HYDROLOGICAL RESPONSE SIMULATION UNDER LAND USE AND CLIMATE CHANGE SCENARIOS

Ph.D. THESIS

by

BRIJ KISHOR PANDEY

DEPARTMENT OF WATER RESOURCES DEVELOPMENT & MANAGEMENT
INDIAN INSTITUTE OF TECHNOLOGY ROORKEE
ROORKEE - 247 667 (INDIA)
NOVEMBER, 2017

HYDROLOGICAL RESPONSE SIMULATION UNDER LAND USE AND CLIMATE CHANGE SCENARIOS

A THESIS

Submitted in partial fulfilment of the requirements for the award of the degree

of

DOCTOR OF PHILOSOPHY

in

WATER RESOURCES DEVELOPMENT

by

BRIJ KISHOR PANDEY

DEPARTMENT OF WATER RESOURCES DEVELOPMENT & MANAGEMENT
INDIAN INSTITUTE OF TECHNOLOGY ROORKEE
ROORKEE - 247 667 (INDIA)
NOVEMBER, 2017

INDIAN INSTITUTE OF TECHNOLOGY ROORKEE
ROORKEE

CANDIDATE'S DECLARATION

I hereby certify that the work which is being presented in the thesis entitled "**HYDROLOGICAL RESPONSE SIMULATION UNDER LAND USE AND CLIMATE CHANGE SCENARIOS**" in partial fulfilment of the requirement for the award of the Degree of Doctor of Philosophy and submitted in the Department of Water Resources Development and Management of the Indian Institute of Technology Roorkee is an authentic record of my own work carried out during a period from July, 2014 to November, 2017 under the supervision of Dr. Deepak Khare, Professor, Department of Water Resources Development and Management, Indian Institute of Technology Roorkee, Roorkee.

The matter presented in this thesis has not been submitted by me for the award of any other degree of this or any other Institution.

(BRIJ KISHOR PANDEY)

This is to certify that the above statement made by the candidate is correct to the best of my knowledge.

(Deepak Khare)
Signature of Supervisor

The Ph.D. Viva-Voce Examination of BRIJ KISHOR PANDEY, Research Scholar, has been held on March 28, 2018.

Chairman, SRC **Signature of External Examiner**

This is to certify that the student has made all the corrections in the thesis.

Signature of Supervisor **Head of the Department**
Date:

ABSTRACT

Water is one of the most essential components of the environment and requires proper planning and management to achieve its sustainable utilization. Changes in climate and land use have significantly influenced the hydrological cycle and hence affect water resources. Due to uncertainty in climate change projection and land use change, improved knowledge of basin hydrology and resources availability are indispensable for policy formulation and sustainable development of the water sector.

The aim of this research was to improve understanding of hydrological response for a large river basin under land use and climate change scenarios. This study investigates the changes in water balance components under different land use and climate change scenarios over Upper Narmada Basin (UNB), a river basin in the sub-humid area of central India. Moreover, identification of climate change and selection of climate models were carried out at regional scale as well as local scale (UNB). For regional scale studies, India has been categorized in to seven zones, considering the geography and homogeneous annual precipitation i.e. North Mountainous India (NMI), North Central India (NCI), Northwest India (NWI), East Peninsular India (EPI), West Peninsular India (WPI), South Peninsular India (SPI) and North East India (NEI).

The comprehensive assessment of spatial and temporal variability in annual and seasonal precipitation and temperature was carried out at regional scale and local scale. In order to identify climatic variability over the region, parametric and non-parametric tests were performed to detect trend, periodicity and break points in long term precipitation and temperature data. At regional scale (seven Indian zones), regression analysis was carried out on long term (1851-2006) monthly precipitation. The results imply mean values of precipitation are decreasing in most of the zones in the last 30-year period while both positive and negative trends existing in each zone for the monsoon datasets. Therefore, wavelet analysis is quite popular tool for trend analysis and periodicity identification in hydrological time series. Discrete Wavelet Transform (DWT) Daubechies wavelets db6 and db10 were selected to decompose the annual and monthly datasets, respectively, applying criteria minimum MRE and the minimum criterion relative error (E_r). The Z statistic was evaluated for trend analysis of the decomposed periodic components and the original annual and monsoon series. Application of DWT on annual series implied 2-, 4- and 8-year fluctuations in the NMI zone, indicating a positive trend in rainfall, whereas zones WPI, SPI and WPI (with 2- and 4-year fluctuations)

experienced a negative trend at the same periodicities, at the 0.05 (5%) significance level. In the monsoon series, a positive trend was found over NMI and NEI decomposed series at 2-, 4- and 8- year periodicity, whereas WPI, EPI and SPI indicated a negative trend at the same periodicity. Considering India as whole (AI), it was found a negative trend in all zones except NMI and NEI.

Furthermore, at local scale analysis, trend in monthly and annual precipitation and mean temperature data were identified at 16 stations of UNB. However, results imply that 8% stations exhibit the negative trend for precipitation, while 100% stations show positive trend for mean temperature over 16 stations of UNB. A comparative study was carried out between three methods i.e. innovative trend analysis (ITA), Mann Kendall (MK) test and Sen's slope, to check the suitability of ITA against nonparametric tests. In result, ITA show the strong agreement with both methods (MK test and Sen's slope), 97.5% and 77.5% in 'ITA versus MK test' and 'ITA versus Sen's slope'. Change year obtained from sequential Mann Kendall (SQMK) were compared with the change year of CUMSUM. Results indicated most of the stations exhibit significant abrupt change year is 1955 (77.78%) for precipitation, and 1960 (100%) for mean temperature. However, finding from this analysis has improved understanding of variability, at spatially and temporally, at current and future climate change.

Evaluation of changes in land use land cover are extremely important and must be monitored to assess the impact on environment. In this study, mapping of LULC and change detection were carried out using the Landsat TM satellite image and geospatial tools. The development of LULC classes were evaluated from 1990 to 2000 to 2010 to 2015. The reduction in natural vegetation and increase in settlement as well as cropland are reflected in the analysis of LULC mapping. Understanding of trend patterns were demonstrated and predicated for the year 2030 using CA-Markov model. The model were validated with simulated and actual LULC of 2015. The projected LULC of 2030 classes indicated the continuing of same trend of recent past. These future projection indicate the expected changes in near future. Therefore, the LULC changes in classes in near future recommend the planning and management of the study area.

To assess the impact of climate change on hydrology, Global Climate Models (GCMs) are the primary data source. Therefore, performance of GCM models are required to evaluate for choosing the best representative GCM for the region. To identify the best representative climate models, performance of 24 GCMs were evaluated against reanalysis models, based on Skill Score (SS) and Root Mean Square Error (RMSE) of six climatic variables. After applying multi-criteria analysis on evaluation parameters (SS and RMSE), results indicate that there is no single

GCM which can recommend for whole Indian regions. However, GCM models for representation of precipitation have been proposed as ensemble of MPI_ECHAM4.0, MIROC3.2_HIRES, UKMO_HADCM3.0 and INGV_ECHAM4 for Indian regions. Climate models of CCCMA groups are performing well for atmospheric temperature in most of the Indian regions. At local scale, three climate models MIROC5, CNRM-CM5 and MPI-ESR-LM were evaluated as best performing models for hydrological modelling of future climate change over UNB.

In order to assess the hydrological response under land use and climate change, Soil and Water Assessment Tool (SWAT), a semi-distributed hydrological model was calibrated applying multi-site calibration techniques. In monthly simulation, Nash Sutcliffe Efficiency (NSE) and Coefficient of Determination (R^2) were computed, 0.77 and 0.76 for calibration (1978-1995) and 0.73 and 0.70 for validation period (1996-2005), respectively, indicating good performance for basin. Calibrated hydrological model used to simulate the change in water balance components under three different land-use and two climate-change scenarios from three representative GCMs (MIROC5, CNRM-CM5 and MPI-ESR-LM). Hydro-meteorological response under land use change indicate that increase in settlement and decrease in natural vegetation, affect as increase in the water yield and surface runoff, but decrease in evapotranspiration (ET). The actual ET decreases with time due to decrease in natural vegetation, maximum in 1990 (460.04 mm) while projected in 2030 is lower (407.19 mm). Water balance components under climate change scenarios indicated annual precipitation decreasing from -1.65% (MPI) to -16.55 % (MIROC) during P1 (2011-2040) and P2 (2041-2071) under RCP4.5, whereas in RCP8.5 scenarios it varies from -26.19% (CNRM) in P3 (2071-2100) to 21.24 % (MIROC) in P3, with reference to baseline scenario. Changes in green and blue water varying from 16.22% (MIROC, P3) to -14.10% (CNRM, P3) under RCP4.5 and from 38.25%(MIROC, P3) to -22.57% (CNRM, P3) under RCP8.5 with reference to baseline scenario. This study established the sensitivity of UNB to future climatic changes employing projections from CMIP5 climate models and exhibited an approach that applied multiple climate model outputs to estimate potential change over the river basin. Moreover, adaptation strategies are proposed against climate change impact.

In general, the study provide a scientifically important and practically relevant, to identifying the historical climate variability and hydrological assessment under land use and climate change scenarios considering representative climate models output, in contributing to water resources planning and management in the context of river basin.

ACKNOWLEDGEMENTS

I wish to express my deep sense of gratitude to my supervisor Dr. Deepak Khare, Professor, Department of Water Resources Development and Management, Indian Institute of Technology Roorkee, for his invaluable guidance, thought provoking discussions and untiring efforts throughout the course of this work. His timely help, encouragement, constructive criticism and painstaking efforts made it possible to present the work carried out by me in the form of this thesis.

I am thankful to Prof. Ajit Kumar Chaturvedi, Director, IIT Roorkee; Prof. S. K. Mishra, Head, Department of WRD&M; Dr. Ashish Pandey, OC, Computer Lab, Department of WRD&M; Dr. R. D. Garg, Department of Civil Engineering & External Member (SRC); and others faculty members at IIT Roorkee, for providing support, constructive suggestions and boosting moral during the study period.

I thankfully acknowledge the moral and technical support received from my friends, Dr. Prabhash Mishra (NIH-Scientist), Dr. Harinarayan Tiwari, Dr. Nitin Joshi, Dr. Shakti Suryavanshi, Dr. Subhas Rai, Mr. Amarkant Gautam, Mr. Ayush Chandrakar, Mr. Kumar Amrit, Mr. Shailendra Kumre, Mr. Santosh Palmate, Mr. Sushil K. Himanshu, Mr. Deen Dayal, Mr. Radha Krishna, Mr.Tesfa Worku and my B.Tech friends 'KCIANS'.

This thesis dedicated to my grandfather (my first teacher) Late Sri Tara Chandra Pandey. It will be unjust on my part to bind in words the spirits of unparalleled sacrifices made by my parents, Shri Shambhu Nath Pandey and Smt. Madhavi Pandey for their blessings and moral support. This work would not have taken shape as it is now, without involvement of my wife Aastha Pandey. She helped me at each and every step during this work and actively participated in compilation of thesis. I also thank my brothers Mr. Nand Pandey, Anand Pandey and nephews Shivansh and Shreyansh for their help, love and care for me. I also feel obliged to my family members who has always supported me spiritually throughout writing this thesis and my life in general.

I thankfully acknowledge the financial support received from the Government of India through MHRD fellowship during the period of study. The scholarship provided from 'Netherlands Fellowship Program (NFP)' to attend the short course program at UNESCO-IHE, Delft, The Netherlands, and the travel support provided by ITS (DST-SERB), Government of India to attend the summer program on 'Sustainable Water Management in an Era of Big Data' is greatly acknowledged.

Further, my humble thanks are due to all those who in any manner, directly or indirectly, put a helping hand in every bit of completion of this research work.

I thank almighty God for the energy and strength to conquer the difficulties in the way and completion of the work.

(BRIJ KISHOR PANDEY)

TABLE OF CONTENTS

LIST OF FIGURES

Figure No.	:	Description	Page No.

LIST OF TABLES

LIST OF ABBREVIATIONS AND SYMBOLS

Abbreviations	Description
Alpha_bf	Baseflow Alpha Factor
AMC	Antecedent Moisture Condition
ANN	Artificial Neural Network
AR5	Assessment Report 5
AVSWAT	ArcView-SWAT
AWC	Available Water Capacity
CA	Cellular Automata
CANMX	Maximum Canopy Storage
CC	Correlation Coefficient
CH_K2	Effective hydraulic conductivity in main channel alluvium
CH_N2	Manning's "n" value for the main channel
CMIP	Coupled Ocean-Atmosphere Model
CN	Curve Number
CORDEX	Coordinated Regional Downscaling Experiment
DEM	Digital Elevation Model
DWSM	Dynamic Watershed Simulation Model
DWT	Discrete Wavelet Transform
ERDAS	Earth Resource Data Analyzing System
ESCO	Soil Evaporation Compensation Factor
ETM	Enhanced Thematic Mapper
FAR	False Alarm Ratio
GCM	Global Climate Model
GCMs	Global Climate Models
GHGs	Green House Gases
GIS	Geographic Information System
GPS	Global Positioning System
GW Delay	Groundwater Delay Time
GW_REVAP	Groundwater Revap Coefficient
GWQ	Groundwater contribution to stream flow
ha	Hectare
hrs	Hours

Abbreviations	Description
HRUs	Hydrological Response Units
IMD	India Meteorological Department
IPCC	Intergovernmental Panel on Climate Change
IWRM	Integrated Water Resources Management
K	Saturated hydraulic conductivity
km	Kilometer
Sqkm	Square Kilometer
LANDSAT	Land Satellite
LULC	Land Use Land Cover
MCA	Multi-Criteria Analysis
MCM	Million Cubic Meters
mm	Millimeters
NASA	National Aeronautical and Space Administration
OAT	One-factor-at-a-time
PBIAS	Percent Bias
PET	Potential Evapo-transpiration
POD	Probability of Detection
PRMS	Precipitation Runoff Modelling System
R^2	Coefficient of Determination
RCM	Regional Climate Models
RCP	Representative Concentration Pathways
RMSE	Root Mean Square Error
SB	Sub-basin
SCS	Soil Conservation Service
SHE	Système Hydrologique Européen
SLSUBBSN	Average slope length
SOL_AWC	Available Water Capacity
SOL_K	Saturated hydraulic conductivity
SOL_Z	Soil depth
SQMK	Sequential Mann-Kendall
SUFI	Sequential Uncertainty Fitting
SURLAG	Surface runoff lag coefficient

Abbreviations	Description
SURQ	Surface Runoff
SW	Sub-watershed
SWAT	Soil and Water Assessment Tool
SWAT-CUP	SWAT Calibration and Uncertainty Programs
UNB	Upper Narmada Basin
WMO	World Meteorological Organization

CHAPTER 1
INTRODUCTION

1.1 GENERAL

In the recent past, there is remarkable change in nature of the global discussion of issues of climate change and land use land cover (LULC) change and its effect on water resources availability. These issues in particular are disturbing the sustainable development planning and management of water resources. Water resources are very important for agricultural sector, power generation, ecosystem and human health, moreover its requirement is raising day by day with population growth. However increasing water demand can be anticipated but changes in environment and its impacts on human and other ecosystems are locally unpredictable. Therefore, it is important to plan and manage the water resources considering anthropogenic effect and environmental changes.

Climate projections for the 21st century indicate that rising temperatures and changing precipitation regimes are likely to affect the hydrological cycle and water resources availability. Assessment of water resources availability under climate change impact and anthropogenic activity at regional and global scale have been intriguing issue to hydrologic research community in recent past. It is important to assess the exact knowledge of water availability for policy makers to accomplish the sustainable development and management for providing various adaptation strategies. Global Climate Models (GCMs) are the basic tools and sole means to detect and evaluate the climate change impact. GCMs were developed to assess the current climate as well as to project the future climatic conditions at synoptic scale (300 to 450 km spatial resolution). Moreover, GCMs accuracy decreases by increasing finer resolution, which is not suitable to evaluate significant impact studies at local scale. It is a complex numerical model to formulate the global climate system. However, due to climate change, temperature is rising and altering the frequency and intensity of precipitation extreme values, which advances the flood and drought events. In the recent past, many studies indicate that global warming has reduced the water availability in many regions. Moreover, water is the basic need for development at regional or local scale but its availability influenced by many factors including hydro-meteorological and climate variability, and anthropogenic activities. The aim of this study is to identify the contribution of climate change, human intervention and its combined effect on the future projection of water resources at basin scale.

1.2 BACKGROUND OF STUDY

The impact of climate change and anthropogenic activity on climatological parameters influence the hydrological processes and water resources availability. Under the global warming, occurrence of extreme events are altered which causes water scarcity and hurdle in sustainable development. In the recent past, many studies indicated that global warming has altered the water availability in many regions of India. Many researchers and scientific community have proved that global warming is caused by rising greenhouse gas (GHGs) concentrations and influences the rise in temperature and alter the rainfall pattern. Under projected climate change, the extreme events (flood and drought) normally will rise across most of the Indian River. In India, during the monsoon season floods are most vulnerable natural disasters and affect the settlement as well as cropland. In the recent past, many researchers highlighted the climate change impact on Indian rivers (Gosain et al. 2006; Mall et al. 2006; Pandey et al. 2016; Revi 2008; Singh and Kumar 1997).

1.2.1 Potential Effects of Climate Change on Water Resources

The mean annual precipitation in India is about 1170 mm, and it varies from 100 mm (Rajasthan) to 11000 mm (Meghalaya). Most of the rainfall occurs in monsoon season. Moreover, average surface runoff estimated to be about 1869 billion cubic meter from rainfall and snowmelt. It is expected that water demand will increase around two times (552 to 1050 billion cubic meter) by 2025 from 1997 (Chatterjee, 2014). Climate change and climate variability are altering the intensity and frequency of extreme events. Instrumental and proxy observations indicate about global warming due to emission of greenhouse gases, particularly in last four-five decades of the 20th century. Houghton et al. (2001) indicated that cause of global warming, surface temperature is rising and intensification will occur in global hydrological cycle which will alter the frequency and intensity of annual precipitation and weather extreme. It is expected that change in annual precipitation will likely to increase flood magnitude and frequency. Moreover, change in climatic condition and land use land cover dynamics will affect the surface discharge, water yield and water availability, particularly on catchment or basin scale. Gosain et al. (2011) simulated the runoff of 12 Indian River basins under climatic conditions of different scenario. Authors present the worst affected two river basins (Krishna and Mahanadi), one is under droughts and other with respect to floods under climate change effect. Narsimlu et al. (2013) assessed the climate change impact on water availability of Upper Sind River Basin and found that mean annual runoff would increase by 94% at the end of 21st century.

Furthermore, many recent research indicate the availability of water resources, assessment of vulnerability of water infrastructure and proposed mitigation strategies to climate change, population growth, and industrial development.

1.2.2 Effects of Anthropogenic Activities (Particularly Land use Change)

Large scale deforestation, expansion of urbanization and industrialization due to increasing population growth contribute to global warming. Moreover, increasing urbanization and population alter the ecological system, environment, ground water recharge, surface water flow, water demand for agriculture, power generation and other purposes. The human interference and GHGs emission are the driving forces behind the climate change. Increasing population and their livelihood demands exerts the pressure on existing LULC resources. Thus, it is important to monitor the information about dynamics of LULC along with population growth and rising requirement. In central India, due to rising population there is a continuous over-exploitation of natural resources such as expansion of cropland at the cost of deforestation and subsequent urbanization from cropland and deforestation. Due to modification of LULC, many problems generated such as deficit in soil moisture, high rate of soil loss, depletion of ground water level and scarcity of water demand. Thus, it is crucial to assess the dynamics of LULC for long term land resources planning and management for decision makers. Currently, there are many tools such as remote sensing technologies available to assess and develop the land use land cover map. Jaiswal, (1999) suggested that geospatial tools and remote sensing data along with toposheets obtained from Survey of India are appropriate tools to analyse and mapping to LULC. Mondal et al. (2014) examined part of Narmada River Basin in Madhya Pradesh, India considering different GHGs emission scenarios and show that rise in precipitation will increase the soil erosion. Khare et al. (2017) investigated the effect of past, present and future LULC change on runoff change and evaluated the hydropower potential on Narmada river basin, Madhya Pradesh, India.

1.3 PROBLEM IDENTIFICATION

In recent times, various literature from worldwide indicate climatic change and anthropogenic activities are significantly affecting the water resources availability at regional and basin scale. In India, water resources demand has already raised manifold in field of agriculture, ecological life, power generation, domestic and industries due to rapid growth in population. In current scenario, rise in temperature, change in cropping pattern, over exploitation of groundwater and stream water

altering the hydrological cycle, and precipitation rate in many climatic zones and water availability of river basins in India. In terms of climate impact on agriculture field, many crops such as rice, wheat, maize and sorghum are the worst hit by extreme weather conditions. Considering the food security, climate change affects 4-9% per year production on different crop, and 15% to India's Gross Domestic Product (GDP). Therefore, it is important to assess the water availability under the climate change and dynamics of land use land cover for long term strategic planning and sustainable development of a region or basin for country.

1.3.1 Research Gaps

Increased concentration of GHGs and anthropogenic activities are expected to change the climatic conditions causing rise in temperature and change in precipitation frequency and intensity. The following research gaps are summarized:

1. In most of the studies, annual average precipitation and mean temperature were considered for trend detection, extreme values were not considered to measure the climate change impact. Additionally very few studies were focused on periodicity rather than trend and shifting.
2. There are limited studies based on selection of best suitable GCMs/RCMs considering the six climatic variables. To project the future climate and water availability, it is important to identify representative climate models for the region.
3. Due to mismatches between hydrological model requirements and GCMs ability, it is not suitable to couple hydrological models with crude spatial resolution GCMs output to assess the impact studies at local scale. To bridge the gap between GCMs output and hydrological model inputs, dynamic downscaling output have been attempted.
4. There are very few studies available to project the virtual water foot print (blue and green water) considering the climate change, which is relatively a new concept in the field of water resources planning and management.

1.3.2 Research Objectives

In order to assess the climate change impact considering GCMs output by integrating with hydrological model, it is important to select suitable GCMs over the region. The general aim of this study is to evaluate the water availability under climate change impact and land use land cover

change, on Upper Narmada Basin, a river basin in the sub-humid area of central India. The following specific objectives are outlined for the present study:

- To analyse the historical trends, shifting (change year) and periodicity of climatic variables such as precipitation, temperature and reference evapotranspiration at regional scale (seven zones of India) and local scale (Upper Narmada Basin).
- To assess the pattern of land use land cover change and project the near future land use land cover of study area.
- To select the best representative Global Climate Models (GCMs) considering six climatic variables at regional (seven zones of India) and local scale (Upper Narmada Basin).
- To estimate the changes in hydrological response under dynamics of land use land cover, and projection of virtual water for three climatic periods of 21th century under climate change scenarios of representative GCMs. Based on the outcomes, propose subsequent adaptation and coping strategies.

1.3.3 Methodologies

In order to achieve the expected results of the above objectives the statistical analysis and hydrological modelling approach were considered in this study. Trend detection was carried out by various non-parametric and parametric test, namely Mann-Kendal test, Sen's slope test, linear regression, innovative trend analysis and discrete wavelet transform (DWT) methodology, while identification of change year (abrupt/sudden shifting) was carried out by Pettitt's test, Buisand's test and sequential Mann Kendall (SQMK) test. Moreover, periodicity of precipitation parameters at regional scale were carried out by discrete wavelet transform. To select the suitable representative GCMs (at regional and local scale) out of 24 GCMs from Intergovernmental Panel on Climate Change (IPCC) Fifth Assessment Report (AR5), multi criteria approach was applied on evaluated parameters skill (SS) score and root mean square (RMSE) values of six climatic variables. Land use land cover classification was carried out by supervised classification, whereas land use in near future were simulated by Markov and Cellular Automata (CA). In this research hydrological model, soil and water assessment tool (SWAT) was calibrated and validated by SWAT-CUP at monthly time step. Based on statistical analysis (trend, shifting, and periodicity) and water balance components, results obtained from hydrological modelling are important to assess the effect of climate change

and anthropogenic activities. These results will support in long term planning and management of sustainable development of the study area.

1.4 STRUCTURE OF THESIS

The outline of the chapters and framework of objectives are as follows:

Chapter One explains the background and importance of the subject in the context of climate change impact on water availability. This chapter also identifies the specific objectives considering the research gaps based on previous studies over the central India.

Chapter Two presents the review on the assessment of climate change at regional and local scale, including the studies based on trend detection and identification of change year. Studies based on global climate models (GCMs) and regional climate model (RCMs) outputs were considered in this literature review chapter. This chapter includes the assessment of previous studies of land use/ land cover mapping and future projection by geospatial tools. Moreover, this chapter covers the hydrological modelling studies based on different hydrological model, especially Soil and Water Assessment Tools (SWAT).

Chapter Three covers the information about the study area, Upper Narmada Basin (UNB) is located in Madhya Pradesh state, Central India. Additionally, this chapter describes the information about data collection such as distribution of land use land cover, soil type etc.

Chapter Four discusses historical trend and periodicity of precipitation at regional scale (India) by using discrete wavelet transform, a relatively new tool in hydrology. Moreover historical trend and shifting year of precipitation, temperature (maximum, minimum and mean), and reference evapotranspiration were detected by several methodologies for 102 years (1901-2002). Spatial and temporal distribution of climatic parameters were also plotted using geospatial tools.

Chapter Five describes the change in land use land cover pattern for last 25 years (1990 to 2015), from 1990 to 2000 to 2010 to 2015. The supervised classification technique was used to classify the classes. The classification were verified with ground truth data points observed during site visit. This chapter also discuss the projection of land use land cover map for 2030 by Markov and Cellular Automata (CA-Markov) approach.

Chapter Six includes the performance evaluation of 24 GCMs by root mean square value (RMSE) and skill score (SS) of six climatic variables (precipitation, air temperature, mean sea level pressure,

outgoing solar radiation, zonal wind and meridional wind) applying Multi-Criteria Analysis (MCA) at regional scale (seven zones of India). Same methodology was applied to get representative (best) climate model at local study area (UNB), and best performing GCM outputs used for hydrological modelling of the basin. Moreover, outputs from climate models were bias corrected by using distribution mapping approach.

Chapter Seven includes the hydrological model (SWAT) setup for UNB study area. Six discharge gauging sites were selected during the model calibration. Model calibration and validation were performed by using SWAT-CUP (SWAT Calibration and Uncertainty Programs) based on monthly time-setup. The sequential uncertainty fitting algorithm version 2 (SUFI-2) of SWAT-CUP was applied with multiple sets of SWAT parameter to assess the performance of model in terms of coefficient of determination (R^2) and Nash–Sutcliffe Efficiency (NSE). Calibrated model was used to simulate the response of river basin under climate change scenarios and land use land cover dynamics. Future projection (2011-2100) of hydro-meteorological components were assessed using representatives GCM outputs, under moderate and high emission scenarios (RCP4.5 and RCP8.5), for three climatic periods (P1: 2011-2040, P2: 2041-2070, P3: 2071-2100). Spatial and temporal distribution of water availability in terms of blue and green water were shown for study area.

Chapter Eight discusses the summary and important conclusions drawn from the study. Additionally, the chapter also focuses on limitation and future scope of the study.

CHAPTER 2
LITERATURE REVIEW

2.1 GENERAL

Assessment of water availability in a river basin under climate change impact and land use land cover change is very important for the sustainable development and management of water resources in the near future. As indicated by Intergovernmental Panel on Climate Change Fifth Assessment Report (IPCC AR5), current global average temperature raised by 0.85^{o}C from 1880 to 2012 and by end of 21th century it may rise by 2^{o}C (IPCC, 2013). The increase in global temperature due to emission of greenhouse gases and anthropogenic activities induced higher evapotranspiration rates that alter the rainfall rate globally. Change in temperature influences the hydrological process and hydrological events such as flood and drought. In order to get better understanding of hydrological process, many hydrological tools were used to assess the water balance under climate change scenarios.

2.2 CLIMATE CHANGE IDENTIFICATION

In the recent past many scientific community analysed the trend of hydro-climatic variables for last decades. Numerous studies were carried out at regional scale and local scale to examine the trend periodicity and change point in climatic variables such as temperature and precipitation. The purpose of understanding the trend is to detect the expected changes and uncertainties. The most popular methods are Mann-Kendall (MK) test, Spearman Rank Correlation test, and Kendall's Rank Correlation test. However, this section covers the work done on climate change assessment by different tools and approaches.

2.2.1 Trend Analysis

In recent years, many researchers were concerned about the temporal and spatial variability of temperature and precipitation rate cause of attention given to global warming. Trend analysis for rainfall distribution was carried out by scientist community from different countries using different methods. Most of the trend detection study were based on parametric and non-parametric test such as Mann-Kendall (MK test) and regression analysis.

Kothyari et al. (1997) identified the changes in climatological variable like rainfall and temperature in upper and central part of Ganga basin, North India. Data used in this study were collected from 3 stations (Agra, Delhi and Dehradun) and non-parametric test performed to detect the trend in this data. The results evidence that in monsoon season the number of rainy days decreases, whereas, there is increase in maximum yearly temperature. Moreover, magnitude of trend were found to be significant at 95% of confidence level. Kunkel et al. (1999) investigated the trend in extreme precipitation events given a certain duration and a site- specific threshold and tested liner trend in the frequency of extreme precipitation events using the nonparametric Mann-Kendall test. Lal et al. (1999) reported that, when maximum and minimum temperatures rise by 1.0 ° C and 1.5°C and then the gain in the yield of the soybean crop comes down to 35%. Furthermore, the study also reported that, when maximum and minimum temperatures will rise by 3.0 ° C and 3.5 ° C and then soybean yields reduces by 5% as compared to 1998. Mirza et al. (1998) analysed trends and persistence of precipitation data were carried out over the three major river basins Ganges, Brahmaputra and Meghna (GBM) of the Himalayan region, India. Basins were examined for trends applying variety of trend test namely Mann-Kendall rank statistic, Student's t-test and regression analysis, whereas first order autocorrelation was applied for persistence.

Ragab and Prudhomme (2002) examined the global warming effect on water resources in arid and semi-arid regions of the world. Study results indicate the variability in rainfall and temperature in most of the parts of the arid and semi-arid regions. Moreover the average annual rainfall has decreased by 5-25%, while average annual temperature rise is reported between 1.59^{o}C to 2.5^{o}C in winter and from 2^{o}C to 2.5^{o}C in summer of the Thar region (India-Pakistan-Afghanistan). The models and empirical considerations suggested that frequency, intensity and area of tropical disturbances may increase. Yue et al. (2002) examined the trend in daily maximum discharge series of employing two non-parametric rank-based statistical tests (Mann–Kendall test and Spearman's rho test) on 20 observed points in Ontario, Canada. Moreover this study analysed the power of the tests by Monte Carlo simulation. Simulation results suggest that their test power relies upon the many factors such as pre-assigned significance level, order of magnitude of trend, size of series, and the variability within discharge series. However test may be more robust in the case of large series while it may decrease by amount of variation increase within the time series. Additionally if a trend is detected, the power is also contingent the distribution and skewness of the series. It has also observed that both test have similar power in detecting the significant trend.

Xu et al. (2003) observed the monotonic long-term trends and step change in rainfall data time series over Japan, by using parametric method (student t-test) and nonparametric methods (Mann-Kendall and Mann-Whitney test). Limitation of study is that in this investigation only 46 rainfall gauges were used with long data records. Results specify that although many shift changes occurred in Japan but the time series did not display major evidence of monotonic trend during the previous century. However magnitude outcome indicate that if the step change reaches one or two times of its standard deviation, the previous fifty years of record together with five years or more of new data will be obtainable for detecting the probable trend. This decision may be helpful for the revealing step changes in the regions where the rainfall has near-normal distributions.

De and Rao (2004) have assessed the rainfall trends for major Indian cities, namely, Ahmedabad, Bangalore, Chennai, Hyderabad, Jaipur, Kanpur, Kolkata, Lucknow, Mumbai, Nagpur, New Delhi, Patna, Pune and Surat, wnith more than one million population. The significant increasing trends were found in annual and monsoon rainfall over Chennai, New Delhi, Kolkata and Mumbai. Arora et al. (2005) detected the trends of temperature at annual and seasonal temporal scale using the MK test at the country and regional spatial scales. It has been observed that the increase in annual mean, mean maximum and mean minimum temperature were at a rate of 0.42, 0.92 and 0.09 ° C (100 years)$^{-1}$ respectively. On a regional basis, stations of southern and western India shows a rising trend of 1.06 ° C and 0.36 ° C (100 years)$^{-1}$ respectively while North Indian plains stations shows a decreasing trend of 0.38 ° C per 100 years. The seasonal mean temperature had increased by 0.94°C/100 year for the post-monsoon season and by 1.1°C/100 year for the winter season.

Tebakari et al. (2005) analyzed the pan evaporation for Kingdom of Thailand .The analysis has been carried for the 19 years (1982-2000) for considering 27 observation stations. In the result, 19 station obtained as decreasing trend and 8 stations found as increasing trend and no station found as no-rise, no-fall trend with in significant level. Gong et al. (2006) evaluated climatic variables which affecting the ET_o in the sensitivity analysis for Changjiang basin, China. The sensitivity of ETo were analysed with climatic parameters (air temperature, relative humidity, solar radiation and wind speed) of 41 years historical data have been used for the study from 150 observation stations. The results showed that relative humidity or solar radiation are sensitive parameters and quite predictable under with help of sensitivity coefficient.

Partal and Kahya (2006) studied the long term trend in average annual monthly Turkish rainfall data series using Mann- Kendall and Sen's slope test. Autocorrelation method is applied to determine the significant level in outcome of Mann Kendall test. In this study 96 rainfall stations are used, which reflect the turkey regional hydro-climatic conditions. The study concludes that rainfall trend detection results gives some significant trend in months of September, January and February, and in the average annual. However outputs of trend analysis confirms the decrease in average annual rainfall in western and southern part of turkey and also in coasts of the black sea. Basistha et al. (2008) assessed the spatial trends of rainfall over Indian region over a period of 1872-2005 using the MMK test. The results show falling trends of rainfall in North India (except Punjab, Haryana, West Rajasthan and Saurashtra) and increasing trends in the south India (except Kerala and Madhya Maharashtra). Further, MMK test and PMW test were used to detect the shift in rainfall pattern from the year 1901 to 1980. The increasing trend of rainfall was found upto the year 1964 and decreasing trend during year 1965-1980. The year 1964 was observed as the year of most probable annual and seasonal change in rainfall in the region. Ezber et al. (2007) used a statistical and numerical modelling technique to temperature data in urban, sub-urban and rural areas to find the urbanization effect on climate of Istanbul. The MK test was used to determine significance of trends and the years in which changes were started. The effect of urbanization on climate was studied using meso-scale atmospheric model. Both the statistical and atmospheric models have found significant warming in atmosphere over urbanized area. The MK test found significant positive trend in average monthly minimum temperature over urban and rural areas. The seasonal analysis shows that the effect of urbanisation was more pronounced in summer season. The significant changes in temperature were observed in the year 1970 and 1980 due to dramatic increase in population.

Gowda et al. (2008) studied the local region of Devangere district over a period of 32 years using statistical analysis. The climatic parameters i.e. rainfall, relative humidity, maximum temperature, minimum temperature, sunshine hour and wind speed were analyzed to assess the climate change. The mild climate change was found in and around the Devangere region in India. The statistical analysis showed that such a small data set may not represent the correct picture of the climate change and requires long term data. Similar, study was also carried out at local region of Roorkee (Tripathi et al. 2007). Matouq (2008) presented a case study of the impact of global warming on the meteorological parameters like rainfall, temperature and relative humidity. The result showed no changes in rainfall but, annual average temperature increases rapidly, about 1.5-2^{o}C since 1990 at

Jordon. The future scenario of climate change has not considered in this study. Bandyopadhyay et al. (2009) carried the trend analysis of ET_o using Mann-Kendall for India. 133 stations have been selected from the different agro-ecological regions from India and study carried out for the duration of 32 years. In the results, ET_o is rising for the whole India during the selected 32 years of the study period. Authors indicated the main cause of this raising trend is increase in relative humidity and decrease in wind speed for the study duration.

Basistha et al. (2009) concluded in their study that more research is required to assess the spatial patterns of trends of other climatic variables i.e. minimum, average and maximum temperature, relative humidity, wind speed, ET, number of rainy/wet days etc., and their inter-relationship. Literature review shows that climate related studies are restricted to statistical analysis of few meteorological parameters only. The study also concluded that arid portion i.e. western part of India has not been investigated well. Mishra et al. (2009) analyzed the climate variability on rainfall of Kansabati basin, India. However trend and persistence were investigated of projected precipitation for annual, monsoon and pre-monsoon periods. Results implied that there will be likely an increasing trend based on CMIP3 scenarios A2 scenario and decreasing trend based on B2 scenario for both annual and monsoon periods during 2051–2100. Sahoo and Smith (2009) analysed the change in various hydro-climatic variables in the speedily urbanizing semi-arid San Antonio River Basin, particularly changes in fresh water inflows to the Guadalupe Estuary. A bigger number of significant trends were found in all hydro-climatic variables throughout all seasons at stations in the lower catchment area, and the percentage contribution of baseflow to stream flow was increased all around the seasons for average, high and low rainfall. Some significant positive trends of rainfall were found in the winter season without significant spatial pattern.

Jhajharia and Singh (2011) observed declining trends in daily diurnal temperature range (diurnal temperature range (DTR) = maximum temperature – minimum temperature) at four station in northeast for almost all time scales. On the other hand, the DTR trends were significant increased mainly at annual, seasonal (pre-monsoon and monsoon), and monthly (May, June, August, September, and November) time scales. Significant rising trends in DTR are observed at three stations in the month of October and in the monsoon and post-monsoon seasons. Four sites showed significant increasing trends for T_{mean} in monsoon and post-monsoon seasons. However, post-monsoon changes for T_{max} and T_{min} were more than the monsoon season, indicating an element of a seasonal cycle. Significant decreasing trends in the sunshine duration were noticed at annual,

seasonal (winter and pre-monsoon), and monthly (January–March) time scales. Kothawale et al. (2010) investigated from the period 1901–2007, all-India mean, maximum, and minimum temperatures have significantly amplified by 0.51, 0.71, and 0.27 °C per 100 years respectively. In addition to this from year 1971-2007 an accelerated warming was observed.

Xu et al. (2010) carried out the study for trend detection on precipitation and runoff for Naoli River watershed, northeast China. Precipitation and discharge data from 160 meteorological stations were considered in the study. Results suggest that during 1951 to 2000 precipitation was increased in the south region and decreased in north region.

Revadekar et al. (2011) studied the observational analysis by taking 121 stations spread all over India to examine extreme event in daily time series data of maximum and minimum temperature. The study found that the temperature is rising throughout the year but variation in winter season are probable to be conspicuous. Overall conclusion is that widespread warming through an increased in intensity and occurrence of warm events. Tabari and Marofi (2011) analyzed the trend for 20 meteorological station of West Iran using Mann Kendall and regression method. Analysis has been carried on the basis of monthly, seasonal and annually for about 40 years. In the results, it has been found that 70% station showing the positive trend using Mann-Kendall where as 75% stations showing the positive trend using the regression method.

Tabari et al. (2011) mentioned the temporal variability of rainfall in their study, where 41 gauge stations data of Iran were used for a period of 1966-2005. The statistical methods (Mann-Kendall test, the Sen's slope estimator and linear regression) were employed to detect the rainfall trend over Iran. To remove the effect of auto correlation over Mann-Kendall test the effective simple size method was used. Annual precipitation output shows the decline trend over 24 stations with significant value at 7 stations having 95% and 99% confidence level. Extent of significant decline trends is varied from -1.99 to -4.26 mm/year at Zanjan and Sanandaj stations. Seasonal precipitation output shows decline trend in spring and winter seasons while significant trend occurred in winter at most of stations. However, maximum and minimum positive significant value observed in summer is 0.110 mm/year and 0.036 mm/year over Semnan and Mashhad stations.

Tabari and Talaee (2011) analysed the monthly, seasonal and annual maximum and minimum temperature for 20 stations in western part of Iran from the period of 1966-2005. Statistical methods (i.e. Mann-Kendall test, the Sen's slope estimator and linear regression) were employed to detect the

temperature trend over Iran. In monthly time series maximum number of the station in month of August shows the rising significant trend while the minimum number of stations showed in month of November and March. Seasonal output gives strong positive trend in summer seasons in maximum and minimum temperature time series. Annual maximum and minimum temperature results shows the rising trend is 85% and decline trend is 15% of the total stations. In addition, the highest positive value of maximum and minimum temperature at Kermanshah is 0.597 ^{0}C/decade and in Ahwaz is 0.911 ^{0}C/decade. Overall study concludes that the minimum temperature is generally rises at a higher rate as compared with maximum temperature.

Jhajharia et al. (2012) worked on rainfall trend in North East India, highlighting shifts in the trend, using MK test. The Indian climate is primarily characterized by monsoon rainfall which generally occurs from June to September and fulfils a major part of the agricultural water needs. Patra et al. (2012) investigated the rainfall trends in 20th century using the parametric and non-parametric statistical trend analysis tests. The temporal variation in monthly, seasonal and annual rainfall was studied for the Orissa state using the data from 1871 to 2006. The results revealed a long term significant declining trend in annual and monsoon precipitation, while increasing trend in post-monsoon season. Precipitation during winter and summer seasons showed an increasing trend. However, in these studies trend analysis was not performed to determine the shift in precipitation at annual and seasonal temporal scales. Further in different studies only trend analyses of isolated climatic parameters like, precipitation or temperature have been discussed with limited statistical trend detection tests.

Shadmani et al. (2012) investigated the temporal trend of arid region of Iran using Mann-Kendall and Spearman's Rho Tests. For the purpose of the study, 13 meteorological stations selected for the ET and the analysis have been carried out for the 41 year period. Trend detected on the basis of monthly, seasonal and annually for the duration. In the result, rising (positive) as well as decreasing (negative) trend have been found for some region but in the most of the region no trend found under the verified significance level. Some'e et al. (2012) studied the spatial temporal trends and change point of rainfall in Iran by employing the MK and Mann–Kendall rank statistic tests, respectively. In their study 28 synoptic station of Iran (1967–2006) were selected to determine spatial and temporal trends. They found that decreasing trends were larger in spring and winter precipitation as compared with other seasonal series. Their study found evident decrease in winter precipitation series along northern Iran and coasts of the Caspian Sea and during summer precipitation at Mashhad

and Torbateheydarieh stations, two significant positive trends were observed. Therefore in autumn precipitation, no significant positive or negative trends were detected by trend tests.

Duhan et al. (2013) examined the climate variability and trends in annual and seasonal temperature variables over 45 stations of Madhya Pradesh, India. Results of the study imply that annual minimum, maximum and mean temperature significantly increased by 0.62°C, 0.60 °C and 0.60 °C in 102 years (19901-2002). Moreover maximum, minimum and mean temperature is high during more urbanization period than during less urbanized period which indicate ascending in temperatures with increment in urbanization.

Sonali and Kumar (2013) analyzed trend of maximum and minimum temperature of annual, monthly, winter, pre- monsoon, monsoon and post-monsoon. The studies were carried out for three time slots 1901–2003, 1948–2003 and 1970–2003, for India as a whole and seven homogeneous regions of India. Authors assessed the trend applying MK test, Sen's slope estimator and other non-parametric methods. Shi et al. (2014) identified the precipitation concentration index (PCI) and the concentration index (CI) for measuring seasonality and daily heterogeneity using precipitation time series. Mann–Kendal test is used to measure the trends of PCI and CI. The linear correlation examines the rainiest day, which contributes the % of precipitation, CI and PCI. Results of this study shows increasing trend at most of the stations in CI and PCI indices but in PCI no trend is significant. The study concludes that the climate shift zone, the concentration of precipitation on a few rainy days is actually bulky in places with large amount annual precipitation.

Adarsh and Janga Reddy (2015) investigated the rainfall trend for southern India using non-parametric methods and wavelet transforms. Sequential Mann-Kendall test was applied to analyse the sequential changes in annual and seasonal trend. Rahmani et al. (2015) analyzed the daily precipitation of Kansas (USA) applying statistical methods and detected significant change points which were useful to manage the water resources system. Nam et al. (2015) showed that the climate variation has triggered spatial temporal changes in climatological components in North Korea. Statistically robust technique is used to define spatio-temporal outlines of precipitation and temperature in particular time phases. Thirty years period of data were collected from twenty seven gauge station used in the study. The results revealed that the maximum and minimum temperatures temporal trend were expressively unlike in the western farming areas and southwest urban areas during 1996 to 2010 compared with 1981 to 1995. However, in case of precipitation number of

events were expressively altered for portions of the northern and north-east regions. Overall in spatial and temporal scale significant transformations were non-uniform in each month and season.

Numerous of studies have been carried out to investigate the trend in temperature and rainfall in India as well as in abroad, however the studies on trend analysis of other climatological variable (relative humidity, evapotranspiration and wind speed) are limited. Therefore, it was important to carry out the detailed analysis of changes in climatic variable and their impact on regional water requirement.

2.3 ASSESMENT OF LAND USE LAND COVER

The land use land cover (LULC) of an area is a result of natural and socioeconomic components and their utilization by man. Land is turning a scarce resource due to huge farming and demographic pressure. Hence, knowledge about land use land cover pattern and possibilities for their utilization is essential for the planning and execution of land use strategies to cope with raising needs for basic human demands and benefit. This information also helps in supervising the dynamics of land use resulting out of changing demands of increasing population. LULC change has become an important factor in present strategies for coping natural resources and supervising environmental changes.

In last few decades the advancement in space technology and powerful computers, Remote Sensing (RS) and Geographic Information Systems (GIS) proved as excellent tools in the study of land use analysis. Satellite remote sensing data available are cost effective, reliable and timely. In the last decades the land use and land cover changes were detected by conventional surveying and mapping techniques. But these are very expensive and time consuming methods.

In this section, literature review shows that different land use land cover mapping for watershed and basin level. However due to increasing human pressure in recent times land use and land cover changes are being significantly influenced by human activities. It is necessary to study changes in land use and land cover in a micro level for its effective management. Therefore, in this part the stress is given to review the LULC change detection studies and simulated LULC future prediction.

2.3.1 Land Use Land Cover Mapping and Change Detection using Geospatial Tools

Many studies were carried out to identify the change detection in LULC cover on the basis of remote sensing satellite data or imagery applying different classification methods.

Vitousek (1994) expressed that "three of the well-documented global changes are increasing concentrations of carbon dioxide in the atmosphere; alterations in the biochemistry of the global nitrogen cycle; and on-going land use and land cover change." Globally nearly 1.2 million km² of forest and woodland and 5.6 million km² of grassland and pasture have been converted to other uses during the last three centuries.

Ratanasermpong et al. (1995) investigated the natural resources evaluation of Phuket Island (Thailand) by coupling of visual and digital analysis of Landsat-TM data. Applying the method of overlaying, change in natural resources during 1987, 1990, 1992 and 1995 were assessed. Analysis revealed that during period of 8 years (1987-1995), 19% of the mangrove forest land has been dropped by urban expansion, on-shore mining, solid waste disposal and particularly coastal aquaculture called shrimp farming. The results of the study were found to be useful for natural resources management revolving on mangrove forest conservation and protection.

Mendis and Wadigamangawa (1996) observed land use changes using existing land use survey data of year 1983, satellite TM data of year 1992 and aerial photograph of year 1994 for Nilwala River Watershed in the Southern Province of Sri Lanka. TM image of band combination 3, 5, 7 was classified based on maximum likelihood classifier. The aim of this study was to determine the changes of LULC pattern due to execution of the Nilwala Ganga Flood Protection Scheme. Study revealed that paddy cultivation has been replaced by habitations and other plantations due to social economic development and topographic factors. Lwin et al. (1998) monitored forest degradation of lower part of Myanmar. Forest degradation have been extracted from Landsat TM data sets of year 1989 and 1995 and annual forest change by using AVHRR time series images (1989 to 1995).The satellite imageries of different sensors and spatial resolution were classified using clustering and supervised classification. Supervised classification uses spectral differences in classified image, topographic features, previous knowledge for identifying land use classes and selecting its training area for the maximum likelihood classifier. Changes in land cover between the two dates (i.e. 1989 and 1995) were detected using post classification comparison algorithm. Based on detected deforestation changes, future deforestation risk area map was prepared. Deforestation risk map provided guidance or regulation against irrational use of forest resources.

Wu et al. (2002) detected land use changes in an arid and semi-arid region North Ningxia, in Northwest China by utilizing the multi-temporal remotely sensed data (Landsat TM dated 1987,

1989 and ETM 1999). Indicator differencing technique utilizes seven bands information to transform into three indicators such as brightness, greenness and wetness. These three spectral properties of indicators have been used to observe the land use changes by visual comparison. Study revealed that farmland increased so as to increase agricultural output while urban extension was triggered by urban population growth. Rural built-up increase was attributed to agricultural output increase, food product increase, and rural labour force increase. Conversion of land to water-body has relation with agriculture output increase while conversion of water-body to land has relation with sown area increase. Hietel et al. (2004) described the major spatial-temporal processes of land-cover changes and identified the correlations between environmental attributes and land cover changes in a German marginal rural landscape. The role of potential environmental drivers to cause land-cover changes also has been identified. Land cover dynamics from 1945 to 1998 was correlated with the physical attributes (elevation, slope, aspect, available water capacity and soil texture) of the underlying landscape. Kucukmehmetoglu and Geymen (2006) analyzed the land use changes in water resources basins using Landsat images of year 1990 to 2005. The GIS was used for assessing the water resources of Istanbul city at spatial scale. The urbanization impact on water resources in Istanbul city was studied. While classifying the satellite images, the emphasis was given to built-up area and changes of respective built up areas were analyzed. This study not considered the inter–relationship between land use changes, precipitation and temperature of urban region to assess the water resources in changing climate scenario.

Chen et al. (2006) discussed the effect of LULC change (1990-2000) on the land surface temperature (LST) using Landsat TM/ETM+ satellite data of Zhujiang Delta. The remote sensing and GIS technique used to assess the LST at spatial and temporal scale with the different LULC classes. The results revealed that strong and uneven urban growth cause LST to raise 4.56°C in the newly urbanized part of study areas. The LULC change on land surface temperature was assessed. The spatial and temporal behaviours of precipitation and ET along with LST with various LULC classes were not studied in the urban catchment. Stathopoulou and Cartalis (2007) had used the Landsat 7 ETM+ thermal band data to identify the hottest surface within the urban settings and correlated with urban surface characteristics in major cities of Greece. The Corine land cover (CLC) data base was also used to define links between surface emissivity, land surface temperature and urban surface characteristics.

Matouq et al. (2008) had presented a case study of the impact of global warming on the meteorological parameters like rainfall, temperature and relative humidity with the help of GIS. The result showed no changes in rainfall but, annual average temperature increases rapidly about 1.5-2°C since 1990 at Jordon. The future scenario of climate change has not considered in this study. The effect of global warming was assessed without considering the LULC change and, water resources were also not considered. Schilling et al. (2008) had quantified the impact on LULC cover change on the water balance of large agriculture watershed using the SWAT model. It was found that the future LULC will affect the seasonal and annual water balance of the watershed. The effects of LULC change were not quantified on evapotranspiration (ET)/precipitation (P) and evapotranspiration (ET)/temperature (T) for historical and future events. The impact of LULC change on water balance of agricultural watershed was studied without considering climate change scenario. Raj and Fleming (2008) have estimated the surface temperature using the landsat ETM+ satellite imagery for a part of Baspa basin, north-west Himalaya, India. The Top of atmospheric (TOA) radiance was extracted from the digital (DN) values and then surface radiance was estimated from TOA using reference channel emissivity method. The good correlation was found between the surface temperatures from surface radiance and the observed surface temperature. The emissivity of study area was assumed constant (0.97, the emissivity of glacier ice). The surface temperature was estimated without assessing the climate change due to LULC change and, the impact on water resources was not studied.

Prakasam et al. (2010) detected the LULC changes in Kodaikanal, Western Ghats (Tamilnadu), India for noticing changes during the time period of 1969 to 2008 (40 years) by using Landsat satellite data and performing supervised classification techniques.

Setiawan and Yoshino (2012) used remote sensing data and geospatial tools to detect and classifying changes on the land use. This study indicates the temporal vegetation changes and complexity during the time applying the hypothesis that land cover might be dynamics. Moreover pixels represent a change when the inter-annual temporal dynamics is altered. They examined the dynamics pattern of long-term satellite data of wavelet-filtered MODIS EVI from 2001 to 2007. The change of temporal natural vegetation dynamics was found by differentiating distance between two successive annual EVI patterns. Moreover, it was determined the type of changes applying the clustering method, which were then verified by ground check points and secondary data sets. Mohanty et al. (2015) analysed the land use and land cover changes in the coastal area of Odisha state over a period of

twenty four years (1990-2014) by using remotely sensed LANDSAT satellite data for the years 1990, 1999 and 2014 and studied the different classifications of land use and land covers like built up area, agricultural land, forest area, water bodies for creating GIS database and concluded that industrial growth and built up area had increased while a decrease in forest area was observed due to the constructional activities.

Khare et al. (2015) investigated the hydrological response of a river basin, Narmada, Madhya Pradesh, India under dynamics of LULC change. The water yield are normally altering due to decrease of initial abstraction that influence and enhances the runoff volume. However, it is essential to measure the changes in the water availability of basin that occur due to changes in LULC. The study was based on a physically based conceptual model, Soil Conservation Service Curve Number (SCS-CN) that acquired to find the surface runoff. The study includes the formulation of a LULC map of various years using satellite imageries, and drainage network, and preparation of a database by applying GIS.

2.3.2 Land Use Land Cover Future Prediction applying various Approach

Several empirical models were developed to predict the land use and land cover (LULC) conversion process. In the recent past, transition probability models and Markov model have been extensively used for analysis and stochastic modelling of LULC changes and prediction. These tools were used in several case studies to explain changes in LULC conversion under constraints.

There are several empirical models help to build the system's dynamic models; the necessary characteristic being the employ of direct observations of spatial processes. In general, modellers used linear statistical models, such as logistic regression and non-linear approaches, like artificial neural networks, because the relationships between the predictor variables and LULC change are not always linear (Li et al. 2015; Sayasane et al. 2016; Shalaby and Tateishi 2007; Srivastava et al. 2012). Moreover various model are developed in last decade to predict the LULC on the basis of past satellite imagery by the many researchers (Abd El-Kawy et al. 2011; de Noblet-Ducoudré et al. 2012; Gamon et al. 2013; Ghosh et al. 2014; Li et al. 2015; Meshesha et al. 2016; Mondal and Mujumdar 2012; Niraula et al. 2015; O'Brien et al. 2004; Olofsson et al. 2013; Pervez and Henebry 2014; Shalaby and Tateishi 2007; Wu et al. 2006).

Pijanowski et al. (2002) used artificial neural networks (ANN) to project the LULC change. An acceptable relationship between settlement expansion and independent variables were obtained by

neural net training. Similar tools were also used in the study. Agrawal (2001) investigated that lacking of fundamental resources is the main force to drive the LULC change. This leads to enhance in the pressure of production on resources, and provide the changing opportunities created outside policy intervention, departure of adaptive capacity and enhanced vulnerability and alters in social organization. Pontius et al. (2001) simulated the spatial pattern of land use change for Costa Rica using GEOMOD 2 model. GEOMOD is a LULCC model designed to simulate a one-way transition from one category to one other category (Pontius et al., 2001; Pontius and Malanson 2005; Pontius and Spencer 2005). The model quantities factors associated with land use, and simulate the spatial pattern of land use forward and backward in time. Schneider and Pontius Jr. (2001) modeled the land use change in the Ipswich watershed, Massachusetts, USA using logistic regression, multi-criteria analysis and spatial filters.

Verburg et al. (2004) employed dynamic Cellular Automata (CA) model consisting of three spatial levels. At the country level, the model integrate the national wide economic and demographic statics, and disperses them at the regional scale. The regional level employs a dynamic spatial interaction model to evaluate the count of habitants and issue of problems over forty regions, and then continues to model the land use requirements. Allotment of the land use requirements on the 500 meter grid is fixed by a weighted sum of the maps of zoning, suitability, accessibility, and neighborhood potential.

Koomen et al. (2005) used a GIS based model, Land Use Scanner (LUS) which employs logit model and technical opinion to simulate succeeding land use patterns. The anticipated amounts of interchanges are established on a linear extrapolation of the national trend in land use statistics from two time data. The regional demand for each land use is allocated to individual pixels based on suitability. Suitability maps are generated for all different land uses based on physical properties, operative policies, relations to nearby land use functions, and expert judgment.

Verburg (2006) developed CLUE-S (2005), which is a basically revised version of the model named as Conversion of Land Use and its Effects (CLUE 1996). CLUE-S (2005) is a spatially-explicit, multi-scale model that projects land use change. CLUE (1996) is the predecessor of CLUE-S, so the two models contribution many common philosophical methodology and computational characteristics. The CLUE model structure is based on organizations theory to provide the integrated analysis of land use change in relation to socio-economic and biophysical driving components.

Clark Labs (2006) developed the Land Change Modeler (LCM) for ecological sustainability. LCM is a software solution designed to address the problem of accelerated land conversion and the specific analytical needs of biodiversity conservation. It provides tools for the assessment and projection of land cover change, and the implications for species habitat and biodiversity.

Konstantinos et al. (2009) developed MABEL model which utilizes sequential decision-making process simulations for base agents in multi-agent based economic landscape. The sequential decision-making process reported that data-driven Markov-Decision Problem (MDP) coupled with stochastic properties. Utility acquisition attributes in our model are generated for each time step of the simulation. Mubea K W et al. (2010) reported that LULC change is one of the major global environmental issue and simulating the changes is crucial to assess the environmental impacts. In this study, stochastic modelling tools such as Markov Model were employed projecting the LULC changes. The results suggest that there has been a noteworthy and uneven settlement development, result of significant loss in natural vegetation. Moreover the study shows that using the satellite based remote sensing imaginary data and geospatial tool GIS can be an effective approach for examining LULC change with reference to the space and time.

Mondal et al. (2013) employed the Cellular Automata (CA) and Markov model to simulate the LULC changes in the Brahmaputra River basin utilizing LULC maps derived from multi-temporal satellite images. Moreover likelihood map was used for basin information to likely spatial procedure in CA Markov model. The simulated quantity and location alteration have been examined and statistically measured. The validation statistics suggested the good comparison map agreed and disagreed with the reference map. Simulated results precision is marginally higher when compare to others studies of LULC change using CA Markov tools.

Nouri J. et al. (2014) employed a CA–Markov model as one of the planning support tools for analysis of temporal changes and spatial distribution of urban land uses in Anzali, located in Gilan province in the northwest of Iran. In the first step, area changes and spatial distribution of land uses in the town were analyzed and calculated using geographic information systems technology for a time span 1989–2011. In the next step, using the transition matrix, the spatial distribution of urban land uses in 2021 was simulated, the changes were predicted and the possible growth patterns were identified as well. The results showed a declining trend of 10.64 % in forest, 8.52 % in Anzali wetland and 11.54 % in barren land during 1989–2011, and also an increasing trend of 7.1 % in urban areas for

a time span 1989–2021. Major expansions in urban areas were witnessed around western and eastern borders of the city, particularly close to the eastern border. Scattered expansions were also predicted in the Anzali wetlands registered in the Ramsar Convention (southern borders). This study provides an opportunity to define and apply better strategies for environmental management of land use to make an optimized balance between urban development and ecological protection of environmental resources.

Within reviewed models, no single model was available, which can fulfil all needs of LULC change analyst community. Each and every model has some merits and demerits. Some models technical limitations (i.e., spatial interaction, temporal complexity etc.), some models considered limited human decision making or socio-economic factors, some model considered limited biophysical factors. It is also observed that one single model cannot be sufficient for LULC modeling that is suitable worldwide. It is due to regional variation of human dimension and biophysical factors. Much modelling work remains to be done to understand LULC changes. LULC modelling for developing regions with considering regional factorial specification requires to be developed in future.

2.4 CLIMATE MODELS AND OUTPUT ASSESMENT

In the recent past many researcher from several research community around the world have concluded, based on an analysis of thousands of studies, that most of the aspect of life on Earth has been affected by global warming. The assessment of climate change impacts on hydrology and water resources availability are normally evaluated by deriving the scenarios. Moreover these scenarios based on emission of greenhouse gases scenarios (GHGs) for changes in climatic inputs to a hydrological model, these scenarios of the future emissions of greenhouse gases as an input for their calculations. Emission scenarios are developed based on socio-economic projections for the world. Moreover climate models output at different emission scenarios required to assess and predict the future water availably.

2.4.1 Global and Regional Climate Models

Climate is already changing, and quite rapidly. With rare unanimity, the scientific community warns of more abrupt and greater change in the future. To assess the futuristic projection and impact scientific community and research institute develop the mathematical model named Global climate model (GCM).

Global climate models (GCMs) represent the coupling of atmosphere, oceans, sea ice and land surface and have substantial potential for assessment of climate change. GCMs are the models for evaluation of climate change based on emission of greenhouse gas concentration. GCMs grids data are available at coarse resolution so it is not able to predict reliably the most crucial features at local and regional impact analyses. Moreover, various climate change prediction models are available for the assessment and modelling of the climate change. The greenhouse effects are included in all of these models, which are based on physical laws, phenomenon of atmospheric and oceanic effect (WMO report survey). GCM is the global climate model, RCM the regional climate model, MHM the macro scale land-surface hydrological model, MWB the macro scale water balance model and CHM the catchment scale hydrological model (Xu and Singh, 2004). These models are useful to assess, model and simulate the future climate change scenarios either at global or regional level.

In order to analyse local and regional climate impact study, it is required to downscale the GCM data at coarser resolution to finer resolution. To solve this problem two downscaling techniques viz., dynamic and statistical downscaling have been proposed.Transforming coarser scale information to finer scale and making it available is downscaling. Therefore, downscaling methods available in the literature varies from the very simple rule based method to complex modelling of the spatial dynamics downscaling. In general, the downscaling techniques can be classified in dynamic downscaling and statistical downscaling. Both techniques are complementary and have own weakness and strength.

Dynamic downscaling or regional climate modeling (RCM) is the methodology to scale the coarser GCM data grid in to local data grid at finer resolution by applying the complex algorithms. Dynamic downscaling can be further subdivided into one-way nesting and two-way nesting (Anandhi et al., 2008). RCMs represent the tropical cyclones, extreme events, etc. and very useful in study on regional climate change.

Statistical downscaling techniques based on the development of statistical (linear or nonlinear) relationship between regional scale climate variables and local hydrologic variable. In order to calibrate the statistical downscaling model, observed or reanalysis climate data required. There are many advantage of statistical downscaling methodologies over dynamical downscaling approaches such as low cost, rapid assessments of regional climate change impacts. Statistical downscaling is the process of empirical relationship that transform large scale features of GCM (predictors) to

regional scale climate variable (predicted). Regression statistical model is the most popular model among the other statistical downscaling methods which are employed to directly estimate a linear and nonlinear relationship between the predictor and predicted.

It is now widely conceived that climate change will have impacts on water resources availability and management across the Globe. The agriculture, urban sector and hydropower production are the major sectors which are affected by climate change (IPCC, 2013).

According to Wilby (2008) the uncertainty is related to downscaling method, global climate model (GCM) structure and climate change scenario (which is associated with future civilization). With this point of view, few recent studies have been attempted to address the above mentioned uncertainties. McAlpine et al. (2007) reported impact of regional climate change on vegetative cover. They found major changes in regional climate, with a shift from humid and cooler condition to warmer and drier conditions, particularly in southeast Australia. These changes in Australia's regional climate advocated that land cover change is probably a contribution factor to the observed trends in temperature and rainfall at the regional scale. Kay et al. (2009) studied the impact of climate change impact on flood frequency for two river basins in England. Authors used four scenarios (A1F1, B2, B1 and A2) of five GCMs to estimate GCM uncertainty using delta change downscaling approach. They reported that the majority of the uncertainty is due to climate modelling, i.e. selection of GCM and RCM structures. Other research studies have also investigated the different arrangement of above stated sources of uncertainty, the work by Wilby and Harris (2006) examined the climate change based on the comparison of two physically based models and one conceptual model. They reported that the differences in model structure complexities can play an important role in the assessment of model outcome. Finally, Poulin et al. (2011) presented the consequences of model structure and parameter equifinality associated to hydrological modelling in climate change impact studies. This study imply that the impact of hydrological modelling in climate change impact studies. This study reveals the impact of hydrological model structure uncertainty is more important than the effect of parameter uncertainty, under past and recent climate as well as future climate change scenario.

To explore the climate change modelling and use of General Climate Models (GCMs) with different downscaling methods the following research have been discussed.

Loaiciga et al. (1996) have studied the basic process of the hydrological cycle and examined the current predictive capability of GCM that simulate the regional and local hydrologic regime under global warming. This study suggests that GCM is used for large scale. The climate change effect on meteorological parameters using Canadian Climate Centre General Circulation Model (CCCGCM) and University of British Columbia (UBC) watershed model for two hydro-meteorologically different watersheds were studied by Loukas and Quick (1996). Other meteorological variables (like cloud cover, albedo, wind speed, evaporation etc.) were also considered along with precipitation and temperature in hydrologic model to the study climate change. Kondratyev et al. (1998) have reviewed the some of the priority areas in the context of global climate change in Japan. Authors discussed global climate change with special emphasis on the global energy and water cycles. The author suggested that considerations of process, which are overcoming the current uncertainties of numerical climate models, climate prediction and modelling.

Matondo and Msibi (2001) had presented a case study of assessment of water resources and hydrology under the changing climate in Swaziland at country level. The WatBall hydrologic model and General circulation model (GCM) were used to assess the water resources i.e. streamflow and found that WatBall model is suitable for assessing the climate change impact on water resources. First the climatic parameters were derived from selected GCMs (i.e. precipitation, temperature and potential evapotranspiration). Streamflow was predicted from WatBall model using GCMs output for the year 2075 under changing climate scenario. Also, streamflow was predicted considering the effects of population increase and agricultural activities on water resources under climate change. The various adaptations strategies were suggested to cope with climate change. This study did not considered the combined effects of population increase, expanded high growth of industries, commercial activities and land use change on water availability. This study assesses water resources on country level, which could not represent the true picture of climate change at local level.

Xu et al. (2005) reviewed the different existing techniques for assessing the water availability in changing climate. Climate change impact on hydrological regimes were identified both for process research for water and catchment management strategies. It was concluded that climate change related studies includes: 1) Use of GCMs data to provide future climate scenarios under different GHG emission, 2) Use of downscaling techniques (both dynamic downscaling method and statistical methods) to downscale the GCM output to the local scales for hydrological models, and 3) Use of hydrologic models to simulate the effects of climate change . The authors suggested that climate

change models should represent the land-surface process in the prediction of future climate change. They also found that results should be simulated at local sites or region using RCMs. Caramelo (2007) analyzed the spatial and temporal behavior of winter precipitation using principle component analysis (PCA). The monthly observed data from 34 weather stations and a subset of daily precipitation used. The first three PCs represents winter precipitation pattern clearly. So, the data of these three stations were further analyzed. The precipitation variability was assessed using PCA for winter precipitation. It is necessary to analyze the variability of precipitation across all the seasons and same analysis can be extended to other climatological variables to understand the spatial and temporal patterns.

Ojha et al. (2010) formulated the downscaling model by using the Linear Multiple Regression (LMR) and Artificial Neural Networks (ANN) methods to downscale the GCM precipitation for Pichola lake area in Rajasthan, India. Predictor variables data are taken out from; NCEP (National Centers for Environmental Prediction) reanalysis dataset, 1948-2000 years, and replications from CGCM3 (Canadian Coupled Global Climate Model, third-generation) for scenarios A2, B1, A1B and COMMIT for 2001-2100 years. In this study the cross-correlations are utilized to check the consistency of the GCM predictor variables. Downscaling outcome demonstrate that precipitation is expected to rise in future for A2 and A1B situations, while, it is minimum for COMMIT and B1 scenarios. Ghosh et al. (2010) reported that at local and regional scale hydrological parameter can be downscaled by using GCM (General Circulation Model) outputs. In this study SVM (Support Vector Machine) technique is used to downscaled the predictor variable and also develop the best relationship between predictor and predictand variable. During calibration and validation process in SVM model the values of certain parameters is need to be fix, for this purpose PGSL (Probabilistic Global Search Algorithm) technique, is used to give the optimum output. By this the obtained relationship between large scale predictor variables and local scale predictand variables is used to calculate the climate scenarios for multiple GCMs. This multiple GCMs provides the uncertainty condition and those outcome has to be further modified by averaging method. Overall, the performance of the model is evaluated by comparing the earlier developed SVM based downscaling models.

Yang et al. (2012) evidence the potentiality in downscaling extreme precipitation, evaporation and temperature in South China using, SDSM (statistical downscaling method). They downscaled the large scale GCM output to regional scale in direction to inquire the spatial temporal changes in

extreme precipitation, evaporation and temperature over the Dongjiang river basin for the period of 2010 to 2099 under H3A2 and H3B2 radiation scenarios. The consequences for downscaling extreme temperature events would be more substantial during the period of 2010 to 2099 for both scenarios. Yet, the projections of change in extremes precipitation and pan evaporation were not coherent. Therefore the performance evaluation of the SDSM shows the good result in case of extreme temperature and evaporation while in case of extreme precipitation model perform not as much of satisfactory.

Hassan and Harun (2012) applied SDSM (Statistical Downscaling Model) to downscale precipitation from the GCMs into a fine scale. Single gauge station data of Kurau River located in Malaysia are used as input in SDSM model. The study evidence that SDSM model has the ability to perform well during calibration and validation process. For future (2010-2099), models determine that there is rise in sum of mean annual precipitation and the study area become drizzlier. Duhan and Pandey (2014) studied three downscaling methods least square support vector machine (LS-SVM), artificial neural network (ANN) and multiple linear regression (MLR) to formulate the downscaling model for the future projections of average minimum and maximum air temperature for central region of India. The A2 emission scenario from CGCM3 (Canadian Coupled Global Climate Model) is used in this study during the period 2001 to 2100. Reason being, to evaluate Statistical performance of MLR, ANN and LS-SVM models to downscale the future temperature. This study revealed the calibration and verification outcome of the models are good, but the performance of LS-SVM is outstanding as compare to MLR and AAN model.

2.4.2 Climate Model Selection

Evaluation of future projection of climate change impact is very important for human and natural system. For future projection of climatic variables at different scenarios climate models has been introduced (Meehl et al. 2007). Climate models are based on numerical and physical principles which are capable to reproduce the present and future climatic parameters. They provide reasonable confidence in producing future climatic condition by using the numerically coupled Atmospheric Ocean General Circulation Model (AOGCM) (Moss et al. 2010; Su et al. 2012).

For impact studies, climate models output being used. Impact of climate change on climatic variables has been assessed by many researchers (Camici et al. 2014; Chen et al. 2012; Haddeland et al. 2014; Miao et al. 2014; Mondal et al. 2014; Niraula et al. 2015; Zhu 2013). For true impact studies of

climate change, it is necessary to evaluate the model with observed datasets, and model output should perform close to the observed data. The study based on GCM climatic variables has been examined for future projection for 2046-2065 and 2081-2100 time slice. Model results for Malaprabha catchment, India indicated that there is no significant changes in rainfall for the future (Mehrotra et al. 2013). Climate impact on agriculture and crop production can also be carried out using GCM output (Mall et al. 2006).

Several studies have been carried out to inter-comparison the model output with observation (Anandhi and Nanjundiah 2015; Diro et al. 2009; Errasti et al. 2011; Evan et al. 2012; Fu et al. 2013; KS and D 2014; Perkins et al. 2007).The output of GCMs are very uncertain so it is required to compare with the past data and apply bias correction (Ojha et al. 2012). The performance of 10 GCM models for simulating the summer monsoon rainfall variation over the Asian-western pacific region assessed by Kang et al. 2002. Johnson and Sharma (2009) used variable convergence score (VCS) methodology which is based on the coefficient of variation. The authors used this methodology to evaluate the eight different variables from nine GCM output for two emission scenario for Australia. This skill score methodology can be used to evaluate for any GCM at any region. Radić and Clarke (2011) evaluated 22 GCMs for North America using several statistical parameters. Evaluation has been carried out by comparing the model output with reanalysis data for period 1980-99. Frei et al. (2003) investigated daily precipitation simulation has been done for European Alpsused by using 5 regional climate model. Model evaluation using the climatic statistics is important than mean values. There are number of recent studies are using climatic indices and the probability density function (PDF) for examine the best model (Anandhi and Nanjundiah 2015; Frei et al. 2003; McMahon et al. 2015; Ojha et al. 2013; Parth Sarthi et al. 2015; Perkins et al. 2007; Radić and Clarke 2011). Perkins et al. (2007) has been carried model evaluation for 12 region of Australia using Probability density function (PDFs). Evaluation of model on study area have been performed considering daily simulation data of maximum temperature, minimum temperature and precipitation. There are many approaches to compare the simulated or model output with observe values or reanalysis values. Teng et al. (2012) analyzed the datasets from 10 GCM for Australia. After bias correction, data were used for runoff evaluation using hydrological model. A very popular model Taylor diagram has been used for several studies which based on the correlation coefficient, root mean square error (RMSE) and variance ratio to compare the model output with observed values (Lin et al.2014). Fennessy et al. (1994) conducted the sensitivity experiment of the observed seasonal Indian Monsoon with the GCM

model output considering the changes in vegetation, soil moisture and cloudiness. For the evaluation of 10 atmospheric variables over India VCS method used by Ojha (2013). VCS curve generated for quantify the variable performance for different GCMs (Ojha et al. 2013). Das et al. (2012) investigated about six common models from Intergovernmental Panel on Climate Change (IPCC), Second, Third and Fourth Assessment Report - SAR, TAR and AR4 respectively. These models have been considered for the performance evaluation of model for Gangetic West Bengal region of east India. In the results, it has been found that MICRO, Japanese model is the best model for the region. GCM ranking of India region carried out using multicriteria analysis by KS Raju et al. (2014). The authors used the 5 performance indicator for evaluation of eleven GCMs. The study carried at 73 grid points of 2.5 x2.5 resolution covering whole India. The entropy method used for weight the performance indicator, and for removing the systematic bias, nested bias correction has been used (KS Raju and D Nagesh 2014).

In this study, Intergovernmental Panel on Climate Change (IPCC), Fourth Assessment Report (AR4) of global climate model output datasets are evaluated using RMSE and skill score for the Indian region considering six climatic variables. Ranking of model has been carried out for each climatic variables using Akaike Information Criteria (AIC) and combined ranking using Multi-criteria Analysis (MCA) method. This study has been carried for monsoon (June to October), non-monsoon (January to May, November, December) and annual (January to December) basis. The Indian monsoon season has a large socioeconomic impact on the development of the country. Variation in monsoon rainfall affect the flood, drought, agriculture and economy of the country. There are several factors viz. Indian Ocean Dipole (IOD), El Ni˜no-Southern Oscillation (ENSO), and sea-surface temperature (SST) responsible for the interannual variation in Indian monsoon (Srinivas et al. 2013).

2.4.3 Bias correction on climate model outputs

The GCMs are used for the projections of future climate change caused by natural variability or anthropogenic activities (IPCC, 2007). Despite continuous efforts to improve GCM's capability of simulating historical climates, the use of bias correction methods is essential for the impact assessment studies of climate change for more improved projections. The significance of bias correction methods has been described in the special report of IPCC (Senevirantne et al. 2012). In estimating probable hydrologic impacts of climate change (Arnell et al., 2004; Oki and Kanae, 2006), a suitable bias correction has been applied to projected temperature and precipitation for error

free estimation of projections. Dettinger et al. (2004) carried out the climate change impact assessment study in the Sierra Nevada of California to study the climate change impact on river flow by using bias-corrected on GCM projected temperature and precipitation data. Lehner et al. (2006) also predicted the risk of flood and drought due to climate change by applying a hydrologic model embedded with the bias- corrected atmospheric data. In addition, bias correction has also been applied to the Regional Climate Model (RCM) simulations such as the studies conducted in four basins of the United States (Hay et al., 2002) and Ireland (Steele-Dunne et al., 2008).

Number of bias correction methods have been used to improve the regional climate downscaling simulation. Wu and Lynch (2000) examined the impact of climate change on seasonal carbon cycle in Alaska through a dynamical downscaling approach in which they constructed the linear bias correction (LBC) of an RCM by adding projected changes of temperature and specific humidity in a GCM simulation to reanalysis climate. A similar technique has been applied by Sato et al. (2007) to examine the effect of global warming on regional rainfall over Mongolia. The bias correction has also been applied to correct the projected wind speed temperature, geo potential height, specific humidity, and sea surface temperature. The results reveal that the rainfall intensity predicted with new method has been closer to observations than the traditional method. The bias correction approach is used to eliminate the biases from the daily time series of downscaled data (Salzmann et al., 2007). Patricola and Cook (2010) also employed a similar method as applied by Sato et al., (2007). The climatological LBCs in above mentioned studies maintain deviations on the seasonal time scales but eliminate the diurnal and synoptic effects. Holland et al. (2010) proposed a complex bias correction method for hurricane simulation. The bias correction developed by Holland et al. (2010) maintained the diurnal, synoptic effect and the inter-annual variation in the LBC by correcting GCM climatological mean bias with six hourly, National center for Atmospheric research (NCAR) reanalysis data and GCM output. They recommended that the dynamical downscaling prediction with GCM bias correction can generate realistic tropical cyclone frequency because the bias correction reduced the impracticable high vertical wind shear over the tropical Atlantic. Jin et al. (2011) proposed a statistical regression model between GCM and reanalysis data to reduce the GCM climatological bias, and the bias corrected GCM output data have been used to force an RCM to predict winter precipitation over the western United States.

Several studies are carried out worldwide to determine the changes in mainly temperature and rainfall and also other climatic parameters its connection with climate change.

2.5 CLIMATE AND LAND USE LAND COVER CHANGE IMPACT ASSESSMENT

2.5.1 Hydrological Models

Hydrological models are the tools which provide the understanding of active interactions between climatic parameters and land-surface hydrology. Moreover, available water and atmospheric temperature affect the hydrological cycle and water budget components. Thus, it is important to select the suitable hydrological model to assess the dynamic interaction between climatic parameters and surface hydrology. It is also help in assessing the climate change impact on regional water availability and cropland productivity. Various models were developed to estimate the peak flow of the design of several hydraulic structures, irrigation and drainage system (Table 2.1).

Table 2.1: Description about various hydrological model and their characteristics

Model Name	Characteristics/Features	Publications
Stanford watershed Model (SWM)/Hydrologic Simulation Package-Fortran IV (HSPF)	Continuous, dynamic event or steady-state simulator of hydrologic and hydraulic and water quality processes	(Crawford and Linsley, 1966; Donigan et al. 1984; Laroche et al. 1996; Saleh and Du, 2004)
Catchment Model (CM)	Lumped, event-based runoff model	(Dawdy et al. 1965; Kuczera and Parent 1998; Van Griensven et al. 2006)
Antecedent Precipitation Index (API) Model	Lumped, river flow forecast model	(Fedora and Beschta, 1989; Kralisch et al. 2005; Sittner et al. 1969)
Tank Model	Process-oriented, semi-distributed or lumped continuous simulation model	(Lee and Singh,1999; Lee and Singh, 2005; Sugawara,1979; Sugawara, 1995)
Hydrologic Engineering Center—Hydrologic Modeling System (HEC-HMS)	Physically-based, semi distributed, event-based, runoff model Streamflow Synthesis and Reservoir regulation (SSARR)	(Anderson et al. 2000; Feldman, 1994; Feldman, 2000; Scharffenberg et al. 2003)
Storm Water Management Model (SWMM)	Process-oriented, semi-distributed, continuous stormflow model	(Huber et al., 1988; Rossman, 2010; Tsihrintzis and Hamid, 1998)

Hydrological Simulation (HBV) Model	Process-oriented, lumped, continuous streamflow simulation model	(Lindström et al. 1997; Seibert 1997; Uhlenbrook et al. 1999)
Chemicals, Runoff, and Erosion from Agricultural Management Systems (CREAMS)	Process-oriented, lumped parameter, agricultural runoff and water quality model	(Cooper et al. 1992; Knisel 1980; Williams and Nicks, 1981; Wu et al. 1993)
Physically Based Runoff Production Model (TOPMODEL)	Physically based, distributed, continuous hydrologic simulation model	(Beven et al. 1997; Beven and Freer, 2001; Quinn et al. 1995; Saulnier et al. 1997; Wolock and McCabe, 1995)
Generalized River Modeling Package—Systeme Hydroloque Europeen (MIKE-SHE)	Physically based, distributed, continuous hydrologic and hydraulic simulation mode	(Graham and Butts, 2005; Im et al. 2009; Sahoo et al. 2006; Singh et al. 1999; Thompson et al. 2004)
Waterloo Flood System (WATFLOOD)	Process-oriented, semidistributed continuous flow simulation model	(Cranmer et al. 2001; Kouwen and Mousavi, 2002; Soulis et al. 2000)
Rainfall-Runoff (R-R) Model	Semi-distributed, process-oriented, continuous streamflow simulation model	(Duan et al. 1992; Kokkonen, 2003; Sorooshian and Gupta, 1983)
Integrated Hydro-meteorological Forecasting System (IHFS)	Process-oriented, distributed, rainfall and flow forecasting system	(Georgakakos 1987; Georgakakos and Foufoula-Georgiou, 1991; Georgakakos et al. 1988)
Soil and Water Assessment Tool (SWAT)	Distributed, conceptual, continuous simulation model	(Arnold and Allen, 1996; Arnold et al. 1998; Neitsch et al. 2011)

2.5.2 Impact Assessment on Water Availability employing SWAT

Several hydrological models utilized for the computation of water availability and water deficits for present and future scenarios. In general, hydrological models represent the dynamic cycle of water balance components (precipitation, evapotranspiration, surface water, ground water recharge percolation and water utilizes by vegetation).

Jha (2004) examined the climate change impact on discharge using RCMs output in the Upper Mississippi River Basin. A hydrological model, Soil and Water Assessment Tools (SWAT) model

was calibrated and validated against measured discharge utilizing observed climate data from the U.S. Environmental Protection Agency Better Assessment Science Integrating Point and Nonpoint Sources (BASINS) geographic information systems. Model outputs were evaluated based on annual scale considering the observed climate series as the lateral boundary condition in RCM. Impacts of climate change on water availability and other hydrologic components were evaluated by driving SWAT with current and future scenario climates. Results indicated that 21% increase in future precipitation simulated by the RCM produced 18%, 51%, 43% and 50% increase in snowfall, surface runoff, groundwater recharge and net water yield, respectively in the Upper Mississippi River Basin.

Matondo et al. (2004) expected the increase greenhouse gas effect which raise the temperature by 1-3.5^{o}C, resulting change in precipitation by ±20%. The impact of anticipated global warming will strike nearly all the sectors of the human endeavour. However, this study was to evaluate the impact of climate change on water resources availability for Swaziland. The computation of the impact of climate change on hydrology and water resources in Swaziland were implemented in three watersheds namely: Mbuluzi, Komati and Ngwavuma. The gaps in discharge data has been filled applying rainfall-runoff modelling technique. MAGICC-model applied to simulate the climate parameters for Swaziland given the baseline scenarios. Moreover three GCMs were used to project the temperature and precipitation changes for Swaziland for year 2075. Model was calibrated and results indicate that there is an annual streamflow change of ±5% in the Komati watershed and ±2% in the Mbuluzi watershed given climate change scenarios. Projected results indicate a negative annual streamflow change ranging from 4% to 23% in the Ngwavuma watershed under climate change scenarios.

Dibike and Coulibaly (2005) noted that global warming have significant impact on local and regional hydrological regimes, which will in turn affect ecological, social and economic systems. However, more dependable precipitation series of future climate scenarios can be derived from GCM outputs using downscaling techniques. The downscaled data is used as input to two different hydrologic models to simulate the corresponding future flow regime in the Chute-du-Diable and Saguenay watershed, Canada. Moreover, the water availability impact analysis were carried out with the downscaled precipitation and temperature time series as input to the two hydrological models advise an overall raising trend in average annual river flow and reservoir inflow.

Fischer et al. (2007) investigated the climate change impact on irrigation demand for regional and local scale considering with and without mitigation of greenhouse gases emission. Future regional and globally irrigation water demands were calculated as a function of both projected irrigated land and climate change and simulations were performed from 1990 to 2080. Future trends for extents of farmland, irrigation water use, and withdrawals were calculated, with specific care given to the implications of climate change mitigation. Renewable water-resource availability was calculated under present and future climate scenarios. Results advise that mitigation of climate change may have substantial convincing effects compared with unmitigated climate change. Moreover, mitigation measures can cut down the impacts of climate change on farmland water demands by about 40%, or 125–160 billion cubic meter (BCM) equated with unmitigated climate.

Guo et al. (2008) examined the floods occurrence and damages in 1990 due to climate change in the Poyang Lake basin in China. In order to evaluate this issues, it was crucial to get information about climate variability, land-use and land-cover changes in the area impact the yearly and seasonal fluctuations of basin hydrology and streamflow. Moreover this study is crucial for long-term planning for LULC to protect water resources and to effectively handle with floods in the Poyang Lake basin and lower basins. Additionally it is also crucial for ecological and socioeconomic implications for the area.

Franczyk and Chang (2009) investigated the climate changes effect on the hydrology of Pacific Northwest during the 21st century. Several GCMs were used to simulate the output, and simulated temperature and precipitation indicate the higher projection. In last 30 years, Due to sudden growth in urbanization, there is change in climate and land use land cover alter the surface runoff and water availability. A combining of global warming and LULC change for 2040 with the semi-distributed, ArcView Soil and Water Assessment Tool hydrological model was used to evaluate the changes in mean runoff depths in the 2040s (2030–2059) from the baseline period (1973–2002) at the monthly, seasonal, and annual scales. Climate model ECHAM5 outputs were downscaled for the region and it was noticed that the region would experience an increase of 1-2°C in the average annual temperature and a 2% increase in average annual precipitation from the baseline period.

Liu et al. (2011) investigated the climate change impact on streamflow in the Yellow River Basin. A semi-distributed hydrological model (SWAT) is calibrated and validated with records at Huayuankou, Lanzhou and Huaxian hydrological stations. Outputs from climate model HadCM3

were downscaled with SDSM and delta statistical approach to generate the daily temperature and precipitation data from 1961 to 2099. In order to get the change in runoff due to climate change, hydrological model SWAT was used. In results, it is noticed that annual mean maximum and minimum temperature may rise by 5.0°C in the 2080s and annual precipitation would increase by 54 mm to 150 mm. Additionally, raising streamflow in spring and summer can help in crop growth, and raising annual precipitation and runoff can facilitate water demand stress to some degree in the Yellow River Basin.

Due to scarcity of observed data and heterogeneousness of the system, discharge and soil loss evaluation in river basin or catchment is one of the most ambitious tasks in water resources studies. However, Soil and Water Assessment Tools (SWAT) is a semi distributed and physical model that can simulate the discharge as well as soil loss for catchment. SWAT is a physically based model. It requires specific information about topography, vegetation, land management practices, hydro-meteorological data (precipitation, maximum & minimum temperature, relative humidity, wind speed, solar radiation), soil physical properties in the catchment. The physical processes associated with water movement, sediment movement, crop growth, nutrient cycling, etc. are directly modelled by SWAT using these input data. The SWAT model is designed to assess stream flow and sediments from individual watershed (Table 2.2).

Table 2.2 : Latest studies based on climate change impact on water availability and soil erosion using SWAT

Authors (Year)	**Study Area**	**Hydrological Model**	**Major Finding /Remarks**
Murty et al. 2014	Ken Basin, India (Area 28574 km^2)	SWAT	• SWAT applied for Ken River basin • Water balance components calculated (1985-2009)
Gessesse et al. 2015	Modjo Watershed, Ethiopia	SWAT	• Climate and LULC change • Sediment loss and transport estimation • Characterization of runoff estimation
Heo et al. 2015	Neches River (Area: 2221 km^2), Eastern Texas (US)	SWAT	• Climate and LULC change considered • Water budget components evaluated
Liu and Lu, 2015	Changle River basin	SWAT	• Nutrient and Pollution estimation

			• Application of Best Management Practices (BMPs)
Singh et al. 2015	Satluj River Basin (48598 Km2) and Tungbhadra River Basin (14429 km2), India	SWAT, SWATCUP	• Model uncertainties with stream flow (peak and low flow) • Separation of sequential peak and low flow using multicriteria evaluation • Temperature and snow melt identified as sensitive parameters in the region
Chattopadhyay and Jha, 2016	Haw river (4000 km^2), North Central Carolina (U.S.)	SWAT	• SWAT model calibrated and validated • Water balance components evaluated due to climate variability
Pandey et al. 2016	Armur watershed , Narmada river, India	SWAT	• SWAT applied for Armur watershed • Water balance components computed for base line (1961-1990) and future climate scenarios (2071-2100) • Positive changes in annual average temperature and rainfall in future projection
Marhaento et al. 2017	Samin river basin (278 km^2), Indonesia	SWAT	• LULC changes and climate change considered • Ratio of surface runoff to stream flow increase • Ratio of base flow to stream flow and lateral flow to stream flow decrease,
Omer et al. 2017	Hutuo River, China	SWAT	• Integrated effect of Anthropogenic and climate change • Climate change and LULC change reduced the runoff • Proposed framework for sustainable development cause of runoff uncertainties
Trang et al. 2017	3S transboundary River basin (Sekong, Sesan, Srepok), of countries (Laos, Vietnam, and Combodia)	SWAT	• Climate study under rcp4.5 and rcp8.5 • Discharge and nutrient increase in wet season and decrease in dry season

2.6 CONCLUDING REMARKS

In recent literature, detection of changes in time series of hydrological and climatological data has received a growing interest. Different aspect of climate change impact and effect of anthropogenic intervention on hydrology were discussed worldwide. Changes in an historical series often occur in the forms of shifting (change year) and trends. Moreover trend in precipitation, temperature and other hydro-meteorological parameters were identified applying various parametric and non-parametric tools. Furthermore, climate variability and land use changes identified for abrupt shifts and trend. Therefore it was very difficult to separate and quantify the individual effects of different land use changes within the catchment area on the basis of observed evidences in the hydrological response.

Many researchers found the reasonable uncertainty in projections of future climate change and its impacts on hydro-meteorological responses, particularly on regional or basin scale. The spatial resolution of the climate models is too coarse to simulate the impact of global change at local scale. Moreover, the greatest uncertainties in the effects of future projection of climate on water balance components arise from uncertainties in global climate models and scenarios. Based on the research above discussed, plenty work has been carried out to simulate the hydrological response considering different scenarios of General Circulation Models output, therefore, performance of GCMs is still required to assess for particular region. Based on the research discussed above, climate and hydrological model was selected to project the water balance for river basin of central India.

CHAPTER 3

STUDY AREA AND DATA COLLECTION

3.1 GENERAL

The basic description of study area and data collection are given in this chapter. This chapter covers the general aspects of location, extent, physiography, climate, drainage, soil, agriculture and hydrological issues over the study area. In other parts of the chapter description of data collection and processing are discussed.

In this research, studies were carried out based on regional scale as well as at local scale. At regional scale, Indian regions were considered for trend and periodicity detection, in addition to, evaluation of best performing climate model. At local scale, a river basin of central India, Upper Narmada Basin (UNB) has been considered for trend analysis of climatic variables, change detection in land use land cover, and hydrological modelling to evaluate the water availability in the basin. Moreover, descriptions about both areas, Indian regions and Upper Narmada Basin (UNB) were mentioned in the given sections.

3.2 UPPER NARMADA BASIN (UNB): LOCAL SCALE STUDY AREA

3.2.1 Location

Narmada River is the fifth longest river of India and known as 'life line of Madhya Pradesh (central India)'. It is the longest west flowing river of India and falling into the Arabian Sea. Upper Narmada Basin is upstream part (upper) of the Narmada river which is one of the most important and holy rivers of central India (Figure 3.1). UNB starts from a small reservoir 'Narmada Kund' in Amarkantak Plateau (Madhya Pradesh) at an elevation of 1057 meters above mean sea level, spread over from coordinates latitude 22° 40' N and a longitude of 81° 45' E (Gupta and Chakrapani, 2005). The length of main stream is about 350 km. The area of UNB is about 3.27 million hectare (32750 km^2) and lies between longitudes 79° 45' E to 81° 45' E and latitudes 21° 20' N to 23° 45' N. There are mainly four districts that lie in the study area namely Mandla, Jabalpur, Narsingpur, and Dindori of Madhya Pradesh, India. Jabalpur is the largest district among all four districts, as per the graphical area and population. The population growth of Jabalpur district 21.67% and 14.51%, Mandla 14.73%

and 17.97%, Narsighpur 21.92% and 14.01% and Dindori district 18.41 % and 17.39 % were occurred in the periods of 1991 to 2001 and 2001 to 2011 respectively (www.citypopulation.de).

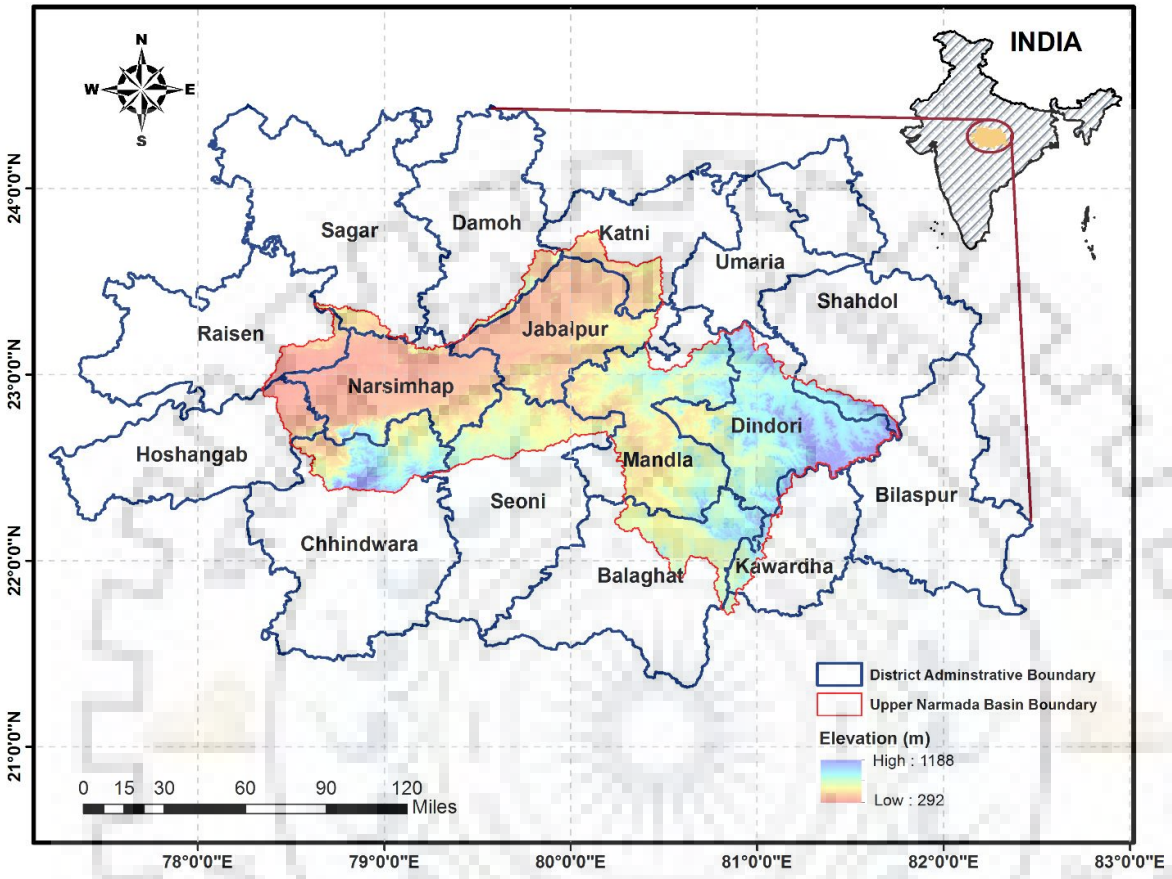

Figure 3.1: Location Map of Upper Narmada Basin, India

3.2.2 Hydraulic Structures

To utilize the water potential of Narmada river for power generation, irrigation, and domestic purposes, State Government of Madhya Pradesh has proposed the about 29 major, 158 medium and about 3000 minor projects to be completed by 2025 (https://en.wikipedia.org/wiki/Narmada_Valley_Development_Authority). Various types of major and minor hydraulic structures are built and proposed along the river basin including dam, barrage, weir and minor structure. However, Bargi Dam is one of the multipurpose major project along the Upper Narmada River, in Jabalpur district. The salient features of the dam is given below in Table 3.1.

Table 3.1: Details of major multipurpose project Rani Avanti Bai Sagar (Bargi dam), Jabalpur

Name of Project	**Rani Avanti Bai Sagar Project (Completed in 1990)**
Location of Dam	Along the Upper Narmada River, Jabalpur district of Madhya Pradesh state; Latitude and longitude are 79º 55'30''and 22º 56' 30''
Hydrology	Catchment Area up to Dam site : 14556 km^2 ; average annual, maximum and minimum rainfall are 1414 mm, 2311 mm and 664 mm, respectively; 75% and 90% dependable yield 5.45 BCM and 4.10 BCM, respectively.
Water Utilization	Irrigation: 2938 MCM, Domestic Water Supply: 170 MCM,
Storage Planning	Gross storage: 3920 MCM; Live storage: 3180 MCM; Dead storage :740 MCM
Submergence Details	Area under submergence at FRL: 27696.50 Hectare
Dam Particulars	Composite earth and masonry dam; Length (Masonry: 827 m, Earth Dam:4540 meter)
Spillway	Central gravity type gated spillway; Length: 385.72m, height: 69.80m, Designed flood : 51510 Cumecs; 21 number of radial gates; sizes of gates :13.716 m x15.25 m)
Canal Command Area	GCA (Gross Cultivable area): 2.60 Lac Ha. CCA (Cultivable Command area) 1.570 Lac. Ha; Annual irrigation 2.20 Lac. Ha.
Hydropower details	Installed capacity 90MW (2x45MW) +10MW (2x 5MW) =100 MW

Note: The above data were collected during site visit of Bargi dam, Jabalpur.

3.2.3 Physiography

Based on physiography, basin can be divided into hilly and plain regions. Upper eastern part of the basin is hilly and mountainous, whereas the lower middle area is mostly covered by natural vegetation and forest. The plain regions in between consist of hilly tracts and in the lower reaches are broad and fertile areas well suited for cultivation. UNB lies in the Madhya Pradesh region, Deccan plateau of central India. The Malwa plateau marks the northern span of Deccan plateau. Satpura range located in the southern part of the state is E-W trending. It has an average elevation of 600 m above mean sea level (amsl) and highest elevation of 1350 m amsl. The Vindhyan ranges

occupies the northern and central part of the region. Moreover, Vindhyan range is extended towards Malwa plateau and Bundelkhand region. In general, the study area has two natural divisions, the valley covering the central and northern parts of the districts and the hills covering the whole of south. The hills in the district belongs to the Satpura range, which rise in continuous chain of forest covered hills. Between these hills and river lies a fertile valley which is a strip of nearly level of about 24 km in width, with slopes gently down towards the Narmada River.

3.2.4 Climatology

Tropic of Cancer crosses the Narmada drainage basin in the upper plains area. A major part of this basin lies just below this line. Thus, there is heavy rainfall in upper parts (hilly and mountainous area) of the basin. However, it decreases from east to west part of basin. Normally, at upper part of the basin, average rainfall is about 1400 mm (near Jabalpur) and lower part receives less than 1000 mm. There is very little rainfall in winter season. The monsoon rainfall accounts for 80% - 85% of the annual rainfall. The heavy rainfall occurs in the upper hilly areas and receives nearly 94% of the annual rainfall in the months of June to October. The annual rainfall in the upper part of the basin is more than 1400 mm and in some pockets it exceeds 1,650 mm. Temperature of basin is like any other part of central India. In general, months of May and January record the maximum and minimum temperature of basin, respectively. Southern portion records higher temperature as compared to northern portion. (*Source: Report of Irrigation Commission, 1972*).

3.2.5 Land use land cover distribution

The major portion of basin is covered by the cropland, natural vegetation, barren land, water bodies and settlement. Agriculture (about 56%) is the dominant class with cultivation during kharif, rabi and summer (Zaid) crop. Paddy is the most common crop in northern part of the basin probably due to heavy rainfall and poor infiltration, whereas wheat is the main crop in lower part of the UNB. Natural vegetation covers about 33% of the total area. Upper part of the UNB are of tropical, moist, deciduous type, whereas southern part of the basins, the vegetation is of tropical dry and deciduous type. Water bodies covered around less than 3% of the total area, including large water bodies of reservoir like Bargi dam etc..

3.2.6 Soil type and distribution

Soil is composition of different types of minerals and organic matters that are different from its parent materials in terms of its texture, structure, consistency, colour, chemical and other

characteristics. The knowledge about the soil profile is very helpful in modelling the hydrological character of the basin. The nature and characteristics of soils is dependent primarily on relief of the area, which influences the variation in soil formation.

In the upper part of UNB basin, the majority of the soil are characterised by shallow black soils. These type of soils are erosional products to hold basalts. The black soils have intrinsic property to hold water and allow less drainage due to presence of smeclite clays. Presence of organic matter is very less in black soils about less than 5%. The black soils in the upper basin are generally in-situ kor collovial. These soils are often interspersed with red sandy or laterite soils. The profile is generally shallow and mainly covers the hilltops and plateau regions. The red soils are the result of intense chemical leaching of basalts whereby all the minerals in the rock are leached out except the oxides of silica, iron and aluminium. Due to intense leaching, these soils have a reasonably good drainage but lacking in nutrients essential for plant growth. Soils in Vindhyan and Satpura plateau region of the middle basin range from shallow black soils to medium black soils. Around Hoshangabad, recent alluviums with varied thickness can be witnessed. Soil erosion is fairly severe in the upper hilly and upper plains regions in the Narmada basin. Severe erosion also occurs throughout course of the river in the lower plains.

3.3 INDIAN ZONES: REGIONAL STUDY AREA

In this research, some studies such as trend detection and periodicity of precipitation, and selection of the climate model were carried out at regional scale, for seven Indian regions.

3.3.1 Location Map

India is located in the south of the Asian continent, bordering the Arabian Sea and the Bay of Bengal. The country is situated north of the equator between 8°4' and 37°6' north latitude and 68°7' and 97°25' east longitude. It is the seventh-largest country in the world, with a total area of 3,166,414 square kilometres. India measures 3,214 kms from north to south and 2,933 km from east to west. It has a land frontier of 15,200 km and a coastline of 7,517 km.

3.3.2 Physiography

In India, north-west to south-west direction is mountain ranges, the most renowned mountain Himalayan range with Kanchenjunga Peak as its highest peak. This mountain peak measures over 8000 meters. The Himalayas are relatively young fold mountains with great magnitude of local

relief, very steep slopes, highly uneven surface, little levelled land and young river valleys. Three important rivers, the Brahmaputra River, Sutlej River and Indus River of India starts from Mansarovara Lake that lies in this zone. Peninsular region of India is oldest and most stable landmass of India and covered by tors, Block Mountains, rift valleys, spurs, bare rocky structures, series of hummocky hills and wall-like quartzite dykes offering natural site for water storage. However western and north western region has emphatic presence of black soil. In northern west part of India is desert (Thar) and Aravali hills. Moreover, Thar desert is 9th The Indian desert is located in the northwest part of Aravali hills. Most of the rivers in the region are ephemeral.

Therefore, Indian regions have been categorized in to seven zones, considering the geography and homogeneous annual precipitation. These regions are North Mountainous India (NMI), North Central India (NCI), Northwest India (NWI), East Peninsular India (EPI), West Peninsular India (WPI), South Peninsular India (SPI) and North East India (NEI) as shown in Figure 3.2 (Li et al. 2014; Sontakke et al. 2008).

3.3.3 Climatology

North Mountainous India (NMI) is the Great Himalayan Mountain of topography elevation more than 7000 m, mean annual precipitation about 1500 mm in which 72% nearly from monsoon season. It is the coldest region of India. Northwest India (NWI) region is arid and semi-arid climate zone of India. In this region, 'Thar' desert located. Mean annual precipitation of this region is 800 mm and 88% contributed by monsoon season. Moreover it is the hottest region of India. North Central India (NCI) is the Indo-Gangentic plains of humid sub-tropical climatic region. The mean annual precipitations 1,212 mm and monsoon contributing 85% of it. The mean annual precipitation for WPI, EPI and SPI regions is 1103, 1162 and 1555 mm, with nearly 85%, 73% and 60 % falling in monsoon period, respectively (Li et al. 2014; Parth Sarthi et al. 2015). NEI is the region of eastern part of Himalaya and includes the mighty Brahmaputra River. It is humid sub-tropical climate region, humid and hot summers, mild winters and severe monsoon. NEI region receives heavy rainfall, however mean annual rainfall varies 1577 mm to 6002 mm that creates the problem of ecosystem and flooding (Jain et al. 2013). It was observed that the region receives overall average annual rainfall of 2156 mm, and major portion (70%) of annual rainfall occurs during the monsoon season.

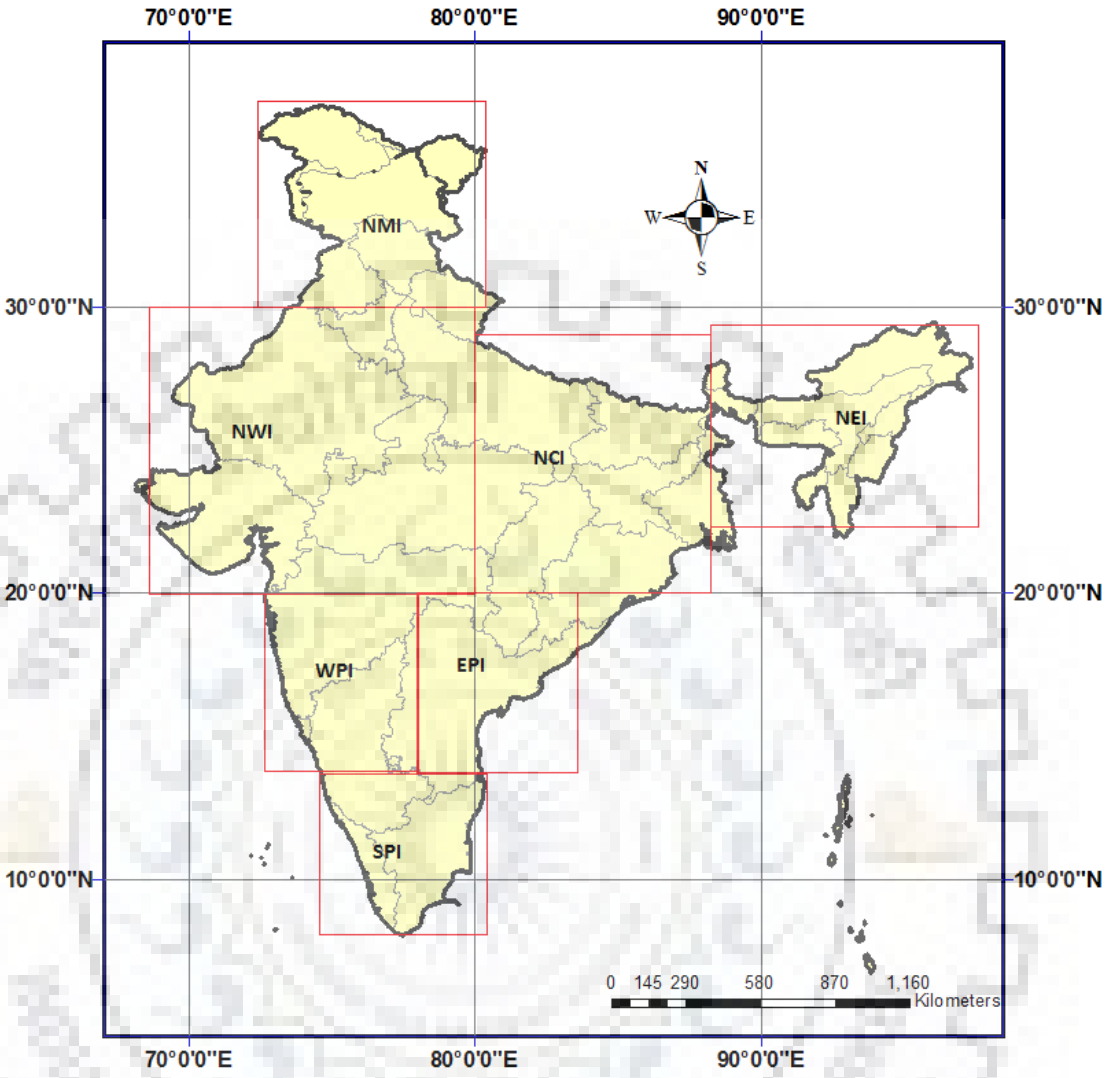

Figure 3.2: Seven Indian zones for regional study (Li et al., 2013)

3.4 DATA COLLECTION AND PROCESSING

Hydro-meteorological and spatial data have been collected from India Meteorological Department (IMD) Pune, India Water Portal (Indian Meteorological Datasets) and other resources.

3.4.1 Hydro-meteorological Data

Mean Monthly meteorological observed datasets of temperature (maximum, minimum and mean) rainfall, reference evapotranspiration and cloud cover data were collected for 102 years (1901-2002) of basin stations UNB that are derived from India Water Portal site for trend analysis study. Moreover daily gridded data of rainfall and temperature (maximum and minimum) for study have

been collected from IMD Pune for 1971 to 2015 for hydrological modelling. The spatial resolution rainfall data is 0.5^o x 0.5^o and 0.25^o x 0.25^o, whereas temperature data was obtained at 1^ox 1^o spatial resolution. Moreover, long term precipitation data series of 156 years (1871-2006) for seven Indian region were obtained from the Indian Institute of Tropical Meteorology (IITM), Pune website (http://www.tropmet.res.in/Data).

3.4.2 Soil Map

The Soil map of the study area presented at 1:250,000 scale has been obtained from NBSSLUP (National Bureau of soil survey and Land Use Planning), Nagpur. It has been carefully scanned and exported to ArcGIS 10.1. Different soils have been traced and the polygons representing various soils are filled with different colours for proper identification. The area under different soils have been identified.

3.4.3 Digital Elevation Model

The Shuttle Radar Topography Mission (SRTM) data are digital elevation on horizontal grid spacing of 90 m resolution. The elevation of UNB area varies from about 300 m to 1200 m from mean sea level (MSL) by Digital Elevation Model (DEM). On west northern and eastern, most parts of the catchment the lowest elevation ranges (Narmada River) and the highest range are located towards lower part of catchment area respectively. In study area the DEM, of 90 x 90 meter pixel size was loaded to the system in an Arc Info grid format. The DEM properties were set up to verify the projection and the horizontal and vertical units of measure were verified. The DEM is acquired to generate the drainage network for the study area.

3.4.4 Observed Discharge

Observed discharge and sediment data are necessary for evaluating the hydrological model. Discharge data of UNB have been collected to calibrate and validate the model. For UNB, seven gauging stations have been established to measure discharge by Central Water Commission (CWC). The seven discharge gauging stations within the basin are Mohgaon, Manot, Patan, Bamni Banjar, Gadarwara, Belkheri, and Sandia.

3.5 CONCLUDING REMARKS

In this research, investigations on the climatic variables have been made at regional scale as well as at local scale to understand the relationship between spatial scale severities of climate change on water availability. The whole country has been divided into seven zones of Indian region to analyze the trend and periodicity of precipitation, and selection of climate model for hydrological studies, which constitute the regional scale of the study. At local scale Upper Narmada Basin (UNB) was selected for trend analysis of climatic variables and evaluation of water balance components at different emission scenarios. UNB has also been selected to describe as a prototype case study area to assess the climate and land use change. Furthermore, UNB is considered as study area to demonstrate the application of integrated hydrological modelling with changing climate scenario. Salient features of the selected study area are described briefly, which includes the location map, physiography, climatology, land use land cover distribution and soil map. The spatial, non-spatial and meteorological data have also been briefly described and presented in subsequent chapters.

CHAPTER 4

IDENTIFICATION OF TREND AND PERIODICITY IN HYDRO-METEOROLOGICAL VARIABLES

4.1 GENERAL

The impact of climate change and human activity on meteorological and hydro-climatological parameters influence the hydrological process and water resources availability. Precipitation and temperature are the most important governing meteorological parameters of hydrological cycle and contribute vital role in water availability (Bae et al. 2008; Dakhlalla and Parajuli 2016; Fennessy et al. 1994; Groisman et al. 1999; Pandey et al. 2016; Sethi et al. 2015; Widmann and Schär 1997; Xu and Zhang 2006). In recent years, many researchers have shown concern about the temporal and spatial variability of precipitation rate cause of attention given to global warming (Arnell 1999; Camici et al. 2014; Fennessy et al. 1994; Ficklin et al. 2009; Fischer et al. 2007; Holman 2005; Liu et al. 2015; Pachauri et al. 2014; Sneyers 1997; Ting and Wang 1997). In the context of climate variability, trend analysis is one of the important tools to analyze the variability in studies of hydrology and climatology. Trend analysis for rainfall distribution was carried out by scientist community from different countries using different methods (Adarsh and Janga Reddy 2015; Bandyopadhyay et al. 2009; Bawden et al. 2014; Jain et al. 2013; Jiang et al. 2002; Mishra et al. 2009; Partal and Kahya 2006; Pingale et al. 2014; Shifteh Some'e et al. 2012; Widmann and Schär 1997). The purpose of understanding the trend is to detect the expected changes and uncertainty. The most popular methods are Mann-Kendall test, Spearman Rank Correlation test, Kendall's Rank Correlation test.

In this chapter, characteristics of hydro-climatic parameters were detected at regional scale (seven Indian zones) and local scale (Upper Narmada Basin) in two sections. In first section, an attempt has been made to determine the trends in monthly, annual and monsoon total precipitation series over India by applying linear regression, the Mann-Kendall (MK) test and discrete wavelet transform (DWT). The linear regression test was applied on five consecutive classical 30-year climate periods and a long-term precipitation series (1851–2006) to detect changes. The sequential Mann-Kendall (SQMK) test was applied to identify the temporal variation in trend. Wavelet transform is a relatively new tool for trend analysis in hydrology. Comparative studies were carried out between decomposed

series by DWT and original series. Furthermore, visualization of extreme and contributing events was carried out using the wavelet spectrum at different threshold values.

In the second section, Upper Narmada river Basin (UNB), a humid subtropical region of India considered as a study area at local scale. Spatial and temporal variation in meteorological data (precipitation and mean temperature) at 16 stations were analyzed based on monthly seasonal and annual series of 102 years (1901-2002). In recent years, there are many trend studies of hydro-meteorological data over the basin, but there are limited studies to detect trend in extreme values. Therefore, a detailed trend analysis was carried out of annual extreme events of precipitation and temperature series applying Innovative Trend Analysis (ITA) for sustainable water management development in terms of climate change. Moreover, discrete wavelet transform (DWT) was applied to identify and for visualization of extreme events. Therefore, Sequential Mann-Kendall (SQMK) and cumulative sum charts (CUMSUM) were used to identify the abrupt change year in precipitation and temperature in 16 stations of Upper Narmada river basin.

4.2 METHODOLOGY

4.2.1 Serial Correlation Test

Serial correlation is also known as Autocorrelation, in which error terms in a time series transfer from one period to another period. Serial correlation coefficient (r_1) at lag-1 computed using following equation:

$$r_1 = \frac{\frac{1}{n-1}\sum_{i=1}^{n-1}(P_i - \bar{P})(P_{i+1} - \bar{P})}{\frac{1}{n}\sum_{i=1}^{n}(P_i - \bar{P})^2} \quad \ldots\ldots\ldots\ldots\ldots (4.1)$$

Where, $P_i, P_{i+1} \ldots\ldots\ldots P_n$ is the time series, $\bar{P}$ is the mean of the time series. If computed 'r_1' is significant at 5% of two tailed test, 'pre-whitened' series should be applying in Mann-Kendall test and Sen's slope method.

4.2.2 Mann-Kendall Test

Mann-Kendall (MK test) is a nonparametric test for trend analysis. It is based on null hypothesis testing for check the existence of trend in the terms of yes or no. It is simple and strong method. In addition to this, it can also handle the missing values and outliers (Yue et al. 2002).

The Kendall's test statistics is given as

$$S=\sum_{i=1}^{n-1}\sum_{j=i+1}^{n}\operatorname{sgn}\left(P_j-P_i\right) \qquad \text{..... (4.2)}$$

$$\operatorname{sgn}\left(P_j-P_i\right)=\begin{cases}+1 & if \quad \left(P_j-P_i\right)>0\\ 0 & if \quad \left(P_j-P_i\right)=0\\ -1 & if \quad \left(P_j-P_i\right)<0\end{cases} \qquad \text{..... (4.3)}$$

for a time series, P_i ,i=1,2,3.....,n.

$$\left(\sigma_s\right)^2=\frac{1}{18}\left[n(n-1)(2n+5)-\sum_{p=1}^{q}t_p\left(t_p-1\right)\left(2t_p+5\right)\right] \qquad \text{..... (4.4)}$$

$$\mathrm{Z_{MK}}=\begin{cases}\dfrac{(S-1)}{\sigma_s} & if \quad S>0\\ 0, & if \quad S=0\\ \dfrac{(S+1)}{\sigma_s} & if \quad S<0\end{cases} \qquad \text{..... (4.5)}$$

When n ≥ 10, S becomes normally distributed with zero mean and variance denoted as σ_s^2. t is the extent of (number of P involved) of any given tie. If $|Z| > Z_{1-\alpha/2}$, there is no trend rejected, according to the null hypothesis. Z is the standard normal variate and α is the significance level for the test (Emori and Brown 2005).

4.2.3 Sen's Slope Estimator

Sen's slope is the tool to estimate the monotone trend of the equally spaced time series data. In this study, it is used to quantify the slope of the series.

$$\beta=\text{Median}\left(\frac{P_i-P_j}{i-j}\right) \text{ for all i< j} \qquad \text{..... (4.6)}$$

Where, β is the slope between data points P_i and P_j (Sethi et al. 2015).

4.2.4 Sequential Mann-Kendall Test

To detect the nonlinear trend with time, Sneyers (1990) introduced sequential or partial values, *z(t)*, from the progressive analysis of the Mann-Kendall test. Herein, *z(t)* is a standardized variable that has zero mean and unit standard deviation. The following steps are applied to calculate *z(t)* (Eq. 4.7 -Eq. 4.10)

1. The values of P_j mean time series, (j =1, . . . ,n) are compared with P_i, (i = 1, . . . , j − 1). At each comparison, the number of cases $P_j > P_i$ is counted and denoted by n_j .

2. The test statistic t is then calculated by equation

$$t_j = \sum_{1}^{j} n_j \quad \text{..... (4.7)}$$

3. The mean and variance of the test statistic are

$$E(t_j) = \frac{j(j-1)}{4} \quad \text{..... (4.8)}$$

$$Var(t_j) = \frac{j(j-1)(2j+5)}{72} \quad \text{..... (4.9)}$$

4. The sequential values or partial values of the statistic *z(t)* are then calculated as

$$z(t) = \frac{t_j - E(t_j)}{\sqrt{Var(t_j)}} \quad \text{..... (4.10)}$$

4.2.5 Discrete Wavelet Transforms

The hypothesis of wavelet analysis was developed based on Fourier analysis. A signal is broken up into smooth sinusoids of unlimited duration in Fourier analysis (Kisi and Cimen 2012). A wavelet is a mathematical function which can be used to localize a given function in both space and scaling (Labat 2005; Labat et al. 2005).Wavelets can be utilized to extract information from diverse kinds of data; such as seismic, finance, heartbeat, hydrological etc. (Agarwal et al. 2005; Ahmad and Simonovic 2005; Chakraborty and Okaya 1995; Ivanov et al. 1999; Ivanov et al. 1996; Michael P. Clementsa 2004; Sinha et al. 2005).Wavelet analysis is often used to learn evolutionary behavior to characterize fluctuated daily discharge time series (Smith et al. 1998; Wang and Ding 2003).The

major improvement of wavelet transforms is their capability to concurrently acquire information on the time, location and frequency of a signal, while the Fourier transform provides only the frequency information of a signal.

The discrete wavelet transform (DWT) is defined as

$$\psi_{m,n}\left(\frac{t-b}{a}\right) = a_0^{-m/2}\left(\frac{t-nb_0a_0^{\,m}}{a_0^{\,m}}\right) \quad \ldots\ldots\ldots\ldots (4.11)$$

Where, *m* and *n* are integers that govern the wavelet scale/dilation and translation, respectively; a_o is a specified fine scale step greater than 1; and b_o is the location parameter and must be greater than zero. The most common and simplest choice for parameters a_o and b_o are 2 and 1, respectively. This power of two logarithmic scaling of the dilations and translations is known as dyadic grid arrangement and is the simplest and most efficient case for practical purposes. For a discrete time series *P(t),* the DWT becomes:

$$DWT(m,n) = 2^{-m/2}\sum_{t-0}^{N-1}\psi^*\left(2^{-m}t-n\right)P(t) \quad \ldots\ldots\ldots\ldots (4.12)$$

Where, DWT *(m, n)* is the wavelet coefficient for the discrete wavelet of scale $a = 2^m$ and location $b = 2^m n$. *Q(t)* is a finite precipitation time series ($t = 0, 1, 2, \ldots, N - 1$), and *N* is an integer power of 2 ($N = 2^M$); this yields the ranges of m and n as, respectively, $0 < n < 2^{M-m-1}$ and $1 < m < M$.

4.2.6 Innovative Trend Analysis

Innovative Trend Analysis (ITA) is used for trend detection proposed by Şen (2011). Traditional trend analysis tools such as Mann-Kendall (MK) and Spearman's Rho (SR) tests based on restrictive assumptions such as independent structure of the time series, normality of the distribution, and length of data. In this new approach, all restrictive assumptions in the MK and SR tests are avoided. Innovative Trend Analysis (ITA) is a handy tool to detect the positive and negative trend.

In ITA, whole time series was divided into two parts. Divided sub-series arranged in the ascending order and plotted on given time series on a Cartesian coordinate system. In this plot, trend free subsections of the series appear along the 45° straight-line. Data lies in the upper portion of the 45° straight line indicates the increasing trends and vice versa (Figure 4.1).

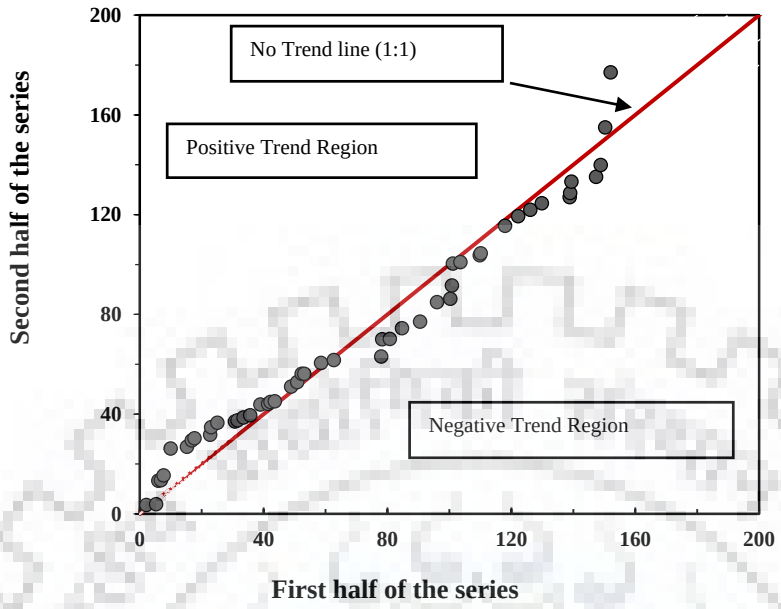

Figure 4.1: Illustration of positive, negative and no trend region in innovative trend analysis

For better understanding of extreme value trend, data could be categories as low, medium and high values clusters. Low rainfall cluster in upper portion indicates the increasing trend in low rainfall. Medium rainfall cluster along the 1:1 straight line indicates the trend free in medium rainfall. High cluster data in lower portion of the plot indicates the decreasing trend in high rainfall. In order to compare with the MK and Sen's, a ITA indicator (D) was proposed by Wu and Qian (2016) expressed as:

$$D = \frac{1}{n}\sum_{i=1}^{n} 10\frac{(Y_i - X_i)}{\bar{X}} \qquad \ldots\ldots\ldots (4.13)$$

Where X_i and Y_i indicate the horizontal axis (first half series) and vertical axis (second half series), respectively, $\bar{X}$ indicate the mean value of horizontal series and n is the length of sub-series. Positive value of ITA indicator (D) indicate the positive trend and negative value indicate the negative trend in the series.

$$z(t) = \frac{t_j - E(t_j)}{\sqrt{Var(t_j)}} \qquad \ldots\ldots\ldots\ldots (4.14)$$

4.2.7 Cumulative Sum Charts (CUMSUM)

This method is used for detection of abrupt change point (shifting) in the meteorological series (Gocic and Trajkovic 2013). Change point is computed based on the cumulative sum *(S_o, S_1, S_2....S_n)* of the time series (P_1,P_2....P_n), where *n* is the series length (Healy 1987).

$$S_o = 0 \; and \; S_i = S_{i-1} + (P_t - \bar{P}) \qquad \text{..... (4.15)}$$

$$i = 1, 2 \ldots\ldots\ldots, n$$

$$S_m = \max_{i=1\ldots n} |S_i| \qquad \text{..... (4.16)}$$

The location of change point is defined by '*m*'. The estimated point 'm' show the last point of occurrence of shifting.

4.2.8 Buisand's Range Test

This method is also known as Cumulative Deviation Test, which is based on the adjusted partial sums or cumulative deviation from the mean.

$$S_o^* = 0 \; and \; S_k^* = \sum_{t=1}^{k} (P_t - P_{mean}) \qquad \text{..... (4.17)}$$

$$k = 1, 2 \ldots\ldots\ldots, n$$

$$S_k^{**} = S_k^* / \sigma \qquad \text{..... (4.18)}$$

$$R = Max|S_k^{**}| - Min|S_k^{**}|, 0 \le k \le n \qquad \text{..... (4.19)}$$

The $R/\sqrt{n}$ is then compared with the critical values given by Buishand (1982) (Peterson et.al.1998).

4.2.9 Pettitt's Test

This test is basically based on the rank of the series and ignores the normality of the series

$$X_k = \sum_{i=1}^{k} r_i - k(n+1) \qquad Q = Max|X_k| \quad 1 \le k \le n \qquad \text{..... (4.20)}$$

where $i = 1, 2, \ldots\ldots\ldots, n$. The change years in the K^{th}year of the max $X_k$value (Bawden et al. 2014; Costa et al. 2008).

4.3 REGIONAL STUDY: SEVEN ZONES OF INDIA

In the recent past, many trend studies were based on long-term and short-term time series of different climatic and hydrological variables, viz. precipitation, temperature and discharge. Hydrological variables exhibit substantial dependence over a wide range of temporal and spatial scales. The spatial variability of a hydrological variable may also have an effect on hydrological modelling. Therefore, the aim of this study are: (a) to carry out trend analysis using climatological categorization of time series (30 years) data, in addition to investigating general long-term trend (156 years) over all seven zones of India based on annual and monsoon precipitation; (b) to study temporal change in trend for monthly, annual and monsoon precipitation to derive changes in climatological time zones, as well as spatial variability of precipitation under Indian conditions; (c) to use a combination of the MK test with DWT to analyse trends in Indian long-term precipitation time series, in which monthly, annual and monsoon precipitation series are decomposed via DWT into approximation coefficient and detailed series using convolution of low pass filter and high pass filter. In order to identify the suitable mother wavelet and decomposed level, to decompose the original series the criteria proposed by Nalley et al. (2012) were used; (d) to apply the SQMK test to the original series and a combination of approximation and detailed series in order to check the trend and periodicity of the series; and (e) to derive a visualization of extreme events and contributing events at different threshold values.

There are three types of precipitation data used in this study: monthly, annual and monsoon data of 156-years period (1851–2006). Monthly data were used to investigate the short-term fluctuations in precipitation, whereas annual data were used to identify the long-term fluctuations, and monsoon data were used to detect the variation in seasonality. Firstly, linear regression was applied on the original series to check the linear changes in precipitation per year for each zone of India. The long-term precipitation series (156 years) was subdivided in to five climatic periods for short-term (30 years) trend analysis, and linear trend analysis was carried out on all five short-term precipitation series. The SQMK test was applied on the original precipitation series to identify temporal changes in precipitation over India.

In the next step, using DWT, the original precipitation series was decomposed into two series: an approximation and a detailed series. The first decomposed series represents the periodic component,

whereas the latter represents the trend of the series. The MATLAB tool box of *Wavelet D-1* was used to decompose the series into wavelet coefficients.

Non-parametric trend detection methods (MK) were applied on the original series and on a combination of the decomposed and approximation series. Additionally, the SQMK test was applied to the original and to a combination of the detailed and approximation components. However, the procedure followed is as follows:

1. Detect linear trend by applying linear regression test on short-term (30-year) and long-term (156-year) precipitation based on monsoon and annual series.
2. Apply the SQMK test to detect temporal variation for the period 1851–2006 based on seasonal and annual precipitation series.
3. Identify the decomposed level of a suitable mother wavelet to decompose the original series using the criteria of mean relative error (MRE) of the approximation series and relative error (RE) of the *Z* value of the MK test (Nalley et al. 2012).
4. Decompose monthly, annual and monsoon precipitation series via DWT into approximation coefficient and detailed series using convolution of low pass filter and high pass filter.
5. To check the trend and periodicity of the series, apply SQMK to the original series and to the combination of approximation and detailed series.
6. Visualize extreme events at different thresholds.

4.3.1 Primary Statistics Analysis

The primary statistical parameters such as mean, standard deviation (SD), skewness (C_S), kurtosis (C_K) and coefficient of variation (C_V) of each zone of India are provided in Table 4.1, which were computed for annual and monsoon precipitation (1851–2006). Average annual precipitation varied between about 773 mm/year (NWI) and 2111 mm/year (NEI), whereas the monsoon season values varied from 686 mm (NWI) to 1507 mm (NEI). The SD in annual series varied between 151 and 227 mm (NCI and NMI, respectively). Skewness parameter represents the measure of asymmetry in a frequency distribution around the centre point; and kurtosis indicates a measure as to whether the data are peaked or flat relative to a normal frequency distribution. Datasets with low kurtosis tend to have a flat top near the mean rather than a sharp peak; its value varies from –0.21 (NEI) to 0.57 (WPI) for average annual rainfall and –0.01 (NEI) to 0.73 (WPI and SPI) for monsoon rainfall. The

C_V represents the ratio of SD to the mean of the data series. The C_V varies between about 8.47 % (NEI) and 17.54% (NWI) for annual values and from 9.28% (NEI) to 20% (NMI) for the monsoon season (Table 4.1).

Table 4.1: Primary statistical parameters value of precipitation series (1851-2006) of Indian Zones

	Annual Precipitation (mm)					Monsoon Precipitation (mm)				
Zones	**Mean**	**SD**	**C_V**	**C_S**	**C_K**	**Mean**	**SD**	**C_V**	**C_S**	**C_K**
NMI	1572.78	227.83	14.49	0.40	0.02	1131.12	225.50	19.94	0.10	0.01
NWI	773.03	135.62	17.54	-0.20	0.30	686.73	128.32	18.69	-0.49	0.02
NCI	1211.49	151.20	12.48	0.03	0.23	1026.68	131.07	12.77	-0.05	0.42
NEI	2155.91	182.64	8.47	-0.38	-0.21	1507.34	139.87	9.28	0.09	-0.01
WPI	1090.64	184.78	16.94	-0.01	0.47	922.59	163.23	17.69	0.07	0.73
EPI	1147.73	155.95	13.59	0.38	0.57	840.68	111.38	13.25	-0.26	0.14
SPI	1525.13	180.02	11.80	-0.07	0.34	906.89	139.43	15.37	0.31	0.73

Note: All the measure in 'mm';SD: Standard Deviation; Cv: Coefficient of Variation (%); Cs: Skewness; Ck; Kurtosis;

4.3.2 Trend Analysis applying Linear Regression

In this study, linear regression was used to detect the trend of long-term precipitation over India. All seven zones were selected for trend analysis with long-term precipitation data (156 years). Trend of precipitation was also carried out on the basis of short time series for annual and monsoon rainfall (June–September).

The World Meteorological Organization (WMO) defines the classical climate period as a 30-year period. For the purpose of short-term trend detection, the 1851–2006 time series was subdivided in to five consecutive classical 30-year periods: C1 (1851–1880), C2 (1881–1910), C3 (1911–1940), C4 (1941–1970), C5 (1971–2006); C5 climate series contains 36 years.

Figures 4.2 and 4.3 show the annual and monsoon precipitation trends of the seven zones of India based on short- and long-term time series. In Figures 4.2 and 4.3, the solid (red) line indicates the short-term trend (30-year period), whereas the dotted (blue) line indicates the long-term trend of the whole 156-year period. On the basis of long-term series of precipitation, zones NMI, NCI and NEI

show a negative trend line, whereas zones NWI, WPI, EPI and SPI indicate a positive trend line for the 156-year precipitation time series.

In past studies, drastic changes were found in climatic parameters in the most recent 30-year climate period (1981-2010) (Gosain et al. 2006; Kahya and Kalaycı 2004; Mirza et al. 1998; Pandey et al. 2016). In this study, negative trend lines were found in the last climatic period (C5) (1971–2006) for zones NMI, NWI, NCI and SPI. However, positive trend lines were found for zones NEI, WPI and EPI for the C5 period based on annual time series (Figure 4.2). Positive linear trends were found over zones NWI, WPI, EPI and SPI, with the other zones (NMI, NCI and NEI) indicating a negative trend for long-term monsoon series (Figure 4.3). For the C5 time period, most of the zones (NMI, NWI, NCI, NEI and SPI) indicate a negative trend line for monsoon series.

4.3.3 Sequential Trend Analysis of Annual and Monsoon Series

In order to examine the trend, the sequential MK test was applied on the annual and monsoon precipitation series. In Figure 4.4, the Z value is shown for annual and monsoon based data (spring, summer, monsoon and autumn) for each zone. Trends were examined at the 0.05 (5%) significance level of a two-tailed test. The standard value of Z at a significance level of 0.05 (5%) is ± 1.96; in Figure 4.4, the straight dotted lines indicate the upper bound (Z = +1.96) and lower bound (Z = –1.96). The SQMK Z values greater than the upper bound indicate a positive trend, whereas Z values beyond the lower bound indicate a negative trend. In Table 4.5 it may be seen that for the monsoon season there is a positive trend in zones NMI (Z = +2.93) and NEI (Z = +1.53), whereas a negative trend was found for zones WPI (Z = –2.23) and SPI (Z = –1.11). For the annual series, zone NMI shows a positive trend (Z = +1.91), whereas in zones EPI (Z = –1.64), SPI (Z = –1.70) and WPI (Z = –2.71), a negative trend was found. The sequential MK test was applied separately to the decomposed series (detail and approximation components) of annual, monsoon and monthly precipitation series.

Trend analysis of annual and monsoon time series shows a similar type of trend for most of the zones. Similarity of trend depend on the contribution of average monsoon rainfall to annual rainfall. For example, for zone SPI, the trend deviation for annual and monsoon series is large because the contribution of average monsoon rainfall is around 59.5% of the average annual rainfall. At the same time, the zone having a higher contribution of average monsoon rainfall with respect to average annual rainfall shows similar trend, for example NWI (88.8%) and NCI (84.7%).

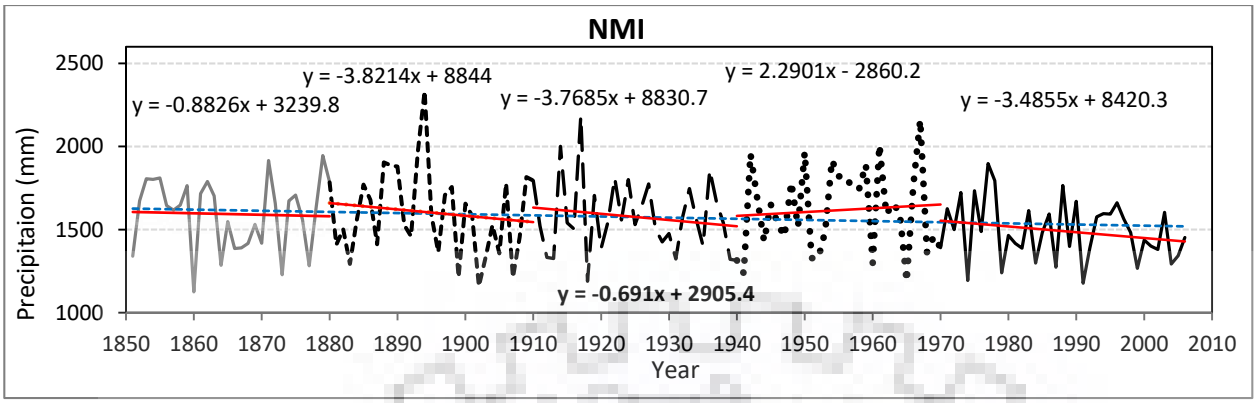
NMI
y = -0.8826x + 3239.8
y = -3.8214x + 8844
y = -3.7685x + 8830.7
y = 2.2901x - 2860.2
y = -3.4855x + 8420.3
y = -0.691x + 2905.4
Precipitaion (mm)
Year

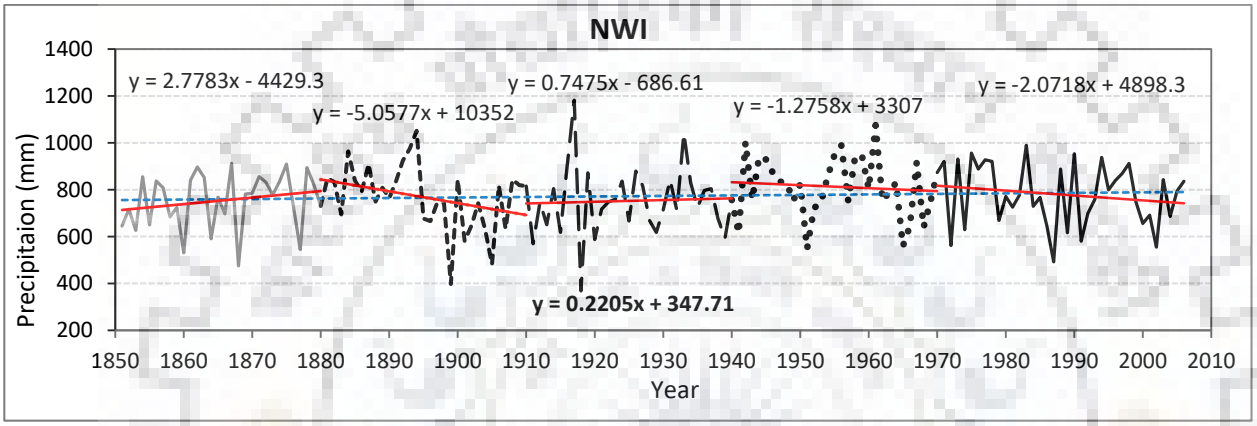
NWI
y = 2.7783x - 4429.3
y = -5.0577x + 10352
y = 0.7475x - 686.61
y = -1.2758x + 3307
y = -2.0718x + 4898.3
y = 0.2205x + 347.71
Precipitaion (mm)
Year

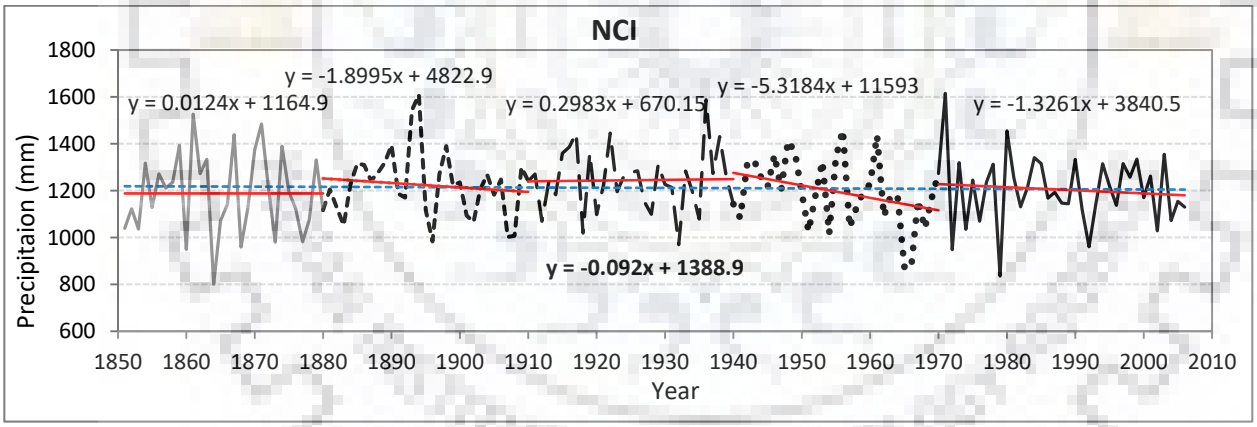
NCI
y = 0.0124x + 1164.9
y = -1.8995x + 4822.9
y = 0.2983x + 670.15
y = -5.3184x + 11593
y = -1.3261x + 3840.5
y = -0.092x + 1388.9
Precipitaion (mm)
Year

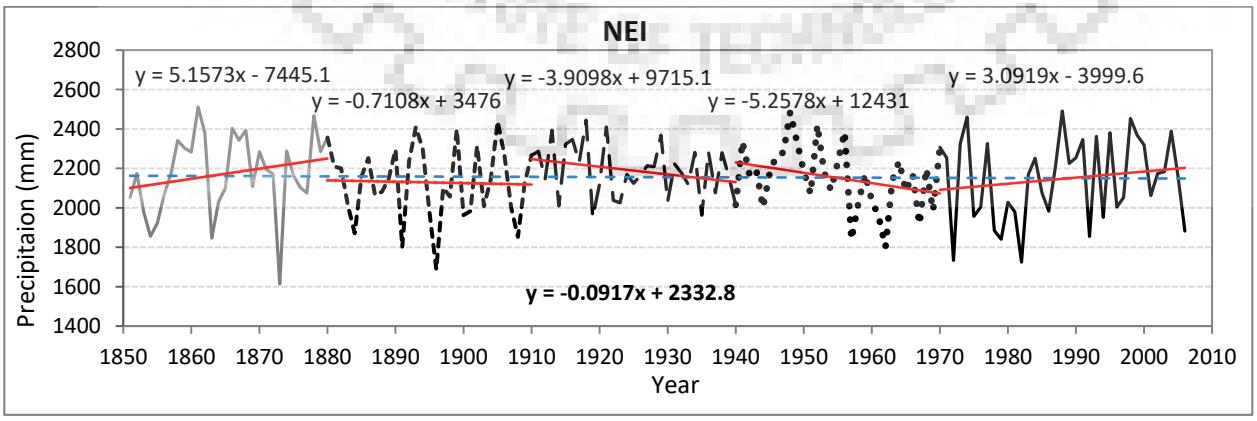
NEI
y = 5.1573x - 7445.1
y = -0.7108x + 3476
y = -3.9098x + 9715.1
y = -5.2578x + 12431
y = 3.0919x - 3999.6
y = -0.0917x + 2332.8
Precipitaion (mm)
Year

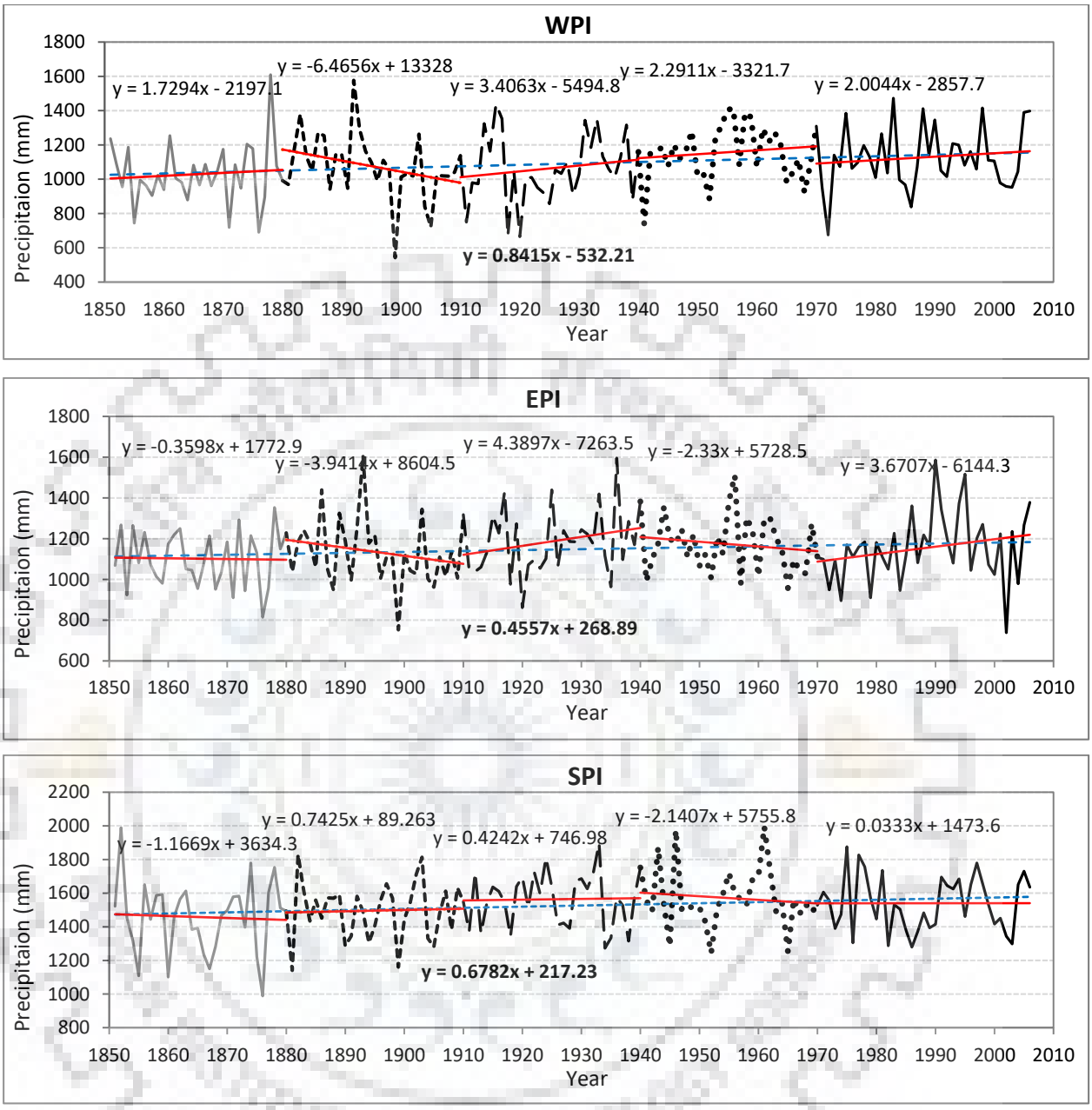

Figure 4.2: Long term and short term linear trend based on annual precipitation series of each zones (red line indicate the short term trend of 30 years period whereas blue dotted line indicate the long term trend of whole period)

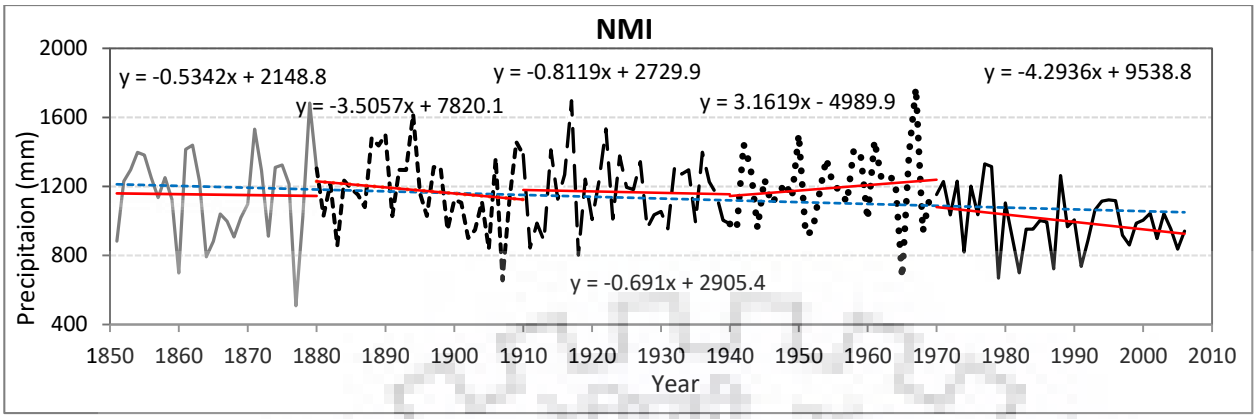
NMI
y = -0.5342x + 2148.8
y = -3.5057x + 7820.1
y = -0.8119x + 2729.9
y = 3.1619x - 4989.9
y = -4.2936x + 9538.8
y = -0.691x + 2905.4
Precipitaion (mm)
Year

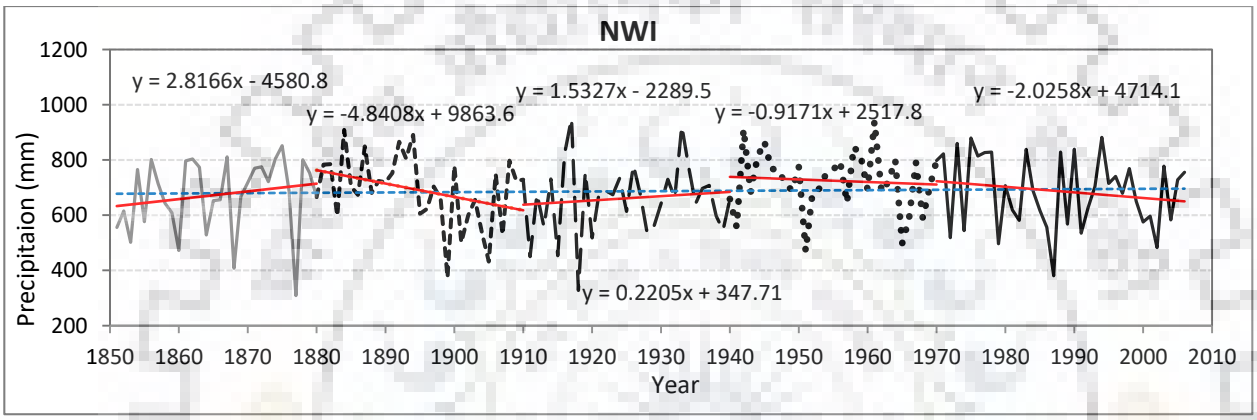
NWI
y = 2.8166x - 4580.8
y = -4.8408x + 9863.6
y = 1.5327x - 2289.5
y = -0.9171x + 2517.8
y = -2.0258x + 4714.1
y = 0.2205x + 347.71
Precipitaion (mm)
Year

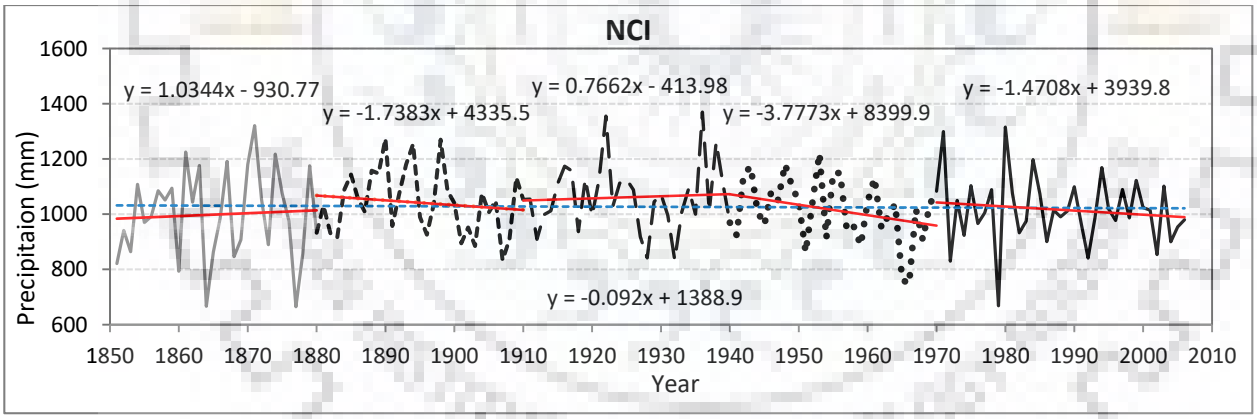
NCI
y = 1.0344x - 930.77
y = -1.7383x + 4335.5
y = 0.7662x - 413.98
y = -3.7773x + 8399.9
y = -1.4708x + 3939.8
y = -0.092x + 1388.9
Precipitaion (mm)
Year

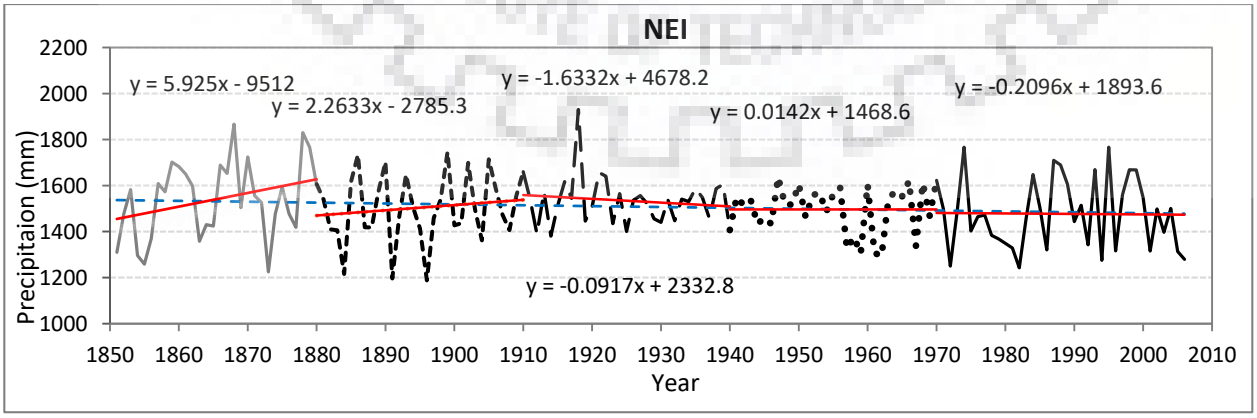
NEI
y = 5.925x - 9512
y = 2.2633x - 2785.3
y = -1.6332x + 4678.2
y = 0.0142x + 1468.6
y = -0.2096x + 1893.6
y = -0.0917x + 2332.8
Precipitaion (mm)
Year

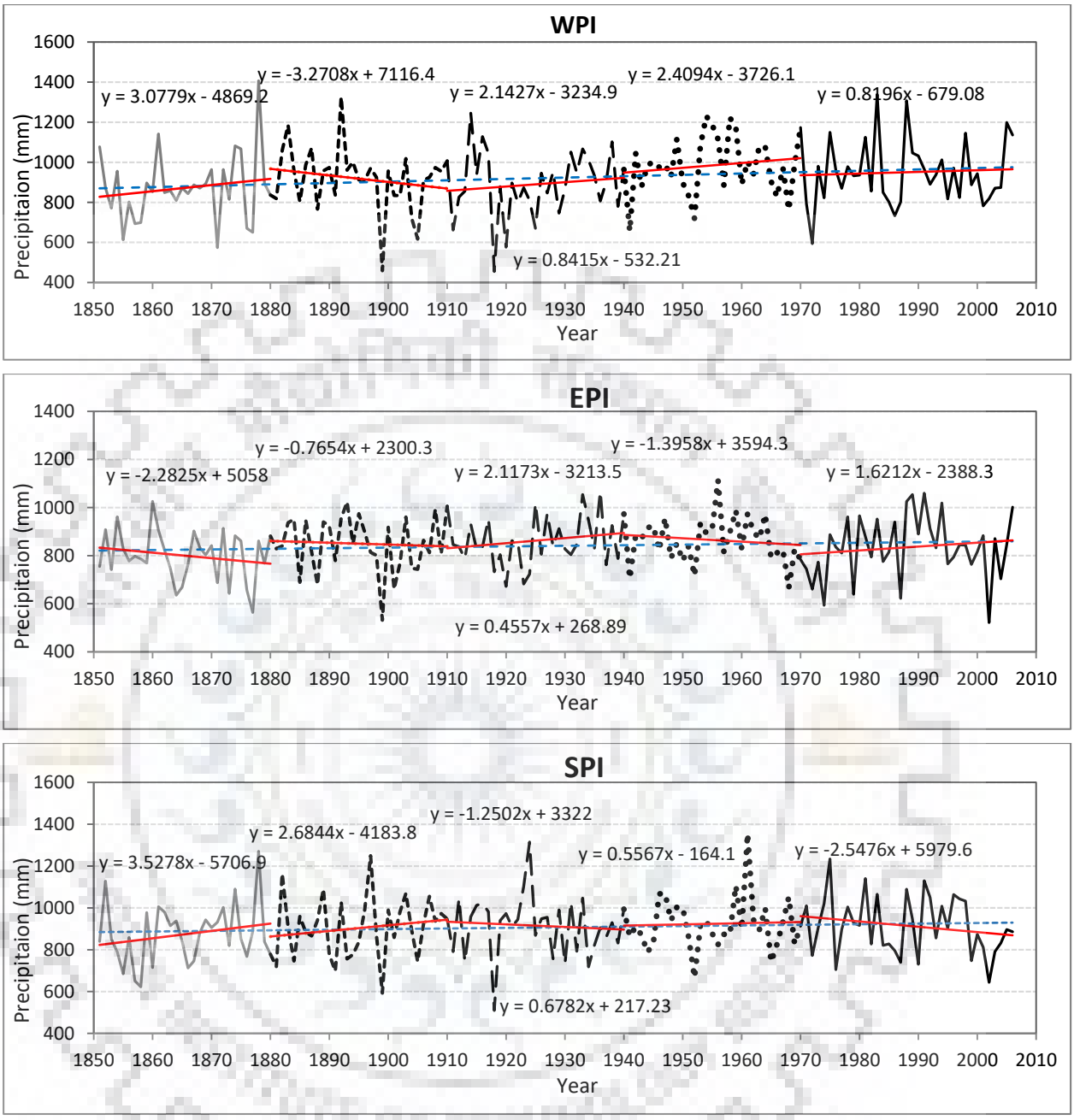

Figure 4.3: Long term and short term linear trend based on monsoon precipitation series of each zones (red line indicate the short term trend of 30 years period whereas blue dotted line indicate the long term trend of whole period)

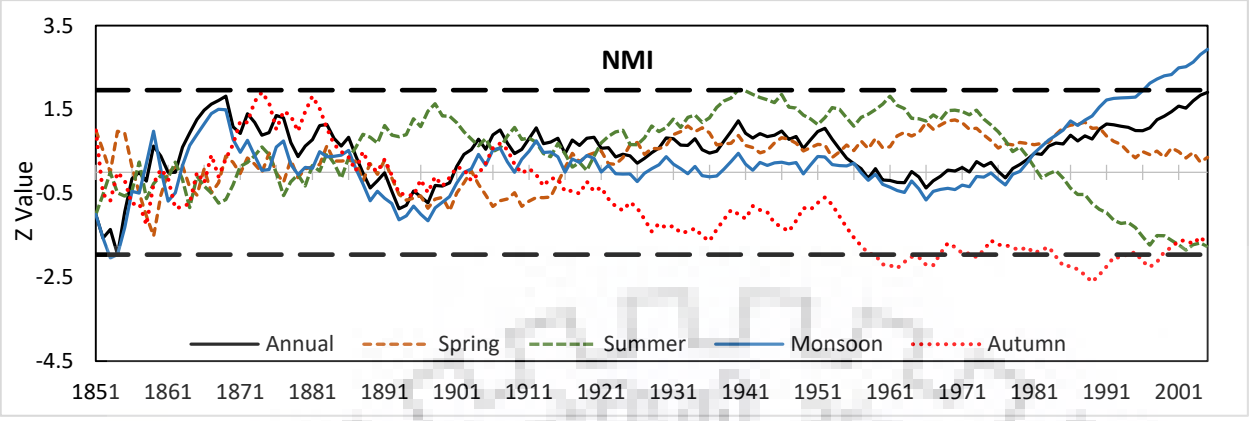
NMI
Z Value
3.5
1.5
-0.5
-2.5
-4.5
Annual
Spring
Summer
Monsoon
Autumn
1851
1861
1871
1881
1891
1901
1911
1921
1931
1941
1951
1961
1971
1981
1991
2001

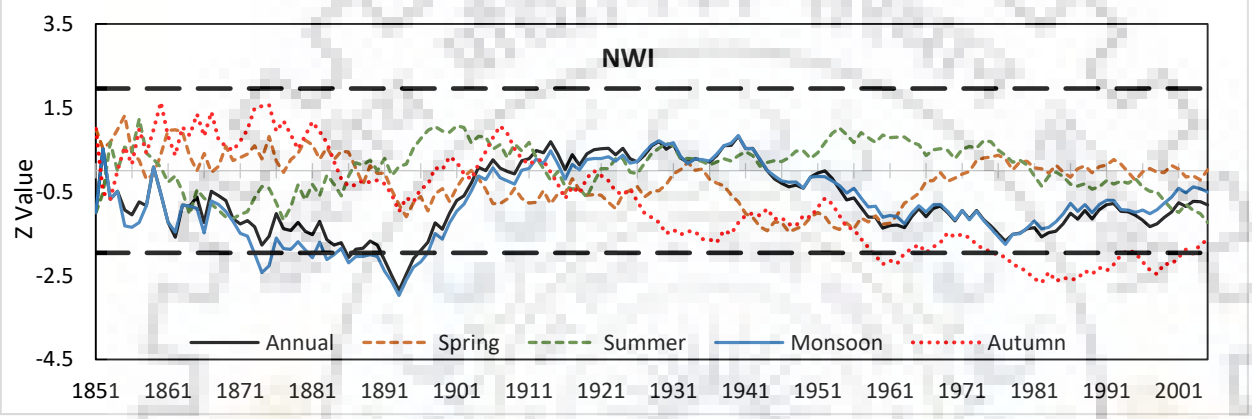
NWI
Z Value
3.5
1.5
-0.5
-2.5
-4.5
Annual
Spring
Summer
Monsoon
Autumn
1851
1861
1871
1881
1891
1901
1911
1921
1931
1941
1951
1961
1971
1981
1991
2001

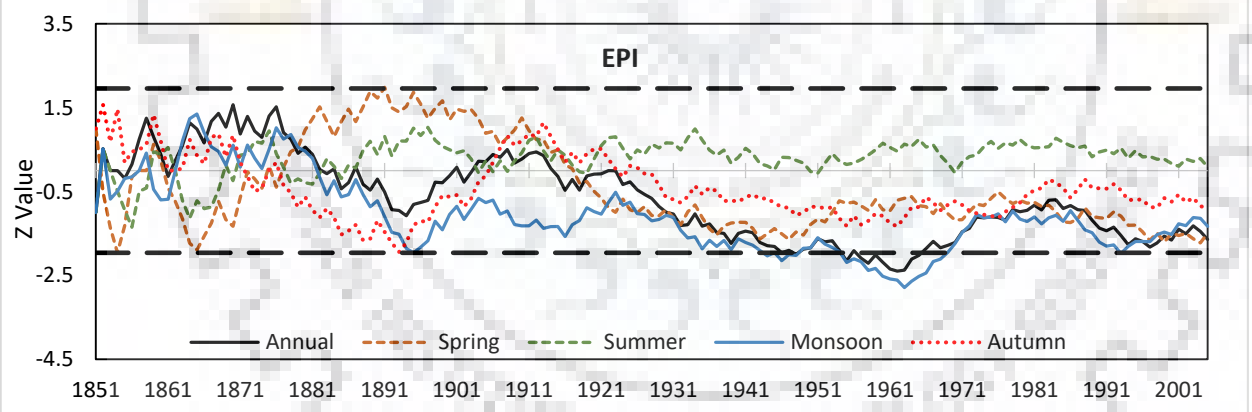
EPI
Z Value
3.5
1.5
-0.5
-2.5
-4.5
Annual
Spring
Summer
Monsoon
Autumn
1851
1861
1871
1881
1891
1901
1911
1921
1931
1941
1951
1961
1971
1981
1991
2001

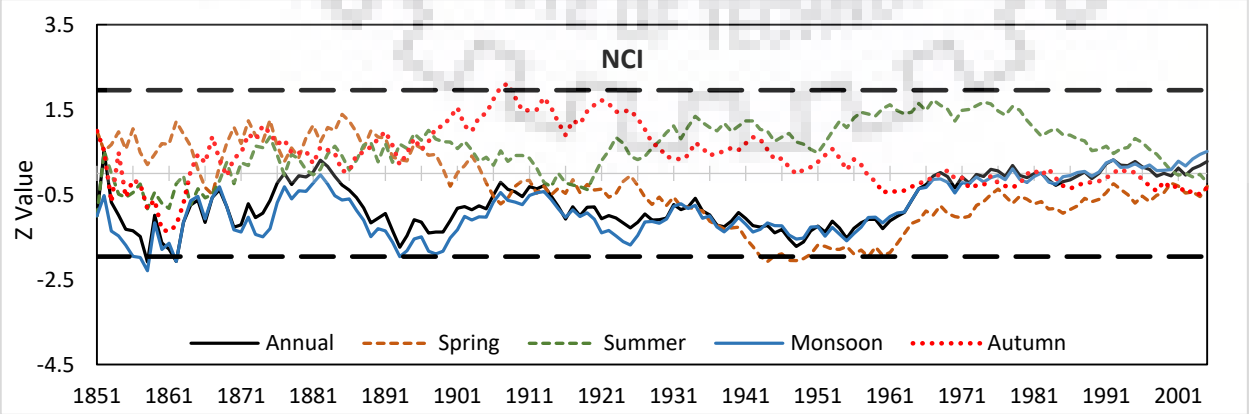
NCI
Z Value
3.5
1.5
-0.5
-2.5
-4.5
Annual
Spring
Summer
Monsoon
Autumn
1851
1861
1871
1881
1891
1901
1911
1921
1931
1941
1951
1961
1971
1981
1991
2001

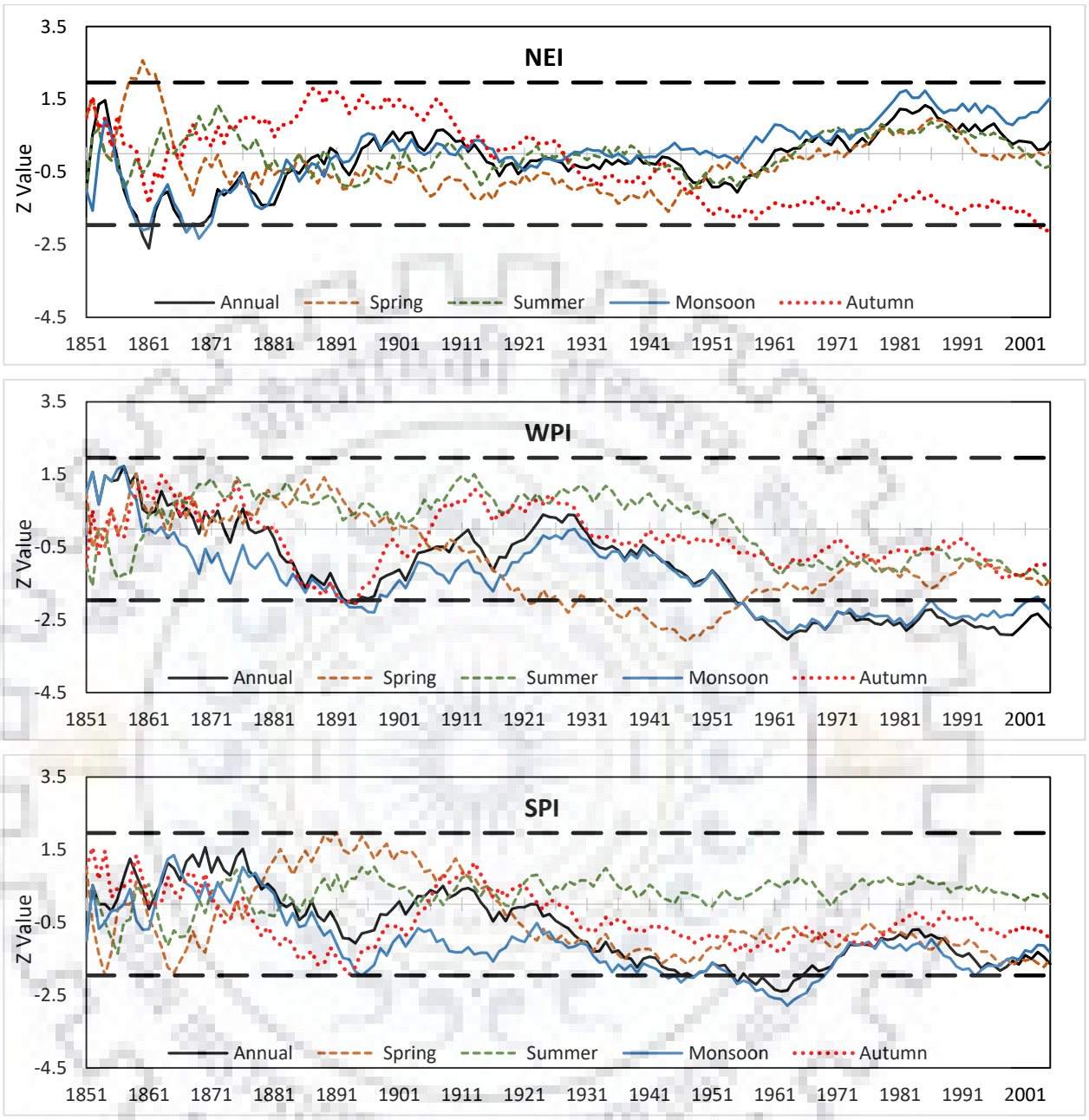

Figure 4.4: Annual and monsoon Sequential MK test (Z value) plot for each zone

4.3.4 Trend analysis using Discrete Wavelet Transform (DWT)

In this study, the Daubechies (db) wavelet was used because it is the most common smooth mother wavelet for hydro meteorological study. The relatively large number of data points used in this study were from the monthly, annual and seasonal datasets. Analysis was carried out for the period 1851–2006, on annual and average monsoon data points of 156 years; there were 1872 (12 × 156) data points for the monthly sets. First, the decomposition level was determined to avoid unnecessary levels of data decomposition of these larger datasets. This level of decomposition is based upon the number of data points and the mother wavelet used Artigas et al. (2006):

$$L = \log_2[n/(2v-1)] \quad \text{..... (4.21)}$$

Where, v is the number of vanishing moments of a db wavelet, n is the number of data points, and L is the maximum decomposition level. The maximum level of decomposition is shown in Table 4.2 for monthly, annual and seasonal datasets.

Table 4. 2: Maximum level of decomposition level proposed for monthly and yearly series (1851–2006)

Series	**Mother wavelet**					
	db5	**db6**	**db7**	**db8**	**db9**	**db10**
Monthly	7	7	7	6	6	6
Yearly	4	3	3	3	3	3
Seasonal	4	3	3	3	3	3

In order to analyse the trend detection, smoother db wavelets (db5–db10) were applied on the monthly and annual datasets. The selection of smoother wavelets was preferred in this study because the trends are supposed to be gradual and represent slowly-changing processes.

The criterion used to determine the smooth mother wavelet and the extension mode of db wavelets for the analysis was the mean relative error (MRE) (de Artigas et al. 2006; Joshi et al. 2016; Nalley et al. 2012). The mean relative error (MRE) was calculated by:

$$\text{MRE} = \frac{1}{n}\sum_{j=1}^{n}\frac{|a_j - x_j|}{|x_j|} \quad \text{..... (4.22)}$$

Where, x_j is the original data value, and a_j is the approximation of x_j. In the results, it was found that there were no significant differences in value of MRE. The second criterion is the relative error (E_r), proposed by (Nalley et al. 2012; Nalley et al. 2013). The lowest value of E_r, based on

approximation of the MK test *Z* value, was examined for each extension mode of the smooth db wavelets. The relative error is calculated by:

$$E_r = \frac{|Z_a - Z_o|}{|Z_o|} \tag{4.23}$$

Where, Z_a is the *Z* value (MK test) of the last approximation for the decomposed level used, and Z_o is the MK test *Z* value of the original data. The results of MRE and E_r calculations are given in Table 4.3 and Table 4.4 for monthly and annual values, respectively. In the results, it was found that the db10 wavelet showed the lowest value of MRE and E_r for monthly datasets, whereas the db6 wavelets was found more suitable for annual data.

Table 4.3: Mean Relative Error (MRE) and Relative Error (Er) at different decomposition level for AI monthly series (1851-2006)

Wavelet	**db5**	**db6**	**db7**	**db8**	**db9**	**db10**
L	7	7	7	6	6	6
MRE	4.1264	4.1394	4.1401	4.1379	4.1323	**4.1336**
Er	14.942	14.392	11.811	11.935	13.358	**10.262**

Table 4.4: Mean Relative Error (MRE) and Relative Error (Er) at different decomposition level for AI annual series (1851-2006)

Wavelet	**db5**	**db6**	**db7**	**db8**	**db9**	**db10**
L	4	3	3	3	3	3
MRE	0.1138	**0.1095**	0.1101	0.1097	0.1094	0.1100
Er	2.154	**1.525**	1.727	1.584	1.777	1.605

Figures 4.5 and 4.6 show the decomposed level for annual and monthly time series using the DWT method. It can be seen in Figures 4.5 and 4.6 that more detailed decomposed levels have lower frequencies, which shows the change in periodicity. The approximation components (a3 and a6) show the long-term change in trend.

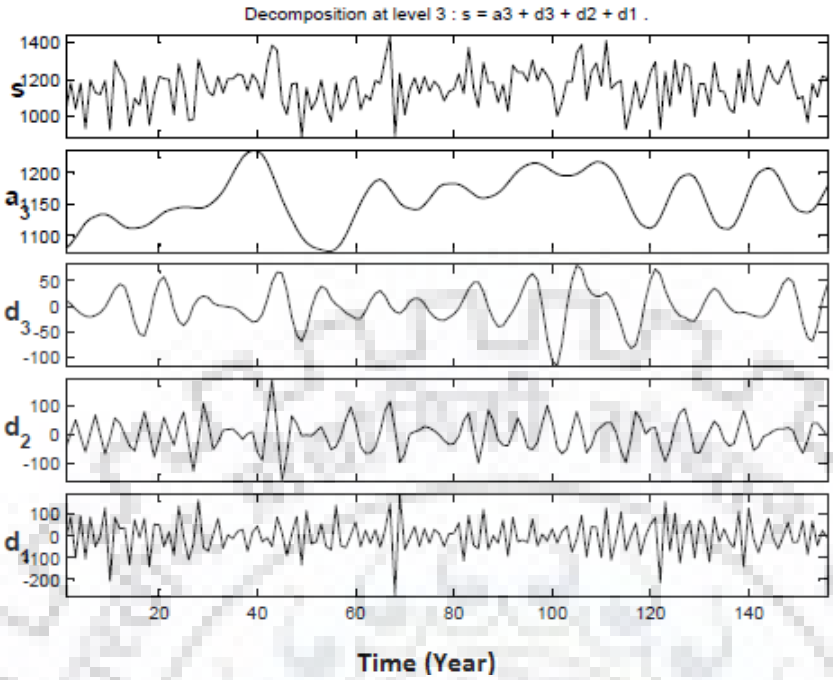

Figure 4.5: Decomposition of original annual precipitation series of AI in to 3 levels (d1-d3) and approximation (a3)

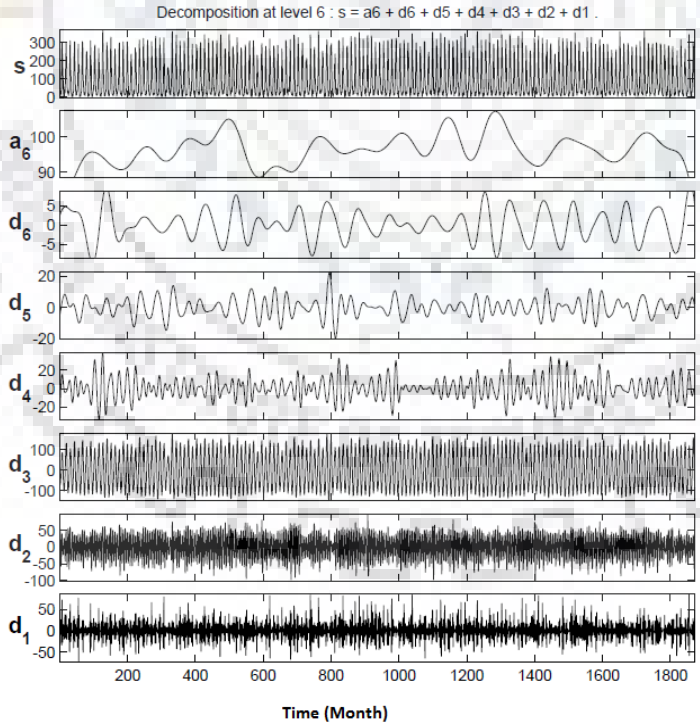

Figure 4.6: Decomposition of original monthly precipitation series of AI in to 6 levels (d1-d6) and approximation (a6)

4.3.5 Trend Analysis of Decomposed Annual, Monsoon and Monthly Series

Each annual and seasonal time series was decomposed into three detailed components (d1–d3) and one approximation (a3), and the monthly series was decomposed into six components (d1–d6) and one approximation (a6). Each detailed component represents the 2^n (dyadic translation) fluctuations, where *n* is the level of detailed components. For annual and monsoon detailed series d1, d2 and d3 represent the 2-year, 4-year and 8-year periodicity, respectively. The approximate component of the wavelet transform represents the high-scale function of the time series. Moreover, it is the low frequency component of the time series and is used to find the key points of the time series to loose minimum potential information (He et al. 2016). For this study, a3 is found as the end point for deriving the optimal (maximum/ minimum) local points of precipitation time series of India. Therefore, for monthly series, detailed components d1, d2, d3, d4, d5 and d6 represent the 2-, 4-, 8-, 16-, 32- and 64-month periodicity, respectively.

A comparison was carried out between the original series and the combination of decomposed series. The values of evaluation parameters, coefficient of determination (R^2) and Nash-Sutcliffe efficiency coefficient (NS), are given in Table 4.5. Table 4.5 indicates that only a few zones showed a significant trend, for example WPI for annual rainfall, and NMI for both annual and monsoon season rainfall. Zone WPI indicates a negative trend for annual and monsoon season, whereas a positive trend was detected for the NMI monsoon season. It was interesting to see the significant trend in decomposed components, where the original series did not show a significant trend, e.g. NMI, NEI (monsoon), EPI and SPI zones (Table 4.5). In general, combinations of detailed and approximation series indicated an increase in MK test *Z* value as compared to single detailed series (without approximation series) and original series. The results shown in Table 4.5 imply that the combination of detailed and approximation series mainly contributed to trend in the original series. However, all the decomposed components of periodicity did not have much influence on trend of the original series.

While analysing the *Z* value of the individual detailed series and the combination of detailed and approximation series, it was noticed that individual detailed series did not show the closeness to the original series (excluding zone NCI for the d1 series) although all zones were examined for significant trend, which was found in WPI and NMI (monsoon). However, in all the cases, the

combination of d1+a3 showed the nearest *Z* value to the original series (annual and monsoon precipitation time series).

Hence, it is clear that the approximation component carries the trend components and affects the trend in the original series, which is similar to the results mentioned by Nalley et al. (2012), in analysing the Quebec and Ontario (Canada) region. For example, for the NMI zone ($Z = +1.91$) the detailed series (d1) *Z* value is 0.20, whereas for the combination series (d1+a3) it is 2.68, which also shows a significant trend. Nalley et al. (2012) proposed a two-step method to identify the most effective periodic components in contributing to trend in the original series. In the first step, the SQMK approach is applied to check the progressive trend line of each individual detailed series and combinations of detailed and approximation series with respect to original time series. Thus, the detailed series, or combination of detailed and approximation series could be identified that follow the same trend as the original data. In the second step, the MK test *Z* value of the detailed series and combinations of detailed and approximation series are compared with the *Z* value of the original time series, and the closet values identified. The component(s) that satisfy these two tests are considered as the most dominant components that affect the trend.

In this study, the combination of detailed components and combinations with approximations were evaluated to identify the most influential component of the trend (Nalley et al. 2012). While analysing the *Z* value of the different combinations, it was noticed that combination of two or more detailed components with the approximation component significantly increased the *Z* value of the series. However, these combinations do not play any crucial role in the decision making, as *Z* value is far away from the *Z* value of the original series, and at the same time the SQMK graph does not match. Hence, we considered a combination of single detailed components with approximation series for comparison of *Z* values and SQMK graph (Figures 4.7–4.9, Tables 4.5–4.6).

In this study, the most periodic component was identified as d1 that contributed a 2-year periodicity trend (with addition to the approximation series) for annual and monsoon series over the study area (Table 4.5, Figures 4.7 and 4.8). This indicates that d2 (4-year periodicity) and d3 (8-year periodicity) did not contribute much in the trend of the annual and monsoon season rainfall in the study area.

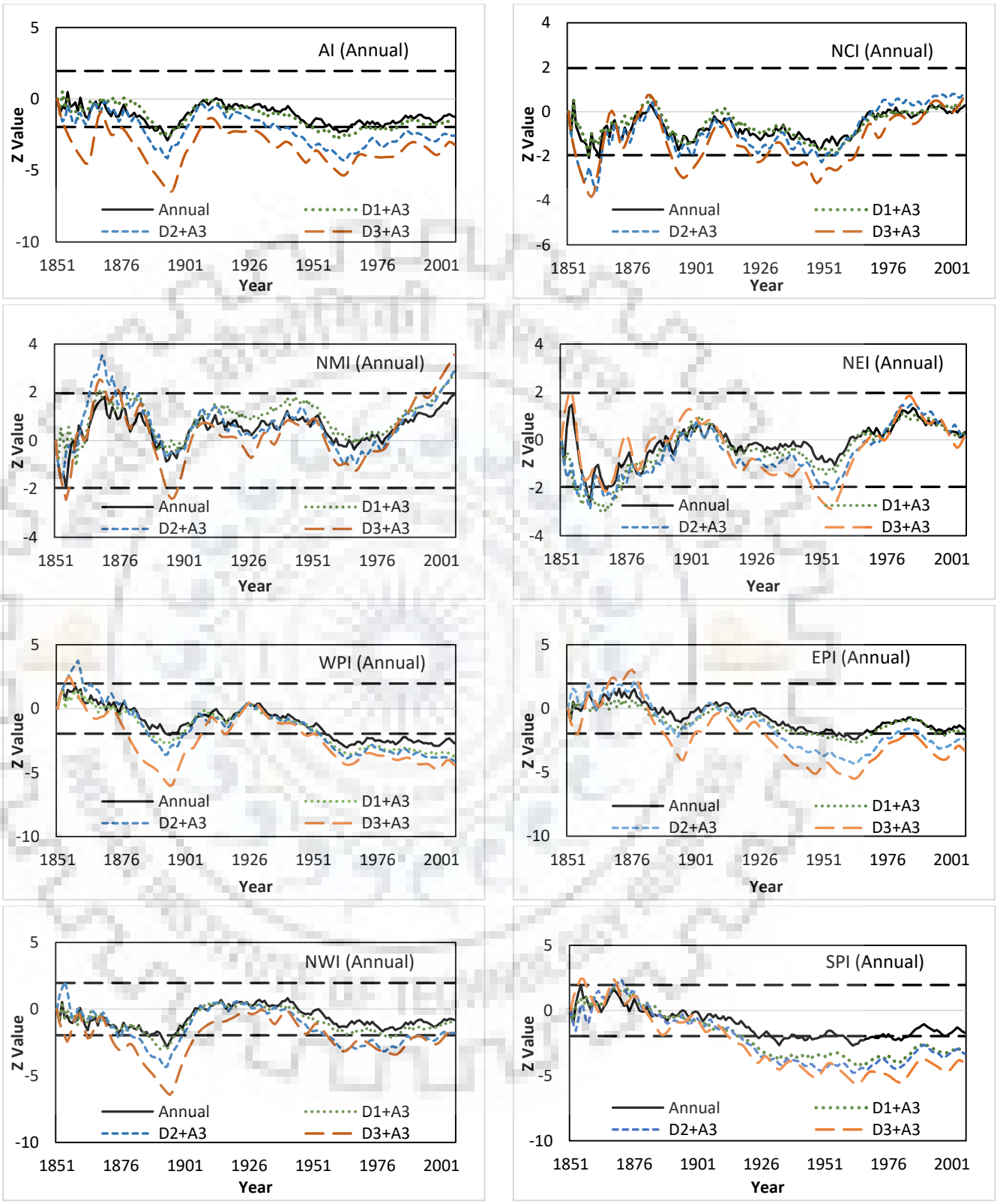

Figure 4.7: Changes in trend along the time for annual original series and combination of detail and approximation series

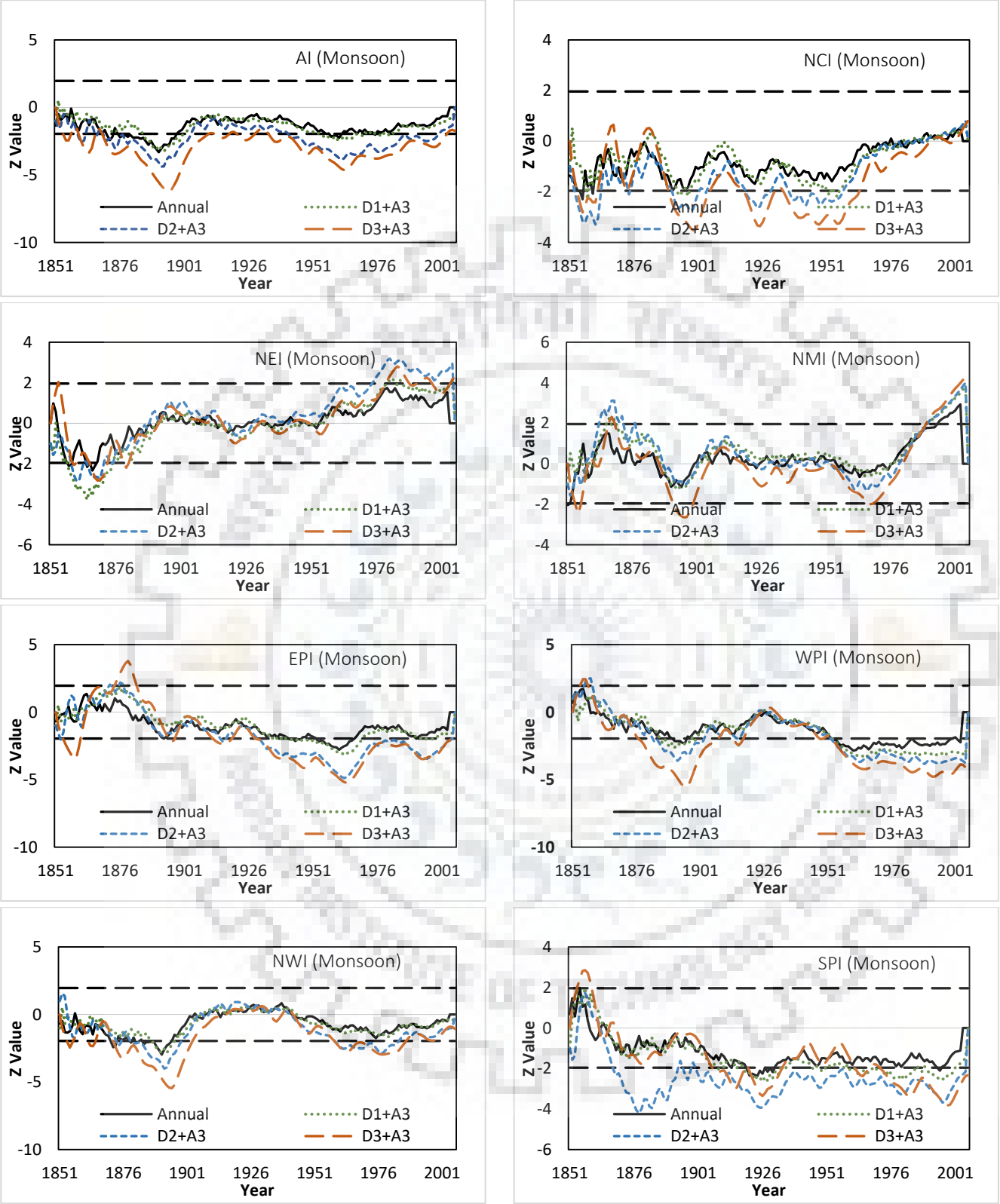

Figure 4.8: Changes in trend along the time for monsoon original series and combination of detail and approximation series

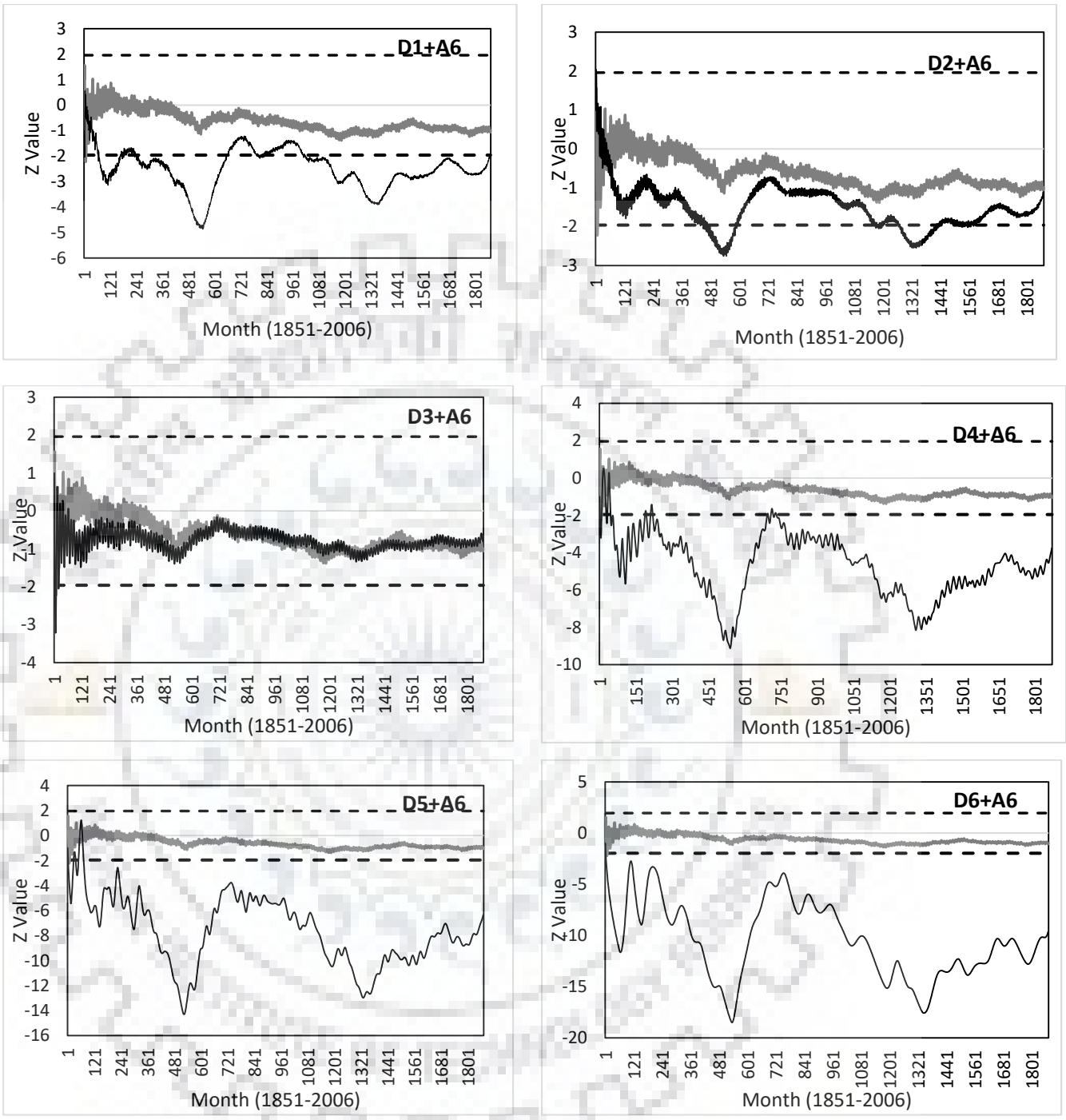

Figure 4.9: Changes in trend along the time for monthly series and combination of detailed and approximation series

Table 4.5: MK test (Z value) for original precipitation series (O) and combination of detailed and approximation series with coefficient of determination (R^2) and Nash Sutcliffe (NS) value

Region		Annual							Monsoon						
		O	**D1**	**D2**	**D3**	**D1+A3**	**D2+A3**	**D3+A3**	**O**	**D1**	**D2**	**D3**	**D1+A3**	**D2+A3**	**D3+A3**
NMI	**R^2**		0.00	0.10	0.00	0.02	0.12	0.17		0.00	0.10	0.00	0.59	0.54	0.54
	NS		-48.11	-48.38	-47.79	-0.82	0.03	0.16		-48.42	-48.45	-47.74	0.59	0.54	0.28
	Z	1.91	0.20	0.03	-0.10	**2.68***	2.88*	3.57*	2.94*	0.01	-0.20	-0.04	**3.80***	4.00*	4.50*
NWI	**R^2**		0.30	0.05	0.10	0.67	0.34	0.26		0.30	0.04	0.07	0.69	0.36	0.36
	NS		-33.83	-32.51	-32.41	0.67	0.34	0.26		-32.01	-32.53	-32.41	0.69	0.36	0.24
	Z	-0.82	0.21	-0.14	0.04	**-1.03**	-1.79	-1.83	-0.51	0.24	0.00	-0.05	**-0.49**	-1.01	-1.06
NCI	**R^2**		0.19	0.03	0.08	0.65	0.37	0.21		0.19	0.03	0.05	0.62	0.45	0.45
	NS		-65.54	-64.46	-64.36	0.65	0.37	0.21		-63.94	-64.44	-64.36	0.62	0.45	0.24
	Z	0.28	**0.20**	0.12	-0.65	**0.37**	0.86	0.74	0.52	0.11	0.10	-0.29	**0.63**	0.81	0.81
NEI	**R^2**		0.09	0.02	0.07	0.62	0.38	0.25		0.03	0.02	0.04	0.60	0.34	0.34
	NS		-142.54	-141.58	-141.77	0.62	0.38	0.25		-141.31	-141.49	-141.77	0.60	0.34	0.31
	Z	0.33	-0.02	-0.66	-0.19	**0.40**	0.17	0.20	1.53	0.02	-0.43	0.15	**2.08***	2.94*	2.36*
WPI	**R^2**		0.19	0.07	0.07	0.65	0.45	0.33		0.17	0.06	0.05	0.65	0.42	0.42
	NS		-36.37	-35.34	-35.33	0.65	0.45	0.33		-34.96	-35.33	-35.35	0.65	0.42	0.28
	Z	-2.71*	-0.19	0.19	0.12	**-3.73***	-4.09*	-4.41*	-2.23*	-0.09	0.13	0.06	**-3.17***	-3.76*	-4.29*
EPI	**R^2**		0.27	0.03	0.07	0.74	0.35	0.26		0.16	0.00	0.03	0.74	0.34	0.34
	NS		-56.08	-54.89	-54.71	0.74	0.35	0.26		-54.48	-54.86	-54.77	0.74	0.34	0.32
	Z	-1.64	-0.07	0.17	0.00	**-1.87**	-2.41*	-3.29*	-1.33	-0.22	0.17	-0.04	**-1.58**	-1.96*	-2.42*
SPI	**R^2**		0.16	0.09	0.06	0.64	0.38	0.31		0.07	0.04	0.02	0.69	0.32	0.32
	NS		-72.83	-71.74	-71.96	0.64	0.38	0.31		-71.63	-71.83	-71.94	0.69	0.32	0.23
	Z	-1.70	-0.13	-0.31	0.03	**-2.98***	-3.32*	-4.07*	-1.11	-0.55	-0.23	0.05	**-1.50**	-2.17*	-2.32*

*(*indicate the trend at 5% significance level, bold format indicate the most effective periodic components)*

Table 4.6: MK test (Z value) for monthly series, detailed components (D1-D6), approximation (A3) and combination of detailed and approximation

Monthly Series (1851-2006)							
	NCI	**NWI**	**EPI**	**NMI**	**SPI**	**WPI**	**NEI**
Original	-0.70	-1.22	-0.77	-0.86	-1.37	-1.35	0.00
D1	0.30	-0.28	-0.04	0.33	-0.16	0.11	-0.12
D2	0.13	0.09	0.01	0.46	0.05	0.12	**-0.02**
D3	**-0.22**	-0.03	0.01	-0.42	-0.11	0.10	-0.16
D4	0.04	0.34	0.49	0.42	0.11	0.21	0.28
D5	0.07	0.13	0.35	**-0.52**	0.42	0.23	-0.17
D6	-0.16	-0.21	0.39	0.70	1.20	0.36	-0.55
A6	3.65*	-5.27*	-11.72*	12.50*	-20.85*	-16.73*	2.32*
D1+A6	0.88	**-1.40**	-2.56*	2.68*	-3.40*	-3.72*	0.95
D2+A6	0.44	-0.59	-2.34*	1.76	-2.71*	-2.77*	0.61
D3+A6	0.03	-0.50	**-0.94**	0.70	**-1.65**	**-1.39**	**0.12**
D4+A6	1.11	-2.62*	-5.53*	5.96*	-7.33*	-7.70*	2.02*
D5+A6	0.90	-2.93*	-7.75*	7.52*	-9.98*	-12.12*	0.94
D6+A6	2.75*	-5.00*	-9.52*	10.41*	-11.75*	-14.42*	0.64

**values indicate the trend at 5% significance level, bold format indicate the most effective periodic component*

Zone-wise MK test *Z* values for monthly series from 1850 to 2006 (1872 data points) for the study area can be seen from Table 4.6. There was no significant trend in the study area for the original monthly time series. In general, the most dominating periodicity was d3 (with approximation series), except in zones NWI (d1) and NEI (d2). Hence, the 8- month periodicity was the most influencing parameter for estimating rainfall trends in the study area (Figure 4.9). The results also emphasize the usefulness of monthly trend analysis along with decomposed components using wavelet techniques as in the present study. Monthly analysis seems important because the periodicity was found less than the annual data.

4.3.6 Visualization and Thresholding of Precipitation Extreme Events

In order to analyse the contributing events for extreme events the method of wavelet analysis is very valuable to decompose the original time series into different frequencies, retaining information in the time domain (Chou 2011; Labat 2005; Nalley et al. 2013). Figure 4.10 presents an example of normalized annual precipitation time series of zone WPI; in the bottom panel the horizontal (blue, red and green) lines represent the three selected thresholds for both positive and negative positions. These thresholds were selected based on the standard deviation ('S' in Figures 4.10 and 4.11) of the original precipitation series. Figure 4.10 clearly shows that the number of exceedance events decreases as the threshold increases. Figure 4.11 shows a visualization of the extreme value of monsoon precipitation at fixed threshold values over the WPI zone. In Figures 4.10 and 4.11, black represents non-exceedance properties of the series. The approach adopted in the present study is inspired by the work of Keylock (2007), but applies to time series of precipitation data. The method could be generalized to gain frequency information from the precipitation time series. An inspection of Figure 4.10 shows that the exceedance of 1.5S at t = 20 (negative fluctuation) is a different type of event to that at t = 65 (positive fluctuation). The different shades indicate the different frequency fluctuations. Keylock (2007) stated that "*the former arises due to relatively small high frequency fluctuations superimposed on a large, low frequency positive departure from the mean. The latter is a sudden and dramatic excursion from the mean that is not superimposed on an obvious larger scale fluctuation*". Therefore, it helps to visualize this information in a clear manner so that the scales of events that actively contribute to an extreme event can be determined.

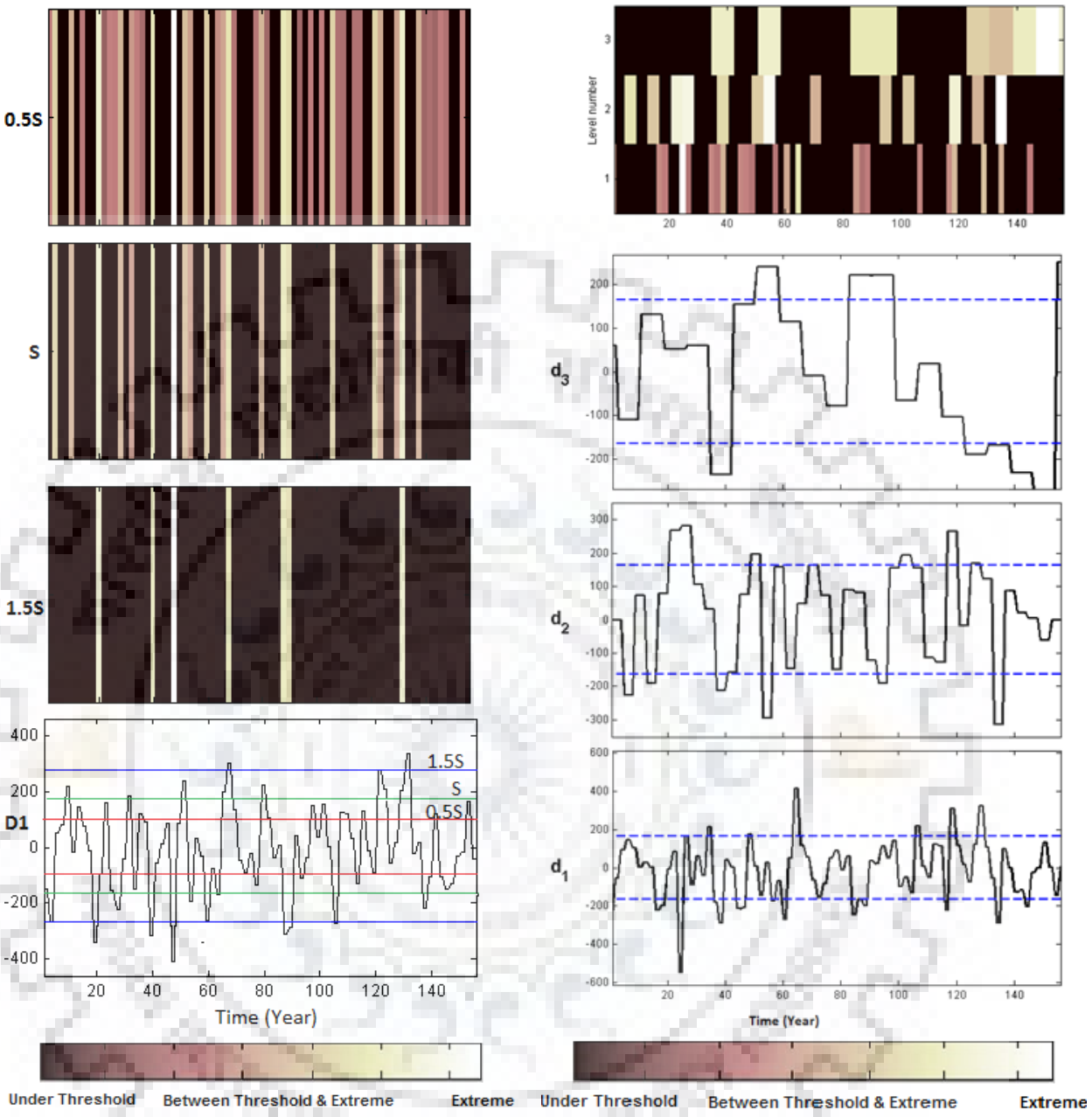

Figure 4.10: Visualization of detailed component (D1) extreme value of annual precipitation at different threshold values of standard deviation (S) over WPI zone of India (red line, green line and blue line indicated the threshold value at 0.5,1.0 and 1.5 times of standard deviation of the observed series respectively)

Figure 4.11: Visualization of extreme value of monsoon precipitation at fixed threshold values over WPI zone of India, where blue lines in D1, D2 and D3 indicate the threshold values (standard deviation of the original series)

4.4 LOCAL SCALE STUDY: UPPER NARMADA BASIN

In the present study, 16 stations of Upper Narmada river Basin (UNB), a humid subtropical region of India considered as a local study area. Spatial and temporal variation in meteorological data (precipitation, mean temperature and reference evapotranspiration) at UNB stations were analysed based on monthly seasonal and annual series of 102 years (1901-2002).

4.4.1 Assessment of Mean Annual Precipitation and Temperature

In recent years, there are many trend studies of hydro-meteorological data over the basin, but there are very limited studies based on trend of extreme values. Therefore, a detailed trend analysis was carried out of annual extreme events of precipitation and temperature series applying Innovative Trend Analysis (ITA) for sustainable water management development in terms of climate change. Moreover, Discrete Wavelet Transform (DWT), a relatively new tool in hydro-climatology was applied to identify and visualization of extreme events. Also the, Sequential Mann-Kendall (SQMK) and cumulative sum charts (CUMSUM) were used to determine the year when significance variation occurred in precipitation and temperature at 16 stations of Upper Narmada river basin. In general, goal of this section are (1) trend analysis using based on monthly, seasonal and annual time series, (2) trend in annual extreme values (low, medium and high) applying ITA, (3) comparison of ITA against nonparametric tests (Mann-Kendall and Sen's Slope estimator), (4) visualization of extreme events applying DWT, (5) to quantitavely detect the shift year of precipitation and temperature using SQMK.

4.4.1.1 Spatial-temporal variation

Temporal-spatial variations of meteorological series shown in Figure 4.12 (a-b) by box-whisker plot. The primary statistical parameters such as mean, standard deviation (SD), coefficient of variation (C_V), skewness (C_S), and kurtosis (C_K) for 16 stations of Upper Narmada river basin were computed for annual precipitation and annual mean temperature series of 102 years (1901-2002) (Table 4.7). Figure 4.12 (a) indicates the variation of the annual precipitation through box-whisker plot of the 16 districts of UNB. Figure 4.12(a) indicates the similar precipitation variability at 25^{th}, 50^{th} and 75^{th} percentile for northern stations (Jabalpur, Katni, Kawardha, Damoh, Seoni and Umaria). The mean annual precipitation is decreasing from south-east districts (Balaghat, Dindori, and Mandla) to north-west districts (Hoshangabad, Narsimhpur, Raisen and Chhidwara). Station Bilaspur in Figure 4.12(a) indicates the substantially lowest precipitation variation as compared to other stations

because of rain shadow region (leeward side) of mountain Satpura range. It can be observed from Figure 4.12(a) that outliers appear at the upper side in most of the stations. Table 4.7 shows the mean annual precipitation varied from 736 mm (Bilaspur) to 1417 mm (Mandla). Therefore standard deviation varied from 176.78 mm to 299.81 mm for Bilaspur and Raisen respectively. The skewness parameter represents the measure of asymmetry in a frequency distribution around the centre point. Kurtosis indicates the measure, whether the data are peaked or flat relative to a normal frequency distribution. Data sets with low kurtosis tend to have a flat top near the mean rather than a sharp peak, it varies from -0.07 (Shahdol) to 0.63 (Raisen) mean annual precipitation. The coefficient of variation (C_V) represent the ratio of standard deviation to mean of the data series. The C_V varies between about 15 % (Dindori) to 25% (Raisen) station for annual precipitation (Table 4.7). Figure 4.12 (b) indicates the variation of the annual mean temperature through box-whisker plot of the 16 districts of UNB. Mean temperature over the study area is about 25.21±0.40^oC (mean ± standard deviation). Most of the western stations (Chhidwara, Damoh, Kawardha, Hoshangabad, Raisen) indicate the similar variability at 25th, 50th and 75th percentile in Figure 4.12(b). Southern part of the UNB districts are covered by forest and vegetation. Therefore annual mean temperature of southern stations are low, in comparison to other parts of the area. It can be observed from Figure 4.12(b) that outliers appear at the upper and lower, both side in most of the stations. Table 4.7 show the highest and lowest annual mean temperature of 102 years (1901-2002) experienced in Balaghat (26.52^oC) and Bilaspur (24.24^oC), respectively. The coefficient of variation varies between 1.98% (Bilaspur) to 1.51% (Jabalpur) station for annual mean temperature.

4.4.1.2 Serial autocorrelation test

Auto serial correlation test at lag-1 was performed for annual and seasonal meteorological data (precipitation and mean temperature) to check the serial correlation in the series. To eliminate the effect of serial correlation, pre whitening could be used in the time series, before applying the MK test.

Annual precipitation series of UNB indicates the positive and negative correlation coefficient within the critical range (Z_c = ±1.96) whereas annual mean temperature indicate positive correlation coefficient (Figure 4.13). Therefore serial autocorrelation were obtained only for annual and autumn mean temperature series. Figure 4.13 indicates the strongest and weakest autocorrelation for Raisen and Balaghat, respectively for both annual and autumn mean temperature series. Pre-whitening was

applied before using the MK test. Therefore, time series used for MK test to detect the trend and Sen's slope to estimate the rate of change at 16 stations of UNB.

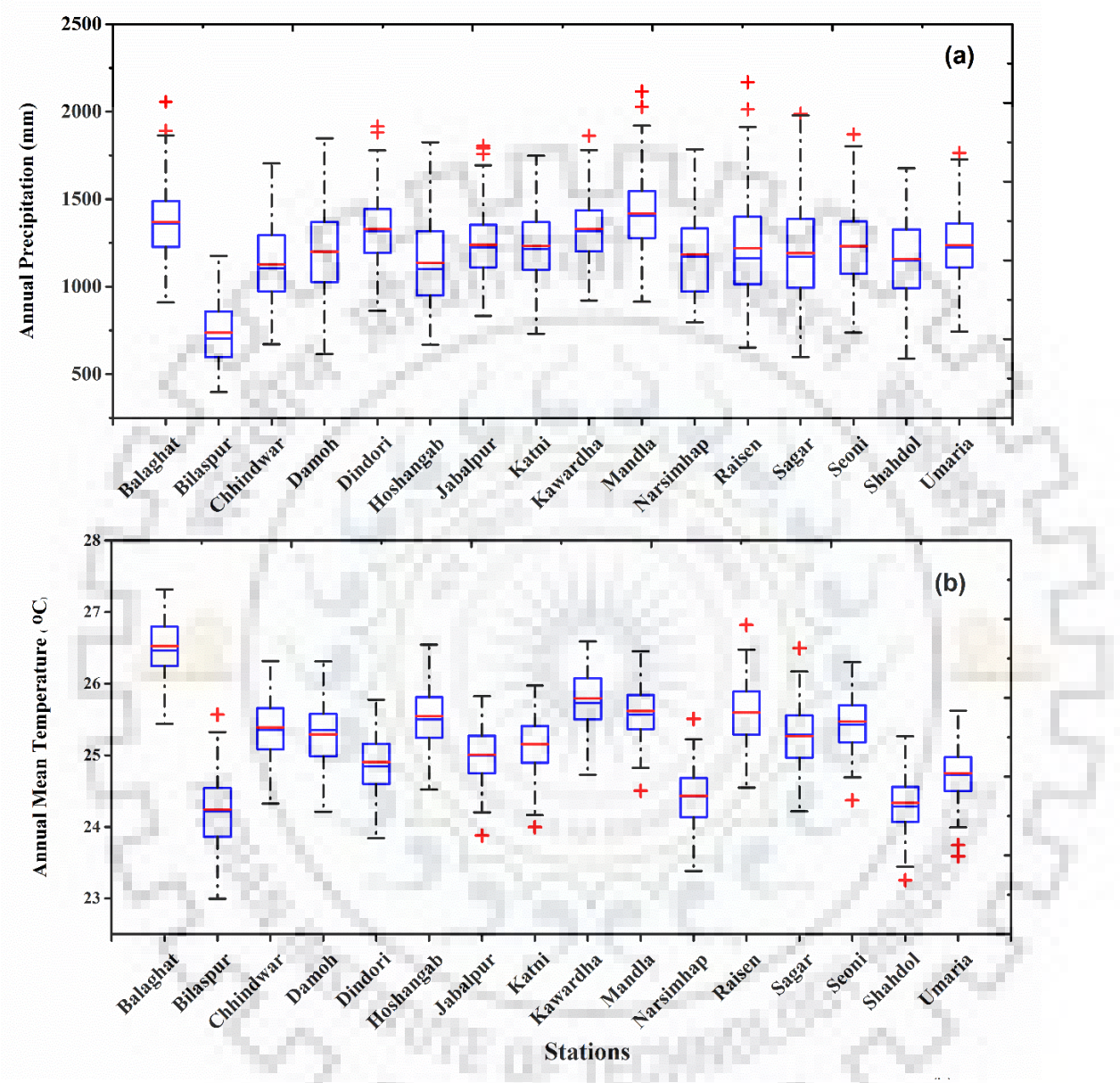

Figure 4.12: (a). Box-whisker plot of annual precipitation and, (b). Box-whisker plot of annual mean temperature of 16 districts of Upper Narmada river basin

(Note: The blue boxes indicate the 25th, 50th, 75th percentiles. Whisker upper/ lower red plus sign indicate the outlier, and red line in box indicate the mean value)

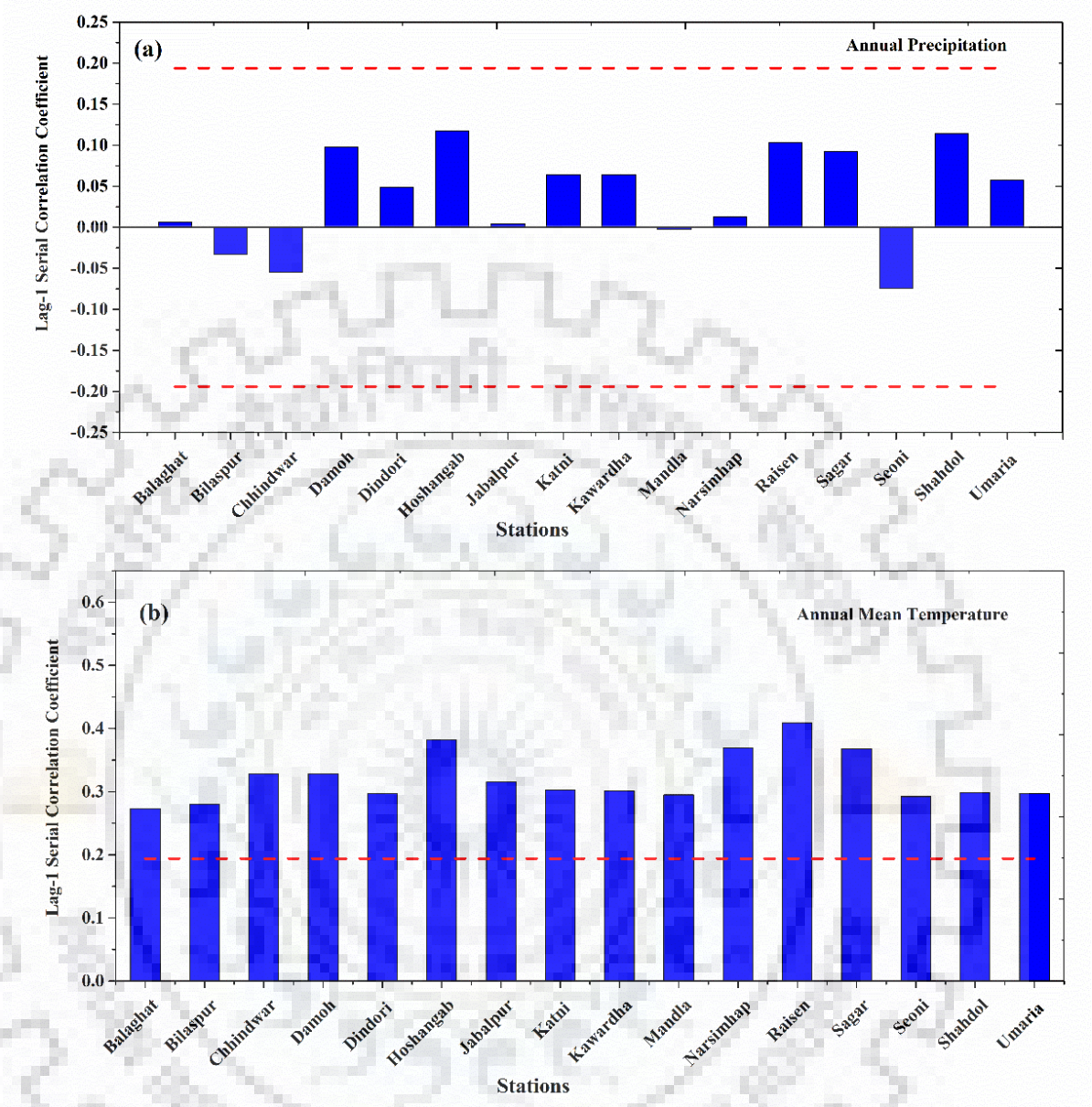

Figure 4.13: Lag-1 serial autocorrelation for (a) annual precipitation and (b) annual mean temperature of Upper Narmada Basin stations

(Note: Red dotted line indicate the critical value (± 1.96) of upper and lower bound at 5 % significance level)

4.4.1.3 Trend detection of mean monthly series

MK test was applied on the original meteorological series without considering the pre-whitening and block bootstrap process assumptions, in order to retain the originality of the monthly time series. Trend detection was carried out based on the null hypothesis, at 1% ($\alpha = 0.01$), 5% ($\alpha = 0.05$), 10 % ($\alpha = 0.10$) of two tailed significance level.

The trends of mean monthly long term precipitation series of the 16 stations of UNB are mentioned in Table 4.7. It can be seen, that most of the month such as January, February, April, June, August, September, October, November, and December were not indicated the significant trend for any stations for mean monthly precipitation series (Table 4.7). However, most of the stations (81.25%) exhibit the significant negative trend in the month of July for long term mean monthly precipitation (1901-2002). Stations Balaghat, Bilaspur and Mandla were not show trend at any significant level. Moreover, Bilaspur station experienced the positive trend for month of March and May. In general, monsoon precipitation may decrease because of decreasing trend of July, one of contributing months in monsoon precipitation over UNB.

Figure 4.14 indicates the trend variability of long term mean monthly temperature (1901-2002) over the central India. In this context, results of the significant trend for UNB stations were summarized in Figure 4.14. This figure shows significant trend in the month of February, March, July, August, November and December as other six months (January, April, May, June, September, and October) seem to have no significant trend. Moreover all the stations did not exhibit trend at any significance level in the months of January, April, May, June, September, and October. However, all stations experienced the positive changes in February, March, November and December. While Bilaspur exhibit the negative trend for the month of July and August at 1% and 5% significance level. In general, rising trend in November and December indicate a warm autumn season.

Table 4.7: MK-Z value of annual precipitation series (1901-2002) for 16 stations of UNB

Stations	Jan	Feb	Mar	Apr	May	Jun	Jul	Aug	Sep	Oct	Nov	Dec
Balaghat	1.058	-0.555	-0.093	0.200	0.231	-1.451	-1.449	0.445	-0.700	0.844	-0.173	-0.535
Bilaspur	-0.694	1.110	2.047**	0.150	1.793*	0.312	1.070	0.243	0.341	0.821	0.541	-0.732
Chhindwara	0.734	0.017	0.043	-0.679	1.015	-1.122	-2.059**	1.133	-0.613	0.708	-0.382	-0.373
Damoh	0.940	-0.272	-0.116	-0.283	1.414	1.064	-2.232**	0.468	-1.018	1.151	-0.272	0.231
Dindori	1.318	-1.272	-0.471	0.477	0.570	-0.532	-1.668*	-0.434	-0.422	0.584	-0.084	-0.234
Hoshangabad	0.873	0.252	0.278	-1.024	1.665*	-0.411	-2.064**	1.573	-1.168	1.162	-0.292	-0.101
Jabalpur	0.838	-0.301	-0.506	0.084	0.853	0.231	-1.943*	0.561	-0.867	0.674	-0.220	-0.211
Katni	1.081	-0.382	-0.593	0.483	1.021	0.723	-2.169**	-0.075	-0.677	0.610	-0.197	-0.012
Kawardha	1.081	-0.382	-0.593	0.483	1.021	0.723	-2.169**	-0.075	-0.677	0.610	-0.197	-0.012
Mandla	1.087	-0.879	-0.448	0.379	0.289	-0.439	-1.532	0.318	-0.561	0.549	0.075	-0.249
Narsimhapur	0.593	-0.072	-0.095	-0.862	1.050	-0.069	-2.151**	1.454	-1.139	0.798	-0.422	-0.081
Raisen	0.833	0.121	0.506	-0.668	1.558	0.202	-1.770*	1.451	-1.290	1.229	-0.159	-0.006
Sagar	0.685	-0.306	0.373	-0.194	1.709*	0.567	-1.816*	1.133	-1.081	1.402	-0.306	0.249
Seoni	0.755	-0.364	-0.052	-0.171	0.390	-0.723	-1.671*	0.966	-0.613	0.691	-0.124	-0.220
Shahdol	1.382	-0.520	-0.625	0.755	1.258	1.480	-1.885*	-1.278	-0.093	0.879	-0.081	0.081
Umaria	1.376	-0.896	-0.775	0.639	0.619	0.492	-2.076**	-0.538	-0.492	0.604	0.159	-0.084

*Note: ***', ** and * values indicate 1% ($Z_{critical}$ = ±2.58), 5% ($Z_{critical}$=± 1.96) and 10 % ($Z_{critical}$= ±1.65) of the significance level of trend, where positive and negative values show the increasing and decreasing trend, respectively.*

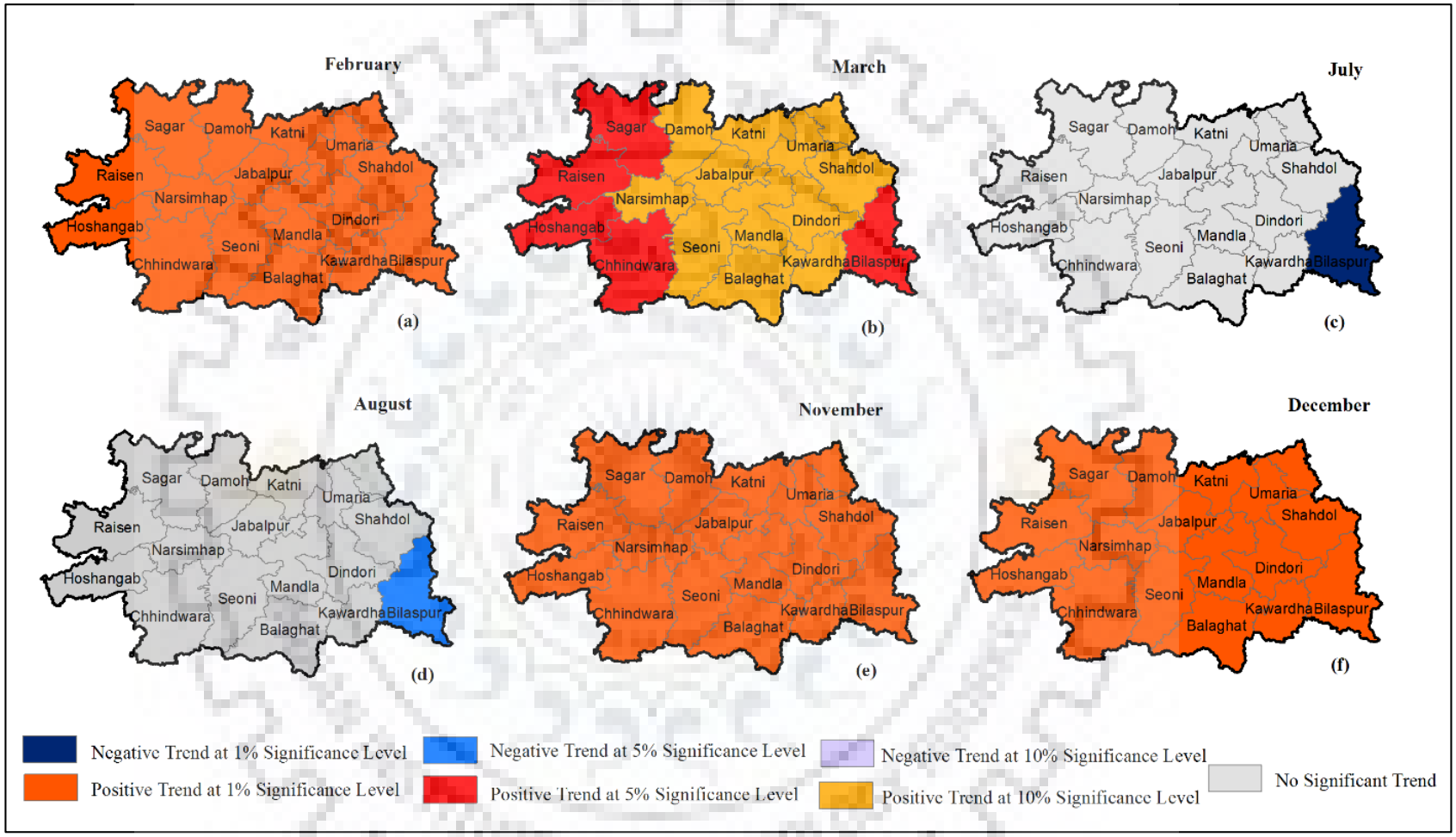

Figure 4.14: Monthly trend variability of annual mean temperature at 10%, 5% and 1% significance level

(Note: Month January, April, May, June, September and October were not included in figure, because of No significant trend at the station during these months)

4.4.1.4 Trend detection of seasonal series

In this section, trends in precipitation and temperature are summarized in Table 4.8 and 4.9 based on four seasons i.e. spring (January-March), summer (April-June), monsoon (July-September) and autumn (October-December).

Precipitation is the main source of water for agriculture, river discharge, domestic purpose and hydropower. Flood is main natural disaster which occur in the monsoon season due to concentrated rainfall over the area. However, severity and frequency of flood reduced from south-east to north-west stations of UNB. The seasonal precipitation trend over 16 stations identified by the three methods are given in Table 4.8. None of the stations exhibit significant trend for spring and autumn precipitation over UNB. However, most of stations indicate insignificant trend for monsoon and summer. Station Bilaspur show the increasing trend ($\alpha = 0.05$) for summer season, while Balaghat, Dindori, Kawardha and Mandla indicate the downward trend ($\alpha = 0.01, 0.05, 0.1$) for monsoon precipitation. Therefore decreasing trend of annual precipitation at Balaghat and Dindori stations (Table 4.8) is due to monsoon negative trend (Table 4.8). Moreover, Balaghat, Dindori, Jabalpur, Kawardha,Mandla, Seoni and Umaria indicate the negative sign by all the three methods (MK, Sen's Slope and ITA) for spring, summer, and monsoon season. Stations Hosangabad, Raisen and Sagar exhibit the same trend sign (positive and negative) for all the seasons by all three methods.

The mean temperature trend over the four seasons, spring (January-March), summer (April-June), monsoon (July-September) and autumn (October- December) were identified (Table 4.9). Spring mean temperature exhibits significant increasing trends (99% confidence level of two tailed test) at the all stations of UNB. Moreover most of stations were also exhibit the strong positive trend at 1% of significance level in autumn season, only at Bilaspur station indicate the positive trend at 5% of significance level. In summer season, five stations (Bilaspur, Chhidwara, Hoshangabad, Raisen and Sagar) indicate the upward trend over the region. Among all the significant stations in all the seasons, only Bilaspur station indicate negative trend (at 99 % confidence level) for monsoon season. However, Bilaspur station is the only station which shows significant trend for all the season; significant positive trend for spring, summer and autumn, and significant negative trend for monsoon season, which is opposing the overall annual trend (Table 4.9). In general, annual positive trend (Table 4.9) of all the significant stations are mainly influenced by spring and autumn seasonal trend.

Table 4.8: Mann-Kendall (MK-Z), Sen's Slope (β) and ITA indicator (D) test results for seasonal precipitation over 1901–2002

Stations	Spring			Summer			Monsoon			Autumn		
	β	MK-Z	D	β	MK-Z	D	β	MK-Z	D	β	MK-Z	D
Balaghat	-0.005	-0.104	-2.236	-0.032	-0.364	-0.888	-1.585	-2.238**	-0.519	0.140	0.931	0.085
Bilaspur	0.010	0.116	-0.013	0.169	2.099**	2.561	0.308	0.619	0.590	-0.018	-0.275	0.524
Chhindwara	0.006	0.110	-1.653	0.004	0.014	-0.753	-0.971	-1.388	-0.508	-0.004	-0.012	-0.943
Damoh	0.012	0.208	-0.371	0.020	0.439	-0.697	-0.398	-0.515	-0.388	0.104	0.729	0.950
Dindori	-0.024	-0.249	-1.933	-0.028	-0.272	-1.169	-1.339	-2.070**	-0.511	0.152	0.977	0.008
Hoshangabad	0.023	0.668	0.205	0.038	0.688	-0.394	-0.752	-0.960	-0.596	-0.023	-0.107	-0.654
Jabalpur	-0.031	-0.347	-1.666	-0.002	-0.006	-0.922	-0.533	-0.885	-0.246	0.055	0.338	-0.295
Katni	-0.015	-0.139	-1.334	0.006	0.098	-0.837	-0.606	-0.919	-0.346	0.080	0.596	0.065
Kawardha	-0.017	-0.208	-1.981	-0.022	-0.243	-0.849	-1.487	-2.868***	-0.575	0.125	0.960	-0.028
Mandla	-0.034	-0.324	-2.026	-0.032	-0.295	-1.123	-1.067	-1.770*	-0.382	0.131	0.682	-0.170
Narsimhapur	0.004	0.098	-1.245	0.013	0.220	-0.751	-0.571	-0.798	-0.286	0.003	0.017	-0.202
Raisen	0.016	0.445	0.764	0.047	0.983	-0.382	-0.881	-0.804	-0.545	0.054	0.477	0.591
Sagar	0.016	0.330	0.319	0.034	0.937	-0.349	-0.421	-0.463	-0.366	0.097	0.804	1.451
Seoni	-0.029	-0.359	-2.221	-0.029	-0.353	-0.958	-1.019	-1.475	-0.363	0.069	0.318	-0.437
Shahdol	0.009	0.110	-0.450	0.020	0.376	-0.567	-0.690	-0.943	-0.513	0.131	1.104	0.745
Umaria	-0.019	-0.156	-1.491	-0.014	-0.168	-1.147	-0.680	-1.041	-0.426	0.096	0.694	0.048

*Note: ***, ** and * values indicate 1% ($Z_{critical}$ = ±2.58), 5% ($Z_{critical}$=± 1.96) and 10 % ($Z_{critical}$= ±1.65) of the significance level of trend, where positive and negative values shows the increasing and decreasing trend, respectively.*

Table 4.9: Mann-Kendall (MK-Z), Sen's Slope (β) and ITA indicator (D) test results for seasonal temperature over 1901–2002

Stations	Spring			Summer			Monsoon			Autumn		
	β	MK-Z	D	β	MK-Z	D	β	MK-Z	D	β	MK-Z	D
Balaghat	-0.857	3.475***	0.253	0.429	1.457	0.098	0.160	0.575	0.029	0.692	4.111***	0.294
Bilaspur	-0.885	2.764***	0.448	1.067	2.816***	0.230	-0.753	-3.241***	-0.076	0.323	1.928*	0.116
Chhindwara	-0.787	3.204***	0.258	0.500	1.663*	0.100	0.117	0.457	0.012	0.692	3.641***	0.319
Damoh	-0.725	2.851***	0.277	0.499	1.596	0.101	-0.147	-0.596	-0.030	0.687	3.835***	0.358
Dindori	-0.840	3.626***	0.290	0.358	1.324	0.099	0.015	0.052	0.012	0.776	4.797***	0.357
Hoshangabad	-0.792	2.755***	0.259	0.575	2.114**	0.107	0.083	0.309	-0.002	0.913	4.475***	0.359
Jabalpur	-0.783	3.394***	0.279	0.438	1.475	0.103	-0.087	-0.353	-0.013	0.712	4.170***	0.350
Katni	-0.733	3.261***	0.280	0.401	1.451	0.108	-0.152	-0.575	-0.021	0.696	4.193***	0.364
Kawardha	-0.880	3.672***	0.269	0.427	1.486	0.100	0.155	0.688	0.031	0.707	4.375***	0.322
Mandla	-0.822	3.533***	0.272	0.411	1.272	0.101	0.005	0.040	0.007	0.716	4.457***	0.331
Narsimhapur	-0.847	3.227***	0.299	0.490	1.556	0.102	0.000	0.000	-0.009	0.676	3.589***	0.360
Raisen	-0.854	2.828***	0.289	0.570	1.926*	0.108	0.061	0.208	-0.016	0.743	3.495***	0.371
Sagar	-0.768	2.735***	0.292	0.541	1.680*	0.102	-0.097	-0.330	-0.037	0.818	3.970***	0.358
Seoni	-0.793	3.441***	0.264	0.461	1.501	0.101	0.035	0.142	0.012	0.684	3.976***	0.312
Shahdol	-0.800	3.536***	0.303	0.312	1.142	0.102	-0.092	-0.344	-0.005	0.665	4.404***	0.375
Umaria	-0.758	3.253***	0.290	0.345	1.394	0.110	-0.150	-0.526	-0.014	0.695	4.369***	0.372

*Note: ***, ** and * values indicate 1% ($Z_{critical}$ = ±2.58), 5% ($Z_{critical}$=± 1.96) and 10 % ($Z_{critical}$= ±1.65) of the significance level of trend, where positive and negative values shows the increasing and decreasing trend, respectively.*

4.4.1.5 Trend detection of extreme events: Application of ITA

Precipitation series

In order to apply the MK test, the original meteorological series were checked for serial correlation considering for the pre-whitening. However, there is no serial correlation observed between annual series (Figure 4.13) and seasonal series. Therefore MK test was applied on the original precipitation series without pre-whitening and trend was analysed based on the null hypothesis theory, at 1% ($\alpha = 0.01$), 5% ($\alpha = 0.05$), 10 % ($\alpha = 0.10$) of two tailed significance level.

The results of trend by three methods, MK test (MK-Z), Sen's slope (β) and ITA (D) for annual precipitation series summarized in Table 4.10. As shown in table, most of the significant trend stations exhibits the negative trend, except Bilaspur station (positive). Based on annual series, only two stations, Balaghat and Dindori showed the significate negative trend at the rate of (-) 1.61mm/year and (-) 1.230 mm/year. Autumn and spring seasonal series, neither positive nor negative trends were detected for any stations at given significance level (α =0.1, 0.5, 0.01). On the contrary, summer indicate the positive trend for single station (Bilaspur), whereas monsoon indicate the negative trend for four stations (Balaghat, Dindori, Kawardha and Mandla). The negative trend of annual precipitation at Balaghat and Dindori stations are mainly influenced by the negative trend of monsoon series. The decreasing trend in precipitation series have been caused by many factors including the deforestation, urbanization, global warming and changes in atmospheric circulation.

The trends of annual precipitation in the three categories (low, medium and high value) identified by applying the ITA method. Figure 4.15 shows the scatter plot for annual precipitation, 1:1 (45^o) line indicate the 'no trend' line, upper and lower data points of 'no trend' line indicate the positive and negative trend in the series. The annual rainfall categorized in to three class: less than 25 percentile data as low values, between 25 and 75 percentile as medium values and greater than 75 percentile as high values. Figures 4.15 (a-p) show the results of ITA trend applied to the 16 stations of UNB of annual series. Most of the stations exhibit the overall decreasing trend for annual precipitation (Table 4.10). The results indicate that ITA indicator (D) for unequal across different precipitation categories (low, medium and high), even in contrary sign. For low and medium precipitation values indicate the downward trend (negative sign), for all the stations (except Bilaspur- medium value), as most points of low extreme and medium values fall below the 1:1 line shown in Figure 4.15 (a-p). At the Bilaspur station (Figure 4.15 (b)), low precipitation decrease

slightly, while medium and high precipitation have strong incline trend and overall increasing trend. Figure 4.15 (d), (g), (h),(m),(o) and (p) show general decreasing trend for low and medium values, while trend changes gradually negative to positive for medium to high values for Damoh, Jabalpur, Katni, Sagar, Shahlod and Umaria, respectively. Stations Katni, Shahdol and Umaria in Figure 4.15 (h), (o) and (p) indicate the strong decreasing trend for low extremes, while increasing trend for high extreme. Significant stations (Table 4.10), Balaghat and Dindori most of the points fall below the 'no trend line', indicating a marked and alike decreasing trend for all the precipitation categories (Figure 15 (a) and (e)). However, Figure 4.15 (f), (i) and (j) indicate the steady negative trend for all categories of precipitation for stations Hoshangabad, Kawardha and Mandla, respectively.

Table 4.10: Mann-Kendall (MK-Z), Sen's Slope (β) and ITA indicator (D) test results for annual extreme values of precipitation over the period 1901–2002

Stations	**MK-Z**	**β**	**ITA Method (D)**			
			Annual	**Low**	**Medium**	**High**
Balaghat	-2.174**	-1.610	-0.547	-0.118	-0.697	-0.573
Bilaspur	1.012	0.686	0.669	-0.159	0.837	0.904
Chhindwara	-1.052	-0.882	-0.575	-0.079	-0.740	-0.544
Damoh	-0.434	-0.352	-0.332	-0.769	-0.488	0.423
Dindori	-1.879*	-1.230	-0.564	-0.585	-0.694	-0.280
Hoshangabad	-0.717	-0.673	-0.583	-0.574	-0.636	-0.486
Jabalpur	-0.758	-0.512	-0.322	-0.687	-0.346	0.050
Katni	-0.763	-0.571	-0.379	-1.105	-0.410	0.342
Kawardha	-0.763	-0.571	-0.594	-0.342	-0.673	-0.627
Mandla	-1.463	-1.038	-0.455	-0.393	-0.556	-0.286
Narsimhapur	-0.549	-0.438	-0.319	-0.267	-0.465	-0.051
Raisen	-0.567	-0.643	-0.477	-0.739	-0.564	-0.006
Sagar	-0.173	-0.218	-0.273	-0.801	-0.420	0.474
Seoni	-1.116	-0.865	-0.452	-0.227	-0.579	-0.334
Shahdol	-0.815	-0.745	-0.461	-1.315	-0.552	0.517
Umaria	-1.099	-0.743	-0.476	-1.089	-0.514	0.194

*Note: ***, ** and * values indicate 1% ($Z_{critical}$ = ±2.58), 5% ($Z_{critical}$=± 1.96) and 10 % ($Z_{critical}$= ±1.65) of the significance level of trend, where positive and negative values shows the increasing and decreasing trend, respectively*

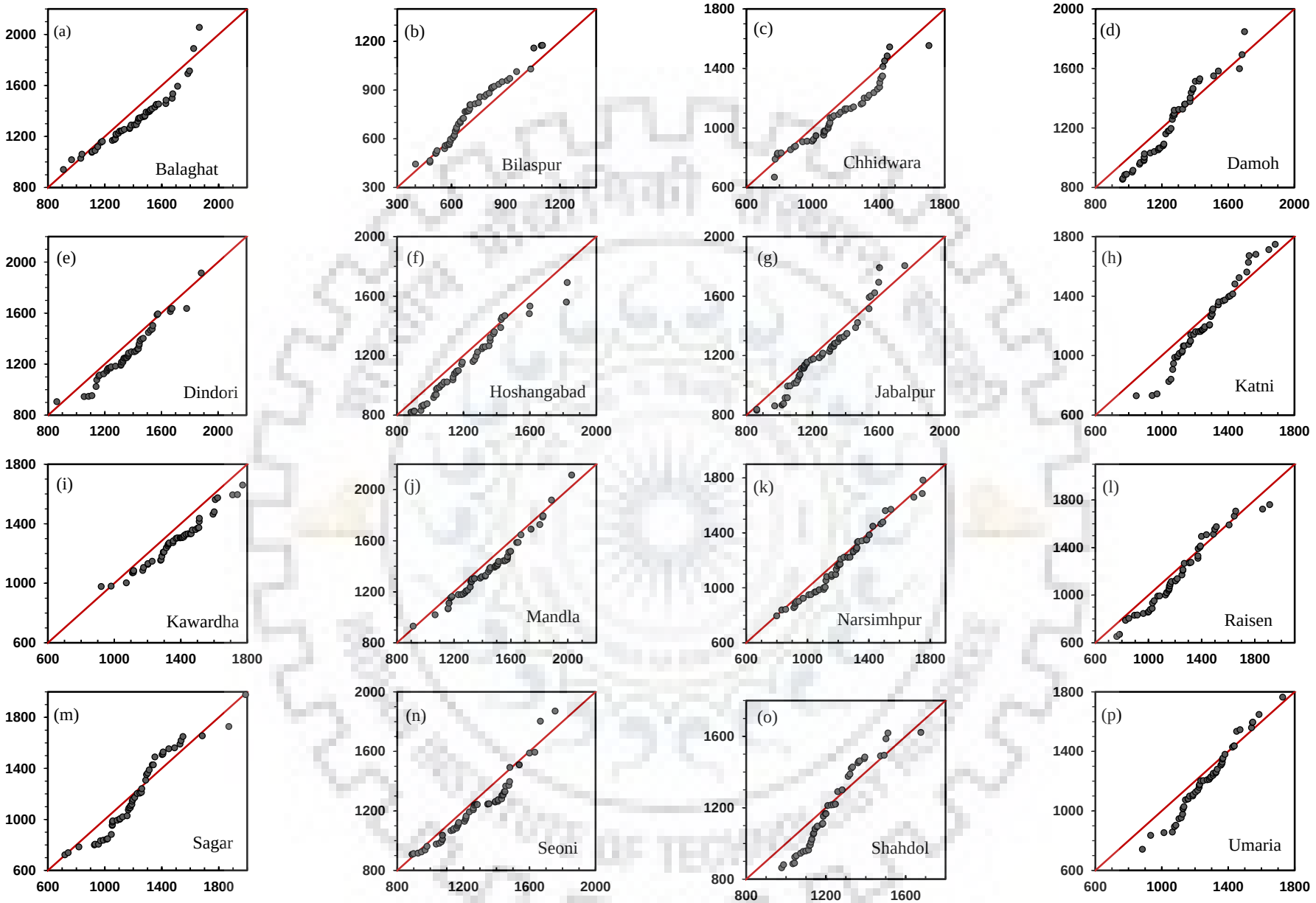

Figure 4.15: The results of ITA for annual precipitation at the 16 stations in Upper Narmada Basin, India

Temperature Series

Summarized results of trend by three methods, MK test (MK-Z), Sen's slope (β) and ITA (D) for mean annual temperature shown in Table 4.11. Before applying the MK test, the original temperature series were checked for serial correlation considering the pre-whitening. However, there is serial correlation observed between annual series, which has already been presented in Figure 4.13(b). Therefore MK was applied on the 'prewhiten' temperature series and trend was analysed based on the null hypothesis theory, at 1% ($\alpha = 0.01$), 5% ($\alpha = 0.05$), 10 % ($\alpha = 0.10$) of two tailed significance level.

Most of the stations suggest the strong significant positive trend at 99% confidence level at the rate of about 0.44°C per decade (Table 4.11). Station Bilaspur indicate relatively weak increase trend at the decadal rate of 0.287°C, at 90% confidence level of two tailed test. Kawardha indicates the high decadal rate as 0.48°C, followed by Raisen with the rate of 0.47°C (Table 4.11). Estimation of trend for low (less than 25 percentile), medium (25 to 75 percentile), high (greater than 75 percentile) values indicate the positive trend for all the stations. Moreover, annual series indicate the overall positive trend by ITA method. Medium and high values show the strong positive trend as compared to lower values.

Figure 4.16 shows the scatter plot for annual mean temperature, 1:1 (45°) line indicate the 'no trend' line, upper and lower data points of 'no trend' line indicate the positive and negative trend in the series. The annual mean temperature categorized in to three class: less than 25 percentile data as low values, between 25 and 75 percentile as medium values and greater than 75 percentile as high values. Figures 4.16 (a-p) show the results of ITA trend applied to the 16 stations of UNB of annual mean temperature series. Most of the stations exhibit the overall strong positive trend for annual mean temperature (Table 4.11). The results indicate that same sign of ITA indicator (D) for all stations, for unequal across different mean temperature categories (low, medium and high). For low temperature values positive trend value is relatively low as compared to medium and high. Therefore, trend in medium and high values mainly contributed the overall trend for the region.

Table 4.11 : Mann-Kendall (MK-Z), Sen's Slope (β) (ºC/10 years) and ITA indicator (D) test results for annual extreme values of mean annual temperature over the period 1901–2002

Stations	MK-Z	β	ITA method (D)			
			Annual	Low	Medium	High
Balaghat	3.565***	0.450	0.135	0.092	0.146	0.132
Bilaspur	1.652*	0.287	0.096	0.055	0.091	0.119
Chhindwara	3.184***	0.423	0.136	0.058	0.153	0.146
Damoh	3.407***	0.454	0.128	0.072	0.144	0.126
Dindori	3.542***	0.461	0.145	0.089	0.158	0.145
Hoshangabad	3.377***	0.462	0.141	0.065	0.159	0.149
Jabalpur	3.436***	0.444	0.134	0.089	0.148	0.124
Katni	3.647***	0.452	0.134	0.102	0.145	0.125
Kawardha	3.542***	0.479	0.144	0.082	0.163	0.141
Mandla	3.559***	0.440	0.137	0.098	0.149	0.128
Narsimhapur	3.154***	0.438	0.140	0.071	0.155	0.150
Raisen	3.189***	0.470	0.141	0.069	0.164	0.145
Sagar	3.119***	0.453	0.129	0.071	0.146	0.130
Seoni	3.354***	0.411	0.135	0.096	0.141	0.136
Shahdol	3.512***	0.448	0.143	0.096	0.154	0.144
Umaria	3.571***	0.446	0.140	0.109	0.148	0.133

*Note: ***, ** and * values indicate 1% ($Z_{critical}$ = ±2.58), 5% ($Z_{critical}$=± 1.96) and 10 % ($Z_{critical}$= ±1.65) of the significance level of trend, where positive and negative values shows the increasing and decreasing trend, respectively*

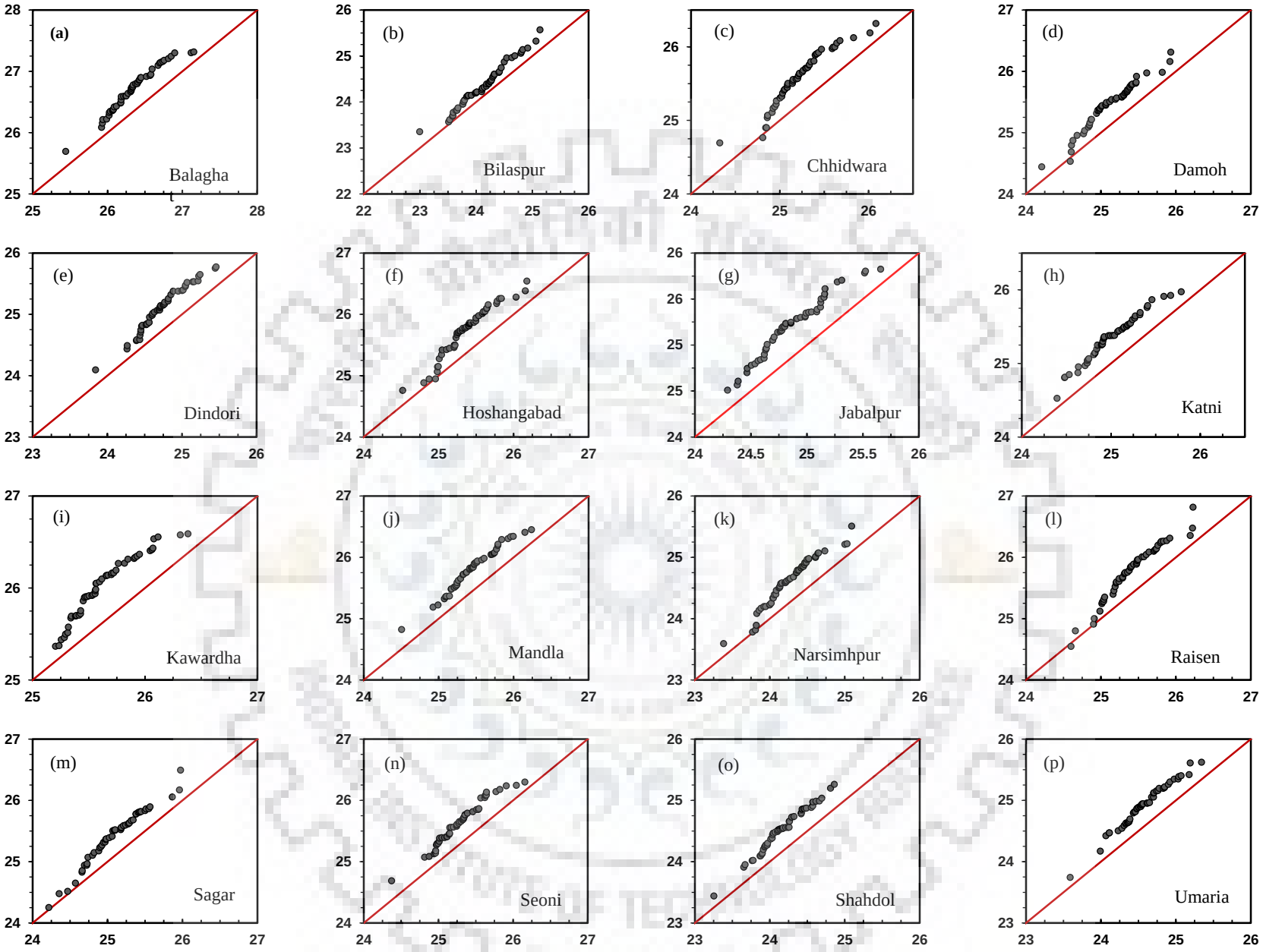

Figure 4.16: The results of ITA for annual mean temperature at the 16 stations of Upper Narmada Basin, India

4.4.1.6 Comparative studies of 'ITA vs MK test' and 'ITA vs Sen's Slope'

For annual and seasonal series, trend were detected over the 16 stations of UNB by three methods: MK-test (MK-Z score), Sen's slope (β) and ITA (D), to compare all the results of precipitation series (statistically significant and insignificant) from three methods. Figure 4.17 shows the scatter plot between ITA *versus* Z score and ITA *versus* SS were plotted to detect the differences in terms of sign of annual and seasonal precipitation test results. Figure 4.17 (a-b) shows the 80 points (16 stations x 5 series) from annual and seasonal precipitation series. Most of the points, 78.75% in Figure 4.17(a) for ITA versus Z score, and 65% lies in Figure 4.17(b) for ITA versus SS, in the first and third quadrants (same sign of X-Y coordinate), which indicate the general acceptance of all the methods. However, annual and monsoon points provide the 100% agreement in the trends among all three methods.

Therefore annual and seasonal temperature data indicate the strong agreement in three methods, as 97.5% for ITA versus Z score, and 77.5% for ITA versus SS lies in the first and third quadrants. Moreover for annual, summer and autumn season results provide the 100% acceptance among the three methods. In general, the wide agreement among the all tests (MK test, Sen's Slope and ITA) exhibit that the ITA method is obviously a viable and good means of precipitation and temperature trend analysis.

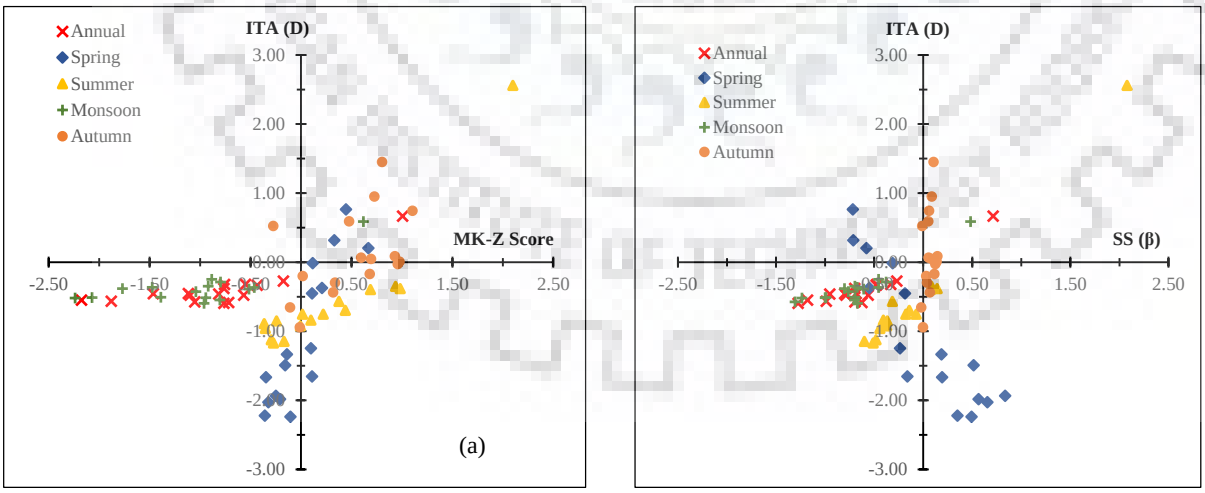

Figure 4.17: (a) A Scatter plot between ITA versus MK-Z score (b) A Scatter plot between ITA (D) versus Sen's slope

4.4.1.7 Visualization and thresholding of meteorological extreme events

Discrete Wavelet Transform (DWT) is very useful tool to detect the contributing events for extreme value, it has the advantage to avoid the effect of noise (Maheswaran and Khosa 2012; Nalley et al. 2013; Nourani et al. 2009; Sang 2013; Sang et al. 2016). This tool can decompose the original time series into different frequencies, retaining information in the time domain (Adarsh and Janga Reddy 2015; Labat 2005; Nalley et al. 2012; Yang et al. 2016). The selection of mother wavelet and choice of temporal scale (level of decomposition) are the most important issues in wavelet analysis (Labat 2005; Nalley et al. 2012; Sang et al. 2016). Selection of mother wavelet is the first task in the wavelet analysis. There are numbers of wavelet available to analyze the time series. Torrence and Compo (1998) divided the wavelet in to two categories, namely, orthogonal (Haar, Daubechies (dbN), Coiflets (coifN), Symlets (symN), BiorSplines (biorM.N), ReverseBior (rbioM.N), and DMeyer (dmey)) which can be use in discrete wavlet transform, and nonorthogonal (Morlet (morl), Mexican hat (Marr), and Gaussian (gaus)), which can be used in discrete wavelet transform or continuous wavelet transform.

Selection of mother wavelet and temporal scale was inspired by previous studies based on hydrological and climatological time series. Considered on the previous studies, mother wavelet, Daubechies (db3) and temporal scale (decomposition level) using tool $\log_{10}N$ (N is the historical data) were used in this analysis (Yang et al. 2016).

In this case, station Balaghat was analyzed for annual precipitation and temperature. Figures 4.18(d)-4.19(d) indicate the normalized precipitation, and normalized mean temperature of Balaghat with six horizontal lines (blue, red and green) representing the three selected thresholds at both positive (lines upper to zero) and negative (lower to zero) positions. These thresholds were selected based on the standard deviation (SD) of the original precipitation and temperature series. Figures 4.18(a-c) and 4.19(a-c) clearly indicate that the number of exceedances events decreases as the threshold increases. Black color (or gray) spectrum indicate the exceedance event at different intensities (positive or negative), white color represent the non-exceedance properties of the series in Figures 4.18(a-c) and 4.19(a-c). It can be observed from normalized series Figures 4.18(d)-4.19(d), only five and four extremes (high and low) are in the annual series beyond the 1.5SD, that can be visualized in the Figures 4.18(a)-4.19 (a), respectively.

The method could be generalized to gain frequency information from the precipitation time series. The different color shades (black and gray) indicate the different frequency fluctuations. Keylock (2007) mentioned that "the former arises due to relatively small high frequency fluctuations superimposed on a large, low frequency positive departure from the mean. The latter is a sudden and dramatic excursion from the mean that is not superimposed on an obvious larger scale fluctuation". Therefore, it helps to visualize this information in a clear manner so that the scales of events that actively contribute to an extreme event can be determined.

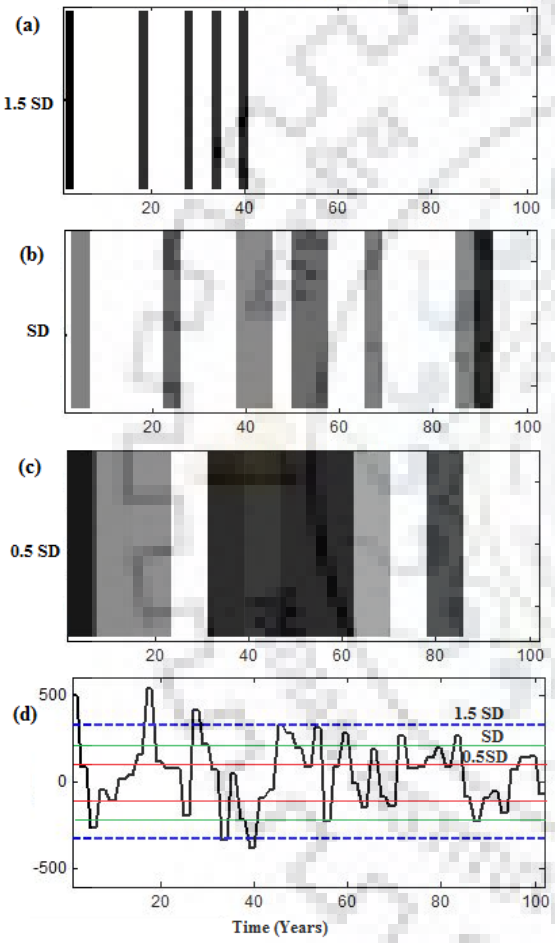

Figure 4.18: A 3-level decomposition of annual precipitation (Balaghat station) for considering the thresholds (SD: standard deviation) of 0.5SD (red line), SD (green line) and 1.5SD (blue dotted line) in (d), solid black curve indicate the normalized precipitation series

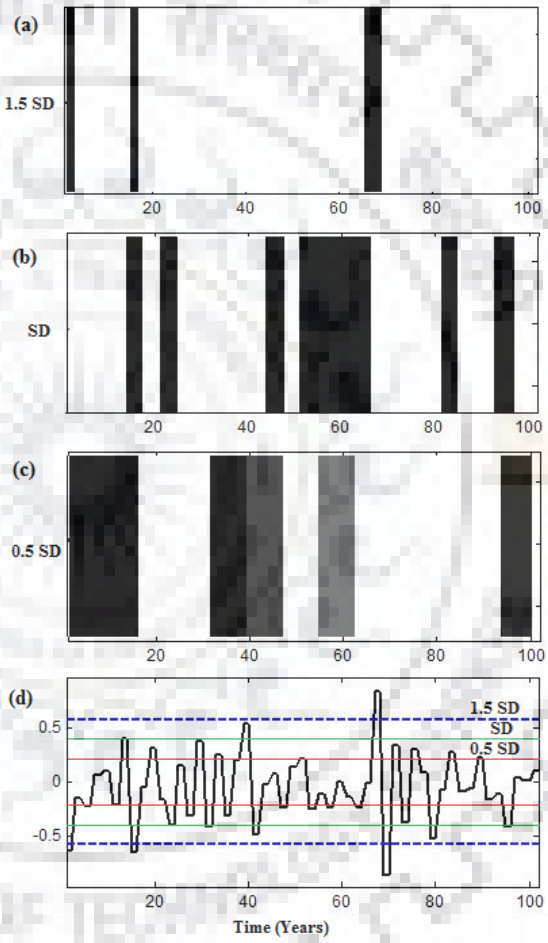

Figure 4.19: 3-level decomposition of annual mean temperature (Balaghat station) for considering the thresholds (SD: standard deviation) of 0.5SD (red line), SD (green line) and 1.5SD (blue dotted line) in (d), solid black curve indicate the normalized precipitation mean temperature

4.4.1.8 Abrupt Change Detection

The Sequential Mann-Kendall test (SQMK) was applied on the original series of annual precipitation and annual mean temperature to detect the abrupt change points. There are many reasons in such abrupt change in meteorological parameters. It may be due to relocations of the stations, changes in instrument exposure, urban influence changes in observing schedules and practices, or abrupt changes in the atmosphere (Alexandersson and Moberg 1997). However, SQMK is a graphically method, used to plot the forward and backward sequential Z score along the time. In Figure 4.20 (a-b) the breakup point of forward curve Z (t), and backward curve (Z' (t)) show the abrupt change in precipitation (Figure 4.20(a)) and temperature (Figure 4.20(b)). The breakpoint of abrupt change lies outside of the red dotted line (Figure 4.20) indicate the significant abrupt change (shifting) at 5% of significance level. Change points obtained from SQMK compare with the results of CUMSUM test.

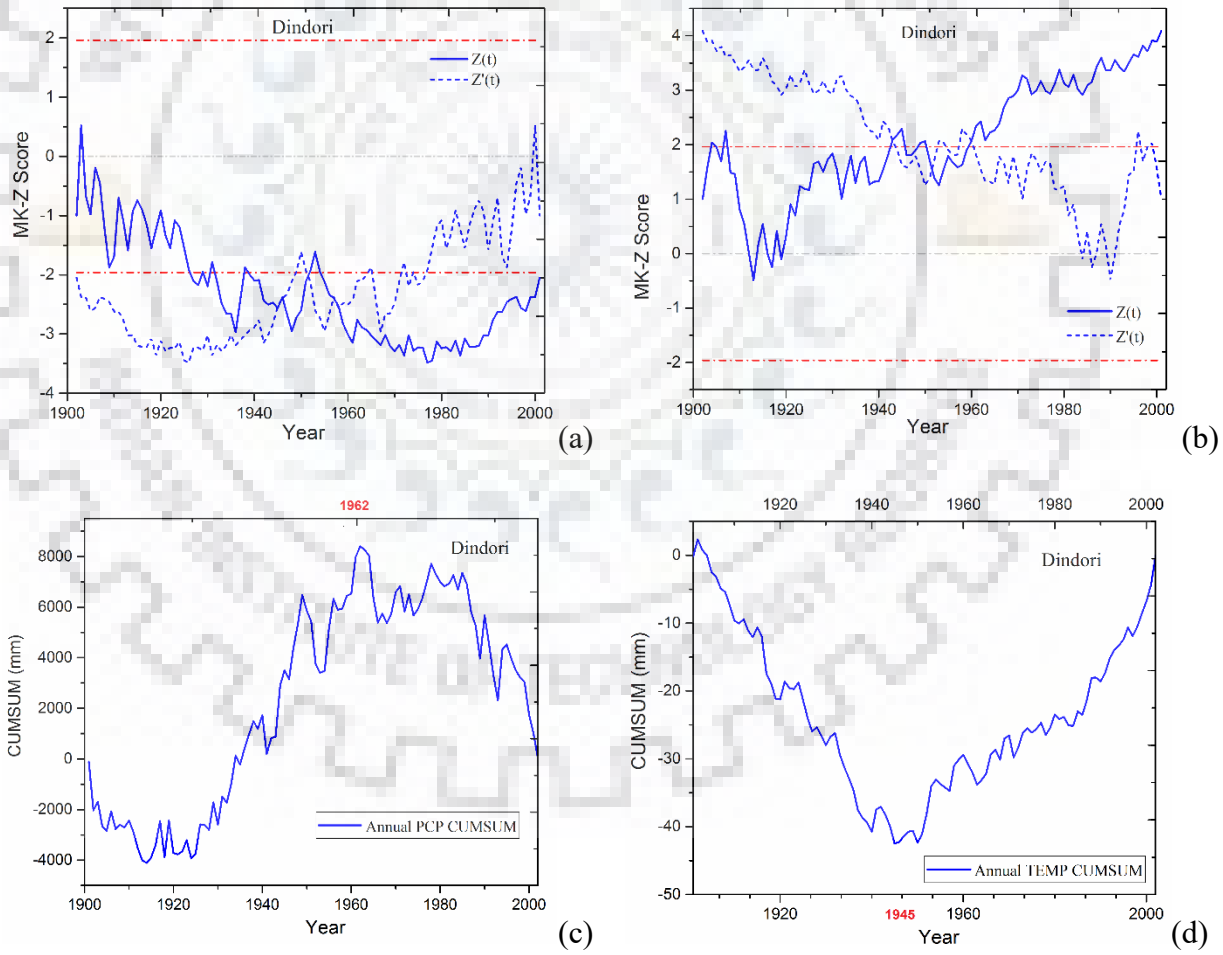

Figure 4.20: Plot of forward (Z(t))and backward (Z'(t)) sequential Z score versus year (a-c) for annual precipitation (b-d) for annual mean temperature

For representation, station Dindori was shown in Figures 4.20(a-d) and results of all 16 stations were summarized in Table 4.12. Applying SQMK, Figures 4.20(a-b) indicate the significant (α=0.05) abrupt change in year 1955 and 1960 , while CUMSUM indicate the abrupt change (Figure 4.20 (c-d)) point 1962 and 1945 for annual precipitation and mean temperature for Dindori station, respectively. Most of the stations (62%) indicate the abrupt shifting year 1955 for annual precipitation, while 93.75% stations exhibit abrupt shifting year as 1960. However, 56.25% and 18.75% stations show significant (α=0.05) abrupt change for annual precipitation and mean temperature, respectively.

In general, 1955-1960 is the duration with abrupt decline in annual precipitation and 1960 is the year with sudden incline in the study area. Precipitation rate starts declining in the area began as early as 1955 and temperature suddenly rise in the year 1960 onwards.

Table 4.12: Abrupt change point (A.S), Start Year of trend (S.Y) and significant trend (S.T) year by SQMK and CUMSUM

Stations	Annual Precipitation				Annual Mean Temperature			
	SQMK			CUMSUM	SQMK			CUMSUM
	A.S.	S.Y.	S.T.	A.S.	A.S.	S.Y.	S.T.	A.S.
Balaghat	1958	1946	1955	1961	1960	1945	1960	1950
Bilaspur	1960	1942	NO	1986	1952	1908	NO	1945
Chhindwara	1955	1948	1958	1962	1960	1942	1960	1945
Damoh	**1955**	1948	1942	1962	1960	1945	1960	1945
Dindori	**1958**	1955	1955	1962	1960	1942	1960	1945
Hoshangabad	**1955**	1948	1955	1962	**1960**	1945	1942	1950
Jabalpur	**1958**	1955	1955	1962	1960	1942	1964	1950
Katni	**1955**	1946	1955	1963	1960	1945	1962	1950
Kawardha	1955	1948	1952	1963	**1960**	1942	1960	1950
Mandla	1967	1936	1958	1963	1960	1945	1960	1950
Narsimhapur	**1955**	1946	1942	1963	1960	1945	1960	1950
Raisen	**1955**	1946	1942	1963	**1960**	1945	1942	1950
Sagar	1955	1948	1942	1963	1960	1945	1942	1950
Seoni	1958	1945	1965	1963	1960	1945	1960	1950
Shahdol	**1955**	1948	1948	1963	1960	1942	1960	1950
Umaria	**1955**	1948	1955	1963	1960	1945	1965	1950

Note: Bold year (Abrupt shifting) indicate the significant abrupt change at 5% significance level

4.4.2 Assessment of Reference Evapotranspiration

Reference evapotranspiration (ET_O) is an important element of the hydrological cycle, and changes in ET_O are of great significance for agricultural water use planning, irrigation system design and management. Furthermore, evaporative demand is expected to alter under climate change and affect the sustainable development. It is governed by several climatic parameters such as temperature, relative humidity, wind speed, and sunshine.

4.4.2.1 Primary statistics of annual reference evapotranspiration

General statistics of average annual reference evapotranspiration is given in Table 4.13 and 4.14 for 12 stations of UNB and across the UNB. The average reference evapotranspiration in basin is 4.79 mm. During summer, the average annual ET_O is about 6.94 mm over the basin, while 3.70 mm in winter season. Maximum average annual value range lies between 4.97 mm (Balaghat) to 4.61 mm (Shahdol) over the basin.

Table 4.13: Primary statistical of average annual ET_O (mm) series of UNB stations

Stations	Mean	SD	C_V	C_S	C_k	Max	Min
Balaghat	4.97	0.06	1.18	0.94	2.63	5.20	4.84
Chhindwara	4.81	0.05	1.02	0.43	0.32	4.96	4.68
Dindori	4.69	0.07	1.47	1.30	4.69	4.98	4.50
Hoshangabad	4.89	0.05	0.99	0.04	-0.46	5.00	4.77
Jabalpur	4.73	0.06	1.17	0.76	2.45	4.94	4.59
Katni	4.80	0.06	1.24	0.66	2.48	5.01	4.63
Mandla	4.82	0.06	1.28	1.10	3.77	5.08	4.65
Narsimhapur	4.62	0.05	1.13	0.58	1.55	4.81	4.49
Raisen	4.88	0.05	1.09	-0.03	0.18	5.02	4.73
Sagar	4.78	0.05	1.15	0.14	0.39	4.93	4.63
Seoni	4.82	0.05	1.11	0.72	1.84	5.02	4.69
Shahdol	4.61	0.07	1.52	1.33	5.03	4.89	4.41

Table 4.14: Primary statistical parameters of average annual ET_O (mm) series of UNB

Season	Mean	SD	Cv	Cs	Ck	Max	Min
Annual	4.79	0.05	1.13	0.74	1.85	4.98	4.65
Spring	4.19	0.08	1.89	0.25	0.05	4.52	4.08
Summer	6.94	0.13	1.84	-0.01	0.74	7.30	6.56
Autumn	4.30	0.07	1.61	1.05	3.71	4.54	4.07
Winter	3.70	0.07	1.86	0.36	0.02	3.88	3.55

4.4.2.2 Trend detection of reference evapotranspiration

In this section, annual, seasonal and monthly trends in the reference evapotranspiration at 12 meteorological stations of UNB during 1901 to 2002 were examined applying the Mann–Kendall test and Sen's slope estimator. Spatial variability and temporal trend of ET_O were investigated over Narmada river basin (India).

Results of the MK test and Sen's slope for long term mean annual, seasonal series and monthly reference evapotranspiration are given in Table 4.15-4.16. Monthly analysis indicate strong trend in the month of October, November and December in the basin, at 1% significance level (Table 2). In upper part of the basin, no significant trend was found in month of January-June and August-September. Moreover, 23% stations experienced significant negative trend for July month. Moreover all the station were exhibit increasing trend at 99% and 95% confidence level, for annual series. For summer, 40% stations exhibit decreasing trend, while no trend was observed in spring. In general, at the temporal scale, 100% of the stations indicate increasing trend at annual, autumn and winter period.

4.4.2.3 Spatial variability of temporal changes in average annual ET_O

Spatial variability over the basin were evaluated and drawn by using a geospatial tool (ArcGIS10.2). Moreover, contour map of spatial variability generated using an Inverse-Distance-Weighted (IDW), interpolation methodology (Shifteh Some'e et al. 2012). In order to compute the annual and seasonal spatial variability in ET_O, magnitude of Sen's slope of natural log series were used. Percent change in mean value of climatic parameters estimated by using equation (4.20):

$$\Delta P = (e^{\beta} - 1) \text{ x } 100 \text{ x } t \qquad \ldots\ldots\ldots (4.20)$$

Where, ΔP = percent change of climatic parameter over period, β = Sen's trend slope (natural logarithmic series), and t = total length of trend period (years).

Spatial distribution of temporal changes in ET_O for annual and seasonal period shown in Figure 4.21. Change in mean annual ET_o series were observed from 3.52% (Shahdol) to 7.36% (Hosangabad). Moreover, 75% stations exhibit decreasing mean values for autumn seasonal series, while 16% stations (Chhidwara and Raisen) observed no change in mean values during 1901 to 2002. Maximum changes were observed in winter series that varies from 14.14% (Raisen) to 11.60% (Seoni) in mean value. Therefore it can be observed that changes in spring and winter season contributing the overall change in mean annual ET_O.

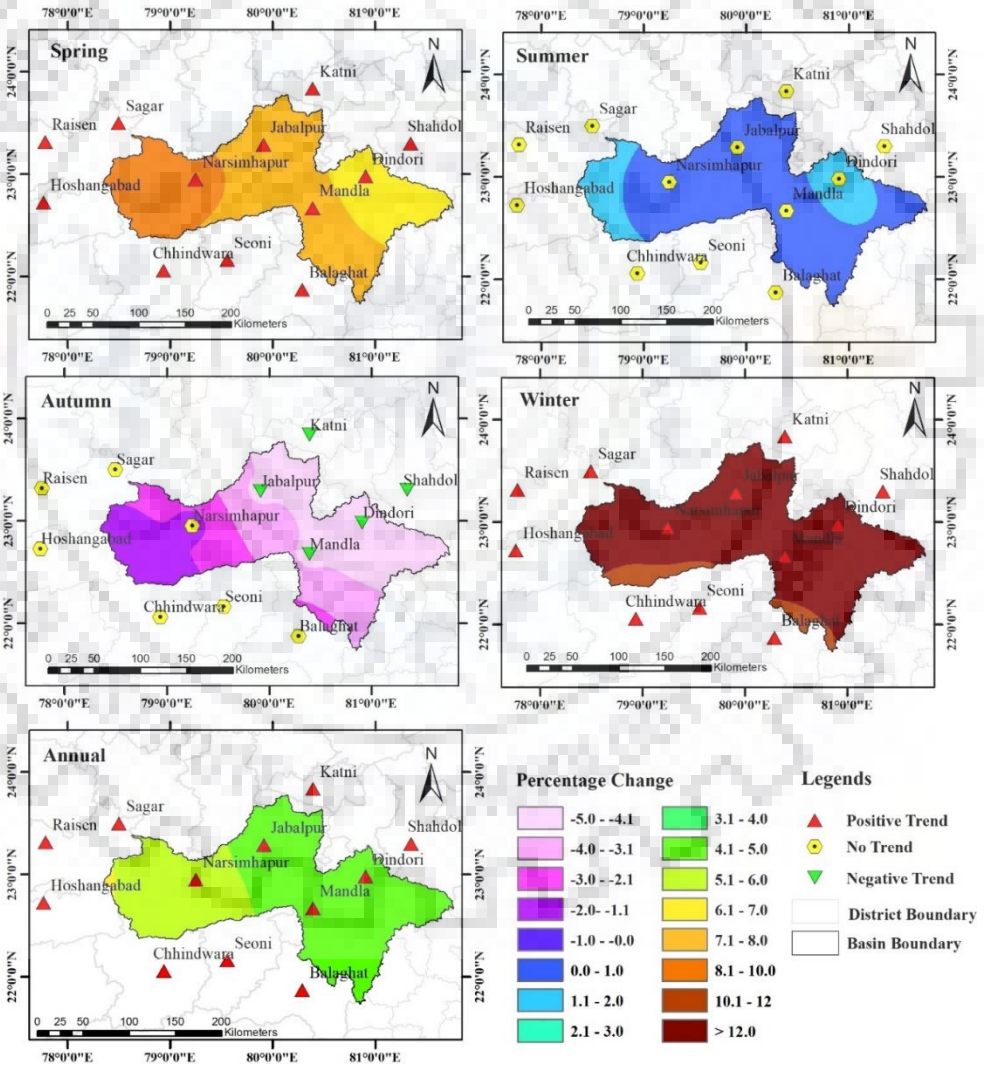

Figure 4.21: Average annual and seasonal evapotranspiration trends and percentage of change during 1901 to 2002 over Upper Narmada basin

Table 4.15: Mann-Kendall (MK-Z) test results for monthly reference evapotranspiration (ET_O)

Stations	Jan	Feb	Mar	Apr	May	Jun	Jul	Aug	Sep	Oct***	Nov***	Dec***
Balaghat	1.00	1.42	1.17	0.08	0.78	-0.43	-1.60	-0.97	1.21	2.87	4.41	4.05
Chhindwara	0.77	1.41	1.68*	0.66	0.60	-0.89	-0.34	-0.59	1.37	2.84	4.20	3.83
Dindori	0.88	1.28	0.75	0.53	0.52	-0.29	-1.77*	-1.51	-0.75	2.97	5.13	4.41
Hoshangabad	0.77	1.33	2.26**	1.44	0.71	-0.80	0.12	-0.31	1.06	2.79	4.43	4.53
Jabalpur	0.88	1.42	1.28	0.65	0.19	-0.73	-0.94	-0.91	-0.92	2.97	5.05	4.67
Katni	0.74	1.18	1.33	0.88	0.22	-0.70	-1.18	-1.21	-1.59	2.70	5.44	4.86
Mandla	0.75	1.33	0.92	0.34	0.60	-0.53	-1.80*	-1.22	-0.30	2.99	5.30	4.39
Narsimhapur	0.66	1.49	1.59	0.53	0.14	-0.94	-0.53	-0.24	0.33	2.75	4.46	4.37
Raisen	1.14	1.29	1.97**	1.28	0.28	-0.91	-0.09	0.02	0.53	2.81	4.51	4.52
Sagar	0.66	1.04	1.64	1.23	0.36	-0.95	-0.69	-0.42	-0.15	2.48	4.26	4.35
Seoni	1.21	1.63	1.34	0.28	0.65	-0.71	-1.31	-0.73	1.29	2.99	4.57	3.90
Shahdol	0.83	1.16	0.71	0.45	0.24	-0.51	-1.54	-1.90*	-1.01	2.86	5.48	4.69

*Note: ***, ** and * values indicate 1% ($Z_{critical}$ = ±2.58), 5% ($Z_{critical}$=± 1.96) and 10 % ($Z_{critical}$= ±1.65) of the significance level of trend, respectively. Positive and negative values shows the increasing and decreasing trend.*

Table 4.16: Mann-Kendall (MK-Z) and Sen's Slope (β) (mm/decade) test results for annual and seasonal reference evapotranspiration (ET_o)

Stations	Annual		Spring		Summer		Autumn		Winter	
	MK-Z	β	MK-Z	β	MK-Z	β	MK-Z	β	MK-Z	β
Balaghat	3.00***	0.0049	0.14	0.0078	-0.99	0.0006	3.46***	-0.0022	2.70***	0.0113
Chhindwara	3.51***	0.0056	0.29	0.0087	-0.04	0.0010	2.83***	0.0000	3.15***	0.0113
Dindori	2.30**	0.0040	0.29	0.0072	-1.99**	0.0015	4.09***	-0.0049	2.60***	0.0126
Hoshangabad	4.18***	0.0071	0.81	0.0094	0.48	0.0031	2.69***	0.0007	3.36***	0.0125
Jabalpur	2.95***	0.0045	0.17	0.0083	-1.69*	0.0008	2.07**	-0.0039	3.00***	0.0128
Katni	2.64***	0.0045	0.15	0.0077	-2.33**	0.0006	4.12***	-0.0059	2.82***	0.0130
Mandla	2.61***	0.0043	0.11	0.0080	-1.68*	0.0000	4.20***	-0.0039	2.72***	0.0127
Narsimhapur	3.29***	0.0052	0.08	0.0089	-0.86	0.0000	3.02***	-0.0018	3.08***	0.0123
Raisen	3.82***	0.0068	0.49	0.0106	-0.10	0.0022	2.61***	0.0000	3.39***	0.0135
Sagar	3.01***	0.0056	0.26	0.0088	-0.81	0.0013	2.48***	-0.0024	2.93***	0.0123
Seoni	3.31***	0.0049	0.14	0.0086	-1.04	0.0000	3.36***	-0.0020	3.22***	0.0111
Shahdol	1.95*	0.0034	-0.02	0.0066	-2.21**	0.0005	4.44***	-0.0058	2.51**	0.0130

*Note: ***, ** and * values indicate 1% ($Z_{critical}$ = ±2.58), 5% ($Z_{critical}$=± 1.96) and 10 % ($Z_{critical}$= ±1.65) of the significance level of trend, respectively. Positive and negative values show the increasing and decreasing trend.*

4.5 CONCLUDING REMARKS

The change in meteorological distribution mainly influenced by the ecosystem and landscape change. However, changes in precipitation rate and temperature are main cause of climate change and deforestation in the upper part of river basin. For planning and management of water resources, it is quite important to understand the distribution and variability of meteorological parameters.

Trend analysis is one of the most significant tools to analyse the global warming problem that indicate the past and future changes in meteorological, hydro-climatological parameters. In this chapter, trend detection has been carried out for long term precipitation data applying regression analysis, MK test and conjunction of DWT and sequential MK tests over India whereas trends of the monthly and annual precipitation and mean temperature data observed at 16 stations of UNB by applying three different trend tests, namely, the Mann-Kendall, Sen's Slope and a relatively new methodology Innovative Trend Analysis (ITA). Regression analysis was carried out on the basis of the classical climate period of 30 years.

The results of this study imply that the mean values of precipitation are decreasing in most of the study area in the last 30-year period. It was found that there are both positive and negative trends existing in each zone for the monsoon datasets. Annual and monsoon precipitation data show a negative trend; however, zones NMI and NEI show a positive trend for annual and monsoon datasets. The most suitable mother wavelet was selected using the criteria of MRE and the criterion relative error (E_r) proposed by Nalley et al. (2012). Applying this criterion, the DWT Daubechies wavelets db6 and db10 were selected for annual and monthly datasets, respectively. Application of DWT on annual series implied 2-, 4- and 8-year fluctuations in the NMI zone, indicating a positive trend in rainfall, whereas zones WPI, SPI and WPI (with 2- and 4-year fluctuations) experienced a negative trend at the same periodicities, at the 0.05 (5%) significance level. In the monsoon series, a positive trend was found over NMI and NEI decomposed series at 2-, 4- and 8-year periodicity, whereas WPI, EPI and SPI indicated a negative trend at the same periodicity. Considering India as whole (AI), it was found a negative trend in all zones except NMI and NEI. Therefore, visualization of extreme events was examined at different threshold limits. The same intensity of positive and negative fluctuations indicated the same colour spectrum, which is one of the limitations of the visualization study and may form the subject of future work in this area.

At local scale, trends of the monthly and annual precipitation and mean temperature data observed at 16 stations of UNB by applying three different trend tests, namely, the Mann-Kendall, Sen's Slope and a relatively new methodology Innovative Trend Analysis (ITA). ITA was employed to detect trend in extreme values of meteorological parameters (annual precipitation and mean temperature). Variation on these meteorological extremes parameters influence the occurrence of hydrologic extremes (floods and droughts). However, results imply that very few stations exhibit the negative trend for precipitation, while all the stations show positive trend for mean temperature over 16 stations of UNB. A comparative study was carried out between three methods i.e. ITA, MK-test and Sen's slope, to check the suitability of ITA against nonparametric tests. In result, ITA shows the strong agreement with both methods (MK test and Sen's slope), 97.5% and 77.5% in 'ITA versus MK test' and 'ITA versus Sen's slope'. Therefore ITA has many advantages over MK test and Sen's slope estimator, as it is based on certain assumption and can be analyzed with less and all ranges of data. In the recent studies, wavelet analysis is considered which is a quite popular for trend analysis and periodicity identification in hydrological time series, but it is quite interesting to analyze and visualize the meteorological extreme events. In this study, meteorological extremes were identified based on three different threshold (0.5SD, SD and 1.5SD) values considering the Daubechies (db3) mother wavelet, and decomposition level as '$\log_{10}$ (N)' ('N' is the length of time series) of DWT. Results of Balaghat station indicates that the 5 and 4 extreme events for precipitation and temperature series employ the 1.5SD thresholding. In addition, abrupt changes analysis were carried out to detect the significant shifting and start of significant change applying sequential Mann Kendall (SQMK) in 16 stations of study area. Further change points obtained by SQMK were compared with the change year of CUMSUM. Results indicate most of the significant abrupt change station indicate the significant change year is 1955 (77.78%) and 1960 (100%) for precipitation and temperature, respectively. Moreover occurrence of abrupt change point investigated as 1955-1960 by SQMK and 1961-1963 by CUMSUM for precipitation, while change point 1960 by SQMK and 1945-1950 by CUMSUM for temperature over 16 stations of UNB.

The observed historical flood Madhya Pradesh received about 362 mm of rainfall between June 1 to July 10 in 2016. This is a 72 per cent increase from the normal monsoon (210 mm) in the state during this time (2016) of the year. Moreover the 1970 flood on the river was the highest for the last 107 years.

The findings in this study provide a new understanding of extreme events trend evaluation that could probably the cause of flood and drought in the area. This will help in short or long term planning and development in water resources of the region. These information can also assist to manage the agriculture water supply, and to update the engineer and stakeholders for decision making.

CHAPTER 5

DYNAMICS OF LAND USE LAND COVER AND FUTURE PROJECTION

5.1 GENERAL

In the recent past, many researchers have investigated the land use land cover (LULC) changes measurements, and examined the reason of changes (Geng et al. 2014; Meshesha et al. 2016; Mialhe et al. 2015). Land cover can be defined as all physical materials at the surface of the earth such as water bodies, natural vegetation whereas land use is described as the land utilized by people for socio-economic activities (Lambin et al. 2003; Meyer and BL Turner 1994; Nagendra et al. 2004). Dynamic LULC changes were investigated by many researchers in recent past using remote sensing satellite images data and techniques and geospatial tools viz. ERDAS Imagine, Geographic Information Systems (GIS) (Dewan and Yamaguchi 2009; Jat et al. 2008; Li and Yeh 2004; Mondal et al. 2014; Mundia and Aniya 2005; Rozenstein and Karnieli 2011; Saadat et al. 2011; Shalaby and Tateishi 2007; Weng 2002; Xiao et al. 2006).

Detection of LULC changes from multi-temporal satellite images is widely used, even though it is a challenging task (Lambin et al. 2001; Meshesha et al. 2016; Prabhakar and Tiwari 2015). These change detection included the monitoring of forest changes, agricultural assessment, changes in land cover and development in built-up area (Abd El-Kawy et al. 2011; Iqbal and Khan 2014; Jaiswal et al. 1999; Kabba and Li 2011; Pervez and Henebry 2015; Rao and Pant 2001; Srivastava et al. 2012). The main reason of changes in land-use and land-cover is governed by many environment-development policies. Kabba and Li (2011) investigated that population and poverty are not alone and sole reason of LULC change, it depends upon the chances and constraints for new land uses that are provided by local as well as national markets and policies. Due to restriction of government agencies over the expansion of agricultural land, deforestation impact by settlement. Jaiswal et al. (1999) quantified the LULC changes by remote sensing data over a period of 30 years in a part of Shahdol, Madhya Pradesh (India). In the results, loss of natural vegetation was calculated to be 22% and 14% of the land was transformed into barren between 1967 and 1996. It was noticed that human settlement and economic development, impact the natural vegetation transformed in to agricultural land. Authors proposed historical cropland datasets might be used for the climate and ecosystem models to understand the climate change and impact on ecosystem.

Furthermore, Narmada River supports meeting agricultural water demand and requirement of people with distinguish culture and traditions ranging from indigenous tribal people inhabitation in the forest areas to the rural population. In last few decades, the LULC of Upper Narmada Basin (UNB) has been changed due to substantial anthropogenic interventions. Construction of hydraulic structure and increase settlement had opened opportunities for resource exploitation and caused rapid change in LULC which continued to the present. Many hill stations have come up and grown beside constructions of new structures and residential areas. These have significantly altered the UNB landscape. Increasing population, became major sources of resource extraction leaving the forest fragmented. Recently, LULC changes in the UNB are driven by economic gains. The "Narmada Bachao Andolan" a campaign initiated in Madhya Pradesh during 1985 opened up forest land for food crop cultivation, which ultimately affected by construction of large dams along the river. Probably, this is the first attempt where projection of LULC in near future is made based on previous decadal LULC and socio-economic datasets.

Moreover, the objectives of this chapter is to estimate the LULC changes based on remote sensing data, and generate the projection of land use land cover changes in near future, using CA-Markov based model. Land-cover changes were investigated on the basis of temporal series of remote sensing multispectral satellite images of Landsat. The chapter presents the (i) identification of classes and distribution percentages of LULC; (ii) estimate the percentage changes in LULC of area between 1990 and 2000 and 2010 and 2015 and quantify the rates of change; (iii) accuracy assessment of classified LULC; (iv) applying CA-Markov to predict LULC allocations in the near future of year 2030.

5.2 BRIEF DISCRIPTION ABOUT DEMOGRAPHY OF MAIN CITIES

On the basis of physiography, the UNB can be divided into hilly and plain regions. Upper eastern part covered by hills, whereas lower middle area are covered by mixed forest. The plain regions in between the hilly tracts and in the lower reaches are broad and fertile areas well suited for cultivation (Figure 5.1). There are mainly four districts lies in the study area, Mandla, Jabalpur, Narsingpur and Dindori. Jabalpur is the largest district among all four the district as per area wise and population (Figure 5.2). The population growth of Jabalpur district 21.67% and 14.51%, Mandla 14.73% and 17.97%, Narsighpur 21.92% and 14.01% and Dindori district 18.41 % and 17.39 % were occurred in the periods of 1991 to 2001 and 2001 to 2011 respectively (www.citypopulation.de).

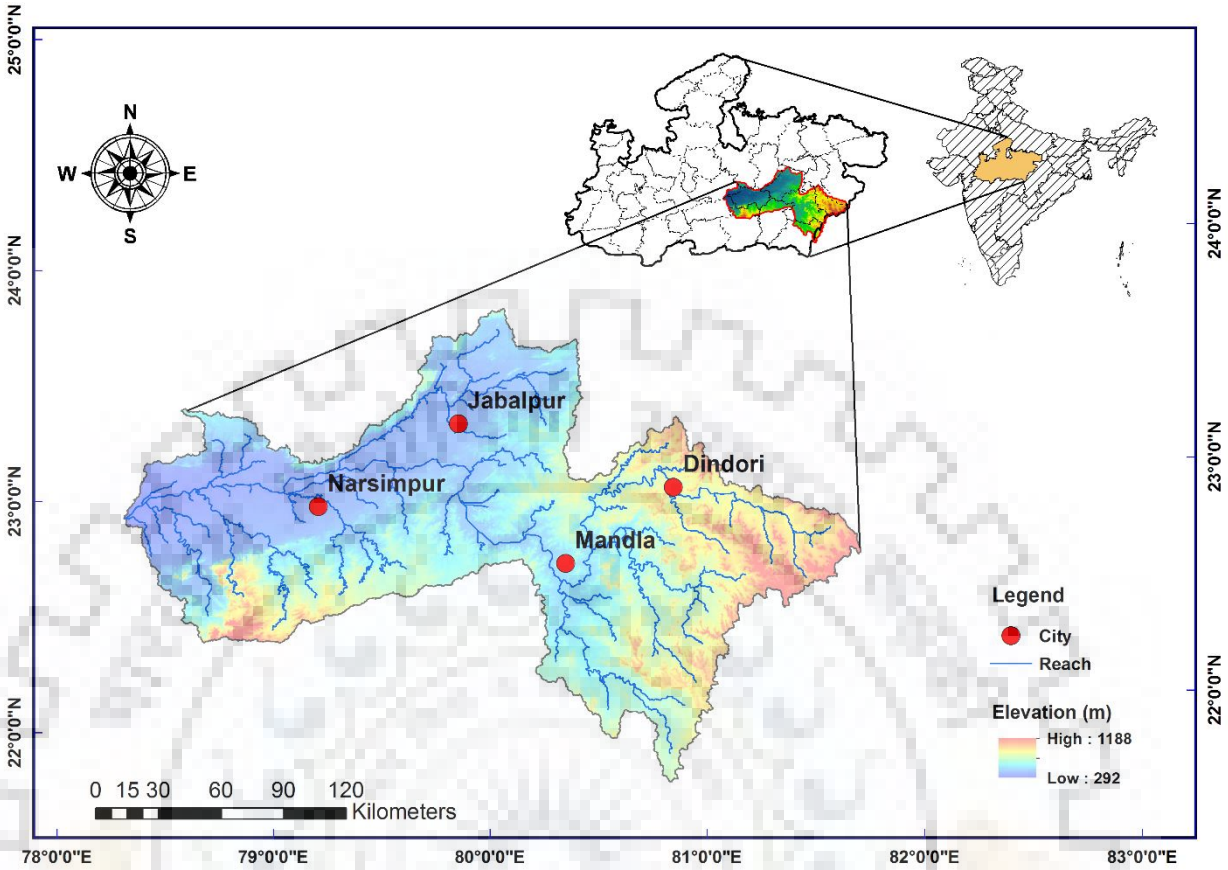

Figure 5.1: Location of main cities of Upper Narmada Basin

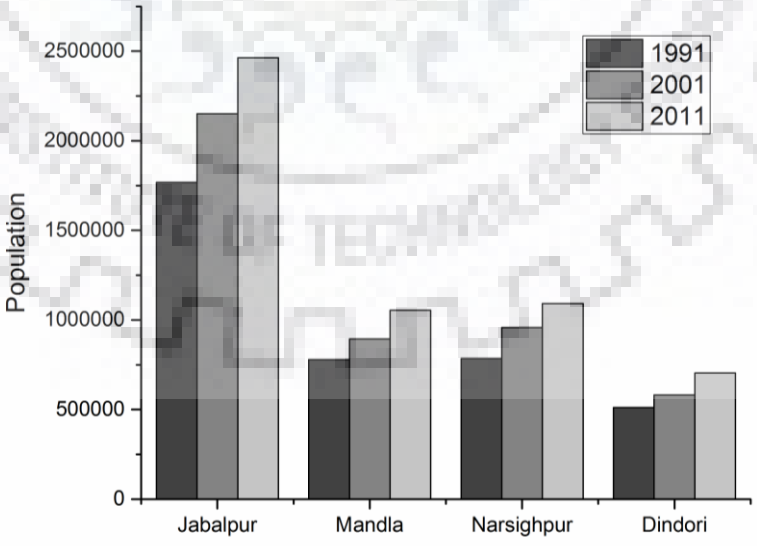

Figure 5.2: Population growth of main cities in UNB for 1991, 2001, and 2011

5.3 SITE VISIT AND DATA COLLECTION

5.3.1 Field Data Collection

Field visits were conducted to collect the 590 ground truth data in the study area. During the field visit data were collected from different locations to validate the classified image. Field data and locations were taken using the global positioning system (GPS) and photographs. Historic land cover data was collected by interviewing the senior native persons. Based on the interview and data collection, study area classified into five categories, viz. water bodies, natural vegetation, barren land, cropland and built-up area. Ground truth points were collected to improve the LULC classification and accuracy assessment. Toposheets from Survey of at 1:250,000 scale were used for ground navigation.

5.3.2 Remote Sensing Data

Remote sensing satellite images of Landsat were used in LULC change detection during 1990 to 2015. Landsat Thematic Mapper and Enhanced Thematic Mapper plus (ETM) images downloaded from the United States Geological Survey (USGS) based website (https://earthexplorer.usgs.gov). The images with less than 10% of cloud cover were downloaded from the website. The study area occupied by the 5 satellite images (Path-Row 143-44, 143-45, 144-44, 144-45, 145-44). Total 20 images of post monsoon (mid October to November) were downloaded for the study for 1990, 2000, 2010 and 2015 (Table 5.1). Landsat images were atmospherically corrected to remove the cloud and cloud cover from all images prior to image analysis.

Table 5.1: Description of satellite images

Year	Acquisition Month	Satellite	Sensor	Spatial Resolution
1990	Oct-Nov	LANDSAT 5	Thematic Mapper	30m
2000	Oct-Nov	LANDSAT 7	Enhanced Thematic Mapper	30m
2010	Oct-Nov	LANDSAT 5	Thematic Mapper	30m
2015	Oct-Nov	LANDSAT 8	Operational Land Imager (OLI) and Thermal Infrared Sensor (TIRS)	30m

5.4 METHODOLGY

Landsat satellite images are used to classify the land use. All four images (1990, 2000, 2010 and 2015) are classified employ supervised classification algorithm in this area. It is one of the most popular classification method, which is usually suitable in identification of few classes. Geospatial tools ERDAS Imagine-2014 and ArcGIS 10.2 were used to process and prepare the LULC map. The overall methodology given in Figure 5.3:

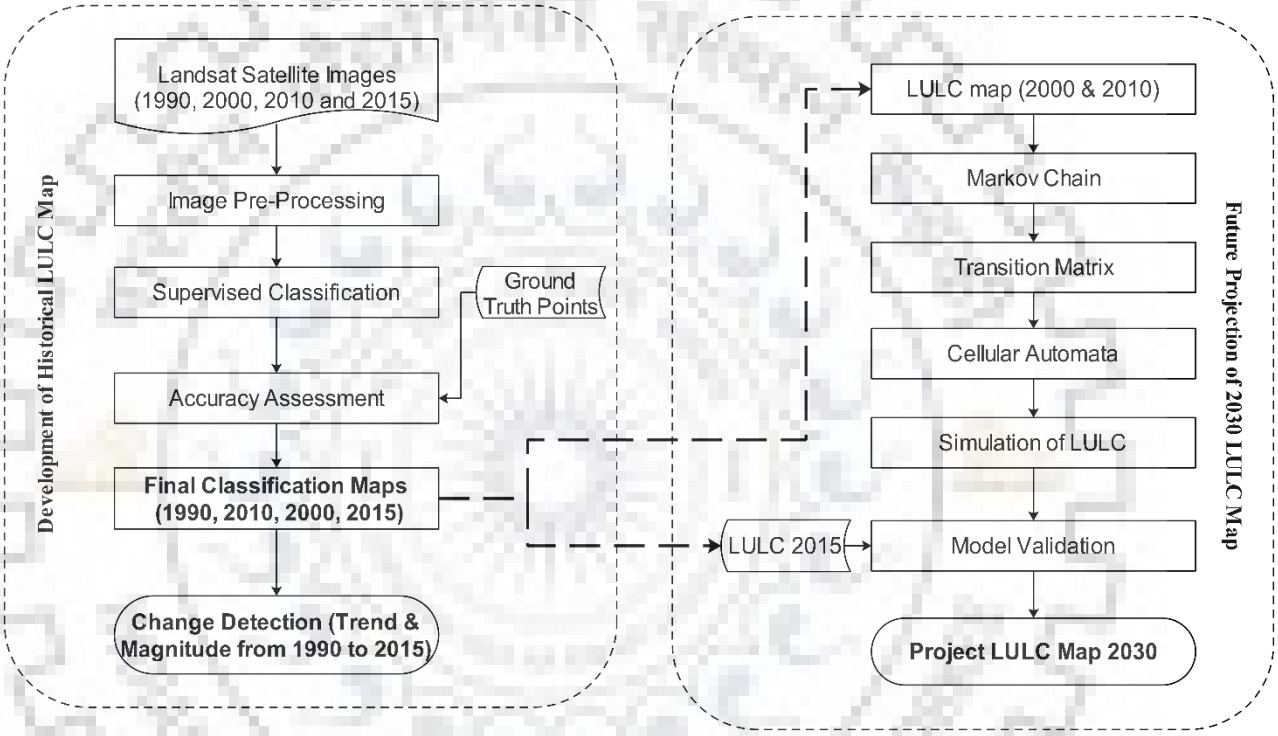

Figure 5.3: Flow chart of land use mapping and future projection

5.4.1 LULC Class Distribution

In order to perform the classification, supervised classification method were applied in the ERDAS Imagine 2014 (a geospatial data processing tool). The ambiguous area and location in classification were recoded by taking help from topography map, ground truth points and by google map. There were five types of LULC identified in the study area, as (1) Built-up area (2) Cropland (3) Natural Vegetation (4) Water Bodies (5) Barren Land, description of these categories are given in Table 5.2.

Table 5.2: Descriptions of land use land cover types

LULC Classes	Classes Code	Description
Water bodies	WB	River, permanent open water, lakes, ponds and reservoirs
Built-up Area	BA	Residential, commercial and services, industrial, transportation, roads, mixed urban, and other urban
Natural Vegetation	NV	Deciduous forest, mixed forest lands, open forest, scrub and others
Cropland	CL	Agricultural area, crop fields, fallow lands and vegetable lands
Barren Land	BL	Open soils, landfill sites, and areas of active excavation, river banks

5.4.2 Image pre-processing

Due to the systematic mistakes and inaccuracy of the sensing devices, the pre-processing is an important step in the land use mapping. In this study, the pre-processing included radiometric and geometric corrections of the satellite images. Radiometric correction is the process of histogram matching of the satellite images from different time periods, whereas geometric correction meant co-registration of the satellite images, so that the images could overlap in the best possible way. This is important because some of the essential methods are based on the comparison of the two images from different time periods, e.g. supervised classification.

The data processing was carried out using ArcGIS10.2 and ERDAS IMAGINE 2014 prior to analysis. After the initial visual image analysis to confirm the agreement of the geo-referenced images, a subset of the image was extracted to include the area of interest and the surrounding areas. Satellite images of extracted area are required radiometric correction for gain and bias correction before LULC classification. In this correction, digital number (DN) derived from the images is converted to the spectral radiance at sensor by data calibration (Shalaby et el. 2005, Yuan et al. 2005).

$$L_{TOA} = \frac{(L_{MAX} - L_{MIN})}{(QCAL_{MAX} - QCAL_{MIN})} * (DN - QCAL_{MIN}) + L_{MIN} \quad \text{……. (5.1)}$$

Where, L_{TOA} is the solar irradiance at top of the atmosphere, L_{MAX} and L_{MIN} represent the maximum and minimum value, $QCAL_{MAX}$ and $QCAL_{MIN}$ are the maximum and minimum DN values (255 or

1) and the L_{MAX} and L_{MIN} are the gain and offset respectively available from the header file of the image.

Precise per-pixel registration of satellite data is requisite for change detection since the possible exists for registration errors to be interpreted as LULC change, leading to an overestimation of actual change (Stow, 1999). Change detection analysis is performed on a pixel-by-pixel basis; therefore any mis-registration greater than one pixel will provide an anomalous result of that pixel. To overcome this problem, the root mean-square error (RMSE) between any two dates should not exceed 0.5 pixel (Lunetta and Elvidge, 1998). In this study geometric correction was carried out using ground control points from topographic maps with scale of 1:250,000 to geocode the image. The RMSE between the two images was less than 0.5 pixel which is acceptable. The RMSE could be defined as the deviations between GCP and GP location as predicted by the fitted-polynomial and their actual locations.

5.4.3 Markov Model

In order to predict the future land use land cover change, hybrid model of Markov and Cellular Automata (CA-Markov) were used in this study. Markov Chain is the tool used for modelling the future prediction. This model consider the past changes (conversion) and rate of changes (conversion) to predict the particular class. This model requires initial state and transition matrix. Conversion from one state to another state is called transition matrix (Halmy et al. 2015) as given in equation (5.2):

$$L = L_{ij} = \begin{bmatrix} L_{11} & L_{12} & \cdots & L_{1n} \\ L_{21} & L_{22} & \dots & L_{2n} \\ \cdots & \cdots & \cdots & \cdots \\ L_{n1} & L_{n2} & \cdots & L_{nn} \end{bmatrix} \quad \dots (5.2)$$

Where, L indicates transition probability state i to state j. Equation (1) must satisfy the next conditions (Equation 5.3):

$$\sum_{j=1}^{n} L_{ij} = 1 \qquad 0 \le L_{ij} \le 1 \quad \dots\dots (5.3)$$

The main step of the Markov model lies in getting a primary matrix and matrix of transition probability (L_{ij}). Then the Markov forecast model mentioned as equation (5.4):

$$L_n = L_{n-1} \qquad L_{ij} = L_{(0)} L^n_{ij,} \qquad \ldots\ldots (5.4)$$

Where, L_n stands for transition probability of any time and L_0 stands for primary matrix (Fan et al. 2008; Li et al. 2015; Singh et al. 2015).

5.4.4 Cellular Automata

To predict the LULC in the study area, output from Markov chain (transition area matrices) was used in the Cellular Automata (CA) model (Foody 2002; Yang et al. 2014; Yuan et al. 2005). In this approach, Cellular automata (CA) integrates with the Markov Chain model to predict the future LULC (Deep and Saklani 2014; Mitsova et al. 2011; Ridd and Liu 1998). The Markov Chain describes the transition probability matrix that indicates the probability of LULC changes from one class to another class in a time interval (Halmy et al. 2015; Marshall and Randhir 2008; Yang et al. 2014). The probability of class changes estimated by Markov model incorporated in the CA approach to add spatial distribution of each class in the study area. The distribution of each class pixel changes by the neighbouring pixel according to probability transition matrix. In CA model, a contiguity filter of 5x5 used to model the changes in predicted LULC. In this study, transition probability matrix was developed using LULC maps from 2000 and 2010 applying Markov model. The transition probability matrix was used in the CA to simulate the LULC of 2015 and compare with the actual map of 2015. Finally, LULC map for 2030 were generated based on the CA-Markov model.

5.5 LAND USE LAND COVER MAP DEVELOPMENT AND CHANGE DETECTION

5.5.1 LULC Classification

The distribution of LULC classes for 1990, 2000, 2010 and 2015 were carried out using Landsat satellite data. The satellite data were downloaded for the post monsoon (late October and November) of each year. Radiometric and atmospheric correction were carried out on Landsat images. Four bands (1-4) of the Landsat TM image, visible and near infrared ranges were selected for the processing. The pre-processed satellite images were classified into five land use land cover classes (Figure 5.4 – Figure 5.5). Ground truth data from field survey of different locations were used for accuracy assessment. Distribution of different classes in developed land use map of year 1990, 2000, 2010 and 2015 were mentioned in Table 5.3 and Figure 5.4. Due to increase in cropland and built-up area, continuously decrease in natural vegetation are observed from 49.18% (1990) to 44.49%

(2000) to 41.42% (2010) to 39.66% (2015). Therefore, built-up area were increasing continuously from 0.20% (1990) to 0.37% (2000) to 0.60% (2010) to 0.72% (2015) due to population migration, cropland area increased from 47.36% (1990) to 52.67% (2000) to 54.99% (2010) to 56.79% (2015).

Table 5.3: Distribution of classes for 1990, 2000, 2010 and 2015

Class	1990		2000		2010		2015	
	Area		Area		Area		Area	
	sq.km	%	sq.km	%	sq.km	%	sq.km	%
Water bodies	398.43	1.23	339.48	1.04	455.81	1.40	408.94	1.26
Built-up Area	63.57	0.20	121.41	0.37	193.62	0.60	233.89	0.72
Vegetation	15983.56	49.18	14460.77	44.49	13462.94	41.42	12890.64	39.66
Cropland	15390.74	47.36	17118.35	52.67	17873.32	54.99	18458.21	56.79
Barren Land	663.71	2.04	459.99	1.42	514.31	1.58	508.33	1.56

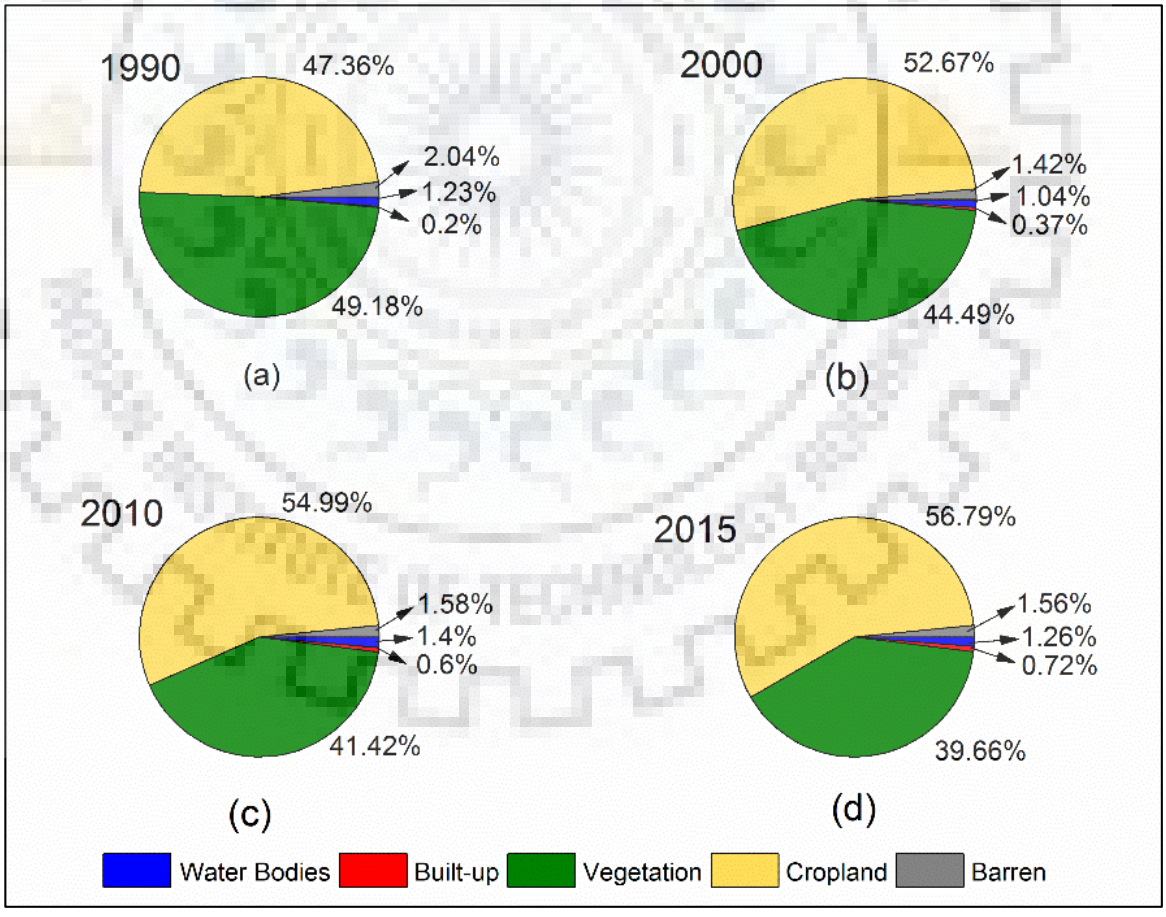

Figure 5.4: Classes of LULC of year of 1990, 2000, 2010 and 2015

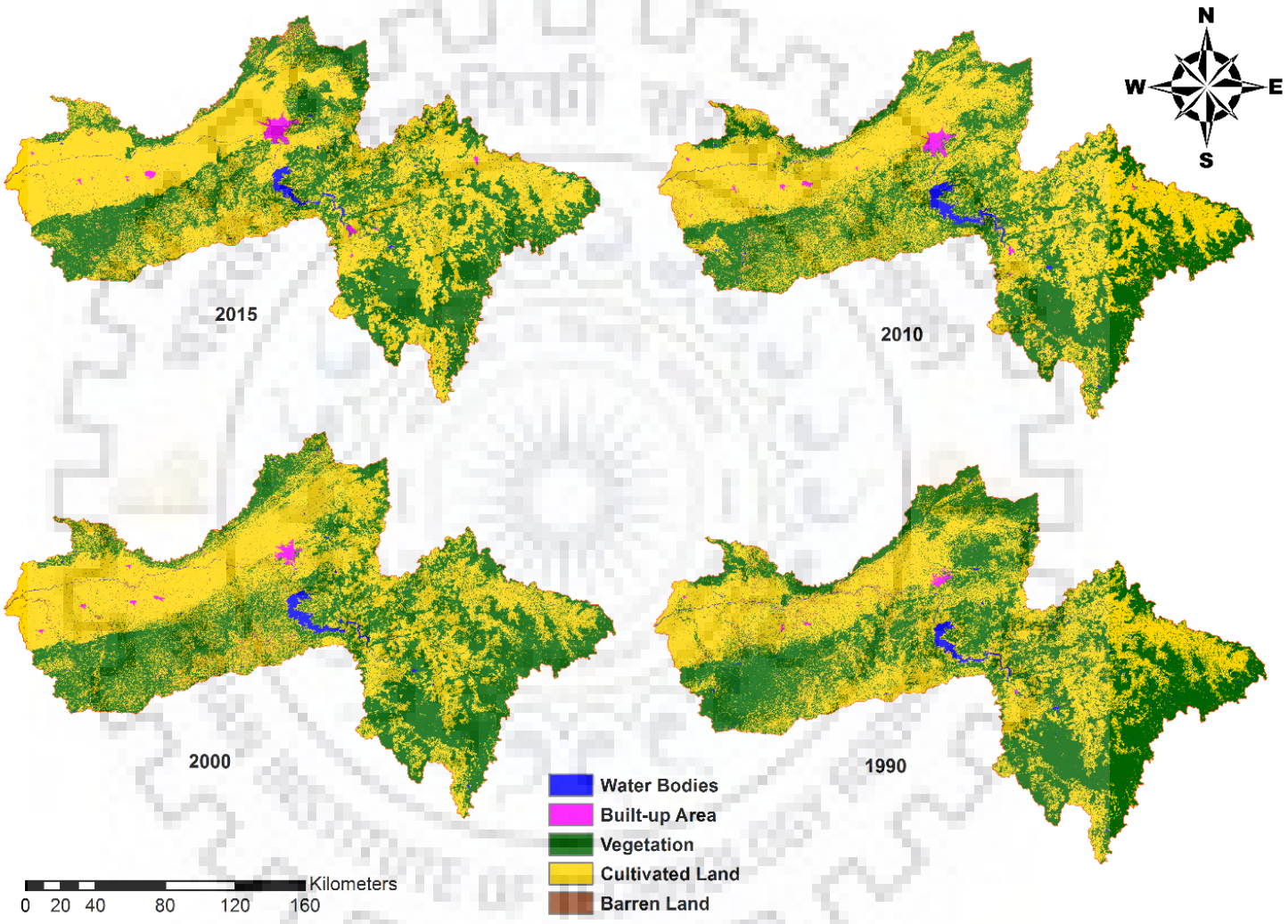

Figure 5.5: Land use land cover map for year of 2015, 2010, 2000 and 2015

5.5.2 Accuracy Assessment

For accuracy assessment, random points were generated across each LULC map. These points were cross-checked with the reference data. In this study, Google Earth integrated in ERDAS Imagine 2014 has been used as reference data for accuracy assessment. In addition to this, ground truth verification was carried out using Global Positioning System (GPS) during field visit. These GPS points were also utilized for classification accuracy assessment. In this analysis, matching points in both satellite-derived LULC map and reference map were denoted by the same class number, otherwise it was replaced with corrected class number. Then, accuracy assessment statistics were generated from the population error matrix of these maps (Jaiswal et al. 1999; Rao and Pant 2001). This matrix included the overall accuracy, user's accuracy and produce's accuracy, and Kappa statics. The user's accuracy is the percentage of points classified in to classes which they belong according to the classified points, and the producer's accuracy is the percentage of reference points that belongs to the classified classes. The average overall accuracy derived based on the estimated user's and producer's accuracy. The kappa statistics is estimated by using observed accuracy (η_O) and expected accuracy(η_E) (Myint et al. 2011).

$$\text{Kappa } (K_p) = \frac{\eta_O - \eta_E}{1 - \eta_E} \quad \ldots. (5.5)$$

The accuracy of the classified LULC was evaluated using error or confusion matrix to compare with the ground truth data based on field survey (Geng et al. 2014; Neupane and Kumar 2015). The random points of 170,190 and 180 were generated for the year 1990, 2000 and 2010 respectively. The location points of 2015 were collected by using the geographical positioning system (GPS) tool. The overall accuracy and Kappa statistics are presented in Table 5.4. For each class of LULC, a contingency matrix was evaluated that represent the user accuracy (UA) and producer accuracy (PA). Table 5.4 indicates overall accuracy 89.88%, 86.11%, 86.84% and 85.88% for the 2015, 2010, 2000 and 1990, respectively. The Kappa statistics (K_p) for 2015, 2010, 2000, and 1990 were 0.87, 0.82, 0.83 and 0.82 respectively. The confusion matrix of year 1990, 2000, 2010 and 2015 are presented in Table (5.5-5.8), respectively.

Table 5.4: Overall accuracy and Kappa statistics (*Kp*) of LULC classification

Year	Classification Accuracy (%)	Kappa Statics (K_p)
2015	89.88	0.87
2010	86.11	0.82
2000	86.84	0.83
1990	85.88	0.82

Table 5.5: Confusion matrix of LULC map of 1990

Classified Data	Water bodies	Built-up Area	Vegetation	Cropland	Barren Land	**CT**	**UA (%)**
Water bodies	**20**	1	2	0	0	**23**	**86.96%**
Built-up Area	0	**24**	0	3	1	**28**	**85.71%**
Vegetation	2	0	**40**	3	3	**48**	**83.33%**
Cropland	0	2	1	**40**	2	**45**	**88.89%**
Barren Land	0	1	0	3	**22**	**26**	**84.62%**
RT	**22**	**28**	**43**	**49**	**28**	**170**	-
PA (%)	**90.91%**	**85.71%**	**93.02%**	**81.63%**	**78.57%**	-	-

Table 5.6: Confusion matrix of LULC map of 2000

Classified Data	Water bodies	Built-up Area	Vegetation	Cropland	Barren Land	**CT**	**UA (%)**
Water bodies	**28**	0	3	1	0	**32**	**87.50%**
Built-up Area	0	**20**	2	2	0	**24**	**83.33%**
Vegetation	0	0	**44**	3	1	**48**	**91.67%**
Cropland	2	1	3	**53**	2	**62**	**85.48%**
Barren Land	0	1	0	3	**20**	**24**	**83.33%**
RT	**30**	**22**	**52**	**62**	**23**	**190**	-
PA (%)	**93.33%**	**90.91%**	**84.62%**	**85.48%**	**86.96%**	-	-

Table 5.7: Confusion matrix of LULC map of 2010

Classified Data	Water bodies	Built-up Area	Vegetation	Cropland	Barren Land	**CT**	**UA (%)**
Water bodies	**27**	0	3	0	0	**30**	**90.00%**
Built-up Area	0	**25**	3	2	0	**30**	**83.33%**
Vegetation	1	0	**45**	3	1	**50**	**90.00%**
Cropland	0	2	4	**41**	3	**50**	**82.00%**
Barren Land	1	0	0	2	**17**	**20**	**85.00%**
RT	**29**	**27**	**55**	**48**	**21**	**180**	-
PA (%)	**93.10%**	**92.59%**	**81.82%**	**85.42%**	**80.95%**	-	-

Table 5.8: Confusion matrix of LULC map of 2015

Classified Data	Water bodies	Built-up Area	Vegetation	Cropland	Barren Land	**CT**	**UA (%)**
Water bodies	**30**	0	3	2	0	**35**	**85.71%**
Built-up Area	1	**44**	0	3	0	**48**	**91.67%**
Vegetation	0	2	**56**	4	0	**62**	**90.32%**
Cropland	0	3	3	**79**	1	**86**	**91.86%**
Barren Land	0	3	0	1	**22**	**26**	**84.62%**
RT	**31**	**52**	**62**	**89**	**23**	**257**	**-**
PA (%)	**96.77%**	**84.61%**	**90.32%**	**88.76%**	**95.65%**	-	-

Note: CT is classified totals, UA is user's accuracy, RT is Reference Totals and PA is producer's accuracy

5.5.3 LULC Change detection

The change detection in LULC were carried out and analyzed for a duration of 25 years (1990-2015) (Figure 5.6-5.8). Due to shifting and growth of population in the region, built-up area increased from 0.18% (2000) to 0.52% (2015) during 25 years, with respect to the base year of 1990 (Figure 5.6). The rate of growth of built-up area were noticed 68126 hectares per year during 25 year of duration (1990-2015). In last two decades, changes were found with rate of 57831 hectare per year and 130047 hectare per year during the period of 1990-2000 and 2001-2010, respectively. In order to analyses the first 10 years (i.e.1990-2000) with respect to the base year 1990, natural vegetation decreased by 9.53%, whereas it was decreased by 19.35% in 25 years of duration. In order to analyze the cropland, it was increased by 19.93% from 1990 to 2015 in 25 years.

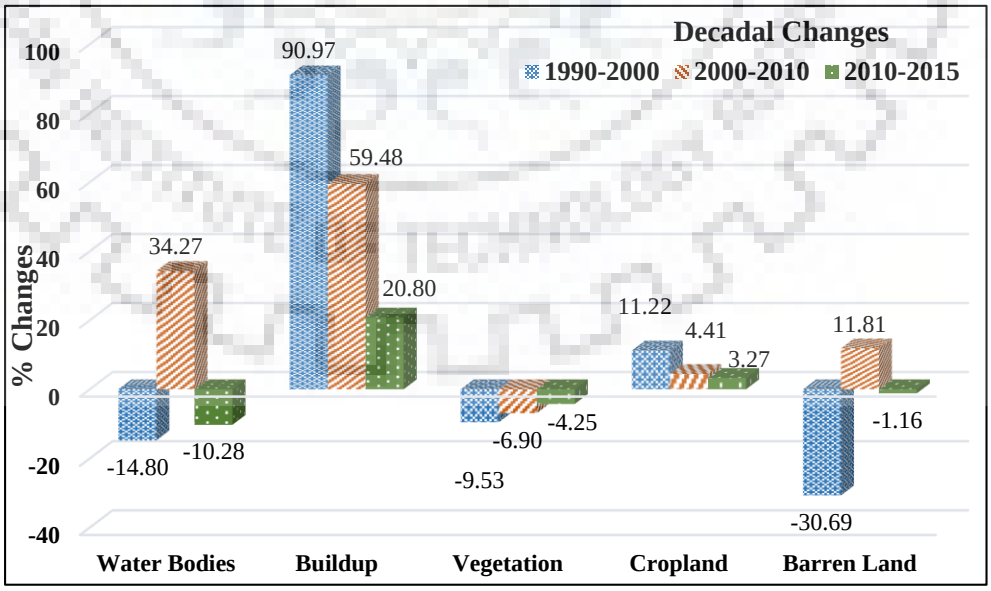

Figure 5.4: Decadal percentage changes in LULC classes from 1990 to 2015

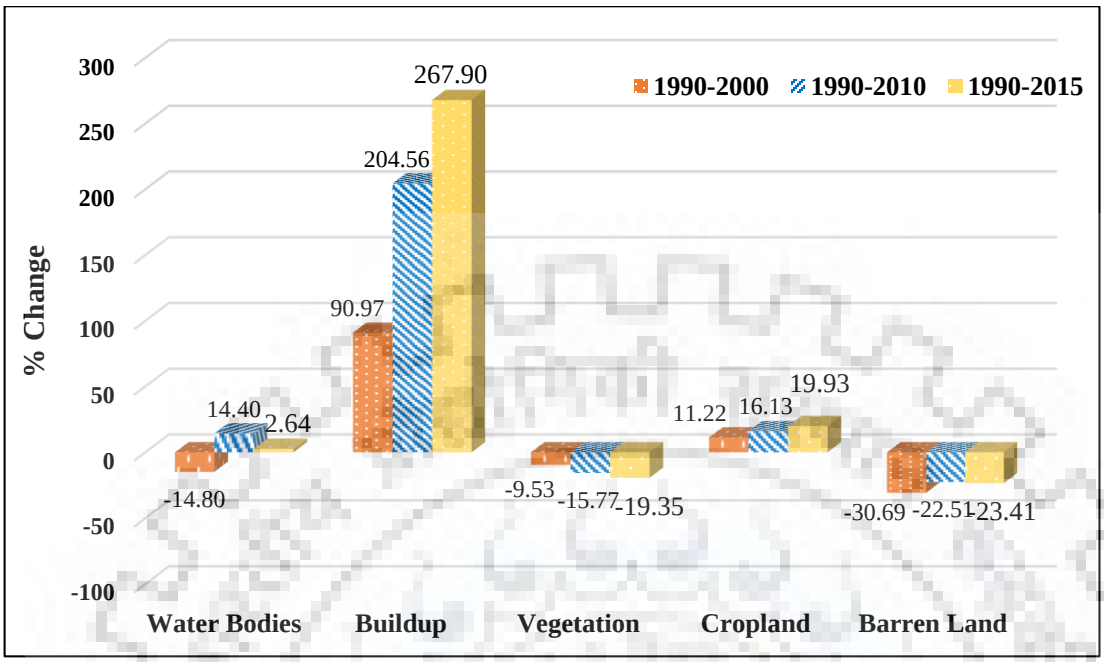

Figure 5.5: Percentage Changes in LULC classes with reference to 1990

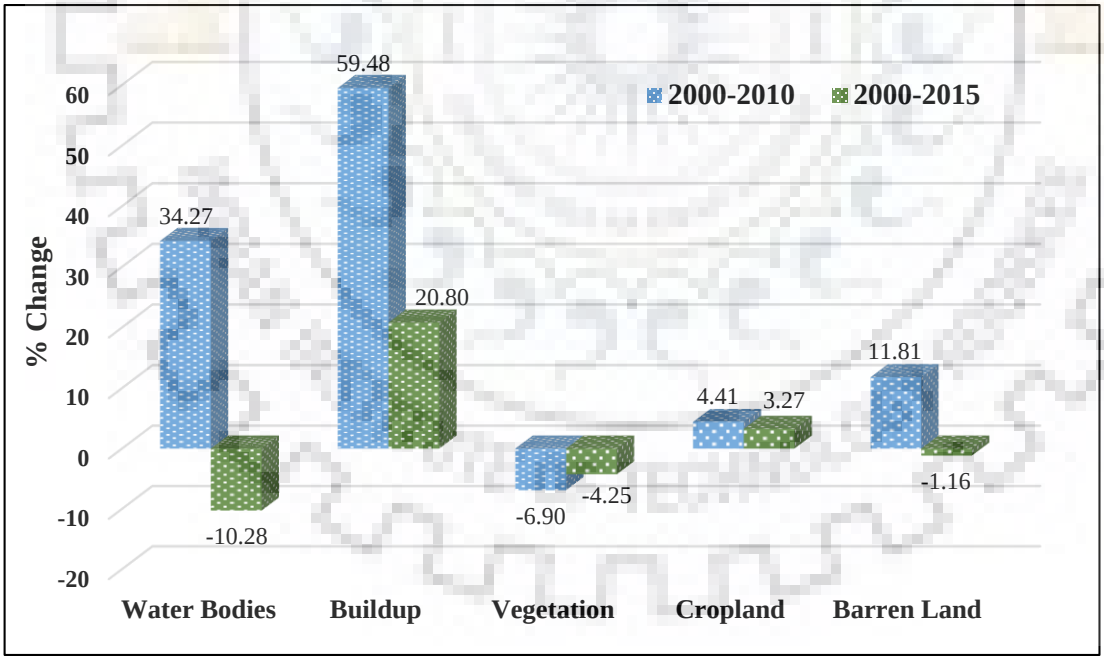

Figure 5.6: Percentage Change in LULC classes with reference to 2000

5.6 SHORT TERM FUTURE PROJECTION OF LAND USE LAND COVER

5.6.1 Future Projection employing CA-Markov

In order to detect the changes in future LULC distribution, it is very important to understand the trend of changes in LULC of past and present. For planners and policy-makers, it is necessary to have information about the change pattern and driving forces responsible for changes. Utilizing the knowledge of past and present LULC changes, LULC change model can be developed to project the future map. Many literature and model are available for this. In this study, integrated model of Markov chain and Cellular Automata (CA-Markov) were applied which is based on transitional probability matrix. Markov model is one of the most popular model for future projection using present pattern. However, this approach does not provide the direction of change but magnitude only. Therefore, Cellular Automata (CA) contains the spatial component provide the direction to modelling (Lambin et al. 2001; Petit et al. 2001). Hence, hybrid model of Markov chain and Cellular Automata Markov (CA–Markov) provides any number of classes and can project the conversion from one class into another.

Three transition rules were considered based on local socio-economic information, land use planning and related policies in Upper Narmada Basin from 2000 to 2010. These rules were used to predict the future land use land cover 2030. The first rule is characterized by natural development in which it is assumed that the factors that currently influence land use keep pace with the trend of LULC change from 2000 to 2010 and will not change greatly from 2010 to 2030. The second rule is characterized by speedy growth, in which it is assumed that areas of LULC change quickly, by considering the growth rate of population, urbanization level, per capita living space and the floating population to obtain the demand for land use in 2030. The third scenario is characterized by ecological and cultivated land protection. In this scenario, water bodies are designated as natural reserves that play an important role in ecological security and cannot change to any other land use categories, and the basic farmland is then taken as a restricted area in which the cultivated land cannot be converted into other land use types other than settlement. Initially, distribution of LULC of 2015 was simulated through transition probability matrix from the LULC map of period 2000-2010 applying CA-Markov approach for validation. The transition of classes from one in to another classes was evaluated based on the generated transition probability matrix. Transition probability matrix for the future year 2015 and 2030 were generated from past actual LULC image of 2000 and

2010 (Table 5.9 and Table 5.10).The accuracy of simulated LULC was compared with the actual LULC of 2015. In the Markov model, transition probability assumed to be stationary that makes suitable for short term future projection. Therefore, it does not provide the spatial distribution of the change, due to this shortcoming it is integrated by CA approach. Applying this approach of CA-Markov, projected LULC of study area was evaluated for year of 2030 as shown in Figure 5.10.

Table 5.9: Transition probability matrix of 2015 derived from the LULC map of 2000 and 2010

Early 2010 / Later2015	Water Bodies	Built-up	Natural Vegetation	Cropland	Barren Land
Water Bodies	0.8528	0.0003	0.1470	0.0000	0.0000
Built-up	0.0021	0.9576	0.0062	0.0277	0.0063
Natural Vegetation	0.0001	0.0000	0.8688	0.1098	0.0214
Cropland	0.0039	0.0019	0.0632	0.9177	0.0133
Barren Land	0.0000	0.0000	0.3335	0.6088	0.0577

Table 5.10: Transition probability matrix of 2030 derived from the LULC map of 2000 and 2010

Early 2010 / Later2030	Water Bodies	Built-up	Natural Vegetation	Cropland	Barren Land
Water Bodies	0.6168	0.0012	0.2919	0.0885	0.0017
Built-up	0.0056	0.8490	0.0391	0.0989	0.0075
Natural Vegetation	0.0028	0.0015	0.7026	0.2730	0.0201
Cropland	0.0085	0.0056	0.1553	0.8161	0.0145
Barren Land	0.0030	0.0030	0.3430	0.6170	0.0340

5.6.2 LULC Change Detection from 1990 to 2030

The projection of 2030 indicates the built-up area, cropland and natural vegetation area are 463.83 km^2, 19222.91 km^2 and 12157.11 km^2 respectively. Built-up area and cropland increased from 0.72% (2015) to 0.98% (2030) and 56.79% (2015) to 59.15% (2030) respectively in next 15 years, whereas natural vegetation area found to be decreased from 39.66% (2015) to 37.41% (2030) for the same duration (Table 5.10). In general, the prediction of 2030 LULC classes distribution indicate the expansion in cropland and reduction in natural vegetation due to deforestation. It also indicate a

substantial growth in the built-up area. The expansion of built-up area and cropland occurring due to the tourist places such as Jabalpur and Amarkantak, and population growth in the region. Study indicates the continuous increase in population in the study area reflecting deforestation and expansion in cropland.

Table 5.11: Comparison of actual and projected LULC classes

LULC Classes	Initial (1990)		Final (2010)		Actual 2015		Simulated 2015		Projected 2030	
	Area		Area		Area		Area		Area	
	sq.km	%	sq.km	%	sq.km	%	sq.km	%	sq.km	%
Water Bodies	398.43	1.23	455.81	1.40	408.94	1.26	364.02	1.12	463.83	1.43
Built-up	63.57	0.20	193.62	0.60	233.89	0.72	223.03	0.69	319.78	0.98
Vegetation	15983.56	49.18	13462.94	41.42	12890.64	39.66	12881.86	39.64	12157.11	37.41
Cropland	15390.74	47.36	17873.32	54.99	18458.21	56.79	18544.31	57.06	19222.91	59.15
Barren Land	663.71	2.04	514.31	1.58	508.33	1.56	486.79	1.50	336.37	1.03

The effect of the present trend in LULC change due to developmental process will result in degradation of natural vegetation. Therefore, nearby area further changes into the barren land around the highways of connecting cities and increase in settlement around these highways. The projected LULC maps provide an idea about the LULC changes in near future of year 2030.These results can be utilized for the future planning towards conservation of natural vegetation, and guide to decision makers to manage the balance growth in all other classes. The study will help to stop expansion of unmannered expansion of cropland and further help in reduce pressure on the natural vegetation area.

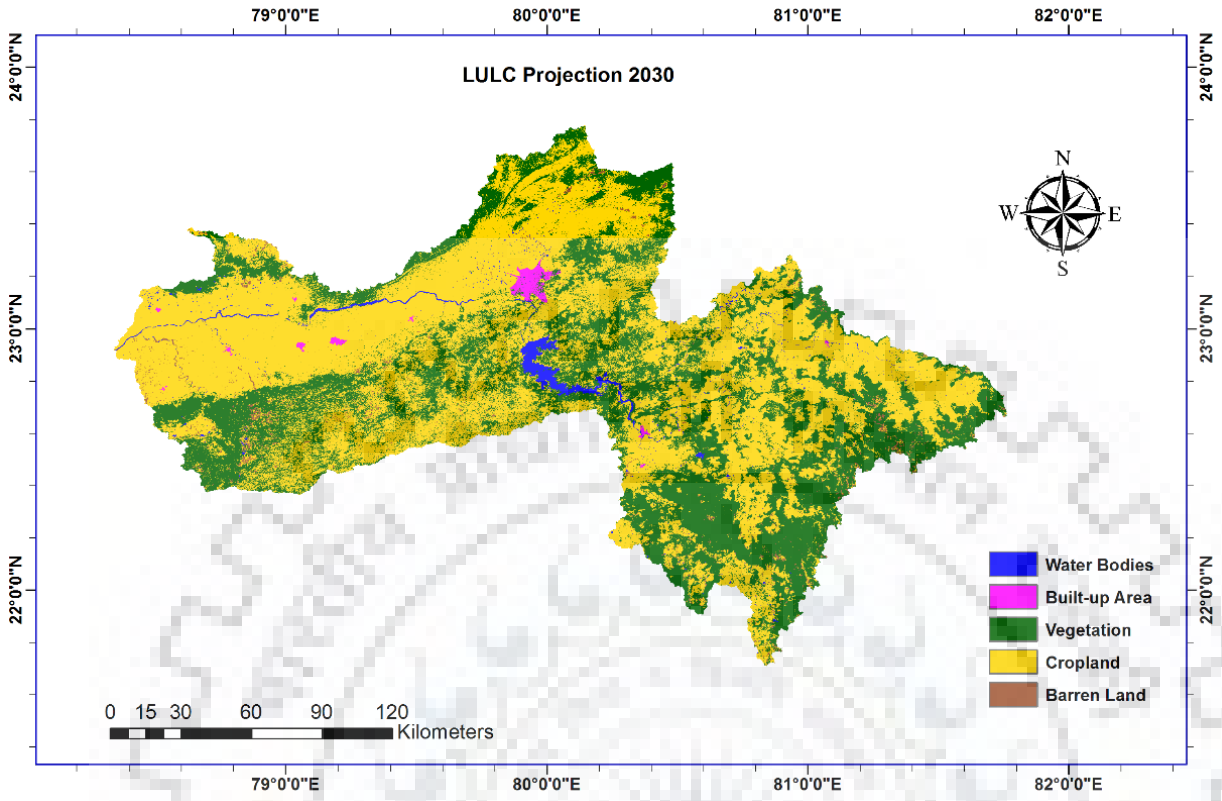

Figure 5.7: Simulated LULC map of projected year 2030

5.7 CONCLUDING REMARKS

The understanding of LULC distribution and transition from one class to another is essential for robust planning, management and help in guiding the direction of development at local, state or national levels. This selective information not only allow to manage the land utilization but also play an important role in future planning and policy making for policy makers. In general, due to increase in population most of the cities and towns are changing their real landscape in unplanned manner and natural vegetation is losing their real characteristics. For securing the sustainable development, it is important to monitor and understand the LULC changes pattern along with time. As trend indicates the continuous increase in settlement, proper planning and development by planners, policy-makers, executives, stakeholders and by local people is required. In order to attain the sustainable development, it is necessary to provide planning model by concerned agencies so that every bit of available land can be used in a proper way without damaging the natural vegetation. However, this type of planning models are only possible by understanding, changes in LULC trend pattern with time. The mapping of LULC and change detection were studied in the Upper Narmada

River basin, one of the east to west flowing rivers in the central part of India. LULC mapping were carried out using the Landsat TM satellite image by application of geospatial tools GIS and ERDAS Imagine. The development in the different classes of LULC were evaluated from 1990 to 2000 to 2010 to 2015. The reduction in natural vegetation and increase in settlement as well as cropland are clearly reflected in the analysis of LULC mapping. Understanding of trend patterns were predicated for the year 2030 using CA-Markov model. The model were validated with simulated and actual LULC of 2015. The projected LULC of 2030 classes indicated the continuing of same trend of recent past. These future projection indicate the expected changes in near future. Therefore, the LULC changes with respect to different classes in near future cautioned the concerned authorities for proper planning and management of the study area.

CHAPTER 6

REPRESENTATIVE CLIMATE MODELS AND BIAS CORRECTION

6.1 GENERAL

Global Climate Models (GCMs) are based on numerical and physical principles aimed at reproducing the present and future meteorological parameters. It provides considerable confidence in producing future climate condition by using the numerically coupled Atmospheric Ocean General Circulation Model (AOGCM) (Moss et al. 2010; Su et al. 2012). Several inter-comparison studies have been done between model outputs and observed data all over the world (Anandhi and Nanjundiah 2015; Diro et al. 2009; Errasti et al. 2011; Evan et al. 2012; Fu et al. 2013; KS and D 2014; Perkins et al. 2007). However, the GCMs output are very uncertain due to initial condition, boundary condition, model structure and emission scenario (Ojha et al. 2012). The performance of 10 GCM models for simulating the summer monsoon rainfall variation over the Asian-western pacific region assessed by Kang (2002). Johnson and Sharma (2009) used variable convergence score (VCS) methodology based on the coefficient of variation to evaluate the eight different variables from nine GCM outputs for two emission scenario for Australia. This skill score methodology can be used to evaluate for any GCM at any region. Radić and Clarke (2011), evaluated 22 GCMs for North America using several statistical parameters. Evaluation has been carried out by comparing the model output with reanalysis data for the period 1980-99.

Frei et al. (2003) investigated daily precipitation simulation for European Alps by using five regional climate model. There are number of recent studies based on indices and probability density function (PDF) to identifying the best model (Anandhi and Nanjundiah 2015; Frei et al. 2003; McMahon et al. 2015; Ojha et al. 2013; Parth Sarthi et al. 2015; Perkins et al. 2007; Radić and Clarke 2011). Perkins et al. (2007) conducted model evaluation for 12 regions in Australia using probability density function (PDFs). Evaluation of the model in the study area have been performed considering daily simulation data of maximum temperature, minimum temperature and precipitation. There are many approaches to compare the simulated or model output with observed values (when data is available) or reanalysis values (for poorly gauged regions with missing or no observed data). For impact studies of climate change, it is necessary to evaluate the model with observed datasets, and

model output should perform close to the observed data. There were many studies carried out to evaluate the GCMs.

In this chapter, Coupled Model Intercomparison Project (CMIP), global climate models are evaluated using root mean square error (RMSE) and skill score (SS) of six meteorological variables for all seven zones of Indian region and Upper Narmada Basin (UNB). Ranking of model has been carried out applying Multi-Criteria Analysis (MCA) method. This study has been carried out for monsoon (June to October), non-monsoon (January to May, November, December) and annual basis.

6.2 CLIMATIC DATA

6.2.1 Global Climate Model Data

Daily data over India have been archived by modelling group of Data Integration and Analysis System (DIAS) for 24 GCMs. Model outputs have been carried out from 1981–2000 for all models. Climate models used in this study are given in Table 6.1.

6.2.2 Reanalysis Data

Reanalysis data precipitation (pr), ongoing long wave radiation (olr), were obtained from Global Precipitation Climatology Project (GPCP) and National Oceanic and Atmospheric Administration (NOAA) respectively whereas, atmospheric temperature (tas) ,mean sea level pressure (ps), zonal wind (uas) and meridional wind (vas) were obtained from the Japanese 25-year Reanalysis model (JRA25) for the period 1981–2000. Annual average climatic data of 20 years (1981-2000) over India represented in Figure 6.1.

Table 6.1: Global Climate Models Centre and location (Randall et al. 2007)

S.N.	GCM	Acronym	Centre and Location	Resolution (Degree)
1.	BCCR_BCM2_0	bcr	Bjerknes Centre for Climate Research (BCCR), Univ. of Bergen, Norway	2.8 x 2.8
2.	CCCMA_CGCM3_1	cc4	Canadian Centre for Climate Modeling and Analysis ,Canada	3.75 x3.75
3.	CCCMA_CGCM3_1_T63	cc6	Canadian Centre for Climate Modeling and Analysis ,Canada	2.8 x 2.8
4.	CNRM_CM3	cnr	Centre National de Recherches Meteorologiques, Meteo, France	2.8 x 2.8

5.	CSIRO_MK3_0	cs3	Atmospheric Research, Australia	1.9 x 1.9
6.	CSIRO_MK3_5	cs5	Atmospheric Research, Australia	1.9 x 1.9
7.	GFDL_CM2_0	gf0	Geophysical Fluid Dynamics Laboratory, NOAA	2.0 x 2.5
8.	GFDL_CM2_1	gf1	Geophysical Fluid Dynamics Laboratory, NOAA	2.0 x 2.5
9.	GISS_AOM	gao	NASA Goddard Institute for Space Studies (United States)	3.0 x 4.0
10.	GISS_MODEL_E_H	gih	NASA Goddard Institute for Space Studies (United States)	4.0 x 5.0
11.	GISS_MODEL_E_R	gir	NASA Goddard Institute for Space Studies (United States)	4.0 x 5.0
12.	IAP_FGOALS1_0_G	iap	LASG/Institute of Atmospheric Physics (China)	2.8 x 3.0
13.	INGV_ECHAM4	mpi4	Max Planck Institute for Meteorology, Germany	1.1 x 1.1
14.	INMCM3_0	inm	Institute of Numerical Mathematics, Russian Academy of Science	4.0 x 5.0
15.	IPSL_CM4	ips	Institute Pierre Simon Laplace (IPSL), France	2.5 x 3.75
16.	MIROC3_2_HIRES	mih	Center for Climate System Research (The University of Tokyo)	1.1 x 1.1
17.	MIROC3_2_MEDRES	mim	National Institute for Environmental Studies, and Frontier Research Center for Global Change (JAMSTEC, Japan)	2.8 x 2.8
18.	MIUB_ECHO_G	miu	Meteorological Institute of the University of Bonn, (Germany and Korea)	3.7 x 3.7
19.	MPI_ECHAM5	mpi	Max Planck Institute for Meteorology, Germany	1.9 x 1.9
20.	MRI_CGCM2_3_2A	mri	Meteorological Research Institute, Japan Meteorological Agency,	2.8 x 2.8
21.	NCAR_CCSM3_0	nca0	National Center for Atmospheric Research (NCAR),	1.4 x 1.4
22.	NCAR_PCM1	nca1	National Center for Atmospheric Research (NCAR)	2.8 x 2.8
23.	UKMO_HADCM3	had3	Hadley Centre for Climate Prediction and Research, Met Office, UK	2.75 x 3.75
24.	UKMO_HADGEM1	had1	Hadley Centre for Climate Prediction and Research, Met Office, UK	1.25 x 1.875

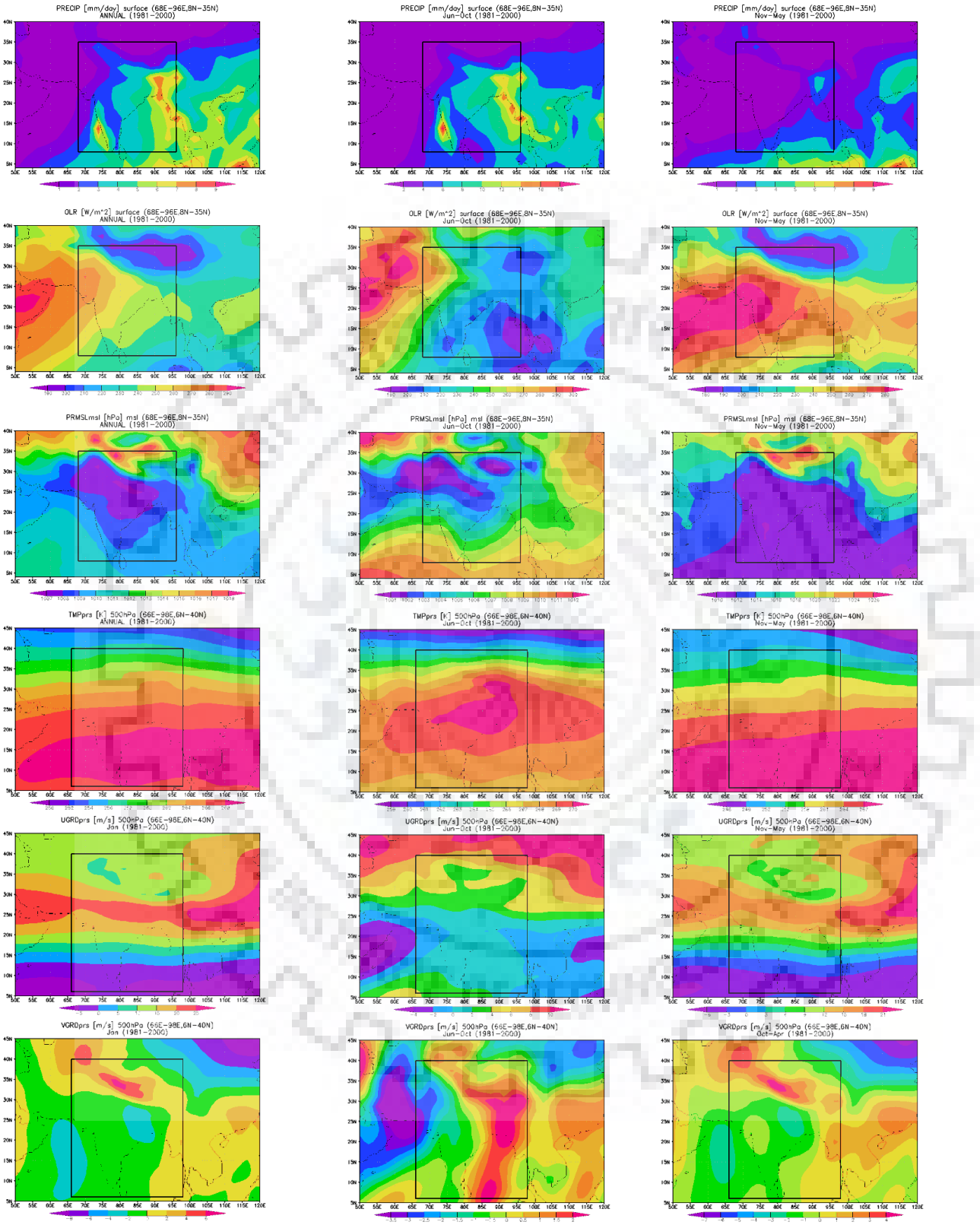

Figure 6.1: Average annual, monsoon and non-monsoon of reanalysis climate data over India

6.3 METHODOLOGY

In this analysis, performance of the model has been carried on the basis of Skill Score (SS) and Root Mean Square Error (RMSE) between model output and reanalysis data for year 1981-2000. There are six meteorological parameters: precipitation (pr), outgoing long wave radiation (olr), air temperature (tas), mean sea level pressure (ps), zonal wind (uas) and meridional wind (vas) considered for the SS and RMSE evaluation. The comparison of GCM data with reference data has been carried out by checking their seasonal cycle and variability using probability density function (PDFs). Ranking of the GCMs have been evaluated based on the Total Grand Scoring (TGS) Index, which is dependent on the SS and RMSE assessment. The overall flow diagram illustrating the methodology is presented in Figure 6.2.

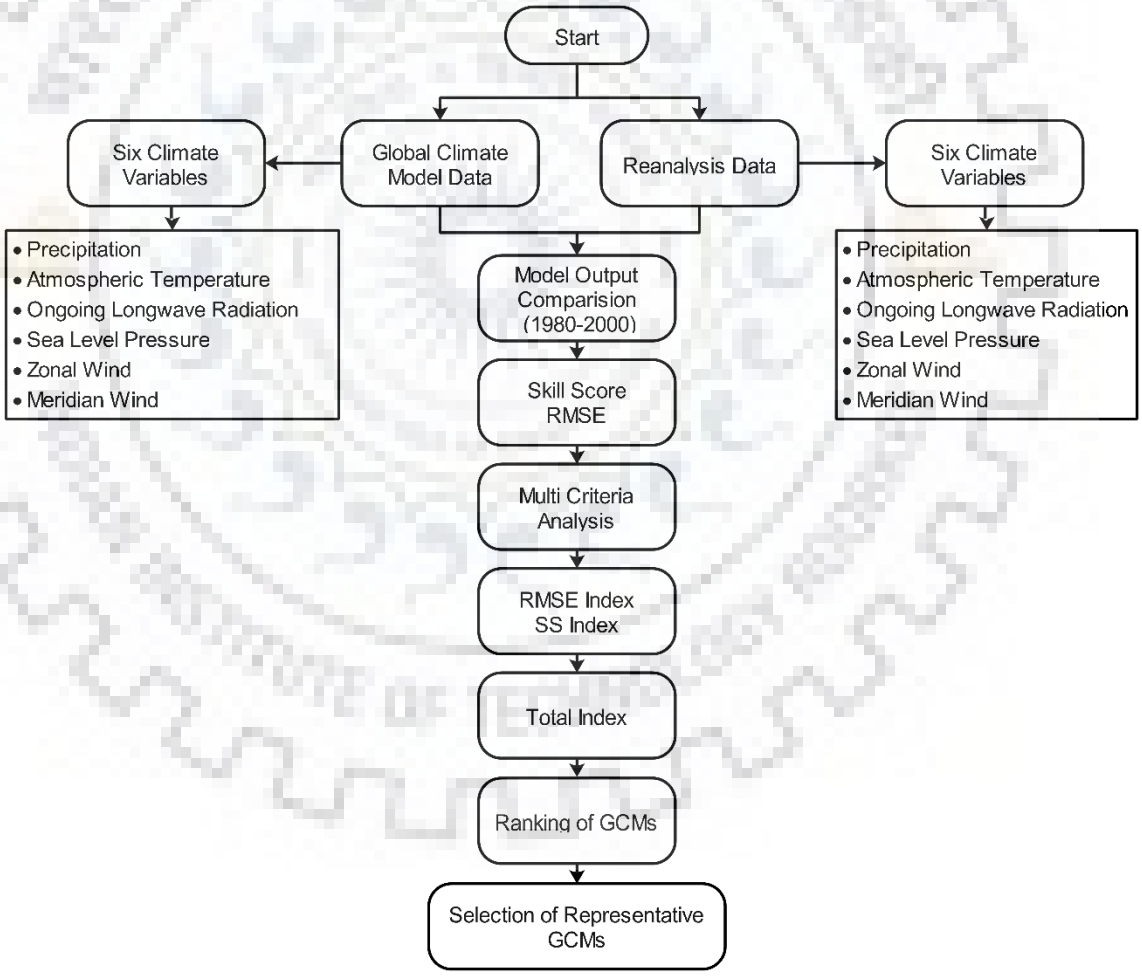

Figure 6.2: Flow diagram illustrating the methodology to select the representative GCMs

6.3.1 Evaluation Parameters

The Root Mean Square Error (RMSE) is a frequently used measure of the difference between values predicted by a model and the values actually observed from the environment that is being modelled. These individual differences are also called residuals, and the RMSE serves to aggregate them into a single measure of predictive power. The RMSE of a model prediction with respect to the estimated variable is defined as the square root of the mean squared error:

$$RMSE = \sqrt{\frac{\sum_{i=1}^{n}(f_i - x_i)^2}{n}} \quad \ldots\ldots\ldots (6.1)$$

Where, x_i is observed values and f_i is modelled values.

Skill is generally defined as the accuracy of forecasts of interest to the standard reference (Murphy et.al 1988). The basic measure of accuracy in this chapter is Mean Square Error (MSE). Let f_i, x_i, c_i can be defined as the climate model outputs and mean of the reanalysis output:

$$MSE(f,x) = \left\langle (f_i - x_i)^2 \right\rangle \quad \ldots\ldots\ldots (6.2)$$

Where, angle bracket denotes the mean of nth grid at a particular time. For perfect model output MSE should be equal zero (i.e. $f_i \geq x_i$ for all i).

$$MSE(c,x) = \left\langle (c_i - x_i)^2 \right\rangle \quad \ldots\ldots\ldots (6.3)$$

Here, c_i is the long term meteorological variables. Then the skill score (SS) defined on the basis of mean square error is

$$SS = \left[MSE(c,x) - MSE(f,x)\right] / \left[MSE(c,x) - 0\right] \quad \ldots\ldots\ldots (6.4)$$

for perfect match, $MSE(f,x) = 0$,

$$SS = 1 - \left[MSE(f,x) / MSE(c,x)\right] \quad \ldots\ldots\ldots (6.5)$$

SS is positive when model output is greater than observed output where as it may be negative if it is less than the observed value (Murphy 1988; Murphy 1993).

6.3.2 Multi Criterial Analysis (Scoring Method)

In order to derive the model ranking of climate models, Skill Score (SS) (Murphy 1988) and Root Mean Square Error (RMSE) of the each model were computed for the study area. Evaluation parameters, SS and RMSE are the model output and reanalysis observed data.

a) Skill Score Index (S_{index}):

$$S_{avg} = \sum_{i}^{n} S_i \qquad \text{….. (6.6)}$$

$$S_{index} = \begin{cases} 1 & S_i \geq S_{avg} \\ 0 & S_i < S_{avg} \end{cases} \qquad \text{..... (6.7)}$$

b) RMSE Index (L_{index}):

$$L_{avg} = \sum_{i}^{n} L_i \qquad \text{..... (6.8)}$$

$$L_{index} = \begin{cases} 1 & L_i \leq L_{avg} \\ 0 & L_i > L_{avg} \end{cases} \qquad \text{..... (6.9)}$$

c) Total Index (TI):

$$TI = \begin{cases} 1 & S_{index} + L_{index} > 1 \\ -1 & S_{index} + L_{index} < 1 \\ 0 & others \end{cases} \qquad \text{.... (6.10)}$$

Total index (TI) calculated for each meteorological parameters based on annual. For each model, grand index, evaluated and corresponding to total grand index ranking has been allotted. Ranking of GCMs showing the top performing model to least capable model.

6.4 RANKING OF CMIP3 MODELS AT REGIONAL SCALE: INDIAN ZONES

6.4.1 Evaluation Parameters of Meteorological Variables

In the present study, the evaluation of IPCC AR4 climate models has been carried out on daily observations using the referenced climate results. Assessment of models based on probability density function (PDF) which is used for parameter evaluation considering the area about 10^{o} x 10^{o}. PDFs for pr, tas, olr, ps, uas and vas for 1981-2000. This study was based on the monsoon season (June-Ooctober) non-monsoon (November-March) and annually (January- December). PDF has the ability to demonstrate the distribution value of climate model values over reference model values (Perkins et al. 2007). There will be shifting in distribution in the case of climate change and variation in the distribution of model output. For regional study, India has been divided into seven rectangular regions based on homogeneous physiography and precipitation zone (Figure 6.3). These regions are North Mountainous India (NMI), North Central India (NCI), Northwest India (NWI), East Peninsular India (EPI), West Peninsular India (WPI), South Peninsular India (SPI) and North East India (NEI).

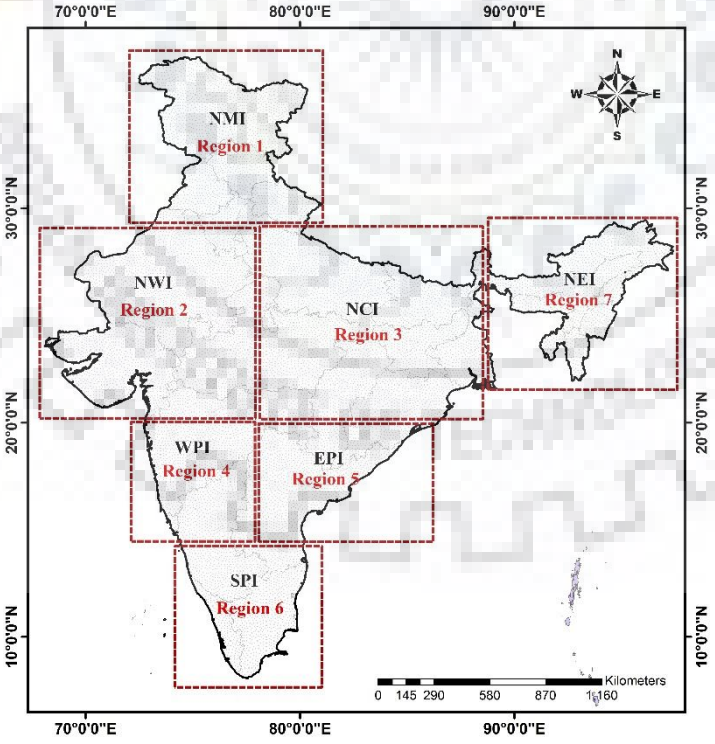

Figure 6.3: Seven regions of India for model ranking (Li et al. 2013)

Root Mean square error (RMSE) and Skill Score (SS) have been evaluated for the climate models with reference to the reanalysis data for each region. Zero value of RMSE and SS value of 1 represents the perfect model. The archive of climate models ensemble by Data Integration Assessment Tools (DIAS) developed by The University of Tokyo, has been used to evaluate the RMSE and SS for each climate model for each region and season.

RMSE value for precipitation based on monsoon, non-monsoon and annual season for all the climate models are given in Table 6.2. Precipitation from different climate model compared with the Global Precipitation Climatology Project (GPCP) rainfall monthly datasets from 1981-2000 over India shown in Figure 6.4. Figure 6.5 shows the skill score of 'pr' for all regions. Temporal assessment has been carried out for each zone corresponding to the annual, monsoon and non-monsoon season. In region 1, climate model 'cc4' (0.02) for annual, 'cs5' (-0.01) for monsoon, 'ips' (0.03) for non-monsoon are represent the minimum SS value for meteorological parameter 'pr'. Minimum RMSE value obtained for GCM 'mpi4' (1.03 and1.22) for annual and monsoon season, and 'cc6' (0.74) for non-monsoon season. For region 2, climate model 'gir' represents the SS value 0.30 and -0.07 for annual and monsoon season respectively. For non-monsoon season, 'nca0' represents the minimum SS value (0.34). GCM 'mih' obtained the minimum RMSE value 0.88 and 1.61 for annual and monsoon season respectively and cc6 (0.34) for non-monsoon. In region 3, minimum SS value represented by climate model 'cnr' for annual and monsoon season (0.04 and -0.16) whereas 'mih' (0.59) represents the minimum value for non-monsoon. Climate model 'had3' represents the minimum RMSE value 1.42 and 2.37 for annual and monsoon season respectively. Model 'mih' (0.59) obtained minimum RMSE value for non-monsoon season. In region 4, model 'gir' represents the minimum SS value for annual and non-monsoon season (0.90 and 0.24 respectively). GCM 'inm' (-0.22) represent the minimum SS value for monsoon season. Climate model 'mpi' represents the minimum RMSE value for all season. In region 5, minimum SS value obtained by mri (0.01), iap (-0.23) and mim (0.00) for annual, monsoon and non-monsoon season respectively. Climate models 'bcr' obtained minimum RMSE value for annual and monsoon season (1.10 and 1.54 respectively) and 'mih' (0.41) represents the non-monsoon 'pr'. In region 6, cnr (0.42), iap (0.10) and nca0 (0.40) represent the minimum value of SS for annual, monsoon and non-monsoon season respectively. Model 'mpi' (1.66 and 0.72) represent the minimum RMSE value for annual and non-monsoon season whereas 'mpi4' (2.46) represent the minimum value for monsoon

season. For region 7, climate model ‘ips’ and ‘nca1’ represent the zero SS value for annually, ‘gao’ (-0.44) and ‘mim’ (-0.24) represent the minimum score for monsoon and non-monsoon season respectively. Minimum RMSE value was obtained by ‘mim’ climate model, 2.23, 3.44 and 1.35 for annual, monsoon and non-monsoon respectively.

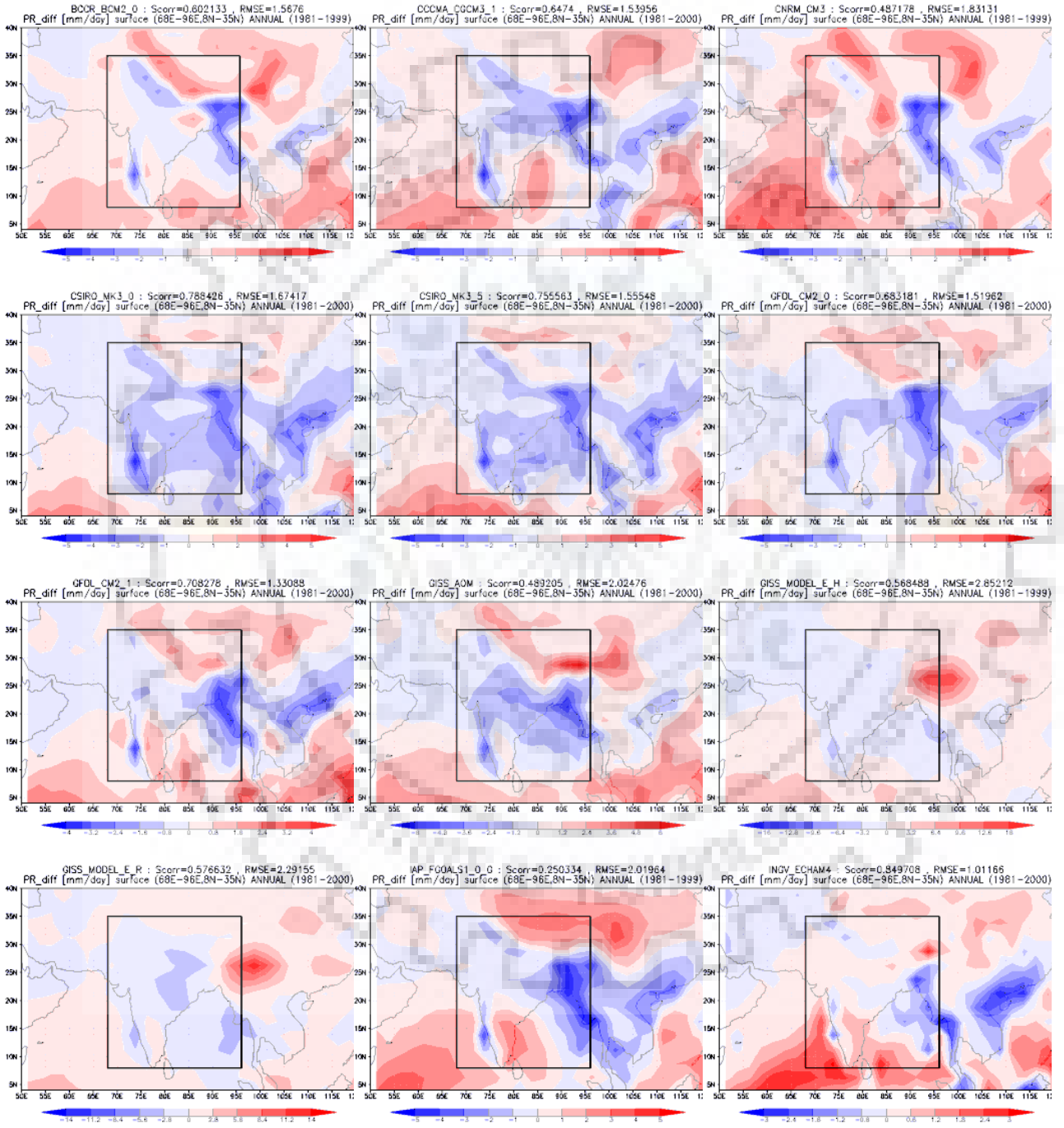

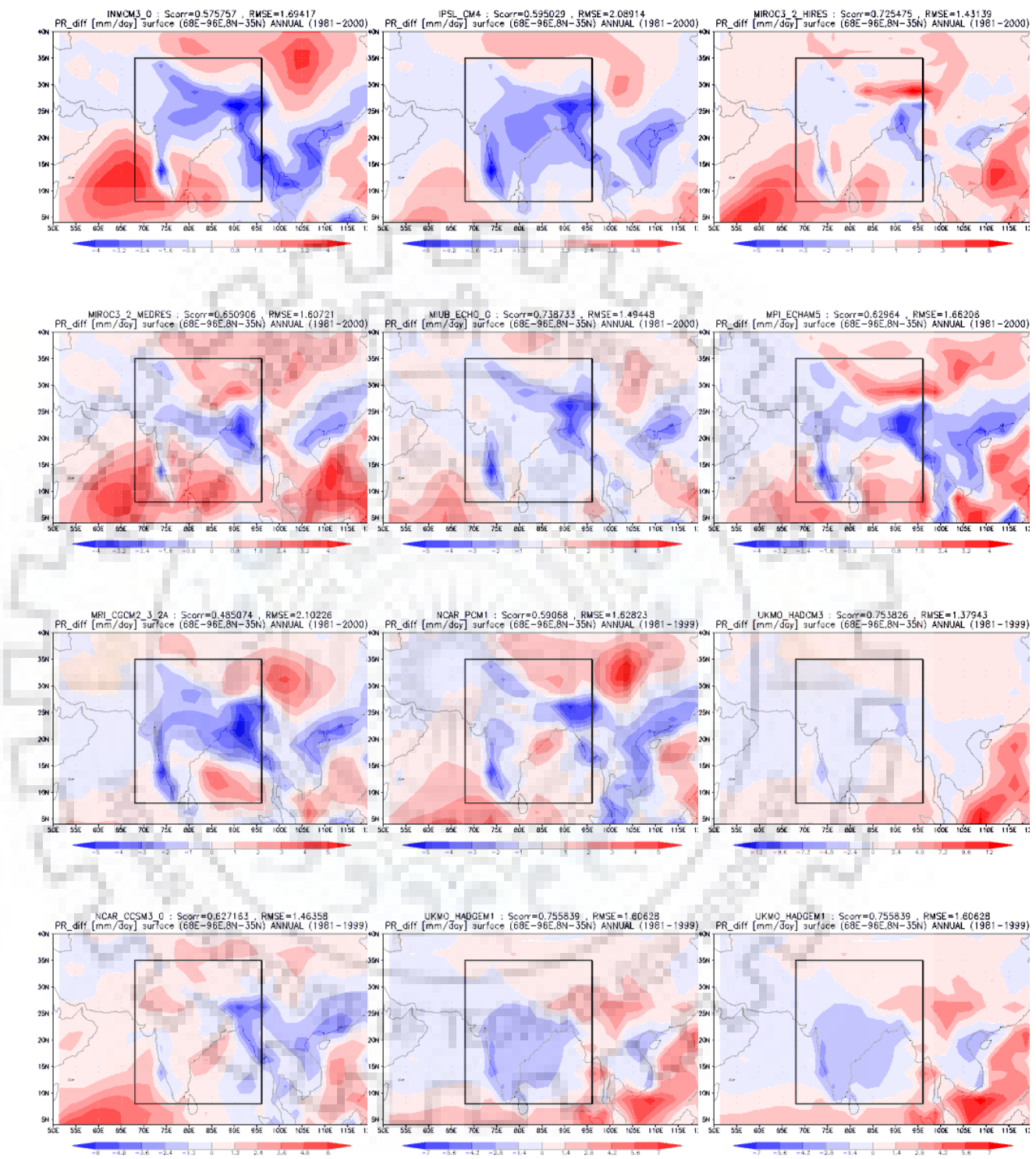

Figure 6.4: Precipitation variations in 24 climate models with reference to reanalysis (GPCP) model

Table 6.2: RMSE value of climate models for precipitation

Model	M1	N1	A1	M2	N2	A2	M3	N3	A3	M4	N4	A4	M5	N5	A5	M6	N6	A6	M7	N7	A7
bcr	2.25	2.96	1.74	1.14	2.13	0.42	2.71	4.13	1.70	1.19	2.16	0.49	1.10	1.54	0.79	2.12	3.27	1.29	6.21	2.09	0.72
cc4	1.37	2.14	0.82	1.20	2.36	0.37	1.90	3.37	0.86	1.32	2.61	0.40	1.48	2.68	0.62	2.17	3.87	0.95	4.95	1.69	0.82
cc6	1.11	1.63	0.74	1.12	2.22	0.34	2.10	3.86	0.84	1.65	3.29	0.48	1.88	3.61	0.64	2.14	3.70	1.02	5.76	1.64	0.54
cnr	2.16	2.41	1.98	1.49	2.68	0.64	3.58	4.26	3.09	1.70	2.30	1.27	1.71	1.73	1.70	2.18	2.64	1.85	6.57	1.80	1.80
cs3	1.72	2.19	1.38	1.36	2.68	0.41	2.09	3.83	0.85	1.46	3.11	0.27	1.80	3.34	0.70	2.19	3.41	1.32	4.83	1.64	0.60
cs5	1.71	2.23	1.35	1.46	2.85	0.46	2.14	3.89	0.89	1.74	3.67	0.35	1.97	3.60	0.80	2.46	4.08	1.31	4.21	1.73	0.82
gf0	1.57	1.62	1.55	1.14	2.05	0.48	1.84	2.89	1.09	1.33	2.64	0.39	1.43	2.47	0.69	1.76	2.81	1.01	5.29	2.01	0.64
gf1	1.52	1.81	1.31	1.10	1.99	0.46	1.48	2.48	0.76	1.28	2.68	0.28	1.20	2.19	0.49	1.87	3.41	0.77	4.00	1.39	0.89
gao	2.60	2.64	2.57	2.02	4.00	0.61	2.66	4.85	1.10	1.53	3.18	0.36	1.61	2.93	0.67	2.08	3.36	1.16	5.54	2.22	0.57
gih	1.80	2.52	1.29	1.99	4.29	0.35	2.89	5.67	0.90	1.52	3.12	0.38	2.07	3.87	0.79	2.58	3.83	1.69	17.42	5.89	0.72
gir	2.00	2.68	1.52	2.05	4.41	0.37	3.15	6.15	1.01	1.82	3.85	0.37	2.49	4.79	0.85	2.73	4.91	1.17	11.10	5.23	0.80
iap	2.73	2.81	2.67	1.55	2.80	0.66	2.49	4.33	1.17	1.88	3.95	0.40	1.45	2.69	0.56	2.10	3.98	0.76	6.92	2.14	0.52
mpi4	1.03	1.22	0.89	1.14	1.94	0.57	1.62	2.68	0.87	1.61	2.78	0.78	1.36	2.01	0.89	1.94	2.46	1.57	3.49	1.59	0.88
inm	1.81	2.76	1.14	1.82	3.71	0.47	2.66	4.75	1.17	1.99	3.93	0.61	1.61	2.54	0.95	2.63	4.19	1.52	5.31	1.94	0.92
ips	2.43	2.95	2.06	2.27	4.63	0.59	3.39	6.67	1.05	2.61	5.74	0.37	2.45	5.04	0.60	2.65	4.99	0.98	7.24	1.97	0.76
mih	1.73	1.75	1.72	0.88	1.61	0.35	1.45	2.66	0.59	1.10	2.29	0.25	1.22	2.37	0.41	1.86	3.27	0.85	4.76	1.96	0.48
mim	1.29	1.60	1.06	1.04	2.00	0.35	1.82	3.16	0.87	1.36	2.49	0.56	1.59	2.15	1.18	2.19	3.85	1.00	3.44	1.36	0.82
miu	1.49	2.44	0.82	1.30	2.59	0.37	2.24	4.09	0.92	1.41	2.95	0.31	1.17	1.95	0.61	2.07	3.51	1.04	5.75	1.49	0.81
mpi	2.00	2.35	1.74	1.19	2.22	0.46	1.77	3.36	0.63	0.90	1.82	0.24	1.44	2.56	0.63	1.66	2.98	0.72	5.22	1.77	0.73
mri	1.99	2.92	1.33	1.87	3.91	0.41	2.62	4.98	0.94	1.51	3.08	0.39	1.80	3.06	0.89	2.27	3.97	1.05	6.43	1.72	0.49
nca0	1.61	1.70	1.54	1.61	2.70	0.82	2.51	3.95	1.49	1.64	2.42	1.09	2.07	3.24	1.23	2.38	3.27	1.75	6.42	1.35	0.43
nca1	1.69	2.35	1.22	1.93	3.68	0.67	2.58	4.81	0.99	2.20	4.12	0.84	2.05	2.76	1.55	2.52	4.37	1.20	7.44	1.74	1.53
had3	1.44	2.01	1.02	1.27	2.56	0.35	1.42	2.37	0.75	1.59	3.25	0.41	1.68	2.99	0.75	1.92	3.01	1.14	3.68	1.44	0.78
had1	1.37	1.80	1.06	1.81	3.82	0.38	2.51	4.64	0.98	2.42	5.27	0.38	2.52	5.14	0.64	2.85	5.19	1.18	5.30	2.15	0.66

Note: M1, N1 and A1 indicate the monsoon, non-monsoon and annual values for zone one and similarly for other zones

There is no single model to represent air temperature (tas) for the whole region for all seasons. In region 1, GCM 'mih' obtained the minimum SS value for all seasons viz. 0.71 (annual), 0.59 (monsoon) and 0.80 (non-monsoon). Climate model 'cs5' (0.76 and 0.53) carried the minimum RMSE value for annual and non-monsoon season. In region 2, there were climate models 'ips', 'gao' represent the minimum SS (0.74 and 0.39) and minimum RMSE value (0.76 and 0.44) for annual and monsoon season respectively. In region 3, model 'nac0' represent the minimum SS value for annual (0.59) and monsoon (0.03) season. Minimum RMSE value was obtained for GCM 'gao' 0.62 and 0.60 during annual and non-monsoon season respectively.

Climate models 'ips'(0.38) and 'gao'(0.03) obtained the minimum SS for annual and monsoon season respectively while for non-monsoon season, model 'nca1'(0.83) and 'had3' (0.83) represent the same value in region 4. For region 5, minimum RMSE value obtained for model 'gih' for annual (0.36) and non-monsoon season (0.33), however 'cnr' (0.26) represent for non-monsoon season. In region 6, model 'ips'(0.11) and 'cnr'(0.21) for annual, 'gih' (0.52) and 'mpi(0.19) for monsoon, 'nca1'(0.01) and 'cnr'(0.22) represent the minimum SS and RMSE value respectively. In region 7, model 'ips' obtained the minimum SS value for annual (0.51) and monsoon (-0.16) season, whereas model 'mpi' obtained minimum RMSE value for annual (0.75) and non-monsoon (0.81).

For ongoing long wave radiation (olr), climate model output compared with the reanalysis data of NOAA. In region 1, ensemble of climate models 'miu'(0.91), 'ips' (0.85), 'mim'(0.94) represent the minimum SS value for annual, monsoon and non-monsoon season respectively. GCMs 'gf0' represent the minimum RMSE value for annual (10.48) and monsoon season (12.73). In region 2, model 'gir'(0.77) for annual, 'ips' (0.63) for monsoon and 'cs5' (0.81) were represent minimum SS value. Minimum RMSE value for region 2 indicated by model 'mpi' (11.27), 'mpi4' (7.36) and 'ips' (6.65) for annual , monsoon and non-monsoon respectively. Therefore, climate Models ips, gir, 'mpi', 'ips' and 'cs5' represent the region 2 for all season. For region 3, ensemble of GMCs mim, mpi, mpi4 and gao represent the all season. Climate model 'mim' obtained the minimum SS value for annual (0.51) and monsoon (-0.06) season, whereas 'gao' (0.78) represent the non-monsoon. Model mpi4 observed the mini RMSE value for annual and non-monsoon season, and minimum SS value for region 5 for annual and monsoon season. For region 6, climate model mpi, mim, mih obtained minimum evaluation parameter for annual monsoon season. Ensemble of climate model gir, mim and mpi4 scored the minimum evaluation parameter for region 7. Figure 6.6, 6.7 and 6.8

indicated the SS value of sea level pressure, zonal wind and meridional wind respectively for all seven regions of India.

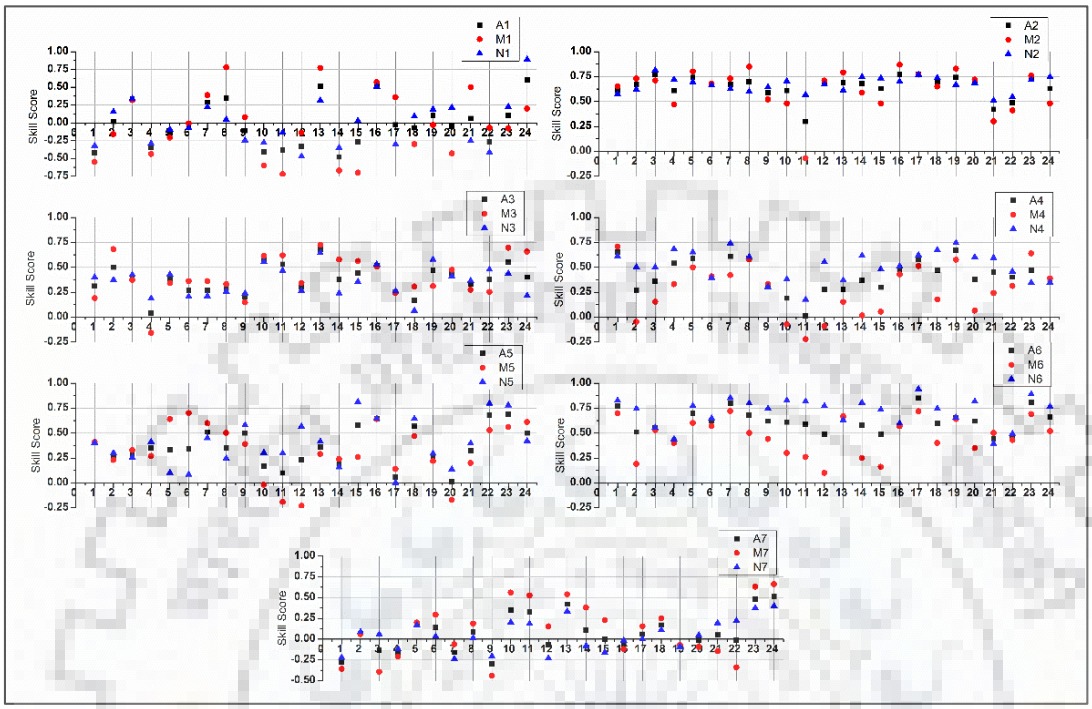

Figure 6.5: Skill score of GCMs for precipitation over India

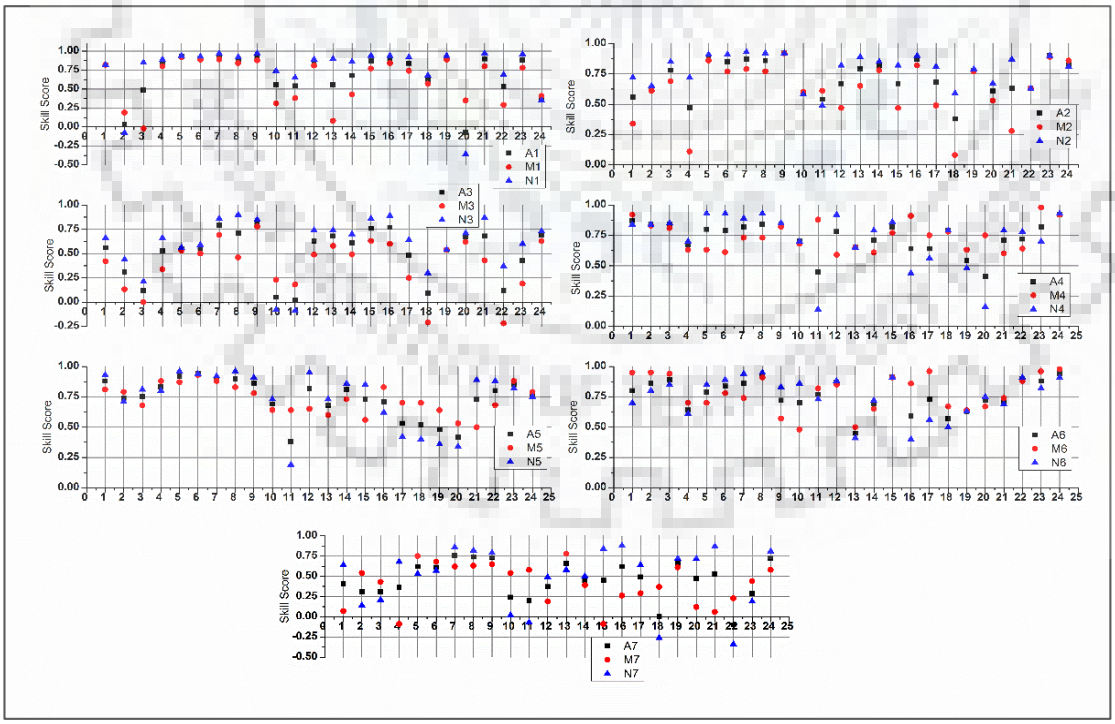

Figure 6.6: Skill score of GCMs for sea level pressure over India

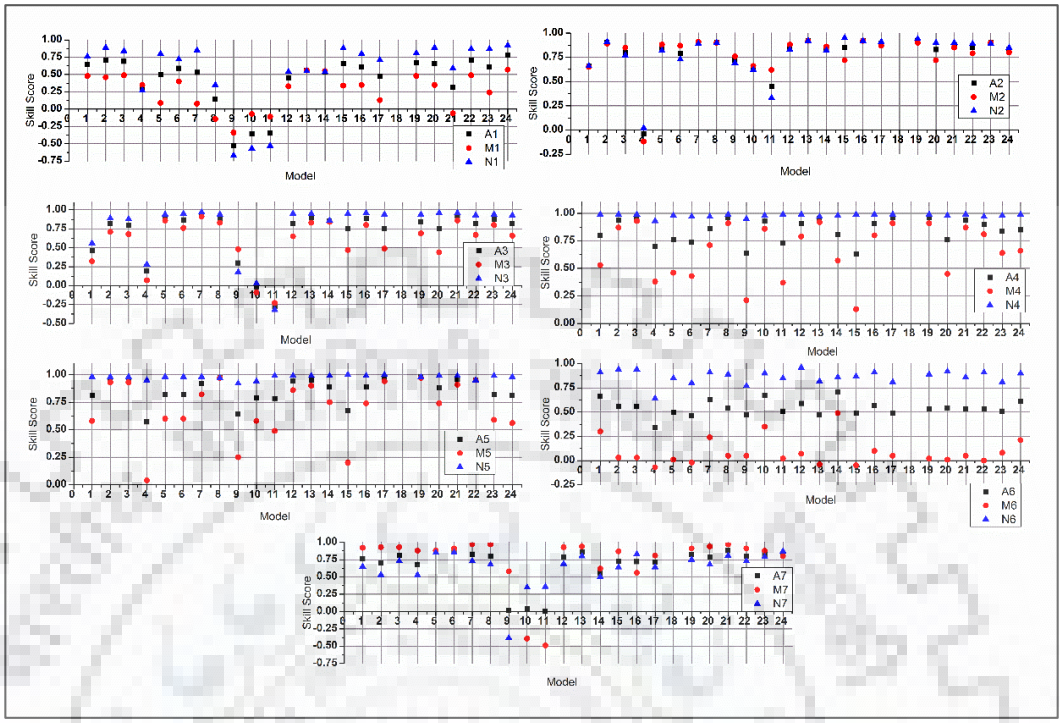

Figure 6.7: Skill score of GCMs for zonal wind over India

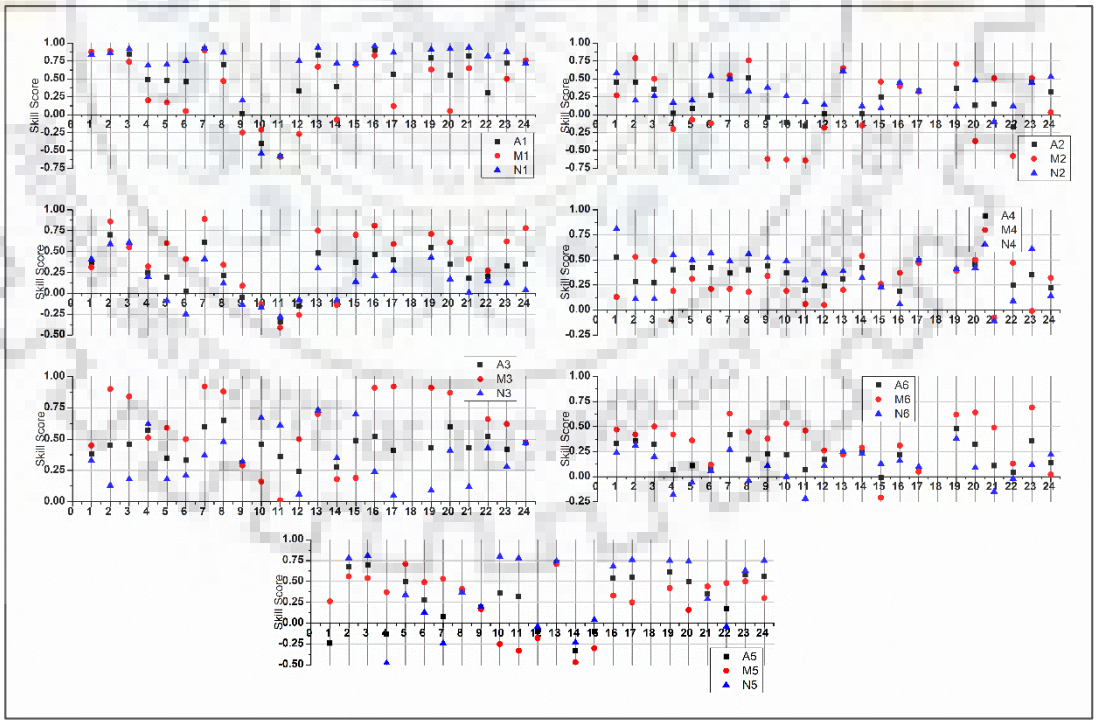

Figure 6.8: Skill score of GCMs for meridional wind over India

6.4.2 Ranking of Climate Model

There are many methods available for model ranking but identification of the 'best' method, is still under debate for climatologists. In this section, ranking of climate models have been proposed based on scoring index using the Multi-Criteria Analysis (MCA).

In this present study, 24 IPCC AR4 climate models selected for ranking over India. Total score index evaluated for each model using the multi-criteria analysis (MCA) method were shown in Table 6.3. Ranking of model over India evaluated considering 6 meteorological variables pr, tas, olr, ps, uas and vas. In order to calculate the total scoring index, skill score and RMSE value of each model for all parameters used. The same index was used for each Indian region during monsoon season, non-monsoon season and annually, Table 6.3 indicate the total scoring index of each climate model. 'High' score value GCM indicates the 'best' performing climate model per region whereas 'lowest' score indicates the 'poor' performing climate model. Score scale of model lies between 6 to -6 as maximum and minimum score achieved by any model. It is important to note that there is no single GCM that can perform 'best' during monsoon, non-monsoon and annual for the same region. Ranking of 24 climate models based on monsoon, non-monsoon and annual period for each region is given in Annexure 1.

Table 6.4 indicated, for annual simulation it has been found that had3 for region 1, mpi for region 2, mpi4 for region 3 and 7, gf1 for region 4, gf0 for region 5 and bcr for region 6, scored maximum total index. Ensemble of gf0, gf1 and mpi scored second highest for India for annual simulation. For monsoon season, climate model mpi scored maximum for region 1, cc6 scored 6 in the index scale for region 2. Climate model mpi4 scored maximum value 6 for region 3 and 7, whereas mih performed 'best' for region 4 and 5 during the monsoon season. Ensemble of cc6, cc4, mpi4, and cs3 performed better in India as whole during monsoon. It has been observed during monsoon that the climate model gir secured the lowest position for region 2,3,4,5 and 7. In order to analyze the climate model for non-monsoon season, had3, mim, mpi, gf1, ips and cc4 was the best model for regions 1 to 7 respectively. Ensemble of gf1, gf0, ips, mpi secured second position for the whole India during non-monsoon season. Climate model 'gir' performed very poorly and scored the lowest score index values for regions 1, 2 and 3.

Table 6.3: Total Index score of GCM Models for Annual, Monsoon, Non-Monsoon

MODELS	*NMI*	*NWI*	*NCI*	*WPI*	*EPI*	*SPI*	*NEI*	*NMI*	*NWI*	*NCI*	*WPI*	*EPI*	*SPI*	*NEI*	*NMI*	*NWI*	*NCI*	*WPI*	*EPI*	*SPI*	*NEI*
	ANNUAL							*MONSOON*							*NON-MONSOON*						
bcr	1	0	0	2	2	5	-3	-1	1	-2	1	2	5	-3	1	-1	-1	2	2	3	-3
cc4	2	4	3	2	1	3	4	2	5	5	4	3	0	4	-2	0	3	2	0	5	2
cc6	3	4	3	1	2	4	1	3	6	3	1	3	3	3	5	2	3	0	1	2	3
cnr	-2	-3	-2	0	0	0	-4	-2	-2	-3	1	1	2	-1	-1	-2	-1	0	1	-3	-1
cs3	2	3	4	3	1	1	5	0	4	4	3	2	1	5	1	2	3	1	2	0	4
cs5	1	3	3	0	-1	-1	4	1	3	3	1	2	-2	5	2	1	0	-1	-2	-1	3
gf0	5	3	4	4	4	5	2	2	3	4	0	2	2	2	3	1	1	2	4	5	2
gf1	3	5	3	5	4	1	4	3	5	3	3	5	3	4	2	4	3	5	2	3	3
gao	0	-1	-2	1	3	1	0	0	-2	-2	2	0	-1	-1	0	2	0	3	4	3	0
gih	-3	-4	-3	-1	-3	-1	-3	-3	-4	-3	-1	-4	-2	-2	-2	-3	-2	-1	-2	1	-3
gir	-4	-6	-5	-5	-4	-2	-4	-3	-6	-5	-3	-4	-1	-4	-3	-3	-3	-2	-2	-1	-3
iap	-2	0	0	1	2	1	-2	-2	1	0	-1	-2	-1	-2	0	2	0	3	4	3	-1
mpi4	3	5	5	1	4	1	6	3	6	6	2	4	2	6	3	1	3	-1	2	-1	3
inm	-3	-1	1	-2	1	1	-1	-3	-2	1	-2	1	-1	-2	0	3	0	2	1	1	0
ips	0	-2	1	-1	0	-1	-3	-1	-4	0	-1	-3	-3	-1	2	3	4	4	6	5	1
mih	2	3	4	1	3	1	2	2	2	5	5	6	3	1	2	3	2	-1	0	0	3
mim	3	3	1	2	1	2	1	2	3	1	4	2	2	1	2	5	4	1	-1	2	3
miu	-1	1	0	2	0	-2	0	-2	1	-1	1	0	-2	0	1	2	1	3	1	0	1
mpi	5	6	5	5	2	4	4	4	6	4	3	2	2	4	5	4	5	5	1	3	5
mri	-1	-1	2	-2	-3	-1	1	-3	-3	0	-1	-3	-1	-1	2	2	3	1	-4	0	1
nca0	1	0	1	0	-3	-3	3	1	1	2	1	-1	2	0	2	3	3	1	0	-4	5
nca1	-1	-1	1	-1	4	-2	0	-1	0	0	3	4	0	2	-2	-1	3	-2	1	-2	1
had3	6	4	3	2	1	3	2	3	4	4	-1	-1	0	3	6	3	2	0	2	3	1
had1	2	2	3	2	2	0	4	3	2	3	3	-1	0	5	0	4	1	1	4	2	2

Table 6.4: Top 5 GCM ranking (best to worst) Model for Indian region

Ranking	NMI	NWI	NCI	WPI	EPI	SPI	NEI
				Annual			
1	had3	mpi	mpi4	gf1	gf0	bcr	mpi4
2	gf0	gf1	mpi	mpi	gf1	gf0	cs3
3	mpi	mpi4	cs3	gf0	mpi4	cc6	cc4
4	cc6	cc4	gf0	cs3	nca1	mpi	cs5
5	gf1	cc6	mih	bcr	gao	cc4	gf1
				Monsoon			
1	mpi	cc6	mpi4	mih	mih	bcr	mpi4
2	cc6	mpi4	cc4	cc4	gf1	cc6	cs3
3	gf1	mpi	mih	mim	mpi4	gf1	cs5
4	mpi4	cc4	cs3	cs3	nca1	mih	had1
5	had3	gf1	gf0	gf1	cc4	cnr	cc4
				Non-monsoon			
1	had3	mim	mpi	gf1	ips	cc4	mpi
2	cc6	gf1	ips	mpi	gf0	gf0	nca0
3	mpi	mpi	mim	ips	gao	ips	cs3
4	gf0	had1	cc4	gao	iap	bcr	cc6
5	mpi4	inm	cc6	iap	had1	gf1	cs5

6.5 SELECTION OF REPRESENTATIVE MODELS OVER UPPER NARMADA BASIN

In order to identify the best representative climate model, 24 climate models (CMs) from CMIP5 of IPCC AR5 were selected for performance evaluation. In this analysis, performance of the model was carried based on Skill Score (SS) and Root Mean Square Error (RMSE) between climate model output and reanalysis data of 20 years (1981-2000) data. However, computation of RMSE and SS were carried out by using Data Integration and Assessment Tool (DIAS) developed by University of Tokyo, Japan (Kawasaki al et. 2017). There were six meteorological parameters: precipitation (PCP), outgoing long wave radiation (OLR), air temperature (AT), mean sea level pressure (SLP), zonal wind (ZW) and meridional wind (MW) considered from each model for the SS and RMSE assessment. The comparison of climate data with reanalysis data has been carried out by checking their seasonal cycle and variability using probability density function (PDFs). Ranking of the CMs have been evaluated based on the Total Index (TI), which depends on the SS and RMSE

computation. The annual SS and RMSE values of each six climatic variables are presented in Table 6.5.

Table 6.5: Annual skill score (SS) and root mean square error (RMSE) of six climatic variables over UNB

	PCP		AT		OLR		SLP		ZW		MW	
Model	**SS**	**RMSE**	**SS**	**RMSE**	**SS**	**RMSE**	**SS**	**RMSE**	**SS**	**RMSE**	**SS**	**RMSE**
ACCESS1.0	0.64	1.55	0.79	1.11	0.78	22.67	0.84	0.89	0.82	1.17	0.73	1.07
BCC-CSM1.1	0.45	2.50	0.71	2.76	0.75	21.51	0.44	1.17	0.76	1.41	-0.11	1.44
CCSM4	0.52	1.12	0.67	1.9	0.69	9.34	0.86	2.39	0.52	1.62	0.42	1.3
CMCC-CMS	0.59	1.43	0.77	1.63	0.84	14.58	0.38	1.37	0.85	1.54	0.62	0.94
CNRM-CM5	0.50	1.58	0.80	0.93	0.62	17.36	0.81	1.12	0.87	0.95	0.76	0.87
CSIRO-Mk3.6.0	0.59	2.54	0.84	2.57	0.84	25.56	0.77	1.91	0.29	1.35	0.40	1.07
CanCM4	0.42	1.44	0.75	1.74	0.86	19.64	0.36	1.13	0.88	1.80	0.32	1.57
CanESM2	0.51	1.56	0.69	1.61	0.90	24.29	0.33	1.30	0.85	1.52	0.40	1.45
FGOALS-g2	0.33	2.17	0.63	1.66	0.69	16.10	0.49	1.47	0.90	1.95	-0.20	1.84
GFDL-CM3	0.69	0.85	0.70	2.02	0.63	14.18	0.73	1.36	0.84	1.49	0.48	1.31
GFDL-ESM2G	0.57	1.13	0.76	1.97	0.48	15.37	0.60	2.66	0.87	1.66	0.51	1.29
GISS-E2-H	0.24	3.06	0.64	4.63	0.19	32.78	0.84	2.11	0.42	1.42	0.65	1.26
GISS-E2-R	0.24	3.00	0.67	4.04	0.24	29.56	0.79	1.62	0.62	1.02	0.71	0.93
GISS-E2-R-CC	0.09	3.00	0.65	4.23	0.27	30.63	0.78	1.76	0.57	1.14	0.68	1.02
HadCM3	0.66	1.41	0.74	2.51	0.72	27.23	0.75	5.51	0.87	1.94	0.63	1.13
INM-CM4	0.56	1.41	0.50	2.20	0.73	16.52	0.54	1.56	0.61	2.02	0.26	1.37
IPSL-CM5A-MR	0.38	1.81	0.66	4.44	0.78	22.09	0.67	0.88	0.83	1.93	0.45	1.66
MIROC-ESM	0.03	1.40	0.29	1.66	0.15	11.10	0.14	2.62	0.77	3.36	0.02	2.32
MIROC-ESM-CHE	0.27	1.40	0.42	1.60	0.28	10.37	0.16	2.54	0.80	3.23	0.02	2.28
MIROC5	0.72	1.94	0.80	0.98	0.94	9.97	0.78	1.33	0.88	1.35	0.61	0.73
MPI-ESM-LR	0.68	1.29	0.81	1.67	0.90	13.91	0.42	1.63	0.87	1.52	0.63	0.78
MRI-CGCM3	0.65	2.68	0.82	2.63	0.84	24.93	0.78	3.34	0.82	1.18	0.53	1.55
MRI-ESM1	0.55	2.71	0.81	2.55	0.80	24.82	0.76	3.38	0.82	1.19	0.52	1.53
NorESM1-M	0.51	1.29	0.82	1.57	0.77	9.99	0.73	1.37	0.85	1.45	0.60	1.17

Performance of climate models were evaluated based on the 'Total Index' (TI) employing the multi criteria analysis. In order to compute the Total Index, multi criteria were applied on the simulated values of SS and RMSE values (Equations 6.6-6.10). However, annual average values of SS were computed as 0.47, 0.74, 0.65, 0.61, 0.76 and 0.44 for PCP, AT, OLR, SLP, ZW and MW, respectively. Moreover, RMSE values evaluated as 1.84, 2.28, 19.35, 1.93, 1.63 and 1.33 for PCP, AT, OLR, SLP, ZW and MW, respectively. Applying multicriteria analysis in S_{index} and $RMSE_{index}$,

TI value may vary in the range from +6 to -6, +6 TI value indicates all six variable are acceptable for particular climate model, whereas -6 exhibit none of climate variables are acceptable of particular model in study area. In this analysis, two climate models MIROC5 and CNRM-CM5 indicate the +6 TI values follow by +5 TI vales of MPI-ESM-LR, GFDL-ESM2M and IPSL-CM5A-MR (Figure 6.9). Lowest TI values was noted -2 for GISS-E2-H and BCC-CSM1.1 (Figure 6.9).

However, to reduce the uncertainly in climate projection, top three climate models: MIROC5, CNRM-CM5 and MPI-ESM-LR were selected as representative climate models for hydrological modelling over the study area. The dynamical downscaled data (regional climate model data) of these three climate models have been coupled with SWAT, hydrological model to estimate the water balance components. Table 6.6 indicate the selected models and description about the centre location.

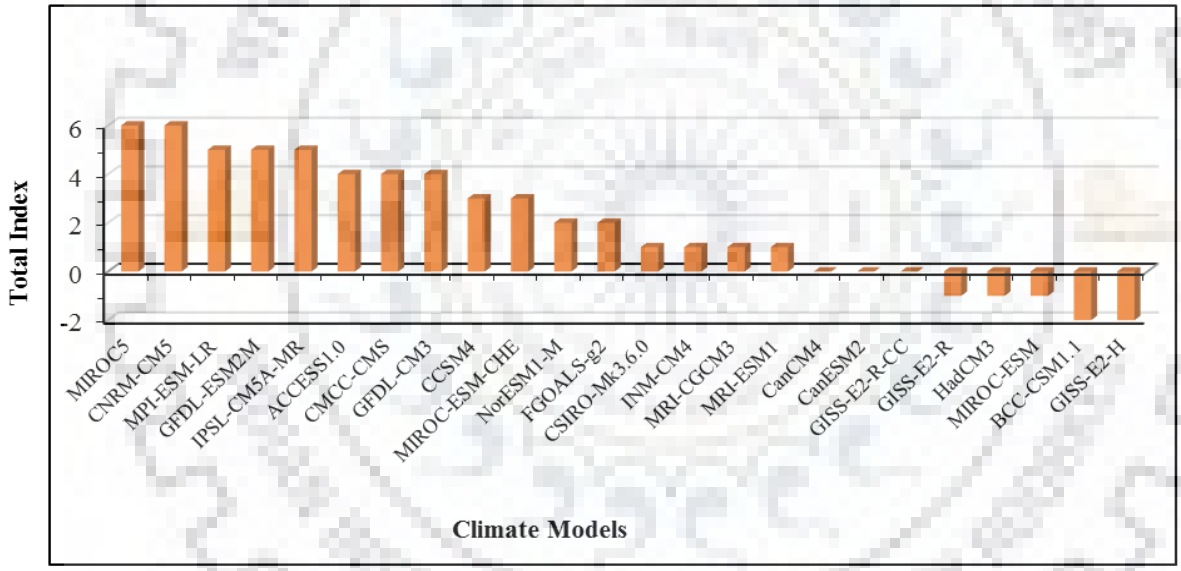

Figure 6.9: Ranking of climate models based on Total Index (TI)

Table 6.6: Description of centre location of selected representative climate models for hydrological studies

Climate model	Short Name	Centre and Location
MIROC5	MIROC	Center for Climate System Research (The University of Tokyo), Japan
CNRM-CM5	CNRM	Centre National de Recherches Meteorologiques, Meteo, France
MPI-ESM-LR	MPI	Max Planck Institute for Meteorology, Germany

Source: http://cmip-pcmdi.llnl.gov/cmip5/availability.html

6.6 BIAS CORRECTION OF RCM OUTPUT

Bias correction process apply a transformation algorithm for correcting the RCM output. The basic approach is to evaluate biases in baseline (control period) RCM climate variables, by comparing the observed climate variables, which is also applicable for correcting the baseline and RCP scenarios runs. In this study, dynamical downscaled GCMs output (RCM data) of driving representative GCMs were selected with integration of hydrological model. The RCM data from Coordinated Regional Downscaling Experiment (CORDEX) was used to assess the climate projections over the river basin under IPCC AR5, representative concentration pathways (RCPs) 4.5 and 8.5 scenarios. The CORDEX-RCM outputs represent daily average at the spatial resolution of 0.44° x 0.44° (~50 km x 50 km) for regional climate impact studies. However, these outputs are not be used directly for hydrological models to assess the local scale studies because of systematic biases. These biases are the results of imperfect conceptualization, discretization while downscaling and spatial averaging within grid cells (Graham et al. 2007a). Therefore, bias correction approach, distribution mapping was applied on precipitation and temperature series to remove the inherent systematic biases.

6.6.1 Distribution Mapping

Distribution mapping method was used to correct the raw RCM output variables. The basic concept of distribution mapping is to adjust the distribution function of raw climate variables (RCM data) to fit with the observed distribution function of observed data by developing the transform function (Johnson and Sharma 2012; Teutschbein and Seibert 2012). In order to correct the raw simulated series (RCM data), Gamma distribution and Gaussian distribution often assumed best suited distribution for precipitation data and temperature data, respectively.

Gamma distribution: $$f(x|\alpha,\beta) = x^{\alpha-1}\frac{1}{\beta^{\alpha}.\Gamma(\alpha)}.e^{-\frac{x}{\beta}}; \quad x \geq 0; \quad \alpha,\beta > 0 \qquad \text{.....(6.11)}$$

Where, α and β are shape parameter and scale parameters, respectively (Block et al., 2009; Ines and Hansen, 2006; Katz, 1999; Piani et al., 2010; Watterson, 2003).

Gaussian distribution: $$f(x|\mu,\sigma^2) = x^{\alpha-1}\frac{1}{\sigma\sqrt{2\pi}}.e^{\frac{-(x-\mu)^2}{2\sigma^2}}; \quad x \in R \qquad \text{.....(6.12)}$$

Where, σ and μ are scale parameter and location parameters, respectively (Christensen et al., 2008; Teutschbein and Seibert 2012).

Firstly, cumulative distribution function (CDFs) were developed for both observed series and baseline RCM output series for all days of corresponding month and baseline simulated CDF shifted to the observed CDF (Lafon et al., 2013; Teutschbein and Seibert, 2012). Therefore, the same CDFs use to correct the baseline and future projected series.

$$P'_{bl}(d) = F_G^{-1}[F_G(P_{bl}(d)\left|\alpha_{bl,m}, \beta_{bl,m}\right)\left|\alpha_{obs,m}, \beta_{obs,m}\right] \quad \text{..... (6.13)}$$

$$P'_{\text{rcp}}(d) = F_G^{-1}[F_G(P_{\text{rcp}}(d)\left|\alpha_{rcp,m}, \beta_{rcp,m}\right)\left|\alpha_{obs,m}, \beta_{obs,m}\right] \quad \text{..... (6.14)}$$

For temperature, Gaussian CDFs transfer indicated as follows:

$$\text{T}'_{bl}(d) = F_G^{-1}[F_G(\text{T}_{bl}(d)\left|\mu_{bl,m}, \sigma^2_{bl,m}\right)\left|\mu_{obs,m}, \sigma^2_{obs,m}\right] \quad \text{..... (6.15)}$$

$$\text{T}'_{\text{rcp}}(d) = F_G^{-1}[F_G(\text{T}_{\text{rcp}}(d)\left|\mu_{rcp,m}, \sigma^2_{rcp,m}\right)\left|\mu_{obs,m}, \sigma^2_{obs,m}\right] \quad \text{..... (6.16)}$$

Where, F and F^{-1} and indicates the CDF and its invers, respectively. For precipitation, Gamma CDF (F_G) was used, whereas Gaussian CDF (F_N) suited for temperature bias correction (Teutschbein and Seibert 2012).

While bias correction on series, cumulative distribution function (CDFs) were developed for both observed series (1971-2000) and baseline RCM output series (1971-2000) for all days of corresponding month and baseline simulated CDF shifted to the observed CDF. Therefore, the same CDFs use to correct the baseline and future projection (2011-2040, 2041-70, 2071-2100) series. It is an assumption that bias correction approaches are stationary, which indicate correction algorithm and parameterization is applicable for future scenarios as well.

6.7 CONCLUDING REMARKS

Global climate models (GCMs) were evaluated and the most suitable model was identified that can best reproduce the meteorological parameters for hydrological and impact studies for the UNB. In this analysis, 24 GCMs were used for assessment from Coupled Model Intercomparison Project, CMIP3 and CMIP5 for regional (Indian region) and local study area (UNB), respectively. Each GCM output was evaluated with reanalysis data, Skill Score (SS) and Root Mean Square Error (RMSE) are the main tools used to assess the performance for six meteorological variables (precipitation, outgoing long wave radiation, air temperature, mean sea level pressure, zonal wind and meridional wind) of GCMs. By considering the combined effect of meteorological variables,

GCM models ranked from 'best' to 'worst' using multi-criteria analysis (MCA). For regional study, the entire Indian region was divided into seven zones on the basis of homogeneous precipitation. These zones are North Mountainous India (NMI), North Central India (NCI), Northwest India (NWI), East Peninsular India (EPI), West Peninsular India (WPI), South Peninsular India (SPI) and North East India (NEI). The study has been carried out for monsoon season, non-monsoon season and for the entire year, and performance of each model was checked and ranked for each individual zone. Result of the study indicate, there is no single GCM which can be recommended for the whole Indian region. The main concluding remarks drawn from the study are:

a) GCM model for precipitation have been proposed as ensemble of MPI_ECHAM4.0, MIROC3.2_HIRES, UKMO_HADCM3.0 and INGV_ECHAM4 are the best model for the Indian region.

b) Climate models of CCCMA groups are performing well for atmospheric temperature in most of the Indian region.

c) Climate models CCCMA, ECHAM and MIROC3.2 models have been evaluated for meridional wind over the Indian region.

d) The resemblance GFDL_CM2.0, MPI_ECHAM5, INGV_ECHAM4, UKMO_HADCM3 and BCCR_BCM2_0 GCM models are recommended for the whole India for the annual study.

e) Three climate models, MIROC5, CNRM-CM5 and MPI-ESM-LR were selected as representative climate models for UNB.

f) Distribution mapping (quantile-quantile) method was used to correct the raw RCM output climatic variables. The basic concept of distribution mapping is to adjust the distribution function of raw climate variables (RCM data) to fit with the observed distribution function of observed data (IMD data) by developing the transform function. In order to correct the raw simulated series (RCM data), Gamma distribution and Gaussian distribution often assumed best suited distribution for precipitation data and temperature data, respectively.

CHAPTER 7

HYDROLOGICAL SIMULATION UNDER LAND USE LAND COVER DYNAMICS AND RCP SCENARIOS

7.1 GENERAL

To maintain the sustainable development, knowledge on water availability of a country or region, strategic information needed for long-term planning to fulfil the water requirement including agriculture and domestic purpose. In the recent past, enough evidences provided by scientific community that 'Climate is changing and it is unequivocally phenomena' (Pachauri et al. 2014). The influencing factors of global warming and changes in climatic system are emission of greenhouse gases (GHGs) and anthropogenic activities (Graham et al. 2007; Solomon, 2007; Zhu, 2013). Increasing concentration in greenhouse gases modifying the hydrological cycle and the frequency and magnitude of hydrological and climatic parameters. The projection of water availability on regional hydrology depends upon land use land cover and simulated climate variables (e.g., temperature, precipitation) from the global climate models (GCMs). It is quite common to estimate the water balance variations under land use land cover change and climate change from GCMs output coupled with hydrological model. Therefore, it is important to examine the performance of GCMs simulation for hydrological studies. However there are very limited studies are available on virtual water variability considering dynamics of land use land cover and climate change impact. In the recent past, water footprint concept has been introduced that is assessed in terms of consumed, evaporated and polluted water and categorized in blue, green and gray water footprint by the scientific community (Aldaya et al. 2012; Chapagain and Hoekstra 2004; Hoekstra 2008; Hoekstra and Hung 2002). Moreover hydrological simulation is not possible without calibrated hydrological model set up for the region. In order to calibrate the model, there are many hydrological parameters that cannot be measured directly in the field, but must be obtained through a model calibration process. Model calibration is thus an essential task to obtain the optimal parameter values, which match simulations with observations as closely as possible.

As already have been discussed in earlier section, there are very limited studies based on assessment of hydrological responses under dynamics of land use land cover and climate change for UNB. Hence the aims of study presented in this chapter are: (1) setup the semi-distributed hydrological

model (SWAT) applying multi-site calibration techniques for Upper Narmada Basin, (2) computation of land use land cover change impact on water availability under constant climatic condition, (3) evaluation and assessment of hydrological components, including blue water and green water, under future scenarios from 2011 to 2100 under IPCC AR5 representative concentration pathways (RCPs), moderate emission scenario (RCP4.5) and high emission scenario (RCP8.5). However, overall process of impact studies is illustrated in Figure 7.1.

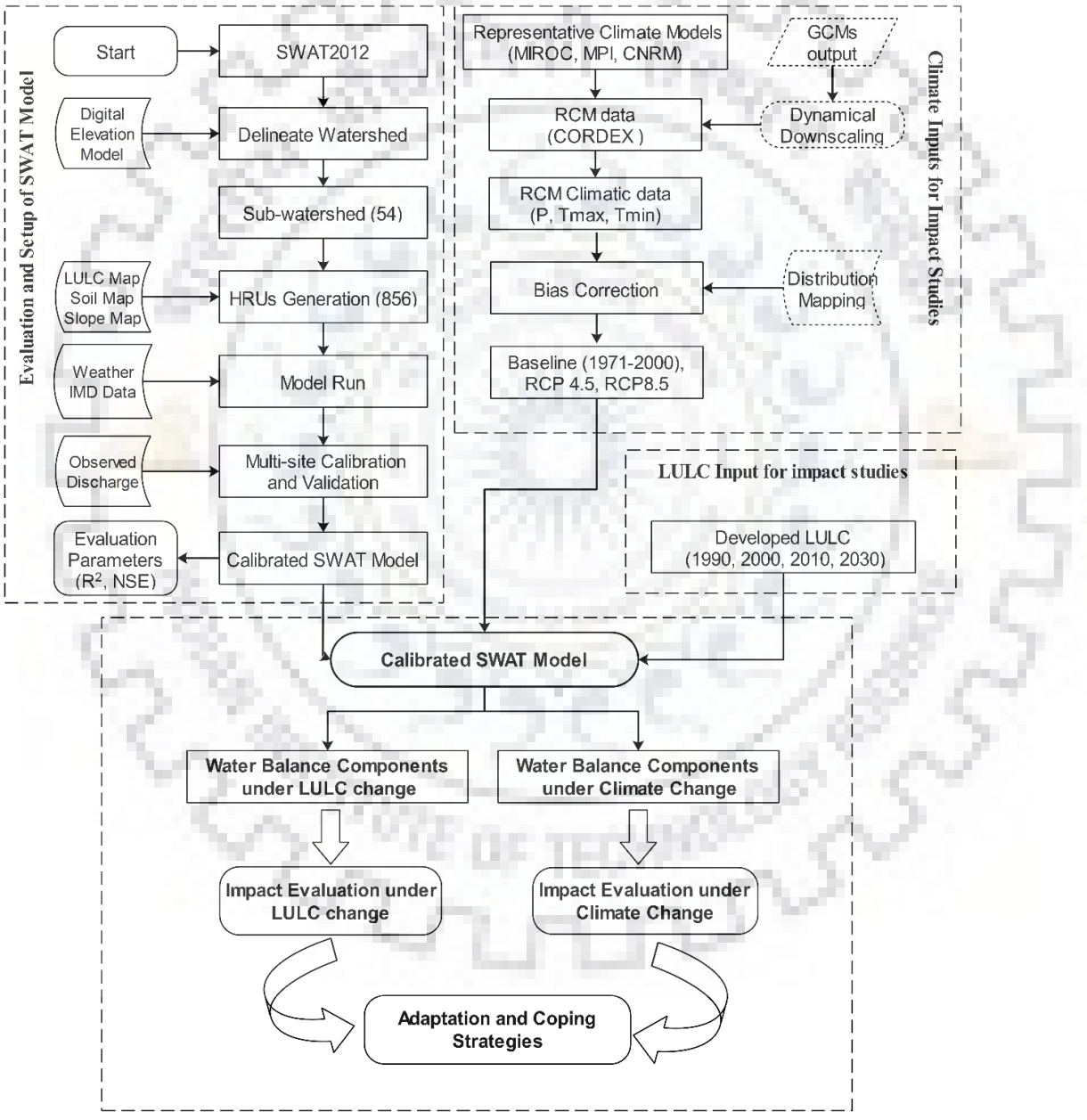

Figure 7.1: Framework of impact assessment on water availability due to land use land cover and climate change

7.2 DATA PROCESSING

7.2.1 Spatial data

Different type of spatial data are required in the SWAT model for simulation. The data required by SWAT for basin simulation are:

Digital Elevation Model: Shuttle Radar Topographic Mission (SRTM) has provided digital elevation data (DEMs) of 90 m resolution. The downloaded digital elevation model from SRTM has projection system of WGS_1984_UTM, Zone_44 N at 90-meter resolution and the position of study area is maximum.

Soil Map: Food and Agriculture Organization (FAO) digital soil map of the world having scale of 1:5,000,000.

Land Use Map: The land use land cover data is essential for hydrological modelling. The land use land cover of an area is one of the major factor which affect surface runoff, evapotranspiration and erosion in the basin. The land use land cover map of 2011-12 was procured from National Remote Sensing Centre (NRSC) Hyderabad, Government of India on 1:50,000 scale used in climate change impact study over the basin.

The distribution of different elevation, slope, land use classes and soil map of basin are presented in Figure 7.2 and Annexure 2.

7.2.2 Hydro-meteorological Data

Discharge Data: Hydro-meteorological stations in India setup by an apex central Government body, Central Water commission (CWC), India. In this study, daily discharge data was downloaded from 'Water Resources Information System India (WRIS-India) website, managed by National Remote Sensing Centre- Indian Space Research Organization (NRSE-ISRO).

Weather Data: High resolution (1^o x 1^o) daily gridded temperature data set for the period 1969-2005 and (0.5^o x 0.5^o latitude/longitude) gridded daily rainfall data for the period 1971-2005 over Indian region developed by India Meteorological Department (IMD) Pune, India.

Regional Climatic Data: The regional climate model (RCM) data provided by Coordinated Regional Downscaling Experiment (CORDEX) was used in this study. Climate change simulation of RCM at a spatial resolution of 0.44^o x 0.44^o.

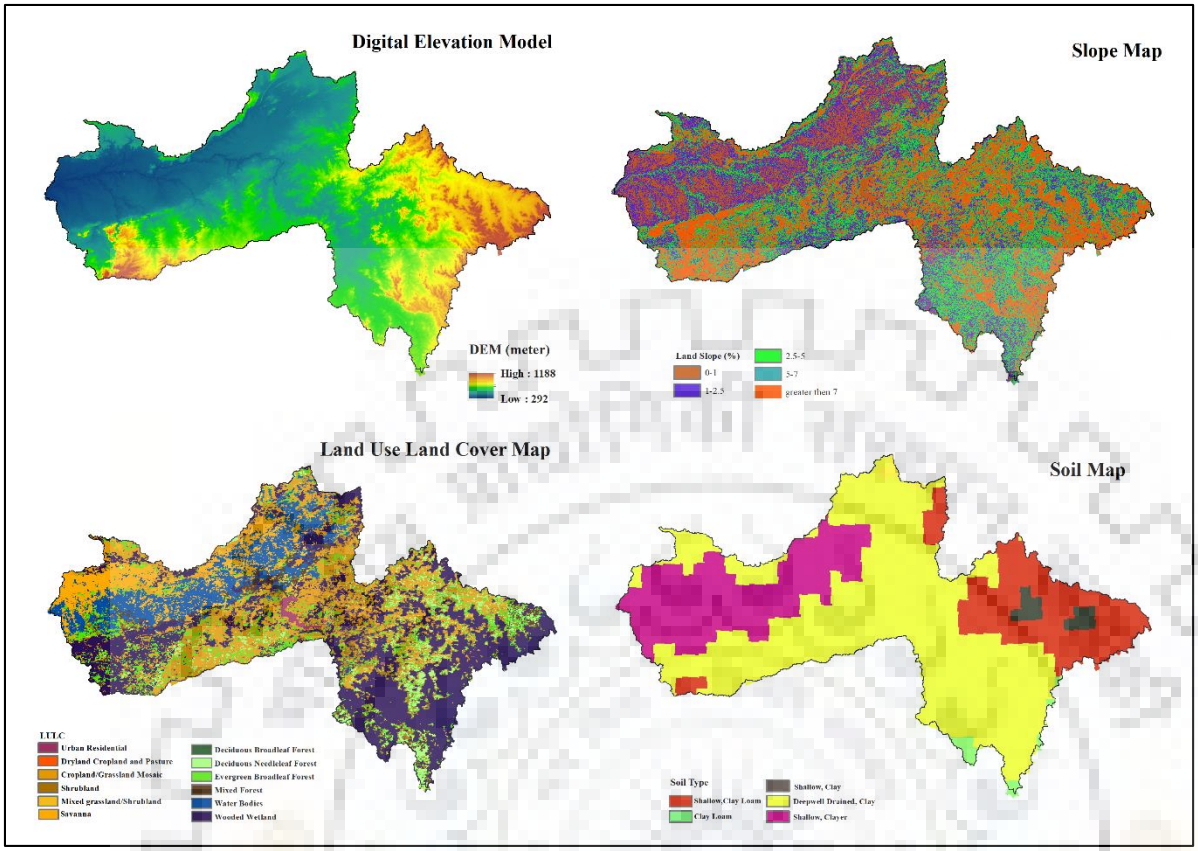

Figure 7.2: Spatial data (elevation, slope, land use and soil map) for hydrological modelling

7.3 HYDROLOGICAL MODEL: SOIL AND WATER ASSESSMENT TOOL

7.3.1 Introduction

To simulate water availability, a physical based, semi-distributed hydrological model, Soil and Water assessment tool (SWAT) was used and operated on daily time step in this study (Arnold et al. 1994; Neitsch et al. 2011). The model has ability to simulating various hydrological process including future hydro-climatic changes considering future climatic projections and land management practices on quantity and quality of water resources in river basin (Ullrich and Volk 2009).

For hydrological response, the model divides the main basin into small sub-basins and sub-basins into small hydrological response unit (HRU) connected through drainage network (Green et al. 2006). HRU is the lumped unit that comprised of unique combination of land use/land cover, soils and slope area that allows routing of flows to the downstream sections (Neitsch et al. 2011).

The main climatic inputs data for hydrological model are precipitation, minimum temperature, and maximum temperature, solar radiation, and relative humidity (Arnold et al. 1998). The spatial data required for SWAT model area digital elevation model (DEM), land use/land cover map, soil map data (Arnold et al. 1998; Neitsch et al. 2011). Observed precipitation and temperature dataset were obtained from the India Meteorological Department (IMD), India. DEM data was delineate the watershed and to derive the basin features such as slope length and gradient, stream network characteristics (channel slope, length and width) were derived from the DEM using the automatic watershed delineation tool in the recent version of ArcSWAT, interface of ArcGIS10.2.

7.3.2 Model Equations

The hydrologic cycle equation in the land phase as simulated by SWAT is based on the governing water balance equation (Arnold et al. 1994; Pandey et al. 2016).

$$SW_t = SW_o + \sum_{t}^{i=1} (R_{day} - Q_{sur} - ET - W_{seep} - Q_{gw}) \quad \text{..... (7.1)}$$

Where, SW_t and SW_o is the final soil water content (mm initial soil water content on day i (mm), t is the time (days), R_{day} is the amount of precipitation on day i (mm), Q_{surf} is the amount of surface runoff on day *i* (mm), *ET* is the amount of evapotranspiration on day *i* (mm), W_{seep} is the amount of water entering the vadose zone from the soil profile on day *i* (mm), and Q_{gw} is the amount of return flow on day *i* (mm) (Setegn et al. 2009).

Surface Runoff

Surface runoff occurs whenever the rate of water application to the ground surface exceeds the rate of infiltration. When water is initially applied to a dry soil, the application rate and infiltration rates may be similar. However, the infiltration rate will decrease as the soil becomes wetter. When the application rate is higher than the infiltration rate, surface depressions begin to fill. If the application rate continues to be higher than the infiltration rate once all surface depressions have filled, surface runoff will commence. SWAT provides two methods for estimating surface runoff: the SCS curve number procedure (SCS, 1972) and the Green & Ampt infiltration method (1911).

The SCS runoff equation is an empirical model that came into common use in the 1950s. It was the product of more than 20 years of studies involving rainfall-runoff relationships from small rural watersheds across the U.S. The model was developed to provide a consistent basis for estimating

the amounts of runoff under varying land use and soil types (Rallison and Miller, 1981). The SCS curve number equation is (SCS, 1972):

$$Q_{surf} = \frac{\left(R_{day} - I_a\right)^2}{(R_{day} - I_a + S)} \quad \text{..... (7.2)}$$

Where, Q_{surf} is the accumulated runoff or rainfall excess (mm), R_{day} is the rainfall depth for the day (mm), I_a is the initial abstractions which includes surface storage, interception and infiltration prior to runoff (mm), and S is the retention parameter (mm). The retention parameter varies spatially due to changes in soils, land use, management and slope and temporally due to changes in soil water content. The retention parameter is defined as:

$$S = 25.4\left(\frac{1000}{CN} - 10\right) \quad \text{..... (7.3)}$$

Where, CN is the curve number for the day. The SCS curve number is a function of the soil's permeability, land use and antecedent soil water conditions. Typical curve numbers for moisture condition II for various land covers and soil types is provided in standard tables (SCS Engineering Division, 1986).

Potential Evapotranspiration

Potential evapotranspiration is the rate at which evapotranspiration would occur from a large area completely and uniformly covered with growing vegetation which has access to an unlimited supply of soil water. This rate is assumed to be unaffected by micro-climatic processes such as advection or heat-storage effects. The model offers three options for estimating potential evapotranspiration: Hargreaves (Hargreaves et al. 1985), Priestley-Taylor (Priestley and Taylor, 1972), and Penman-Monteith (Monteith, 1965).

Lateral Subsurface Flow

Lateral subsurface flow, or interflow, is streamflow contribution which originates below the surface but above the zone where rocks are saturated with water. Lateral subsurface flow in the soil profile (0-2m) is calculated simultaneously with redistribution. A kinematic storage model is used to predict lateral flow in each soil layer. The model accounts for variation in conductivity, slope and soil water content.

Peak Runoff Rate

Predictions are made with a modification of the rational method. In brief, the rational method is based on the idea that if a rainfall of intensity *i* begins instantaneously and continues indefinitely, the rate of runoff will increase until the time of concentration, t_c, when all of the sub-basin is contributing to flow at the outlet. In the modified 'Rational Formula', the peak runoff rate is a function of the proportion of daily precipitation that falls during the sub-basin t_c, the daily surface runoff volume, and the sub-basin time of concentration. The proportion of rainfall occurring during the sub-basin t_c is estimated as a function of total daily rainfall using a stochastic technique. The sub-basin time of concentration is estimated using Manning's Formula considering both overland and channel flow.

7.4 HYDROLOGICAL MODEL SETUP FOR BASIN

The Soil and Water Assessment Tool (SWAT), a semi-distributed hydrological model was used to simulate the hydrological response of Upper Narmada Basin (UNB). To simulate the potential climate change impact on hydrology of river basin, it was important to calibrate and validate the hydrological model (Abbaspour et al. 2015; Green and Vangriensven 2008; Sayasane et al. 2016; Wu and Liu 2012). The major and wide steps of the model setup are: (i) watershed delineation and derive the sub-basin features (ii) HRU definition (iii) model calibration, validation and parameter sensitivity analysis.

In this study, main basin divided into the 54 sub-basins (Annexure 3), and 54 sub-basin further subdivided in to 856 Hydrological Response Units (HRUs). Each HRU is a unique combination of characterized definition of land-use, soil, and slope classes. The drainage networks in the basin were derived by considering the threshold value of 15000 hectare. The runoff from each HRUs routed through the reach network to the sub-basins and sub-basins runoff routed to the river basin applying either the variable storage routing method or the Muskingum method (Neitsch et al. 2011). In this case, variable storage routing methods was opted as routing method cause less requirement of input variables as compared to Muskingum. Moreover, surface runoff can be computed by using either SCS curve number or Green Ampt Infiltration (GAI) method (Neitsch et al. 2011). In this run, SCS Curve Number was preferred over the Green Ampt infiltration because it needs daily precipitation, whereas GAI required sub-daily precipitation input. While computing the potential evapotranspiration (PET), Hargreaves method was applied instead of Penman-Monteith and

Priestley-Taylor because it requires minimum data such as daily precipitation, and maximum and minimum temperature. Additionally, seven G&D sites setup by Central Water Commission (CWC) were selected to calibrate and validate the model. Comparison of measured and simulated drainage area indicated in Table7.1:

Table 7.1: Discharge gauging sites used in calibration and validation of model

S.N.	Gauging Sites	Latitude	Longitude	CWC* Area(km^2)	Simulated Area (km^2)	Difference Area (%)
1	Bamni Banjar	22.48389	80.37778	1864	1836	1.50
2	Belkheri	22.92889	79.33944	1508	1460	3.18
3	Gadarwara	22.92972	78.78806	2270	2190	3.52
4	Manot	22.73583	80.51306	4667	4825	-3.39
5	Mohgaon	22.76083	80.62361	3919	3950	-0.79
6	Patan	23.31167	79.66361	3950	3945	0.13
7	Sandia$^+$	22.91833	78.34889	33953	32795	3.41

*+ Outlet gauging site of Upper Narmada Basin;**Source: Integrated Hydrological Data Book (January, 2015), Central Water Commission (CWC), New Delhi*

7.4.1 Model Evaluation Parameters

In this study, goodness of calibration and validation is evaluated based on the coefficient of determination (R^2), and Nash-Sutcliffe efficiency (NSE). In general, model is acceptable if the Coefficient of determination (R^2) is greater than 0.5, and calculated as:

$$R^2 = \frac{\left[\sum_i (Q_{m,i} - \overline{Q}_m)(Q_{s,j} - \overline{Q}_s)\right]^2}{\sum_i (Q_{m,j} - \overline{Q}_m)^2 \sum_i (Q_{s,i} - \overline{Q}_s)^2} \quad \ldots\ldots (7.4)$$

Nash-Sutcliffe efficiency (NSE) ranges from -∞ to 1, where 1 indicates perfect simulation against observed value. It was used as objective function to identify the best simulation rages of parameters due to its wide applicability and reliability in hydrological modelling (Willmott et al. 2012; Willmott et al. 2015).

$$NSE = 1 - \frac{\sum_i (Q_o - Q_s)^2{}_i}{\sum_i (Q_{o,\mathrm{i}} - \overline{Q}_o)^2} \quad \ldots\ldots (7.5)$$

The ratio of root mean square error (RMSE) and standard deviation (σ) of observed value, it is measured as RSR:

$$RSR = \frac{RMSE}{\sigma_o} = \frac{\sqrt{\sum_{i=1}^{n}(Q_o - Q_s)_i^2}}{\sqrt{\sum_{i=1}^{n}(Q_o - \overline{Q}_o)_i^2}} \quad \ldots\ldots (7.6)$$

Percent Bias (PBIAS) indicated the underestimated or overestimated observed variable.

$$PBIAS = \frac{\sum_{i=1}^{n}(Q_o - Q_s)_i}{\sum_{i=1}^{n} Q_o} X 100\% \quad \ldots\ldots (7.7)$$

Where, Q_o and Q_s represent the observed discharge and simulated discharge respectively, whereas $\bar{Q}_o$ is the mean observed discharge value.

In order to evaluate the performance of calibrated and validated SWAT model, statistics of evaluation parameters in hydrology for monthly time steps proposed by Moriasi et al. (2007) is given in Table 7.2:

Table 7.2: General rating of performance of model for recommended statistics for monthly step

Performance Rating	NSE	R^2	PBIAS	RSR
Poor	≤ 0.50	≤ 0.50	≥ ±25	0.0 – 0.5
Satisfactory	0.5 – 0.6	0.5 – 0.6	±15 – ±25	0.6 – 0.5
Good	0.6 – 0.75	0.6 – 0.8	±10 – ±15	0.7 – 0.6
Very Good	0.75 – 1.00	0.8 – 1.0	≤ ±15	≥ 0.70

7.4.2 Uncertainty and Sensitivity Analysis

The ability of a hydrological model to sufficiently predict water balance for a particular application is assessed by sensitivity analysis of parameters, model calibration and model validation. Sensitivity is evaluated as the response of an output variable to alter in an input parameter, with the bigger change in output response representing to a greater sensitivity. Sensitivity analysis measures how different parameters influence a predicted output. Model parameters identified in sensitivity analysis that influence predicted outputs are often used to calibrate a model. Model calibration entails the modification of parameter values and comparison of predicted output of interest to measured data

until a defined objective function is achieved (James and Burges, 1982). After achieving the objective function for calibration, validation of the model. Validation procedures are similar to calibration procedures in that simulated and observed values are compared to determine if the objective function is met. However, a dataset of observed basin response selected for validation preferably should be different than the one used for model calibration, and the model parameters are not adjusted during validation. Validation provides a test of whether the model was calibrated to a particular dataset or the system it is to represent. If the objective function is not achieved for the validation dataset, calibration and/or model assumptions may be revisited. In this study, SWAT parameters for calibration were selected after reviewing the several publication.

In this study, Latin hypercube one-factor-at-a-time (LHOAT) method of sensitivity analysis (Morris 1991) was used, implemented in SWATCUP. This tools can be used to evaluate the sensitivity of a parameter that assess the model calibration and parameter uncertainty (Veith and Ghebremichael 2009). This global sensitivity analysis approach has the advantage of being fast compared to similar procedures and, as a result, one does not obtain an absolute measure of the sensitivity but rather a ranked order of the parameters. Ranking of sensitive parameters and code description is given in Table 7.3, while best fitted value range of SWAT parameters are shown in Table 7.4.

Table 7.3: Ranking of sensitive parameters for outlet point UNB (at Sandia)

Ranking	Parameter Name	Definition
1	CN2.mgt	Curve number
2	ALPHA_BF.gw	Base flow recession constant
3	GW_DELAY.gw	Groundwater delay (days)
4	GWQMN.gw	Threshold depth of water in the shallow aquifer required for return flow to occur (mm)
5	ESCO.bsn	Soil evaporation compensation factor
6	EPCO.bsn	Plant uptake compensation factor
7	GW_REVAP.gw	Groundwater re-evaporation coefficient
8	REVAPMN.gw	Threshold depth of water in the shallow aquifer for re-evaporation to occur
9	SOL_K(..).sol	Soil hydraulic conductivity
10	OV_N.hru	Manning's n value for the main channel
11	SOL_AWC(..).sol	Available soil water capacity
12	CANMX.hru	Maximum canopy storage

Table 7.4: Maximum (Max), minimum (Min) and best fitted values of parameters for calibration

S.N	Parameter	Change Type	Fitted value of calibrated sites*							Max-Min Range
			SD	BB	BK	GD	MN	MG	PT	
1	CN2.mgt	Relative	-0.05	0.01	-0.01	-0.02	0.015	0.01	-0.01	-0.1- 0.1
2	ALPHA_BF.gw	Replace	0.57	0.46	0.43	0.44	0.43	0.41	0.58	0.5 - 0.85
3	GW_DELAY.gw	Replace	367	220	230	310	240	201	351	30 - 450
4	GWQMN.gw	Replace	0.29	0.34	0.31	0.10	0.16	0.23	0.12	0.1 -1
5	ESCO.bsn	Replace	0.21	0.18	0.26	0.26	0.56	0.14	0.28	0.1 - 0.7
6	EPCO.bsn	Replace	0.11	0.12	0.23	0.19	0.23	0.15	0.14	0.1- 0.7
7	GW_REVAP.gw	Relative	0.04	0.04	0.04	0.025	0.022	0.026	0.037	0.02 - 0.2
8	REVAPMN.gw	Replace	229	182	223	196	129	223	236	120 - 250
9	SOL_K.sol	Relative	-0.04	0.05	0.03	-0.05	0.015	0.02	-0.034	-0.1 - 0.2
10	OV_N.hru	Replace	0.15	0.01	0.09	0.150	0.13	0.07	0.17	0.01 - 0.2
11	SOL_AWC.sol	Replace	0.26	0.36	0.41	0.23	0.25	0.15	0.18	0.1 - 0.8
12	CANMX.hru	Replace	34	32	39	28	41	26	36	20 - 80

Note: SD:Sandia; BB:Bamni Banjar; BK:Belkheri; GD:Gadarwara; MN:Manot; MG:Mohgaon; PT:Patan

Sequential Uncertainty Fitting Version 2 (SUFI-2) in the SWAT-Calibration Uncertainties Program (SWAT-CUP) tool was used to analyze the uncertainties of model calibration and validation and identifying of sensitive input variables (Abbaspour et al. 2015). SUFI-2 algorithm in SWAT-CUP was used because of ability to tune many parameters while running the model. In this study, 12 SWAT parameters were selected for the calibration and model simulation with 500 combination of 3 iteration during 1978-1995. In each model run, parameters tune the values to match the simulated discharge with observed discharge, afterward these values used to validate the model by monthly discharge values from 1996 to 2005. In general, three major sources of uncertainty observed in the outputs of a hydrological model: structural uncertainty, input uncertainty and parameter uncertainty. The structural uncertainty due to adopting a set of assumptions to simplify the modelling of the desired process. The uncertainty in input may be caused by the error in various climatological inputs, whereas model parameters uncertainty is the results of the effects of major and minor construction such as roads and hydraulic structure, which may produce considerable measures of sediment in short period. Input uncertainty is associated with spatially interpolated measurements of model input or initial conditions (Yang et al. 2008). The uncertainties are quantified by a measure known as the 'p' factor, which is the percentage of observed data bracketed by the 95% prediction uncertainty

(95PPU). The 95PPU is calculated at the 2.5% and 97.5% levels of the cumulative distribution of an output variable obtained through Latin hypercube sampling. This is calculated by the 2.5^{th} and 97.5^{th} percentiles of the cumulative distribution of every simulated point. Another measure quantifying the strength of an uncertainty analysis is the r-factor, which is defined as the average thickness of the 95PPU band divided by the standard deviation of the observed data (Abbaspour, 2008). The goodness of fit and the degree to which the calibrated model accounts for uncertainties are assessed by the above two measures. Theoretically, the value of the p-factor ranges between 0% and 100%, while that of the r-factor ranges between 0 and infinity. A p-factor of 1 and r- factor of zero indicates that a simulation exactly mimic the observation. SUFI-2 seeks to bracket most of the measured data (large p-factor, maximum 100%) with the smallest possible value of r-factor (minimum 0).

7.4.3 Calibration and Validation of Multi-site SWAT Model

Normally, most of the time single site calibration approach is adopted, in which observations (e.g., discharge) from a single gauging site (usually at the basin outlet) are used (Bannwarth et al. 2015; Shi et al. 2013). However, the applicability of this technique for complex and spatially heterogeneous basin is questionable because only one output information at the basin outlet is used for model constraint. Such type of method may yield unrealistic parameter values, which may not suitably of the processes within the basin. Therefore, a multisite calibration approach, in which one or more variables and objective functions are considered at multiple sites to appropriately represent the spatial variability of a given basin. This method is anticipated to better performance of spatially distributed hydrologic models by representing the spatial variability with different parameter values. In this way, multisite calibration approach may reduce the chance to optimize the model to physically unrealistic parameter values. Thus, multisite calibration can potentially improve the parameter uncertainty during the calibration process. Hence, model calibration at different locations of a basin is crucial for the SWAT model, particularly for a spatially heterogeneous catchment.

The SWAT model was calibrated and validated for UNB using monthly observed discharge records from seven gauging sites (Figure 7.3). Table 7.2 represents the measured and simulated sub-catchment area and location of gauging sites, whereas Figure 7.3 represents the stream network, sub-basin and calibration locations. Figure 7.4 indicate the monthly calibration and validation result performed at outlet for 18 years (1978 to 1995) and 10 years (1996 to 2005), respectively, considered the 3 years (1975-1977) warm-up period. Moreover, Figure 7.5 shows the scatter plot of calibration

and validation for outlet of basin (Sandia). In this study, Nash-Sutcliffe efficiency (NSE) was used as objective function to identify the best simulation rages of parameters due to its wide applicability and reliability in hydrological modelling (Willmott et al. 2012; Willmott et al. 2015). Table 7.3 indicates NSE value are 0.77 and 0.73 for calibration and validation, respectively at outlet point of basin (Sandia), however NSE values ranges varying from -∞ to 1, and close to 1 values are acceptable performance (Willmott et al. 2012). Figure 7.5 shows the correlation between simulated discharge and observed discharge exhibit 0.76 and 0.70 values for calibration and validation, which is good and satisfactory (Bisantino et al. 2015; Moriasi et al. 2007). However, Table 7.5 indicates other evaluation parameters such as coefficient of determination (R^2), r-factor (observations bracketed by the prediction uncertainty) and p-factor (achievement of small uncertainty band) also considered in model evaluation.

Table 7.5: Model multi-calibration and validation evaluation values

Site	Evaluation	Duration	p-factor	r-factor	NSE	R^2
Sandia+	Calibration	1978 - 1995	0.62	1.21	0.77	0.76
	Validation	1996 - 2005	0.80	0.96	0.73	0.70
Bamni Banjar	Calibration	2000- 2003	0.31	0.30	0.75	0.72
	Validation	2004 - 2005	0.61	0.48	0.80	0.93
Belkheri	Calibration	1978 - 1995	0.81	0.92	0.83	0.86
	Validation	1996 - 2005	0.36	0.72	0.72	0.91
Gadarwara	Calibration	1978 - 1995	0.62	0.68	0.84	0.81
	Validation	1996 - 2005	0.80	0.96	0.69	0.80
Manot	Calibration	1978 - 1995	0.76	0.92	0.76	0.80
	Validation	1996 - 2005	0.80	0.77	0.73	0.91
Mohgaon	Calibration	1978 - 1995	0.89	0.86	0.78	0.72
	Validation	1996 - 2005	0.81	0.95	0.75	0.64
Patan	Calibration	1985 - 1995	0.77	1.20	0.70	0.91
	Validation	1996 - 2005	0.69	1.85	0.78	0.81

+ Outlet Point of Upper Narmada Basin;

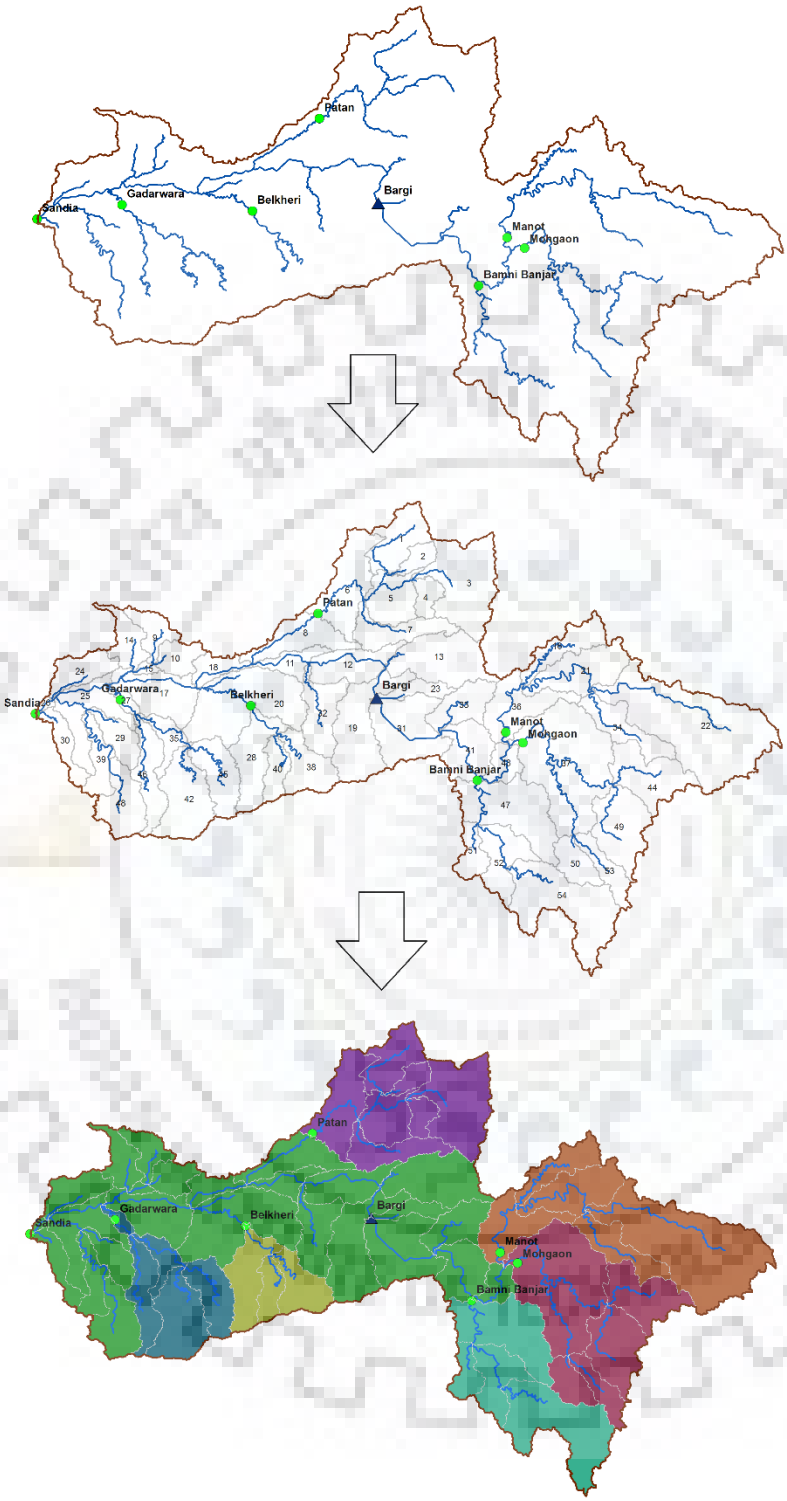

Figure 7.3: Upper Narmada basin stream network, sub-basins and gauging sites used for Model Calibration

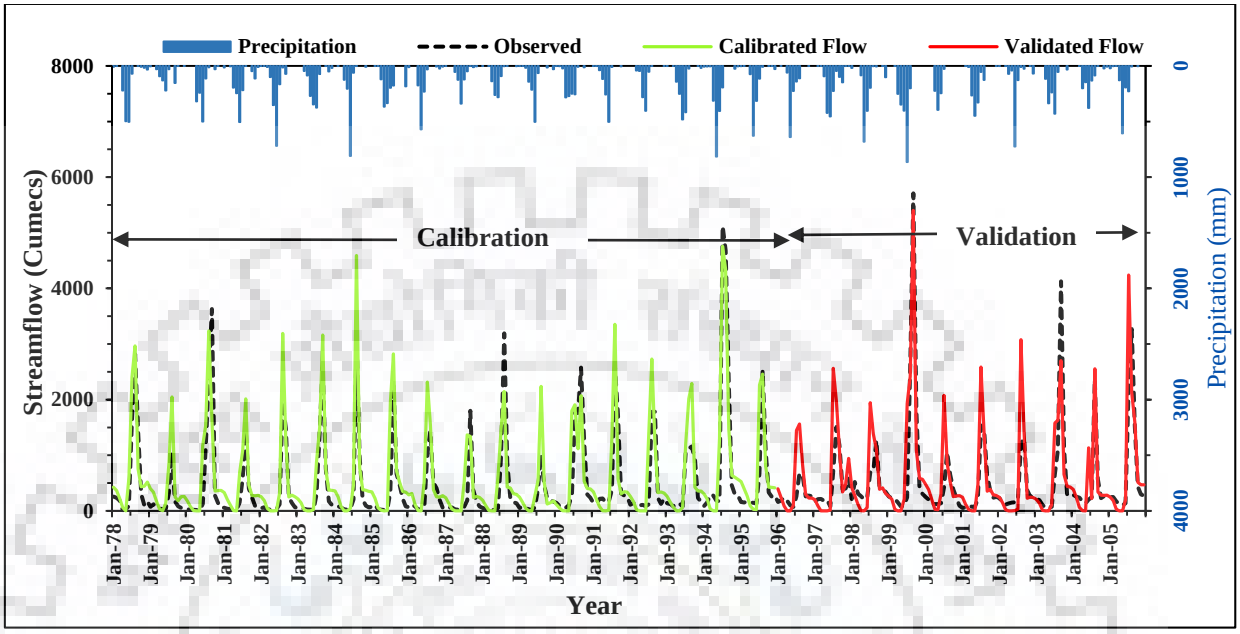

Figure 7.4: Calibration and validation plot of simulated and observed discharge at outlet (Sandia) of UNB

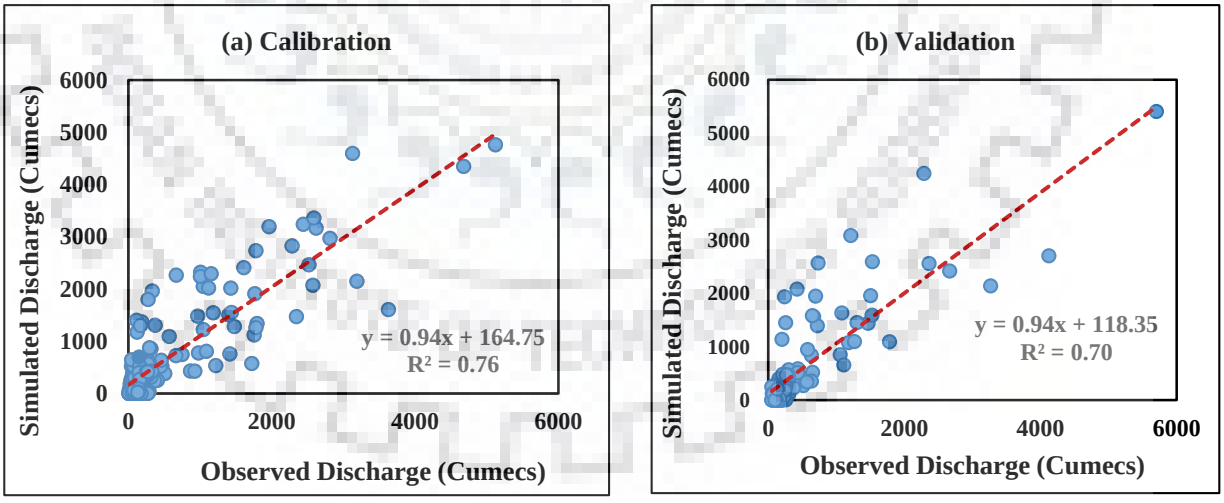

Figure 7.5: Correlation between simulated discharge and observed discharge **(a)** calibration period (1978-1995); (b) validation period (1996-2005) at Sandia gauging site

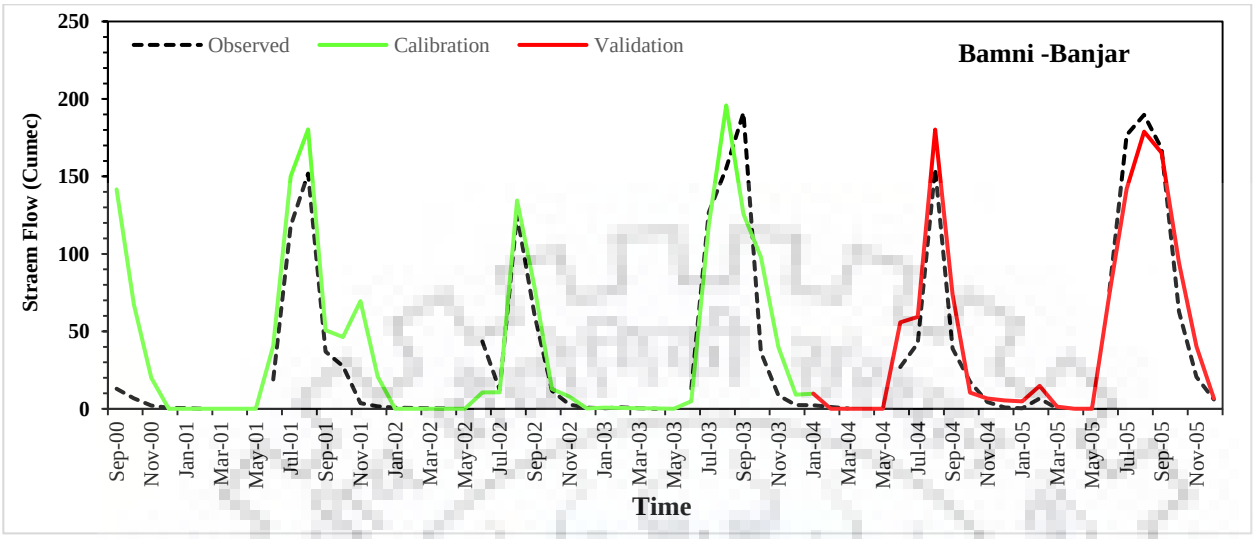
Observed
Calibration
Validation
Bamni -Banjar
Straem Flow (Cumec)
Time

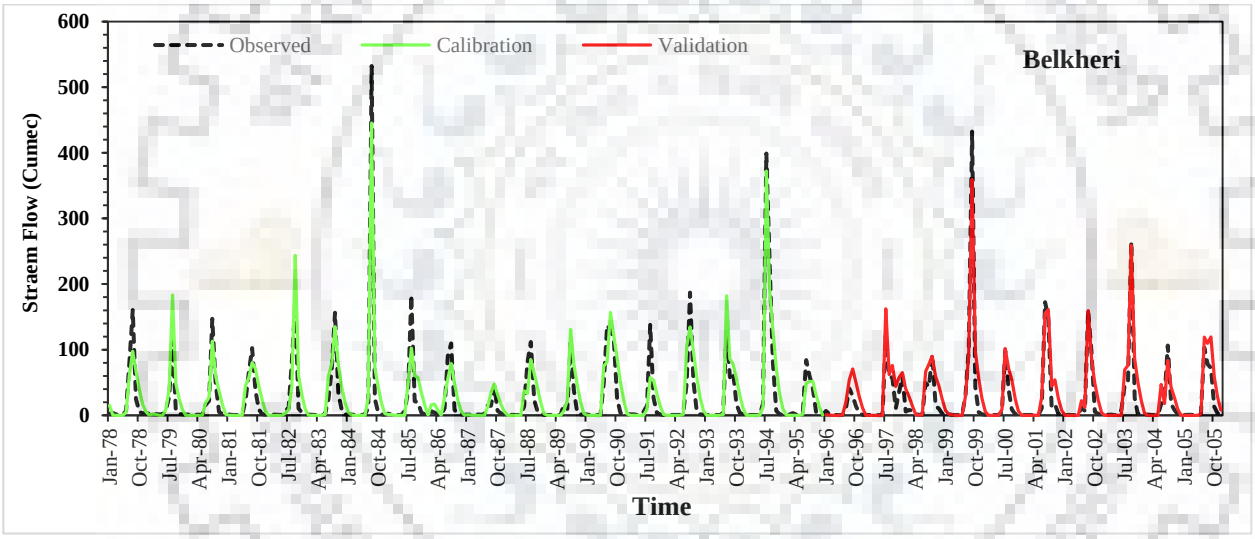
Observed
Calibration
Validation
Belkheri
Straem Flow (Cumec)
Time

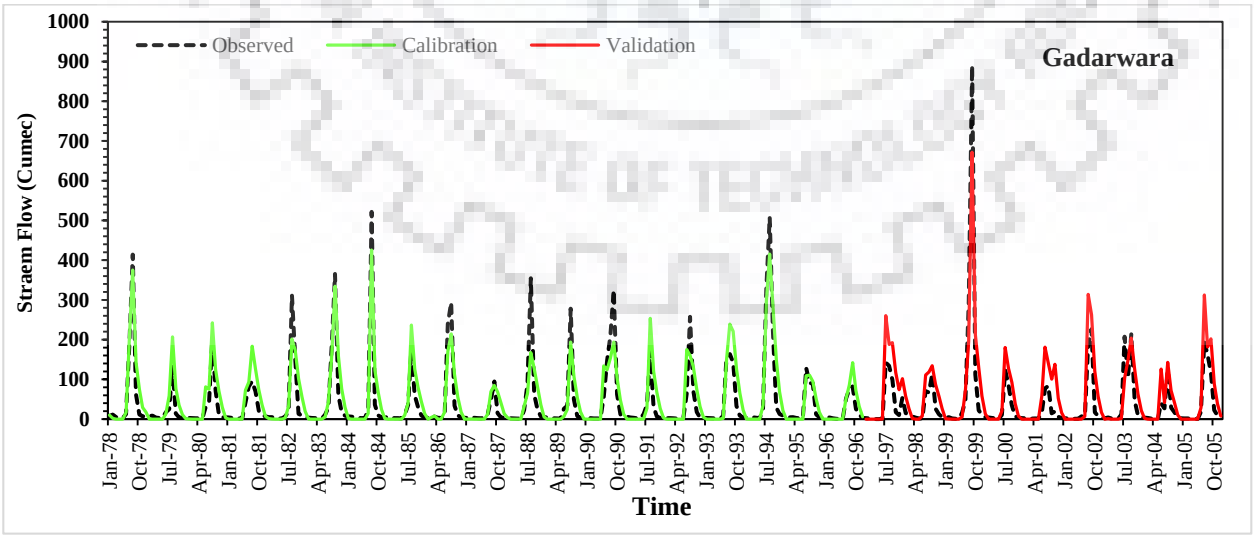
Observed
Calibration
Validation
Gadarwara
Straem Flow (Cumec)
Time

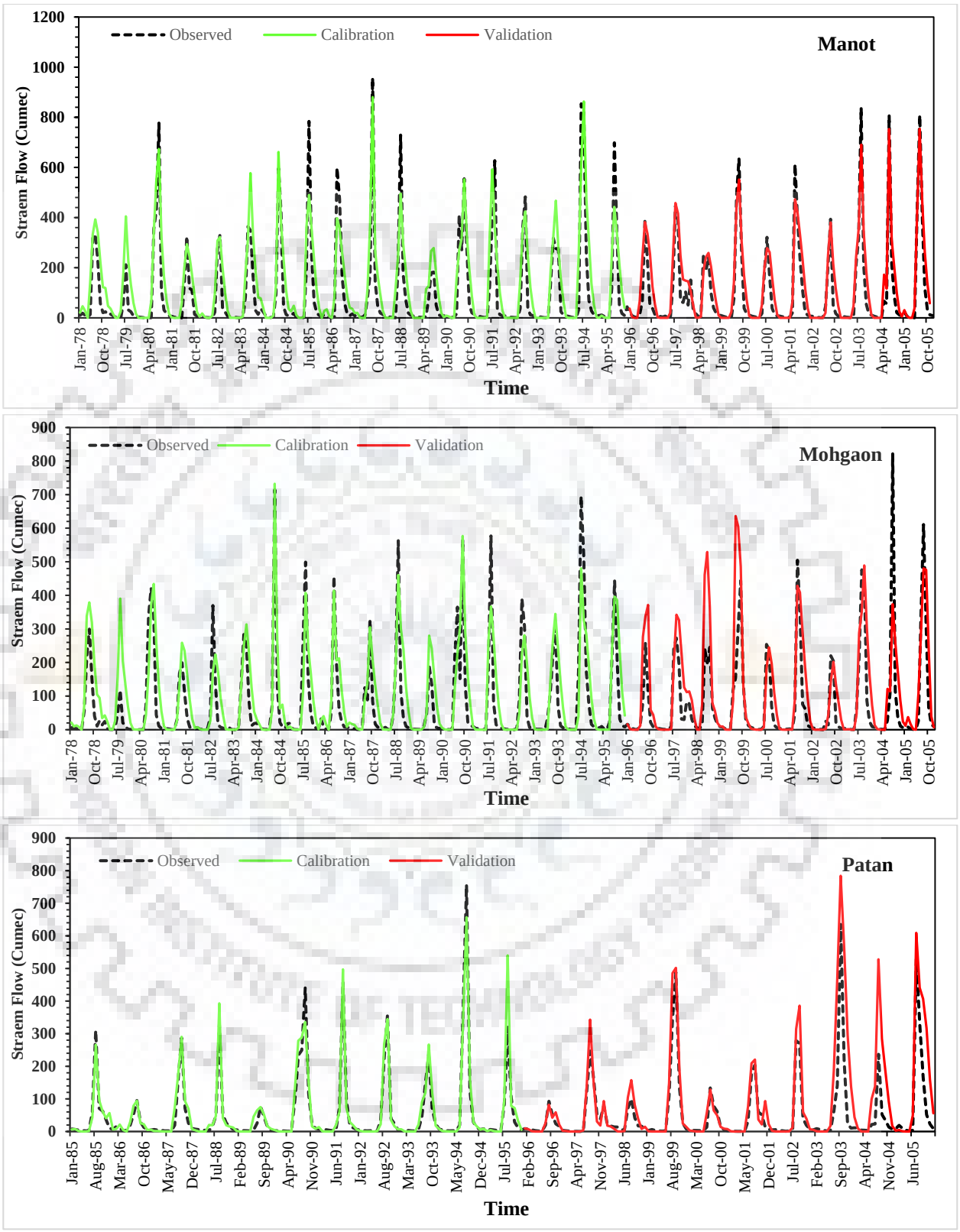

Figure 7.6: Calibration and validation plot of selected sites of UNB

7.5. HYDROLOGICAL RESPONSE UNDER LAND USE LAND COVER CHANGE

7.5.1 Number of SWAT Simulations under Land Use and Climate Change

In this study, the effects of LULC and climate changes on water balance components were evaluated by comparing the SWAT outputs of 26 simulations. Four simulations were performed under dynamics of land use land cover, whereas 22 runs were conducted under different climatic conditions (Figure 7.7). Two GHGs scenarios (RCP4.5 and RCP8.5) from three climate models (representative GCMs) were selected for assess the climate change impact over study area.

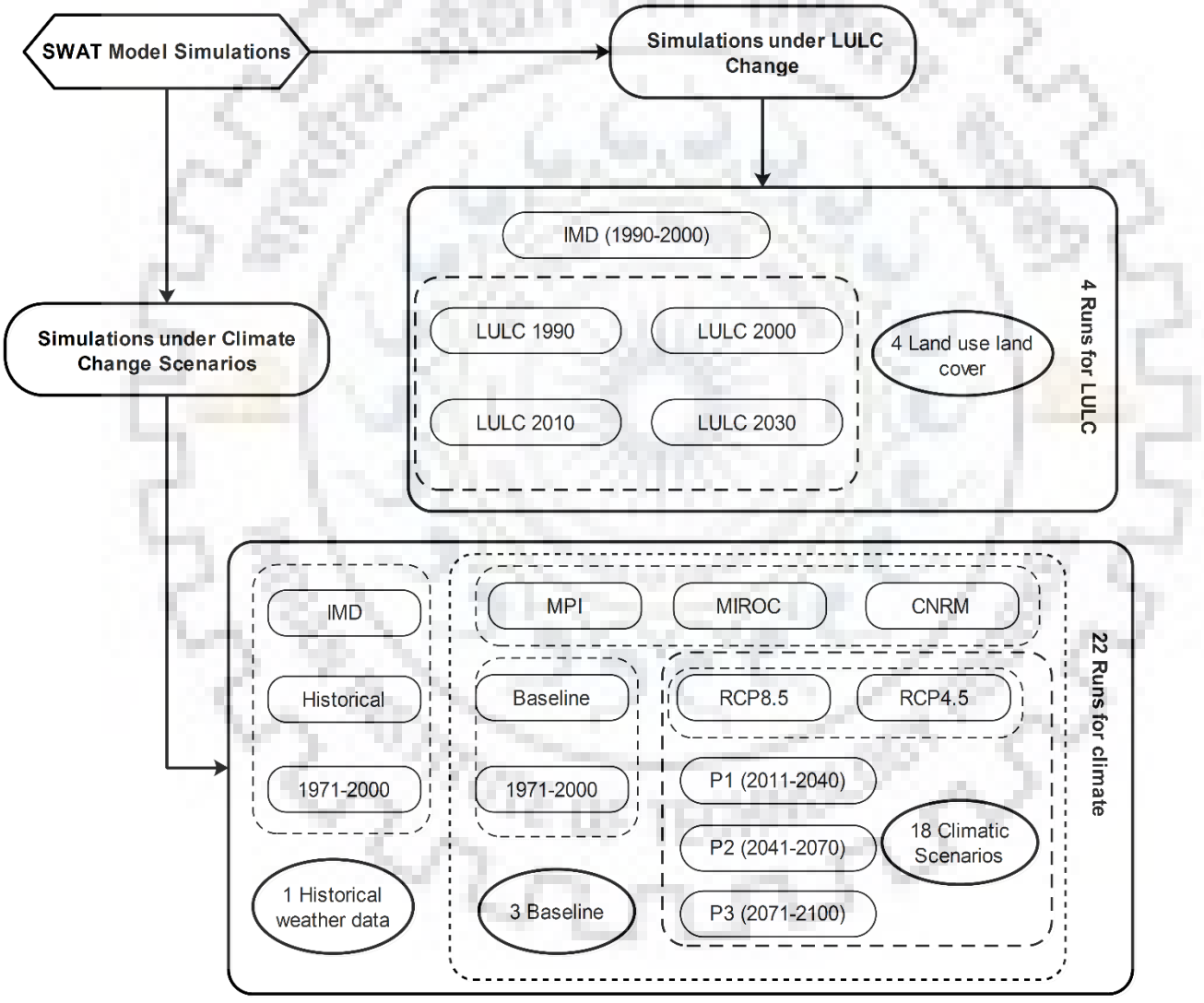

Figure 7.7: Flow chart illustrating 26 number of SWAT simulations under different land use and climate change scenarios

7.5.2 Impact of Land Use Land Cover Change on Water Balance Components

The calibrated SWAT model has been used to simulate the impact of LULC change. Water balance components of the UNB Basin were simulated under four different land use period, 1990, 2000, 2010 and predicted land use 2030. LULC class distribution and changes is given in Table 7.6. The projection of 2030 indicate the built-up area, cropland and natural vegetation area 463.83 km^2, 19222.91 km^2 and 12157.11 km^2 respectively. Built-up area and cropland increased from 0.72% (2015) to 0.98% (2030) and 56.79% (2015) to 59.15% (2030) respectively in next 15 years, whereas natural vegetation area found to be decreased from 39.66% (2015) to 37.41% (2030) for the same duration. In general, prediction of 2030 LULC classes distribution indicate the expansion in cropland and reduction in natural vegetation due to deforestation. It also indicate the substantial growth in the built-up area. The expansion of built-up area and cropland occurring due to the tourist places such as Jabalpur and Amarkantak, and population growth in region. Study indicate the continuous increase in population in the study area influence the deforestation and expansion in cropland.

Table 7.6: Land use land cover distribution of year 1990, 2010, and 2030

LULC Classes	1990		2000		2010		2030	
	Area (Ha)	Area (%)	Area (Ha)	Area (%)	Area (Ha)	Area (%)	Area (Ha)	Area (%)
Water Bodies	39843	1.23	33948	1.04	45581	1.4	46383	1.43
Built-up	6357	0.2	12141	0.37	19362	0.6	31978	0.98
Vegetation	1598356	49.18	1446077	44.49	1346294	41.42	1215711	37.41
Cropland	1539074	47.36	1711835	52.67	1787332	54.99	1922291	59.15
Barren Land	66371	2.04	45999	1.42	51431	1.58	33637	1.03

Impact of LULC change on hydrological components has been analyzed that indicates increased water yield and decreased actual evapotranspiration (ET). The change in LULC influence the surface properties such as curve number (CN) values and evapotranspiration properties. Change in surface parameters values due to changed LULC is the main causes of change in water balance components. In order to compute the LULC change impact only, period of climate data has been fixed for the simulation. In this study, fixed climatic period data from 1990 to 2000 has been considered to simulate the impact of LULC change. The average annual value of water balance (water yield, actual evapotranspiration, surface water and groundwater) is given in Table 7.7. Water yield includes both surface runoff and groundwater. Table 7.6 indicate that increase in settlement and decrease in natural

vegetation, affect as increase in the water yield and increased surface runoff, but there is a decrease in ET. Table 7.7 shows the surface runoff and water yield of 1990 is the lowest (477.79 mm and 699.69 mm, respectively), which increases gradually and highest increase is predicted in the future in 2030 (539.48 mm and 752.54 mm, respectively). The actual ET decreases with time due to decrease in natural vegetation and it is projected to be lower in 2030 (552.86 mm) and highest in 1990 (605.33 mm). There is a gradual decrease in the groundwater due to land use change with time. The value of curve number value increases with urbanization resulting in increased surface runoff and decreased groundwater owing to reduced infiltration. Therefore, conversion of LULC from 1990 to 2030 shows a gradual groundwater decrease. Changed land use and CN have caused increased water yield and decreased ET and groundwater. The average annual values of evapotranspiration and water yield of sub-basin due to LULC change are shown in Figure 7.8 and Figure 7.9, respectively. During last 2 decades (2010-2030), LULC changes increased surface runoff by 28.45 mm and accounted for 5.57% of the total change (539.48 mm). Moreover, ET decreases by 4.19% in the same duration.

Table 7.7: Average annual water balance components under 1990, 2000, 2010 and 2030 LULC

Land use Condition	Rainfall (mm)	Surface Runoff (mm)	ET (mm)	Groundwater (mm)
1990	1248.29	477.79	605.33	58.10
2000	1248.29	495.73	590.06	55.47
2010	1248.29	511.03	577.04	53.28
2030	1248.29	539.48	552.86	49.27

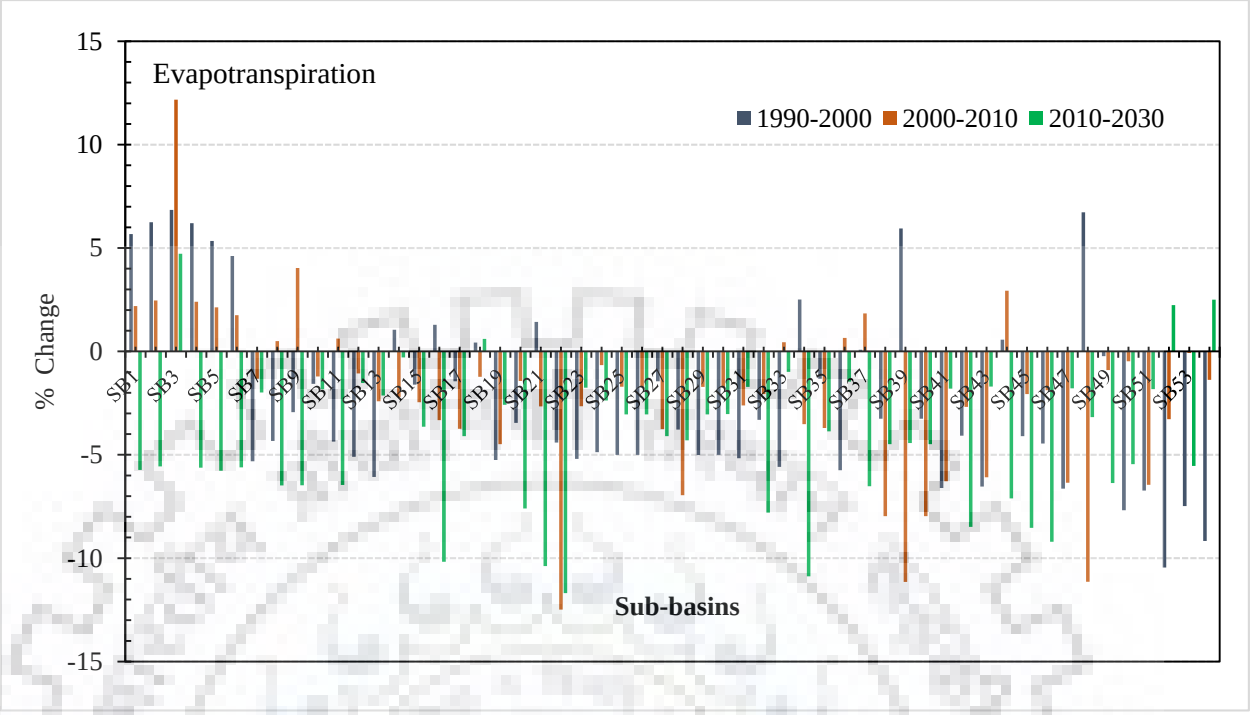

Figure 7.8: Comparison of decadal changes in evapotranspiration due to LULC change

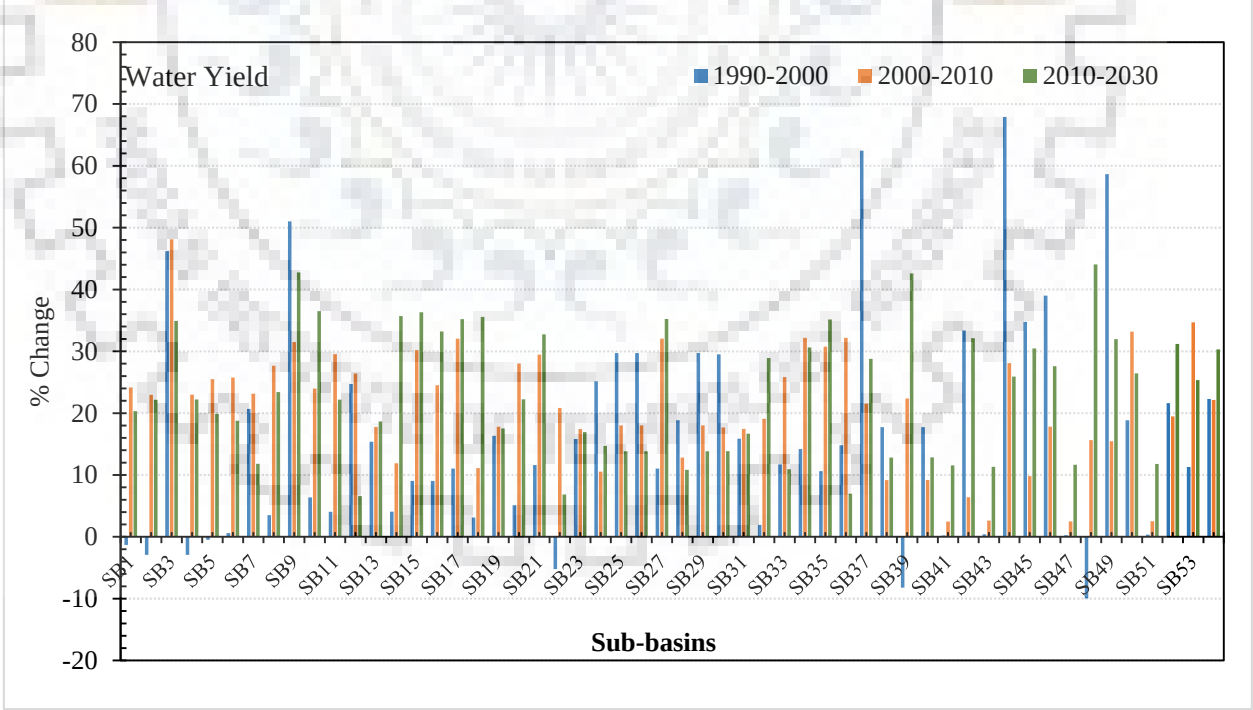

Figure 7.9: Comparison of decadal changes in water yield due to LULC change

7.5.3 Impact of Climate Change on Water Balance Components

7.5.3.1 Precipitation projection under RCP scenarios

Precipitation is one of the most important components of hydrological cycle. It is the main source of water availability in various region. Therefore, it is very important to understand the variability and climate change effect on precipitation over the UNB. Climate model outputs such as precipitation and temperature were bias corrected by distribution mapping before considering in the study. The climate impact on precipitation over the UNB was evaluated by comparing the observed precipitation values (IMD precipitation) with simulated precipitation values from representative climate models. In this study, IMD precipitation (1970-2000) compared with baseline (1970-2000) period of climate model. Results indicate that annual average precipitation of climate models were 1304 mm, 1061 mm and 1354 mm for MIROC, CNRM and MPI, respectively, whereas IMD indicate the 1247 mm. However MIROC model exhibits the closeness with IMD precipitation. The minimum difference was obtained for MIROC (4%) and maximum variation was found for CNRM (-15%) climate model with reference to the IMD precipitation (Figure 7.10).

Climate projections under RCP4.5 and RCP8.5 for each periods P1 (2011-2040), P2 (2041-2070) and P3 (2071-2100) were compared with IMD and respective base line scenario (Figure 7.11). On comparing the results with IMD indicate minimum variation (0.41%) for MPI (1252 mm) model in P1 and maximum variation (-30.37%) for CNRM (868 mm) in P3 were obtained under moderate emission scenario (RCP4.5). Precipitation variation under severe emission scenarios (RCP8.5), minimum variation (4.61%) for MPI (1305 mm) in P1, and maximum variation (-37.20%) for CNRM (783 mm) in P3 were noticed while comparing with IMD precipitation. Figure 7.11 indicate projected precipitation with respective baseline scenarios, MPI P2 (1252 mm) indicate minimum variations (-1.65%) and CNRM P3 (868 mm) exhibit the maximum variations (-18.17%) under RCP4.5 scenario. Whereas MIROC P2 (1336 mm) indicates minimum variation (1.35%) and CNRM P3 (783 mm) indicate maximum variation (-26.19%) under RCP8.5 scenario. Moreover, comparison of average monthly precipitation was carried out for future period (P1, P2, and P3) under RCP4.5 and RCP8.5 scenarios of three climate models (Figure 7.12).

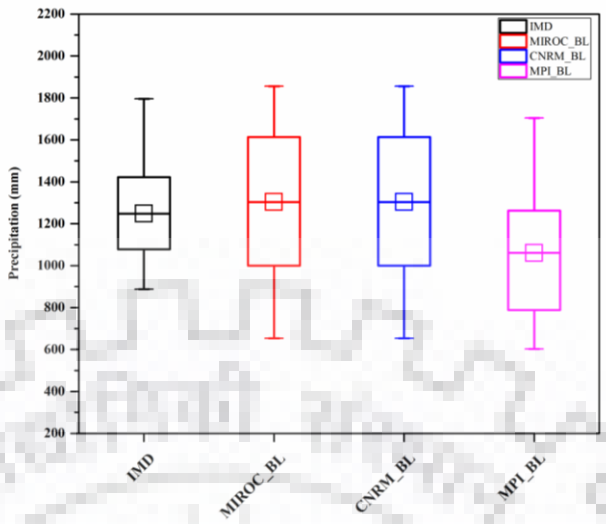

Figure 7.10: Comparison of precipitation variation of observed (IMD) and model simulated for baseline scenario (1971-2000)

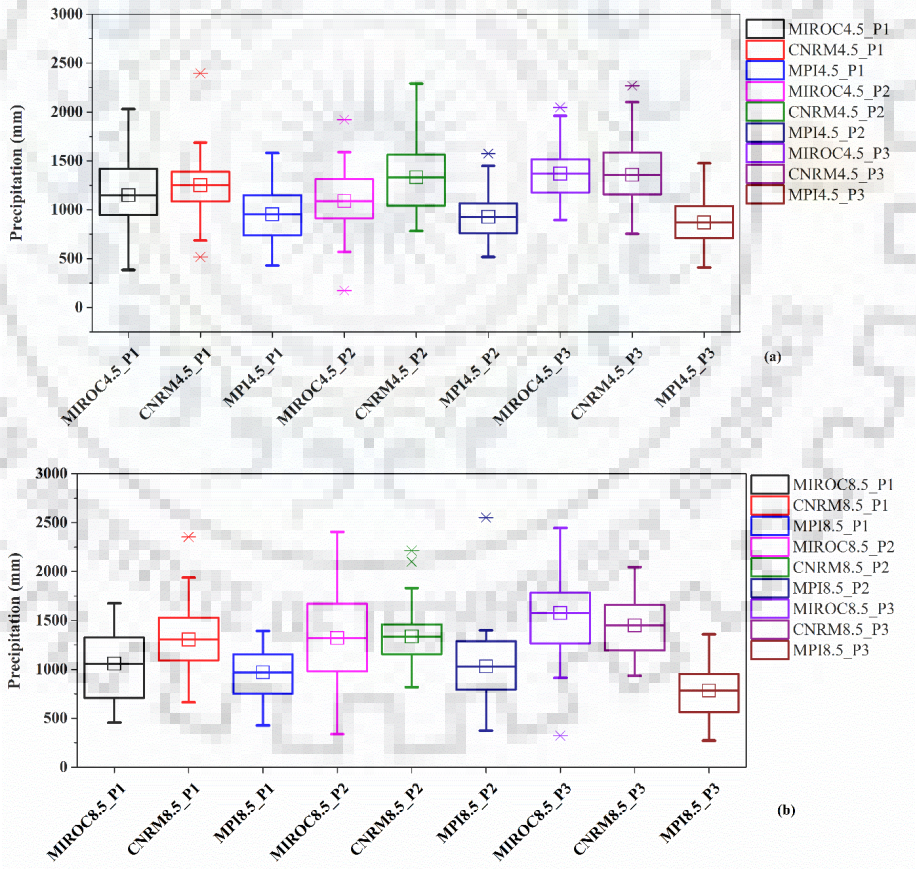

Figure 7.11: Precipitation variations over 3 climatic periods; P1 (2011-2040), P2 (2041-2070) and P3 (2071-2100) in simulated scenario (a) RCP4.5, (b) RCP8.5

(Note: Climate description in Figure as 'ShortnameRCP_climatic period')

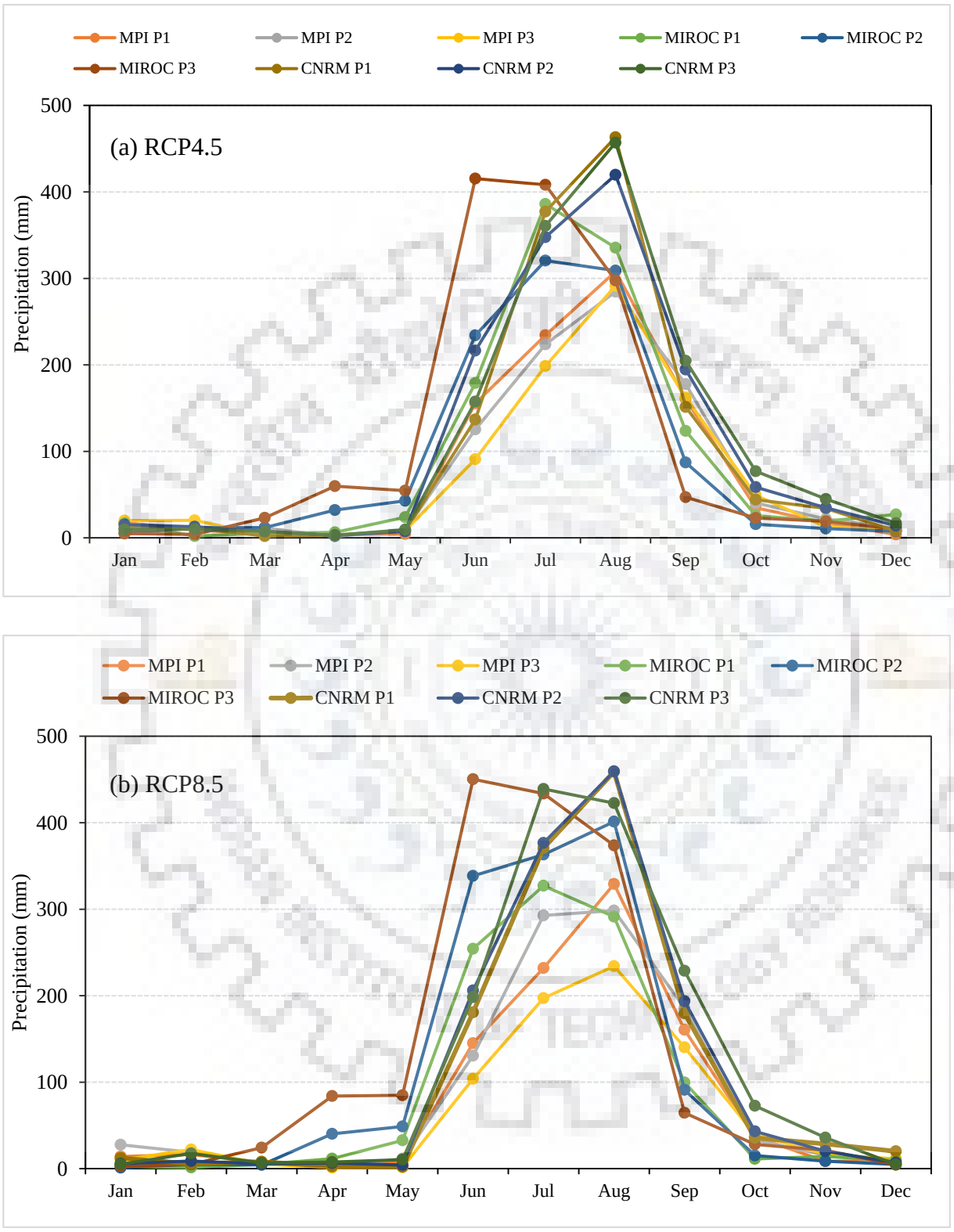

Figure 7.12: Comparison of projected average monthly precipitation under (a) RCP4.5, and (b) RCP8.5 Scenarios

7.5.3.2 Temporal changes on water balance components

Mean annual and monthly simulations

Simulated water balance components considering RCP4.5 and RCP8.5 climate projections were compared with reference to IMD (observed climate data from 1970-2000) and baseline period (GCMs climate data from 1970-2000) (Figure 7.13-7.14).

Furthermore, with reference to simulation under IMD, climate scenarios of MPI model simulations consistently result in an increase in most of the hydrological component (surface runoff), mainly because of increase of precipitation (Figure 7.14(c)). The largest increase in surface runoff (38.05%) is induced by increase in precipitation (22.67%) during 2071-2100 (MIROC5). Largest decrease in precipitation (37.20%) projected during 2071-2100 under RCP8.5 of CNRM climate model, result in a largest decrease in surface runoff (57.17%) and ET (34.66%). Due to consistently increase in temperature, simulated ET is decreasing in each period. However, largest decrease in ET (34.66%) is produced under RCP8.5 by CNRM. whereas the lowest is 6.35% under RCP8.5 scenario by MPI in during the same period 2071-2100. Inter-comparison of projected precipitation of baseline (1970-2000) with IMD (1971-2000) indicates that climate projections are increasing by 4.60% and 8.56% for MIROC5 and MPI, respectively, while decreasing for CNRM by 14.91% (Table 7.8). Considering the increase in precipitation, simulated results indicate increase in surface runoff by 9.78% and 13.33%, and water yield by 10.57% and 15.69% for MIROC and MPI, respectively.

Table 7.8 : Percentage change in hydro-meteorological components of climate model baseline with IMD

Climate Models	PCP (%)	ET (%)	SurQ (%)	WYLD (%)
MIROC5	4.60	-7.55	9.78	10.57
CNRM	-14.91	-19.49	-24.82	-18.50
MPI	8.56	-4.44	13.33	15.69

Mean monthly surface runoff from different scenarios were compared in Figure 7.15. Results of baseline simulation indicate monsoon surface runoff decreases by 22.25% for MPI, while increase in MIROC5 and CNRM estimated as 29.39% and 30.58%, respectively.

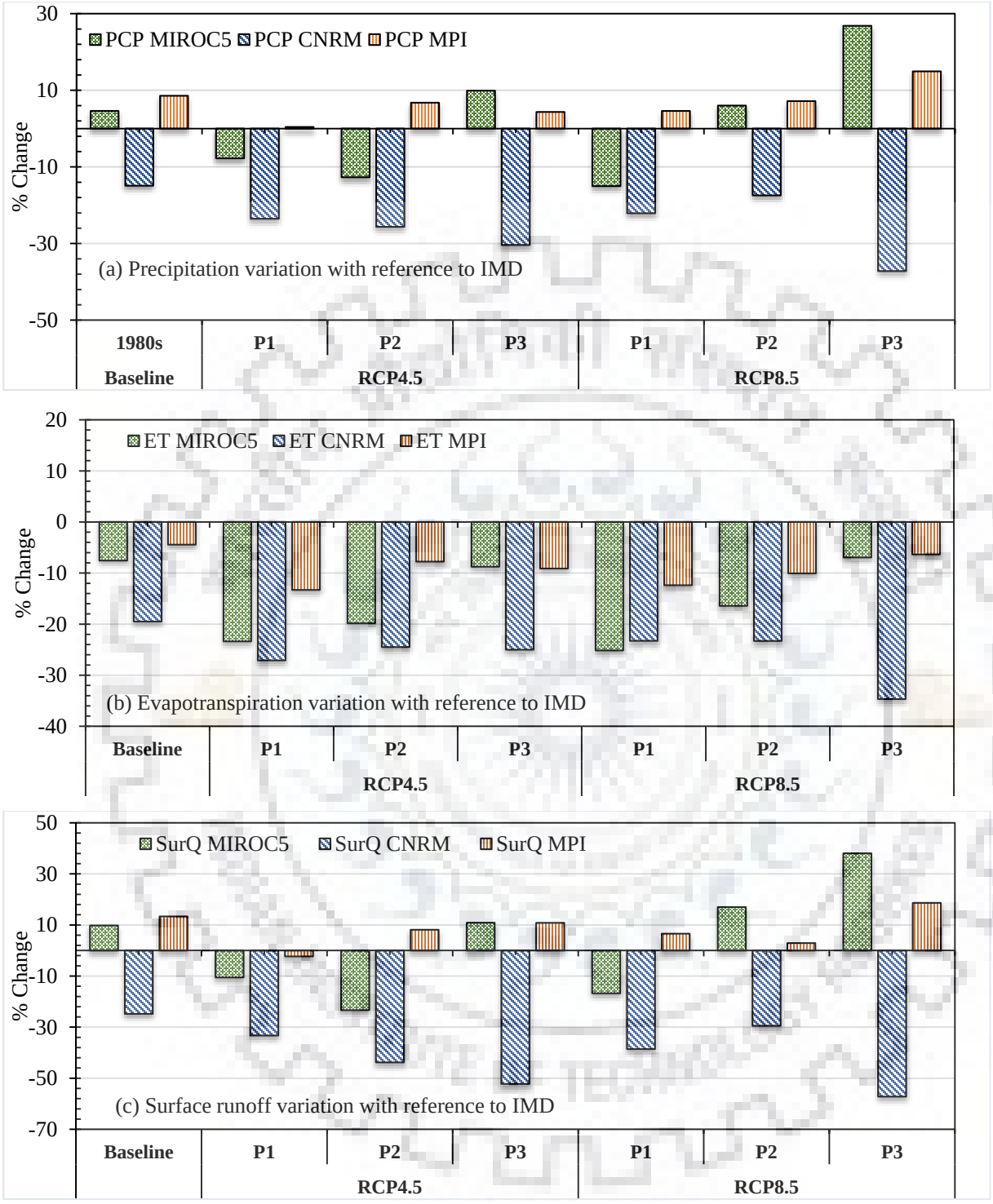

Figure 7.13: Comparison of simulated mean annual water balance components i.e. (a) precipitation, (b) evapotranspiration, and (c) surface runoff, with reference to IMD data (1970-2000)

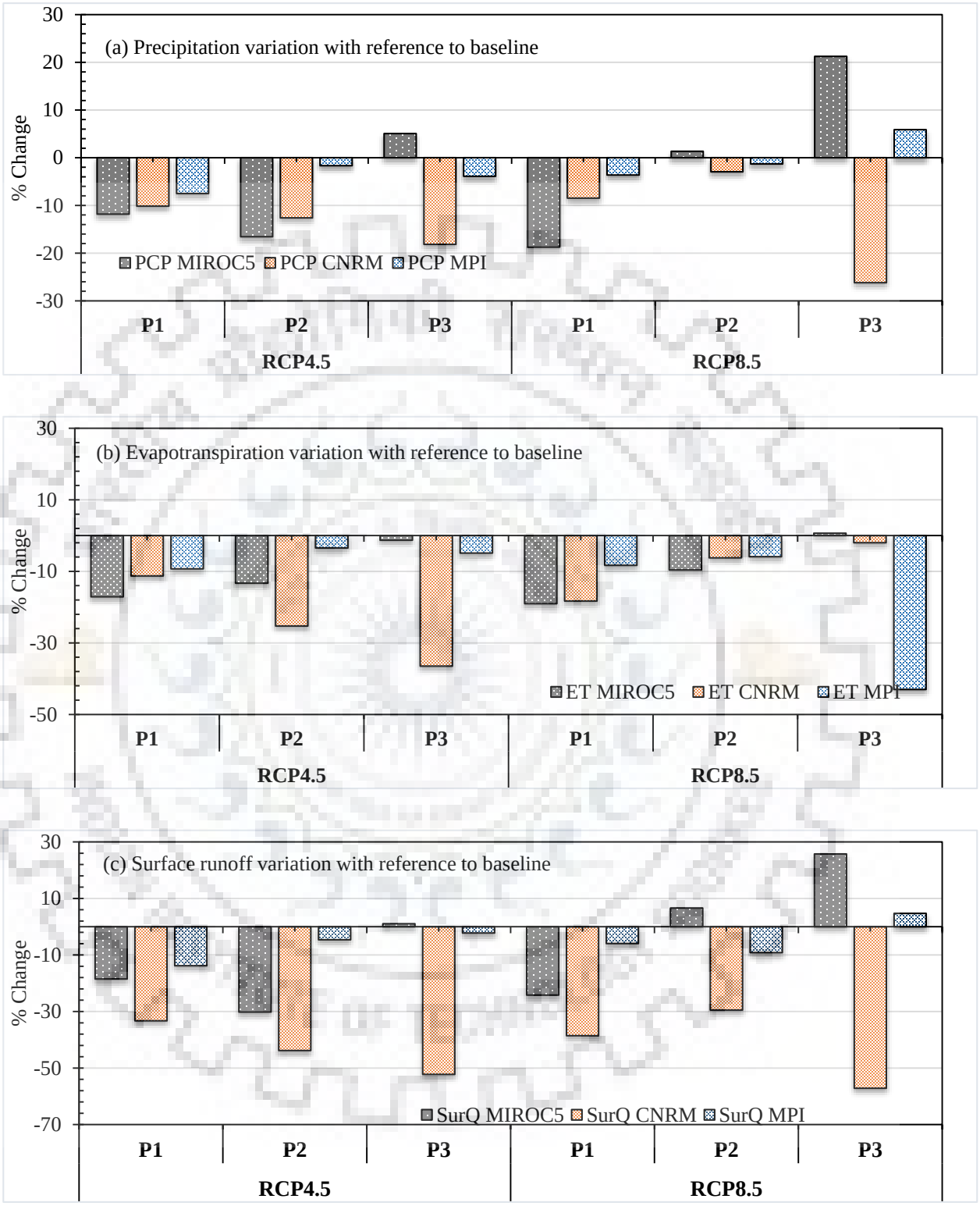

Figure 7.14: Comparison of simulated mean annual water balance components i.e. (a) precipitation, (b) evapotranspiration, and (c) surface runoff, with reference to baseline (1970-2000)

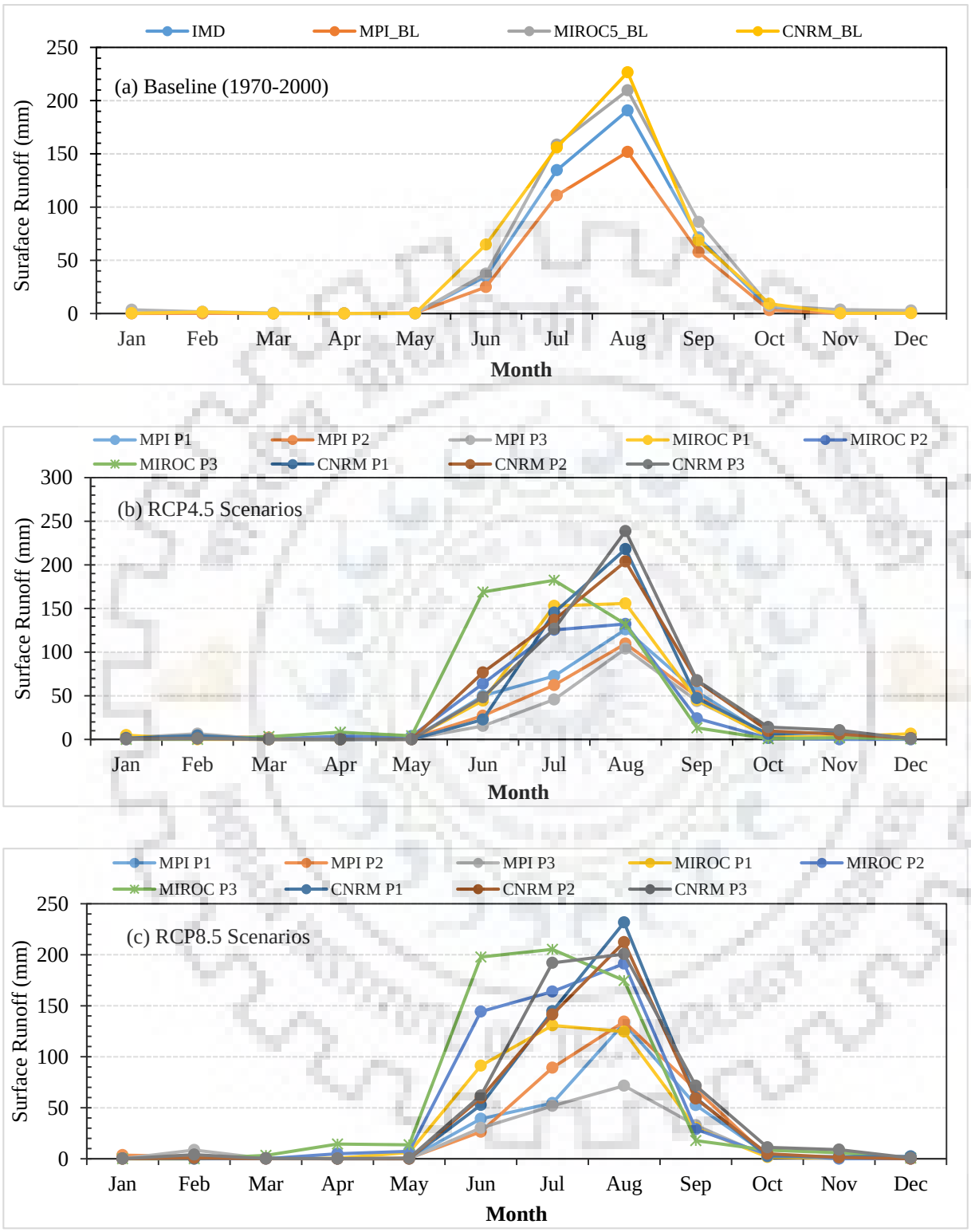

Figure 7.15: Comparison of mean monthly surface runoff under different scenarios

7.5.3.3 Spatial distribution of changes in Green Water and Blue Water

Green Water

Green water computation was carried out for three climatic periods (P1, P2 and P3) under two different scenarios (RCP4.5 and RCP8.5) from three different RCM climate models. Evapotranspiration (ET) and soil water (SW) are the main components of green water and defined as green water flow and green water storage, respectively (Veettil and Mishra 2016). Thus sum of ET and SW indicate the availability of green water. Green water components are very sensitive to the temperature. Table 7.9 and Figure 7.16-7.17 indicate the temporal and spatial distribution of simulated annual mean green water by SWAT. Simulated annual mean ET and SW were 498 mm and 233 mm from IMD climatic data. ET variation in model baseline scenarios were computed as -7.55%,-19.50% and -4.44% for MIROC, CNRM and MPI climate model, respectively.

Figure 7.16-7.17 show the spatial variation in green water over UNB, most of the run indicate 0-(-) 10% variation for RCP4.5 and RCP8.5 because of temperature rise. Output of model run indicate MIROC and MPI exhibit some positive spots in the region for P3 period under RCP4.5 and RCP8.5. However, some upper part (eastern region) of UNB also indicates downfall in green water for same period P3, for same climate model MIROC and MPI.

Blue Water

Water yield (WYLD) and ground water storage (GWS) are the components of blue water, defined as blue water flow and blue water storage, respectively (Veettil and Mishra 2016). However sum of WYLD (surface flow+ lateral flow+ groundwater flow-loss-abstraction) and GWS (percolation – ground water discharge) indicate the total availability of blue water in the area. Blue water components are very sensitive to the precipitation variability (Veettil and Mishra 2016). Table 7.9 and Figure 7.18 -7.19 indicate the temporal and spatial distribution of simulated annual mean blue water by SWAT. Blue water evaluation were carried out for three climatic periods (P1, P2 and P3) under two different scenarios (RCP4.5 and RCP8.5) of three different climate model.

Figure 7.18 indicates WYLD is positive for P3 under MIROC5 and MPI RCP4.5 scenarios, whereas during P2 (MIROC5), P1 and P3 (CNRM) show the decreasing amount with reference to the baseline. However, under RCP8.5 (Figure 7.19), P2 period exhibit increasing availability for most of the UNB region for all the climate models, whereas P1 and P3 show the positive changes for MIROC and MPI climate model.

Table 7.9: Annual average of hydrological response under climate change during base line (2071-2000), P1 (2011-2041), P2 (2041-2070), and P3 (2071-2100) for RCP sceneries

Climate Models	Water Components (mm)		Baseline (1971-2000)	RCP4.5			RCP8.5		
				P1	P2	P3	P1	P2	P3
IMD	Green Water	ET	498	-	-	-	-	-	-
		SW	233	-	-	-	-	-	-
	Blue Water	WYLD	966	-	-	-	-	-	-
		GWS	56	-	-	-	-	-	-
MIROC5	Green Water	ET	460	381	399	454	372	416	463
		SW	214	194	200	218	182	205	228
	Blue Water	WYLD	1068	918	828	1105	842	1125	1351
		GWS	65	79	58	84	60	73	98
CNRM-CM5	Green Water	ET	401	363	376	373	382	382	325
		SW	200	186	188	182	190	194	148
	Blue Water	WYLD	787	694	616	541	679	727	504
		GWS	55	47	59	57	50	67	40
MPI-ESR-LM	Green Water	ET	476	431	459	452	436	448	466
		SW	228	215	221	223	219	220	225
	Blue Water	WYLD	1118	1010	1075	1040	1079	1064	1172
		GWS	58	59	74	73	61	81	82

Note: Unit of Evapotranspiration (ET), Soil Water (SW), Water Yield (WYLD) and Ground water storage (GWS) are in millimetres.

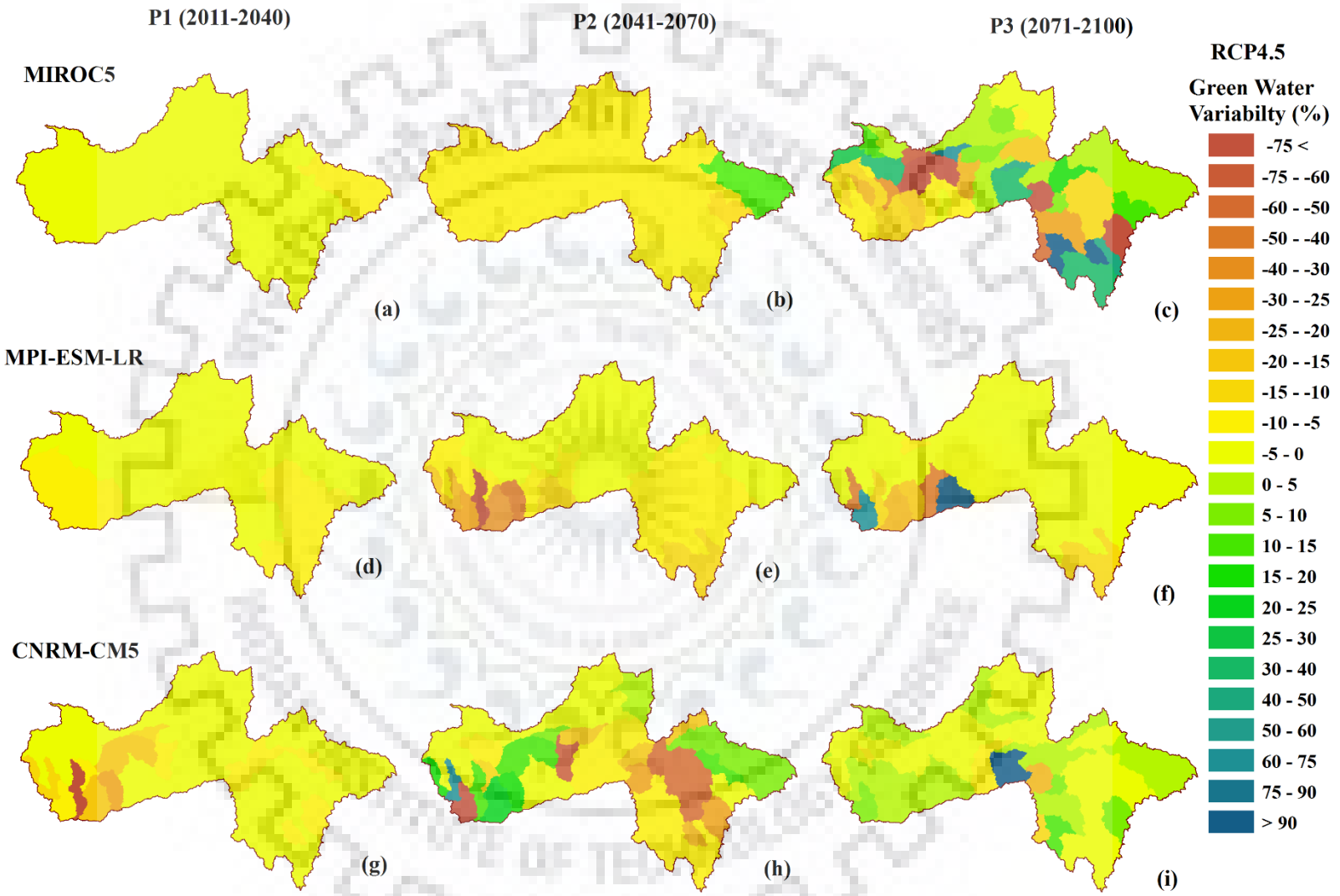

Figure 7.16: Green Water (Evapotranspiration+ Soil Water) variations (%) at RCP4.5 scenarios with reference to the control scenarios

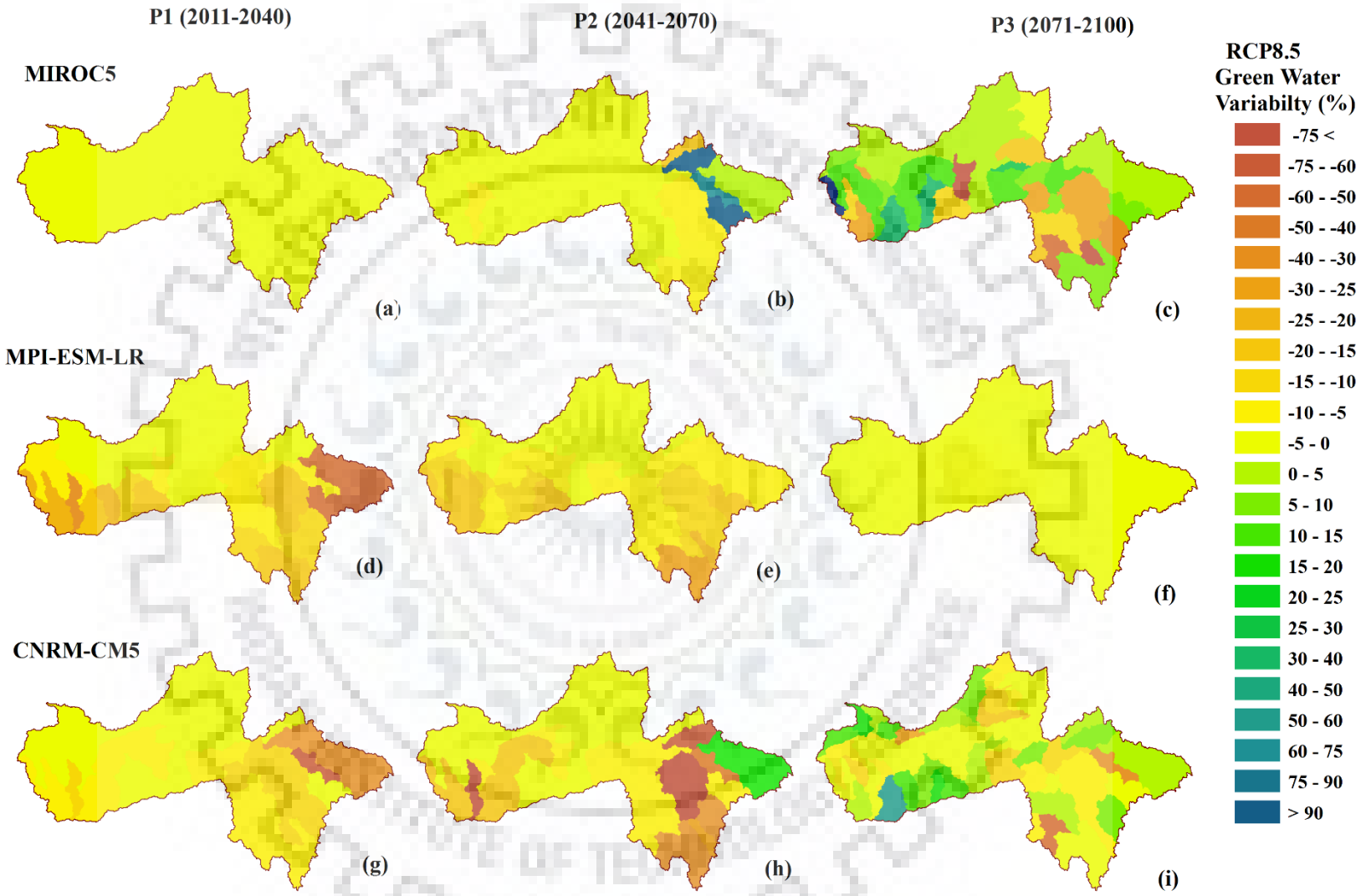

Figure 7.17: Green Water (Evapotranspiration+ Soil Water) variations (%) at RCP8.5 scenarios with reference to the baseline scenarios

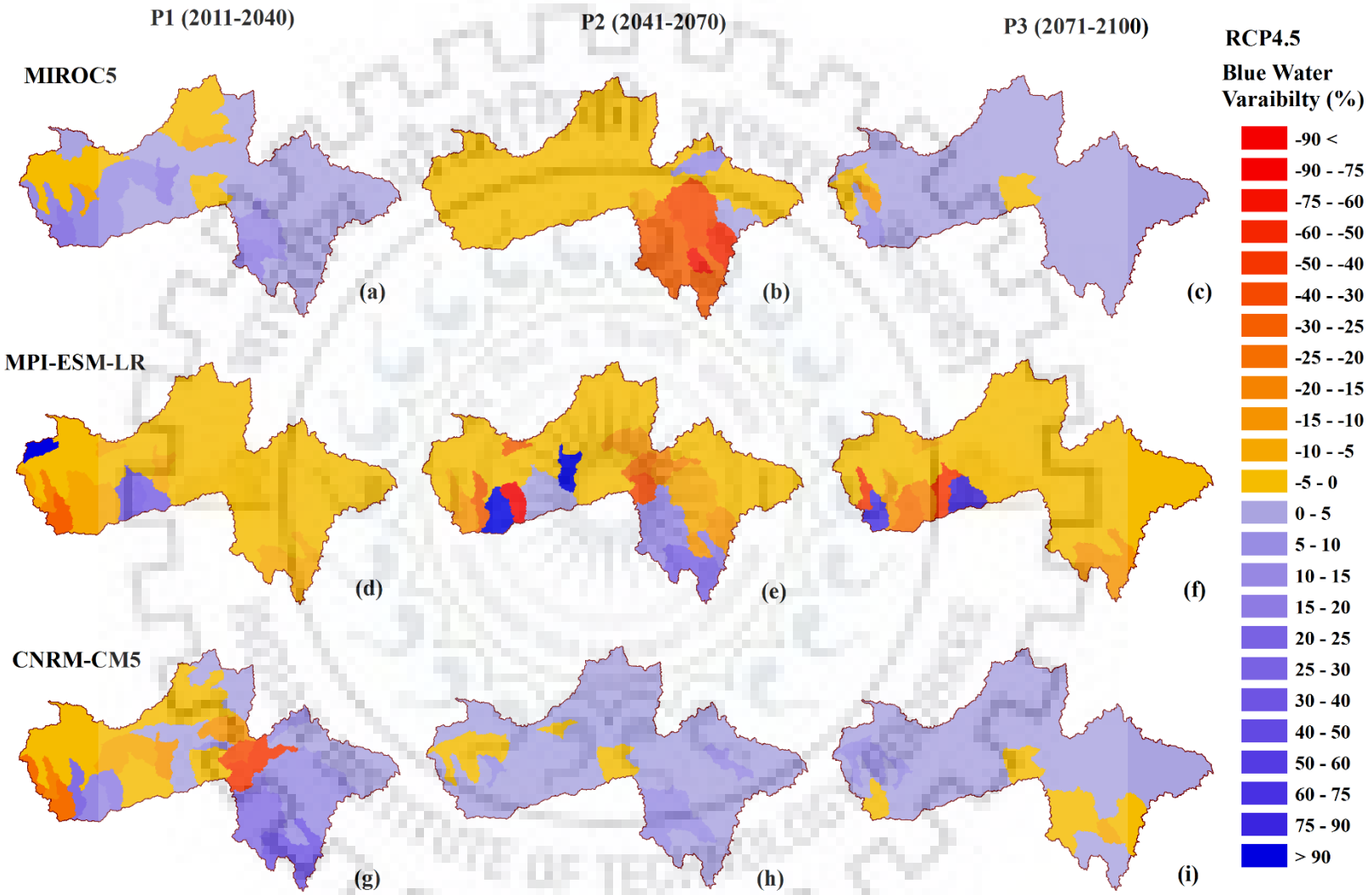

Figure 7.18: Blue Water (Water Yield+ Ground Water Storage) variations (%) at RCP4.5 scenarios with reference to the control scenario

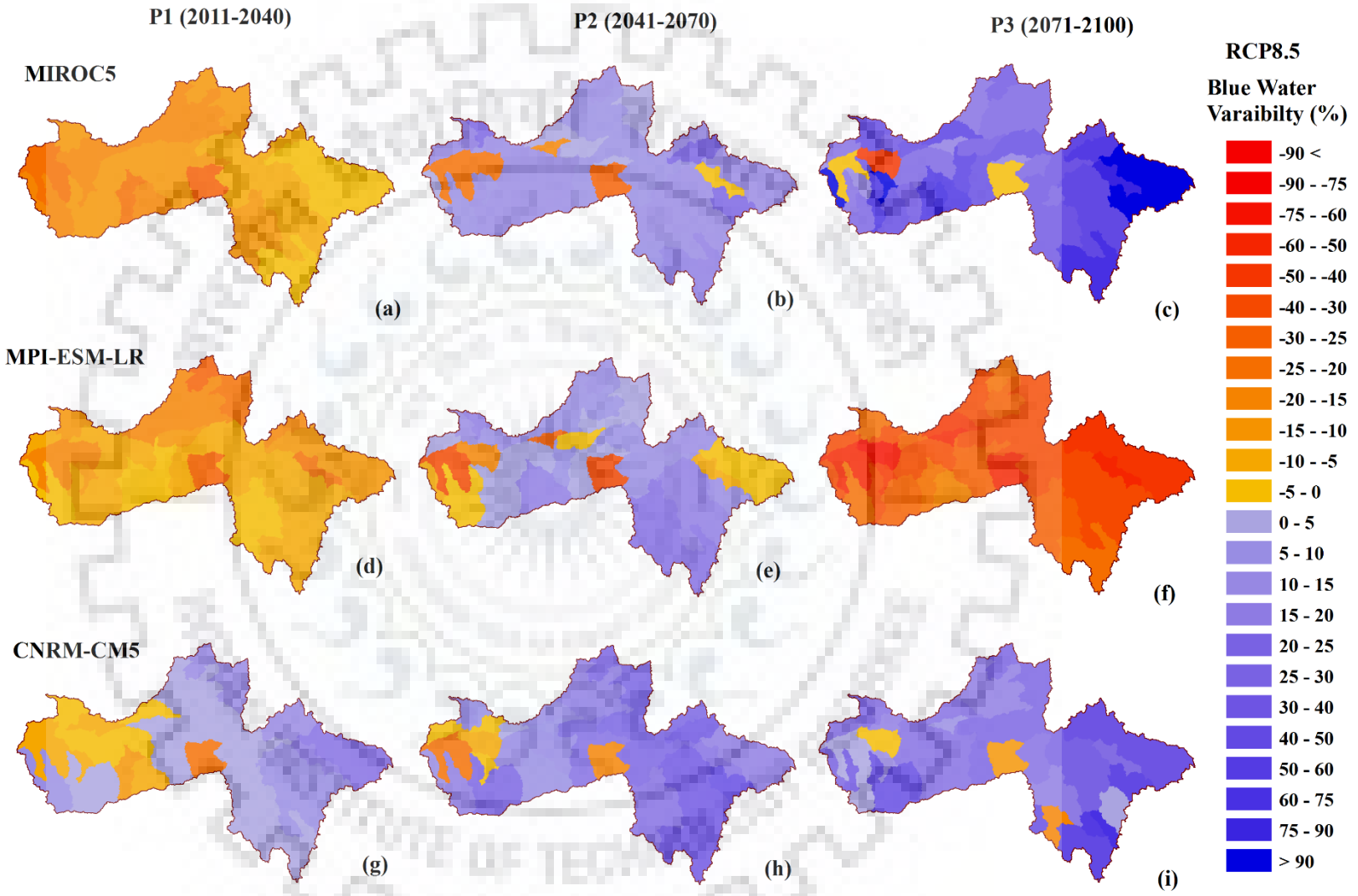

Figure 7.19: Blue Water (Water Yield+ Ground Water Storage) variations (%) at RCP8.5 scenarios with reference to the control scenario

7.6 ADAPTATION AND COPING STRATEGIES TOWARDS CLIMATE CHANGE

According to IPCC AR5, global climate has been changing, thus impacting on temperature, precipitation and altering the regional water balance. However, due to the variation in local circulation patterns and orography, trends may differ from region to region. Overall, the present study suggests that climate change is going to continue and may even accelerate in the future, despite differences in the underlying assumptions regarding economic development (scenario storylines) and model uncertainty.

The United Nations Framework Convention on Climate Change (UNFCCC) proposed two options to cope against climate change. Firstly, mitigation by cutting down GHGs emissions and raising sinks and secondly, adaptation to deal with climate change impact. Under the banner of United Nations Framework Convention on Climate Change (UNFCCC), the Paris Agreement is an agreement addressing with GHGs emissions mitigation, adaptation and finance starting in the year 2020. Most of the countries have committed to establish the long-term goal of keeping the increase in global average surface temperature to below 2°C by 2100. Adaptation and mitigation strategies involve taking practical actions to manage risks from climate impacts, protect communities and strengthen the resilience of the economy. Due to anthropogenic activities and increased GHGs concentration, surface temperature of earth and rate of precipitation is fast changing. Adverse effect of climate change is affecting the global food security, water availability and ecosystem. To minimize this, it is important to reduce the emission of GHGs concentration in the atmosphere. Moreover, proper adaptation and coping strategies may prevent or reduce the adverse effect of climate change.

In order to evaluate the climate change impact and suggest the possible adaptation strategies, it is important to understand the vulnerability under climate change. Vulnerability is a function of exposure to climate variability and change, sensitivity to climate stresses and adoptive capacity to manage the negative impact (IPCC, 2013). The adaptation strategies based on vulnerability was carried out by considering three main problems such as observations of climate change scenarios, impact of climate change on water balance components and climate change impact on extreme events.

Furthermore, Representative Concentration Pathways (RCP), moderate (RCP4.5) and high (RCP8.5) were considered from latest greenhouse trajectories of IPCC AR5, to assess the vulnerability within basin i.e. UNB. Ensemble of global climate models of the basin indicate that

annual mean temperature most likely to rise 1.39^{o}C (RCP4.5) to 3.47^{o}C (RCP8.5) by 21st century (Figure 7.20 -7.21). Precipitation in the basin may increase about 15% (RCP4.5) to 35% (RCP8.5) in next 100 years (Figure 7.22 -7.23). Moreover, extreme events of precipitation in late 21st century can observed from ensembles of GCMs output. There is enough evidence that the expected changes in climate certainly affect the water resources and agriculture. The adaptation and coping strategies in water resources and extreme events (flood) for the basin are need to propose. Moreover simulated annual extreme discharge in 2080s (2071-2100) and mid flow are increasing during 2060s (2041-2070), respectively (Figure-7.24).

Therefore it can be summarized that the vulnerability considering the various sources of uncertainly such as RCPs and GCMs. There will certainly affect the future climate in the basin in following ways:

- Temperature will increase up to 3.5^{o}C under high GHGs concentration.
- Increase in temperature will stimulate the evapotranspiration and contribute in intensification of hydrological cycle.
- Rise in temperature will affect the food production and uncertainty in crop yield.
- It is most likely that increase in total precipitation will continue.
- During mid of 21st century, extreme values will occur frequently which will trigger flooding and soil erosion at large scale.

According to IPCC, "Adaptation is any adjustment in natural or human systems in response to actual or expected climatic effects, which moderates harm or exploits beneficial opportunities" (IPCC, 2001). Adaptation is important factor in reducing vulnerability and cope with the impact of climate change. Moreover it is a responsibility, shared by Governments agencies at national, state and local level, business organization and households each have complementary roles to play. It has been observed that an early adaptation plan will definitely saves resources and livelihood.

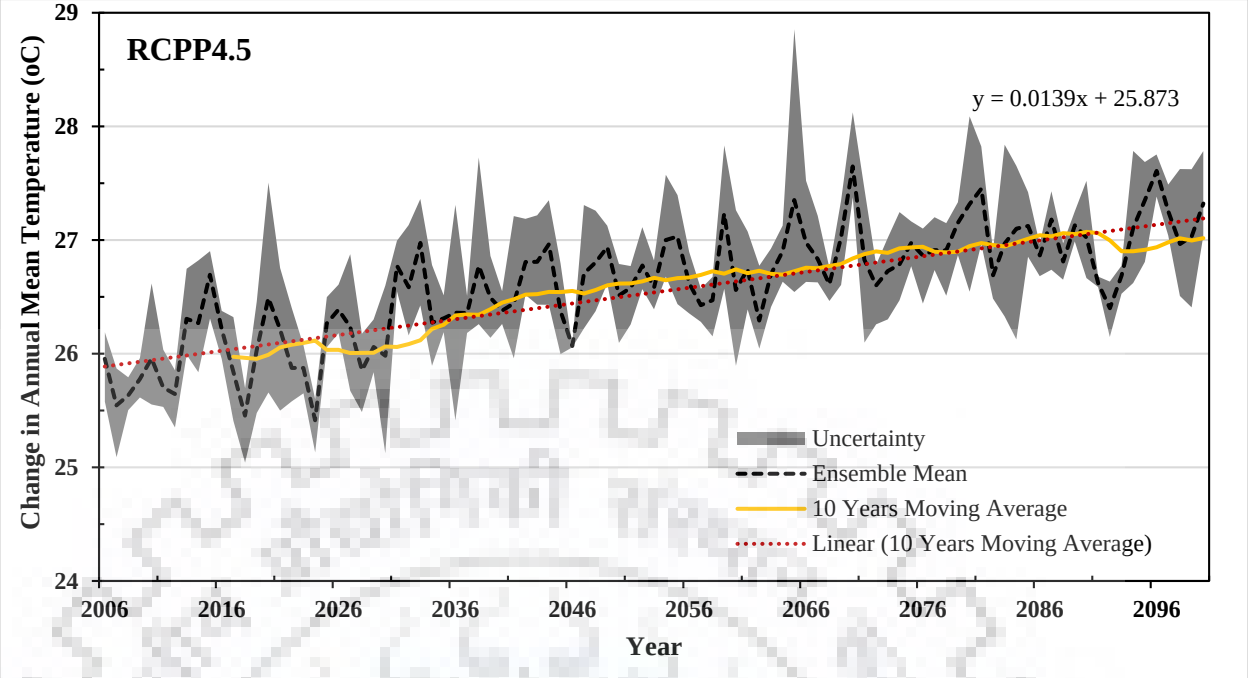

Figure 7.20: Change in mean annual temperature of basin averaged considering GCMs output ensemble of RCP4.5

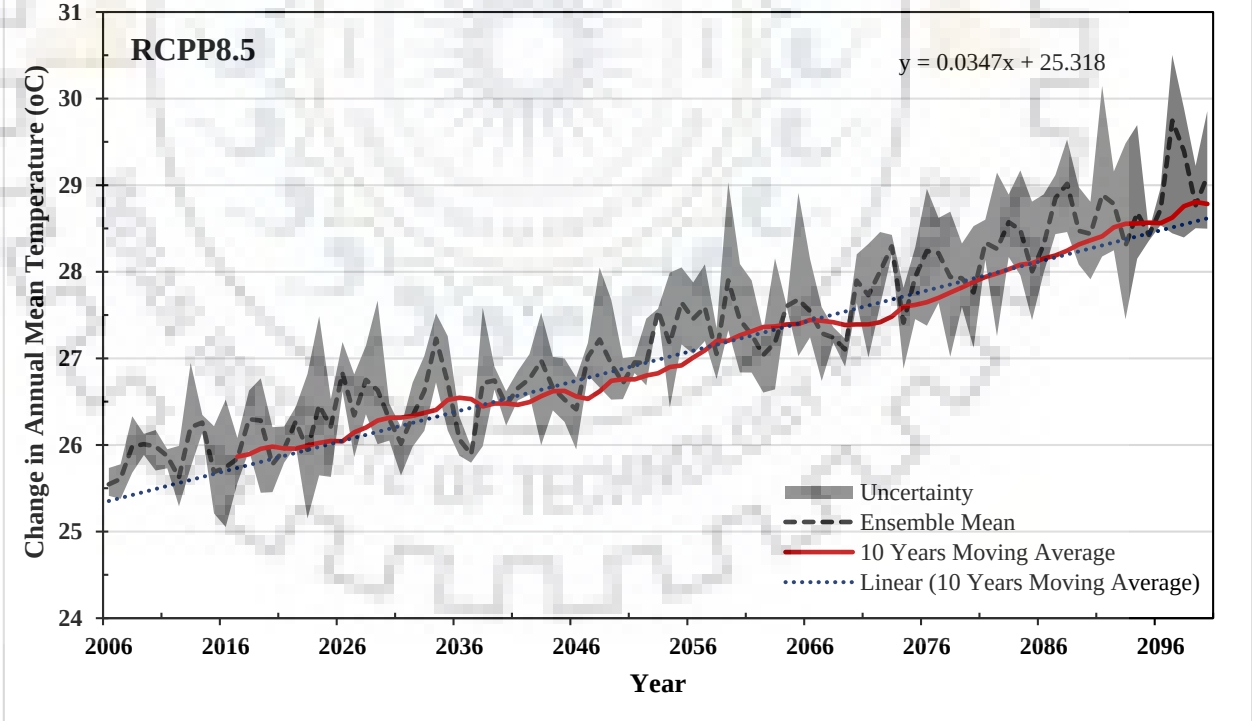

Figure 7.21: Change in mean annual temperature of basin averaged considering GCMs output ensemble of RCP8.5

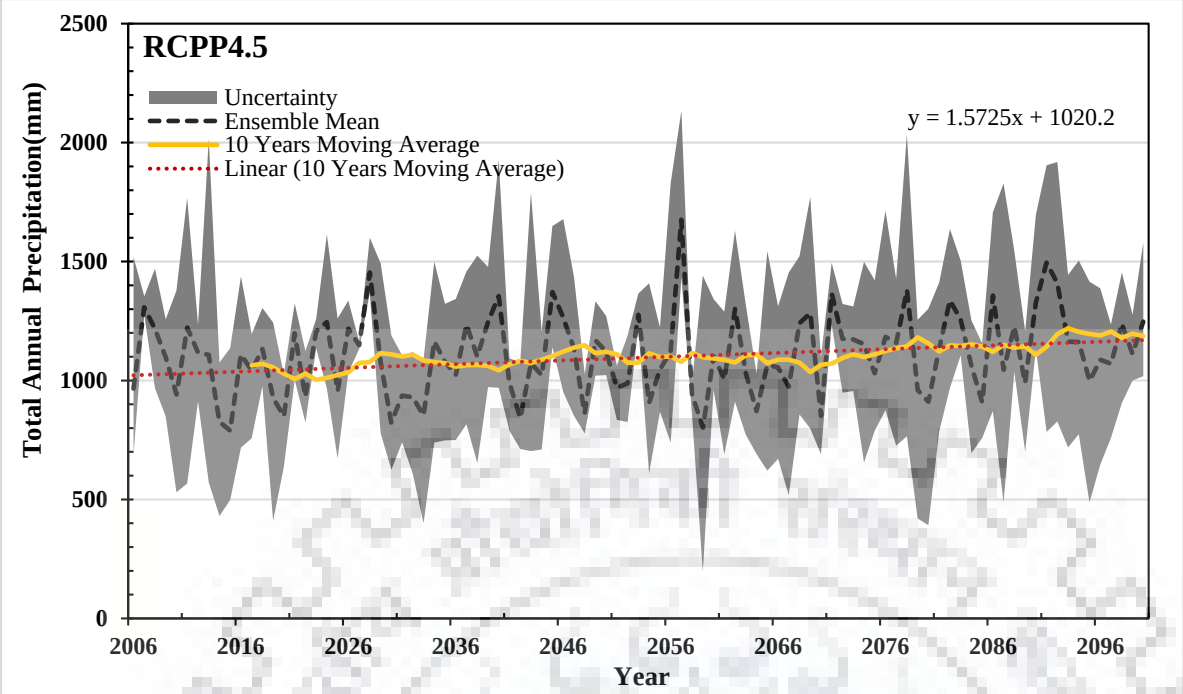

Figure 7.22: Change in total annual precipitation of basin averaged considering GCMs output ensemble of RCP4.5

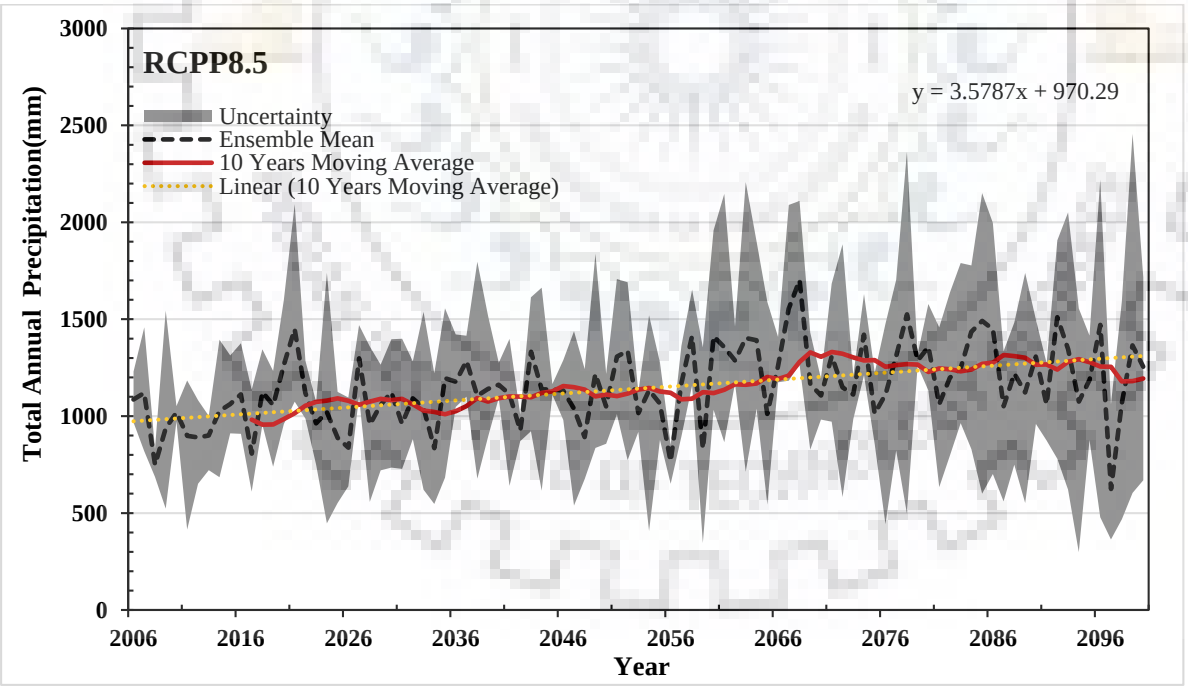

Figure 7.23: Change in total annual precipitation of basin averaged considering GCMs output ensemble of RCP8.5

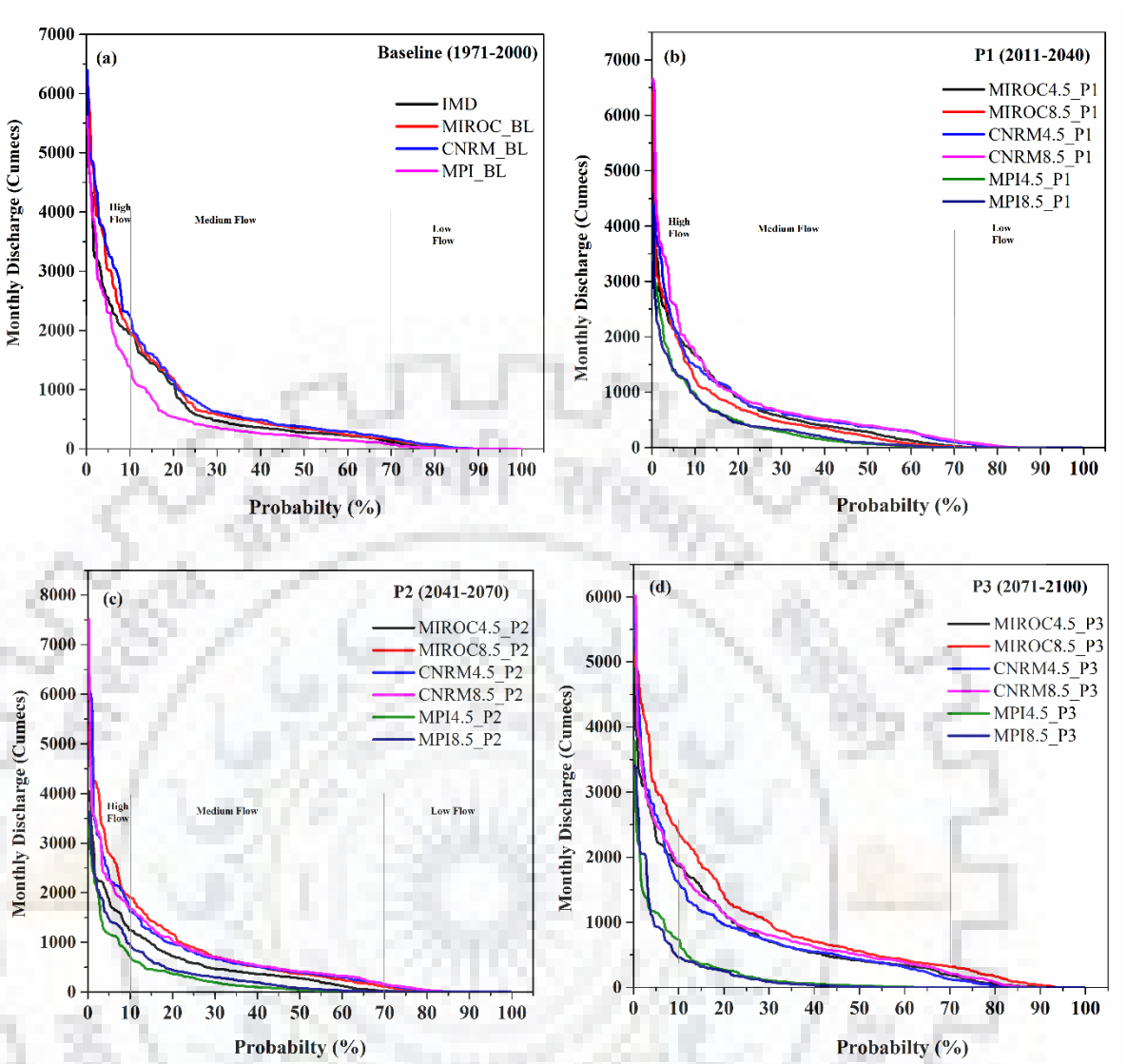

Figure 7.24: Total monthly discharge of basin averaged considering GCMs output ensemble of RCP4.5 and RCP8.5

The IPCC AR5 (2013) gives recommendations on adaptation, vulnerability and capacity enhancement. The main recommendation includes that reducing the vulnerability of any country to climate change requires an increased ability to adapt and mitigate its effects. Both mitigation and adaptation have become essential in reducing the risks of climate change. In order to avoid or reduce negative impacts of climate-driven changes in water resources on farming systems and to exploit potential positive effects, a range of technological and management options are available. The basic principles and elements of adaptation strategies are (Adger 1999; Adger et al. 2007; Epule et al. 2017; Nyong et al. 2007):

1. Assessment and development of flood management, including risk analysis and environmental and social impact assessment;
2. Provide warnings of flood to the general public and civil defence in advance;
3. Monitor the hydrologic regime and related climate factors, especially in the region most likely to suffer from the adverse effects of climate change
4. Develop long-term strategies and practical implementation programmes for agricultural water use under scarcity conditions with competing demands for water;
5. Land management techniques and amendment in policy to manage the natural vegetation and expansion of urbanization;
6. Crop substitution to reduce dependence on irrigation or to increase water availability. Some crops use less water or are more resistant to heat so they cope better with dry conditions than others. In addition, the choice of crops may contribute to adaptation in terms of "evapotranspiration management", in particular in rain-fed agriculture. In regions, a large proportion of the water that falls as precipitation is evaporated and transpired again by the vegetation. Through the appropriate selection of crop types, evapotranspiration from agriculture may be reduced, which could lead to increased runoff and a generally enhanced availability of water for other crops or purposes.
7. Changes in farming systems to make them more resilient against higher variability in climatic conditions. Diversification of production may thus be a way for farmers to increase their management flexibility and adaptive capacity. Also, organic farming approaches may enhance the capacity of agricultural soils to perform under changing and more adverse climatic conditions.
8. Changes in land use and landscape management may help conserve water, for instance replacing arable land by grassland. To reduce sensitivity of farming systems to flood damage, a change of land use in flood risk areas might be necessary. For instance, crop farming in flood risk areas may be replaced by extensive grassland management.
9. Establish and robust the institutional capabilities of countries, including legislative and regulatory arrangements, that are required to ensure the adequate assessment of their water resources and the provision of flood and drought forecasting services;

10. Initiate case-studies to establish whether there are linkages between climate changes and the current occurrences of droughts and floods in certain regions.

11. Furthermore, an integrated approach called Integrated Water Resources Management (IWRM) tool has been proposed to maximize economic and social welfare in an equitable manner without compromising the sustainability of vital ecosystems under climate change. It is defined as a process which promotes the coordinated development and management of water, land and related resources in order. However the potential impacts of climate change and increasing climate variability needs to be sufficiently incorporated in the IWRM plans. IWRM is an extensive tool for coping with natural climate variability and the prerequisite for adapting to the highly uncertain consequences of global warming and associated climate change. Research community needs to introduce the concept and basic overview of IWRM tools in adaptation of climate change impact and recommend as potential tool for implementation. IWRM seems to provide more flexibility and adaptive capacity than conventional water resources management approaches. As such, IWRM has to deal with all natural resources, not only water but also soils, surface water and groundwater, water quantity, quality as well as ecological aspects of water.

In general, water resource management uses both an analytical framework, explicitly identifying the components and different steps in the analysis process, and a computational framework, establishing a capacity for data processing and quantitative comparison of alternatives. Based on scenarios for climate change, demography, economic development and spatial planning, projections of the water demand for irrigation, drinking water supply, industrial water supply and environmental requirements are made. Hydro-meteorological data are used to establish the availability of water as well as its spatial distribution and variation over time. Next, projected future demands are checked against projected available future resources with a river basin simulation model. In case of imbalance, water resources management strategies are designed to improve the situation. Finally, the performance of the strategies, in terms of impacts on the water resources system, the socio-economic system and the environment, is assessed. It seeks to ensure that water is used to advance a country's social and economic development goals in ways that do not compromise the sustainability of vital ecosystems or threaten the ability of future generations to meet their water needs.

Moreover, agriculture may benefit from adaptation measures taken in the water management sector. A need for further research exists both with respect to the integrated impacts of CO_2

increase and climate change on farming systems, and with respect to adaptation strategies that can improve sustainability and resilience of farming systems under more variable climatic conditions. Issues for research include spatial resolution in vulnerability mapping, technological and management-based adaptation measures.

7.7 CONCLUDING REMARKS

This study investigated the land use land cover change and climate variability on water availability of UNB as it plays a crucial role in sustainable development of water resources planning and management. To mimic the basin characteristic, it was important to calibrate the model. Thus multi-site calibration approach has been adopted. The following conclusions can be drawn from the study presented in this chapter:

1. Parameters namely CN2, ALPHA_BF, and GQ_DELAY were found to be the most sensitive parameters for the Upper Narmada Basin.
2. For monthly simulations, the values of R^2 and NSE were found to be 0.77 and 0.76, during calibration, and 0.73 and 0.70, during validation, respectively indicating satisfactory model performance for basin. On the basis of these results, the SWAT model can be successfully adopted for hydrological simulation of Upper Narmada Basin.
3. In order to compute the hydrological components under dynamics of land use land cover, fixed climatic period data from 1990 to 2000 has been considered to simulate the impact of LULC change for 1990, 2000, 2010 and 2030. Results indicate that increase in settlement and decrease in natural vegetation, affect as increase in the water yield and increased surface runoff, but there is a decrease in ET. Moreover, surface runoff and water yield of 1990 is the lowest (477.79 mm and 699.69 mm, respectively) which increases gradually and highest increase is predicted in the future in 2030 (539.48 mm and 752.54 mm, respectively). The actual ET decreases with time due to decrease in natural vegetation and it is projected to be lower in 2030 (552.86 mm) and highest in 1990 (605.33 mm).
4. To project the impact of climate change on water availability, in terms of blue and green water, three representative climate models (MIROC5, CNRM-CM5 and MPI-ESM-LR) output from three classical climatic periods, P1 (2011-2040), P2 (2041-2070) and P3 (2071-2100) were selected under moderate (RCP4.5) and severe (RCP8.5) emission scenarios series (1970-2000). The spatial and temporal variation in green and blue water

of futuristic scenarios were evaluated with respect to baseline scenarios. Results of the analysis indicate climate variability over the green (ET+SW) and blue water (WYLD + GWS) for P1, P2 and P3 under RCP4.5 and RCP8.5. Results indicated annual precipitation decreasing from ranging -1.65% (MPI) to -16.55 % (MIROC) for P1 and P2 under RCP4.5, whereas in RCP8.5 scenario it varies from -26.19% (CNRM, P3) to 21.24 % (MIROC, P3) with reference to baseline scenario. Changes in green and blue water varying from 16.22% (MIROC,P3) to -14.10% (CNRM,P3) under RCP4.5 and from 38.25% (MIROC, P3) to -22.57% (CNRM,P3) under RCP8.5 with reference to baseline scenario.

CHAPTER 8
SUMMARY AND CONCLUSIONS

8.1 SUMMARY

The present research has been carried out with an objective to ascertain the water availability and its distribution under the impact of climate change projection and anthropogenic intervention in Upper Narmada river basin, India. Water is the first sector to be affected by changes in climate. Climate change contributes to intensification of the hydrological cycle and subsequently it has serious effects on the frequency and intensity of extreme events. Sea level rise, increased evaporation, unpredictable precipitation and prolonged droughts are just a few manifestations of climate variability which directly impacts availability and quality of water. The change in meteorological distribution will influence the ecosystem and landscape change. However, changes in precipitation rate and temperature are main cause of climate change and deforestation in the upper part of river basin. For planning and management of water resources, it is important to understand the distribution and variability of meteorological parameters.

8.2 CONCLUSIONS

In the study, Upper Narmada Basin (UNB) and seven regions of India are respectively selected as the local and regional study area. India was categorized in seven regions, considering the geography and homogeneous annual precipitation. These regions are North Mountainous India (NMI), North Central India (NCI), Northwest India (NWI), East Peninsular India (EPI), West Peninsular India (WPI), South Peninsular India (SPI) and North East India (NEI).

1) Initially, trend and break points were identified to detect the climate change. Trend detection was carried out for long term precipitation data applying regression analysis, MK test, Innovative Trend Analysis (ITA) and conjunction of DWT and sequential MK tests over Indian regions as well as Upper Narmada River Basin. Trends of the monthly and annual precipitation and mean temperature data were observed at 16 stations of UNB are as follows:

    a) During regional scale (seven Indian zones) study, regression analysis was carried out for 156 years (1850-2006) long precipitation series. The results indicated that the mean values of precipitation are decreasing in most of the study area in the last 30-year period. Investigation revealed that there are both positive and negative trends existing in each zone for the monsoon period. Annual and monsoon precipitation data show a

negative trend; however, zones NMI and NEI showed a positive trend for annual and monsoon datasets.

b) Wavelet analysis is attempted for trend analysis and periodicity identification in hydrological time series in the study. The most suitable mother wavelet was selected using the criteria of MRE and the criterion relative error (E_r). Applying this criterion, the DWT Daubechies wavelets db6 and db10 were selected for annual and monthly datasets, respectively. The *Z* statistic was evaluated for trend analysis of the decomposed periodic components and the original annual and monsoon series. Application of DWT on annual series implied 2-, 4- and 8-year fluctuations in the NMI zone, indicating a positive trend in rainfall, whereas zones WPI, SPI and WPI (with 2- and 4-year fluctuations) experienced a negative trend at the same periodicities, at the 0.05 (5%) significance level. In the monsoon series, a positive trend was found over NMI and NEI decomposed series at 2-, 4- and 8-year periodicity, whereas WPI, EPI and SPI indicated a negative trend at the same periodicity. Considering India as whole (AI), a negative trend in all zones except NMI and NEI was found.

c) At local scale analysis, trends of the monthly and annual precipitation and mean temperature data observed at 16 stations of UNB were carried out. Results imply that very few stations exhibit the negative trend for precipitation, while all the stations show positive trends for mean temperature over 16 stations of UNB. A comparative study was carried out between three methods i.e. ITA, MK-test and Sen's slope, to check the suitability of ITA against nonparametric tests. ITA shows strong agreement with both methods (MK test and Sen's slope), 97.5% and 77.5% in 'ITA versus MK test' and 'ITA versus Sen's slope'. This indicate that ITA has many advantages over MK test and Sen's slope estimator, as it is based on certain assumption and can be analyzed with less and all ranges of data.

d) Change points were detected to find the significant shifting and start of significant change applying sequential Mann Kendall (SQMK) in 16 stations of study area. Further change points obtained by SQMK were compared with the change points by CUMSUM test. Results indicate that most of the stations exhibit significant abrupt change year is 1955 (77.78%) and 1960 (100%) for precipitation and temperature, respectively. Moreover occurrence of abrupt change point investigated as 1955-1960 by SQMK and 1961-1963 by CUMSUM for precipitation, while change point 1960 by SQMK and

1945-1950 by CUMSUM for temperature over 16 stations of UNB. The finding in this study provide a new understanding of extreme value trend evaluation that probably are the cause of flood and drought in the area. This will help in short and long term water resources planning and development in the region. These information will certainly assist to the engineer and stakeholders to manage the water resources in the region.

2) Mapping of LULC and change detection were carried out using the Landsat TM satellite image utilizing the geospatial tools viz. GIS and ERDAS Imagine over UNB. The decadal development in the different classes of LULC were evaluated from 1990 to 2015. The reduction in natural vegetation and increase in settlement as well as cropland are reflected in the analysis of LULC mapping. Understanding of trend patterns were demonstrated and predicated for the year 2030 using CA-Markov model. The model were validated with the actual LULC of 2015. The projected LULC of 2030 classes indicate the continuing of same trend of recent past. These changes in the LULC in near future call for better planning and management of resources in the study area.

3) In order to identify the best (representative) climate models, 24 Global Climate Models (GCMs) were selected for performance evaluation. Performance of different models were carried out based on Skill Score (SS) and Root Mean Square Error (RMSE) between climate model outputs and reanalysis data of 20 years (1981-2000). The computation of RMSE and SS were carried out by using Data Integration and Assessment Tool (DIAS) developed by University of Tokyo, Japan. Six meteorological parameters, precipitation (PCP), outgoing long wave radiation (OLR), air temperature (AT), mean sea level pressure (SLP), zonal wind (ZW) and meridional wind (MW) were considered from each model for the SS and RMSE assessment.

    a) At regional scale study, there is no single GCM which can be recommended for the whole Indian region. However GCM model for precipitation has been proposed as ensemble of MPI_ECHAM4.0, MIROC3.2_HIRES, UKMO_HADCM3.0 and INGV_ECHAM4 are the best model for the Indian region. Climate models of CCCMA groups are performing well for atmospheric temperature in most of the Indian region. Additionally, model group of ECHAM and CCCMA are proposed for OLR simulation over India during the annual and monsoon season.

b) MIROC5 and CNRM-CM5 are selected as best performing climate models for Upper Narmada Basin, followed by MPI-ESM-LR, GFDL-ESM2M and IPSL-CM5A-MR.

c) Best three representative climate models of Upper Narmada Basin i.e. MIROC5, CNRM-CM5 and MPI-ESR-LR were selected for hydrological modelling over the basin.

4) SWAT Model was calibrated applying multi-site calibration techniques. In monthly simulation, Nash Sutcliffe Efficiency (NSE) and Coefficient of Determination (R^2) were computed as 0.77 and 0.76 for calibration (1978-1995) and, 0.73 and 0.70 for validation period (1996-2005), respectively, indicating good model performance for the basin. Parameters CN2, ALPHA_BF, and GW_DELAY were found to be the most sensitive parameters. Calibrated hydrological model used to simulate the water balance components under land use land cover change and climate change.

   a. Water balance components due to land use land cover change, under constant climatic condition were simulated for 1990, 2000, 2010 and 2030 LULC. Results indicate that increase in settlement and decrease in natural vegetation, results in increased water yield and surface runoff, but there is a decrease in ET. Surface runoff and water yield of 1990 is the lowest (477.79 mm and 699.69 mm respectively), which increases gradually and highest increase is predicted in the future in 2030 (539.48 mm and 752.54 mm, respectively). The actual ET decreases with time due to decrease in natural vegetation and it is projected to be lower in 2030 (552.86 mm) and highest in 1990 (605.33 mm).

   b. To project the water availability under climate change condition, outputs from climate models (MIROC5, CNRM-CM5 and MPI-ESM-LR) were used for periods, P1 (2011-2040), P2 (2041-2070) and P3 (2071-2100) under moderate (RCP4.5) and severe (RCP8.5) emission scenarios. Results of the analysis indicate climate variability over the green and blue water for P1, P2 and P3 under RCP4.5 and RCP8.5. Results indicated annual precipitation decreasing from -1.65% (MPI) to -16.55% (MIROC) for P1 and P2 under RCP4.5, whereas in RCP8.5 scenario it varies from -26.19% (CNRM, P3) to 21.24% (MIROC, P3) with reference to baseline scenario. Changes in green and blue water varying from 16.22% (MIROC, P3) to -14.10% (CNRM, P3) under RCP4.5 and from 38.25% (MIROC, P3) to -22.57% (CNRM, P3) under RCP8.5 with reference to baseline scenario. This study established the

sensitivity of UNB to future climatic changes employing projections from CMIP5 climate models and exhibited an approach that applied multiple climate model outputs to estimate potential change over the river basin.

8.3 RESEARCH CONTRIBUTIONS

The research contribution of the present study are summarised as below:

1. Long-term climatic trend analysis is concluded, applying parametric (linear regression) and non-parametric tests (Mann-Kendall, Sen's Slope), extreme value analysis by Innovative Trend Analysis (ITA), periodicity using discrete wavelet transform (DWT) and change year of precipitation, temperature and reference evapotranspiration at regional scale (seven zones of India) and local scale (Upper Narmada Basin).
2. Land use land cover mapping were carried out using the Landsat TM satellite images utilizing geospatial tools viz. GIS and ERDAS Imagine. The development in the different classes of LULC were evaluated from 1990 to 2015. Understanding of trend patterns were demonstrated and predicated for the year 2030 using CA-Markov model.
3. Ranking of global climate models (GCMs) carried out multi-criteria analysis for each zones of India (regional scale) and for Upper Narmada Basin (local scale). Performance of the model were done based on Skill Score (SS) and Root Mean Square Error (RMSE) between models output and reanalysis data of six meteorological parameters for the period 1981-2000.
4. Development of model setup (SWAT) for Upper Narmada Basin, applying multi-site calibration using SWAT-CUP. Projection of water balance components (surface runoff, evapotranspiration, water yield, surface discharge and groundwater flow etc.) were investigated by integrating bias corrected climate data with calibrated model under high and moderate emission scenarios from 2011 to 2100.

8.4 RESEARCH LIMITATION

There are some limitations in the present study which are given below:

1. There are three climate model considered in long term projection of water balance components for study area.
2. No change in soil layer and land use land cover were considered over the long term period in projection of water availability.

3. Due to limitation of discharge gauging site, it was not possible to calibrate the whole catchment, and part of the basin i.e. Upper Narmada Basin was considered in the presented study.
4. In general, adaptation provides an essential strategy to reduce negative consequences, therefore it does not imply that proposed adaptation can overcome all climate change effects.
5. Small structure along the river has been neglected due to unavailability of proper data.

8.5 FUTURE SCOPE

There are few limitation in the study which can be overcome in the near future listed as:

1. In discrete wavelet analysis (DWT), visualization of extreme events was examined at different threshold limits. The same intensity of positive and negative fluctuations indicated the same colour spectrum, which is one of the limitations of the visualization study and may form the subject of future work in this area.
2. In order to compute the future projection of hydrological components, some more climate models and projections may be considered in the study to reduce the uncertainty.
3. Minor hydraulic structures may also considered in the future study.
4. Digital elevation model (DEM) of coarser resolution (90 meter) used in this study. It is recommended to test the applicability of the approach and replaced by finer spatial resolution of 30 meter or less.
5. To setup the model, limited SWAT parameters were considered in the study that may be extended in future study.

REFERENCES

Abbaspour, K. C., Rouholahnejad, E., Vaghefi, S., Srinivasan, R., Yang, H., and Kløve, B. (2015). "A continental-scale hydrology and water quality model for Europe: Calibration and uncertainty of a high-resolution large-scale SWAT model." Journal of Hydrology, 524, 733-752.

Abd El-Kawy, O. R., Rød, J. K., Ismail, H. A., and Suliman, A. S. (2011). "Land use and land cover change detection in the western Nile delta of Egypt using remote sensing data." Applied Geography, 31(2), 483-494.

Adarsh, S., and Janga Reddy, M. (2015). "Trend analysis of rainfall in four meteorological subdivisions of southern India using nonparametric methods and discrete wavelet transforms." International Journal of Climatology, 35(6), 1107-1124.

Adger, W. N. (1999). Social vulnerability to climate change and extremes in coastal Vietnam. World development, 27(2), 249-269.

Adger, W. N., Agrawala, S., Mirza, M. M. Q., Conde, C., o'Brien, K., Pulhin, J., ... & Takahashi, K. (2007). Assessment of adaptation practices, options, constraints and capacity. Climate change, 717-743.

Agarwal, A., Babel, M. S., Maskey, S., Shrestha, S., Kawasaki, A., & Tripathi, N. K. (2016). Analysis of temperature projections in the Koshi River Basin, Nepal. International Journal of Climatology, 36(1), 266-279

Agarwal, A., Singh, R., Mishra, S., and Bhunya, P. (2005). "ANN-based sediment yield models for Vamsadhara river basin (India)." Water SA, 31(1), 85-100.

Agrawal, A. (2001). "Common property institutions and sustainable governance of resources." World development, 29(10), 1649-1672.

Ahmad, S., and Simonovic, S. P. (2005). "An artificial neural network model for generating hydrograph from hydro-meteorological parameters." Journal of Hydrology, 315(1), 236-251.

Aldaya, M. M., Chapagain, A. K., Hoekstra, A. Y., and Mekonnen, M. M. (2012). The water footprint assessment manual: Setting the global standard, Routledge.

Anandhi, A., and Nanjundiah, R. (2015). "Performance evaluation of AR4 Climate Models in simulating daily precipitation over the Indian region using skill scores." Theor Appl Climatol, 119(3-4), 551-566.

Anderson, M., Chen, Z.-Q., Kavvas, M., and Feldman, A. (2000). "Coupling HEC-HMS with Atmospheric Models for the Prediction of Watershed Runoff." Building Partnerships, 1-10.

Arnell, N. W. (1999). "The effect of climate change on hydrological regimes in Europe: a continental perspective." Global Environmental Change, 9(1), 5-23.

Arnold, J. G., Srinivasan, R., Muttiah, R. S., and Williams, J. R. (1998). "Large area hydrologic modeling and assessment part I: model development." JAWRA Journal of the American Water Resources Association, 34(1), 73-89.

Arnold, J., and Allen, P. (1996). "Estimating hydrologic budgets for three Illinois watersheds." Journal of hydrology, 176(1-4), 57-77.

Arnold, J., Williams, J., Srinivasan, R., King, K., and Griggs, R. (1994). "SWAT: Soil and water assessment tool." US Department of Agriculture, Agricultural Research Service, Grassland, Soil and Water Research Laboratory, Temple, TX.

Arora, M., Goel, N., and Singh, P. (2005). "Evaluation of temperature trends over India/Evaluation de tendances de température en Inde." Hydrological sciences journal, 50(1).

Bae, D. H., Jung, I. W., and Chang, H. (2008). "Long?term trend of precipitation and runoff in Korean river basins." Hydrological processes, 22(14), 2644-2656.

Bandyopadhyay, A., Bhadra, A., Raghuwanshi, N., and Singh, R. (2009). "Temporal trends in estimates of reference evapotranspiration over India." Journal of Hydrologic Engineering, 14(5), 508-515.

Basistha, A., Arya, D., and Goel, N. (2008). "Spatial distribution of rainfall in Indian Himalayas-a case study of Uttarakhand region." Water Resources Management, 22(10), 1325-1346.

Basistha, A., Arya, D., and Goel, N. (2009). "Analysis of historical changes in rainfall in the Indian Himalayas." International Journal of Climatology, 29(4), 555-572.

Bawden, A. J., Linton, H. C., Burn, D. H., and Prowse, T. D. (2014). "A spatiotemporal analysis of hydrological trends and variability in the Athabasca River region, Canada." Journal of Hydrology, 509, 333-342.

Beven, K. (1997). "TOPMODEL: a critique." Hydrological processes, 11(9), 1069-1085.

Beven, K., and Freer, J. (2001). "A dynamic topmodel." Hydrological processes, 15(10), 1993-2011.

Bhattacharya, B., Conway, C., Craven, J., Masih, I., Mazzolini, M., Shrestha, S., ... & van Andel, S. J. (2017, April). Hydrological simulation of the Brahmaputra basin using global datasets. In EGU General Assembly Conference Abstracts (Vol. 19, p. 13758).

Bisantino, T., Bingner, R., Chouaib, W., Gentile, F., and Trisorio Liuzzi, G. (2015). "Estimation of Runoff, Peak Discharge and Sediment Load at the Event Scale in a Medium-Size Mediterranean Watershed Using the Annagnps Model." Land Degradation & Development, 26(4), 340-355.

Camici, S., Brocca, L., Melone, F., and Moramarco, T. (2014). "Impact of Climate Change on Flood Frequency Using Different Climate Models and Downscaling Approaches." Journal of Hydrologic Engineering, 19(8), 04014002.

Chakraborty, A., and Okaya, D. (1995). "Frequency-time decomposition of seismic data using wavelet-based methods." Geophysics, 60(6), 1906-1916.

Change, C. (2007). "The Physical Science Basis, Contribution of Working Group I to the Fourth Assessment Report of the Intergovernmental Panel on Climate Change, 2007, S. Solomon, D. Qin, M." Cambridge University Press, Cambridge, United King& dom and New York, NY, USA.

Chapagain, A. K., and Hoekstra, A. Y. (2004). "Water footprints of nations."

Chatterjee, K. (2014). "Water Resources of India." online www. Climate change centre. net_pdf_waterresources accessed on 31st Jan.

Chattopadhyay, S., and Jha, M. K. (2016). "Hydrological response due to projected climate variability in Haw River watershed, North Carolina, USA." Hydrological sciences journal, 61(3), 495-506.

Chen, H., Xu, C.-Y., and Guo, S. (2012). "Comparison and evaluation of multiple GCMs, statistical downscaling and hydrological models in the study of climate change impacts on runoff." Journal of Hydrology, 434-435, 36-45.

Chen, X.-L., Zhao, H.-M., Li, P.-X., and Yin, Z.-Y. (2006). "Remote sensing image-based analysis of the relationship between urban heat island and land use/cover changes." Remote sensing of environment, 104(2), 133-146.

Chou, C.-m. (2011). "A Threshold Based Wavelet Denoising Method for Hydrological Data Modelling." Water Resources Management, 25(7), 1809-1830.

Christensen, J. H., Boberg, F., Christensen, O. B., and Lucas-Picher, P. (2008). "On the need for bias correction of regional climate change projections of temperature and precipitation." Geophysical Research Letters, 35(20).

Cooper, A., Smith, C., and Bottcher, A. (1992). "Predicting runoff of water, sediment, and nutrients from a New Zealand grazed pasture using CREAMS." Transactions of the ASAE, 35(1), 105-112.

Cranmer, A., Kouwen, N., and Mousavi, S. (2001). "Proving WATFLOOD: modelling the nonlinearities of hydrologic response to storm intensities." Canadian Journal of Civil Engineering, 28(5), 837-855.

Crawford, N. H., and Linsley, R. K. (1966). "Digital Simulation in Hydrology'Stanford Watershed Model 4."

Dakhlalla, A. O., and Parajuli, P. B. (2016). "Evaluation of the Best Management Practices at the Watershed Scale to Attenuate Peak Streamflow Under Climate Change Scenarios." Water Resources Management, 30(3), 963-982.

Dawdy, D., Lichty, R., and Bergman, J. "T. O "Donnell, 1965. Mathematical models of catchment behavior." Journal of the Hydraulics Division, Proc. ASCE, 99.

de Artigas, M. Z., Elias, A. G., and de Campra, P. F. (2006). "Discrete wavelet analysis to assess long-term trends in geomagnetic activity." Physics and Chemistry of the Earth, Parts A/B/C, 31(1-3), 77-80.

de Noblet-Ducoudré, N., Boisier, J.-P., Pitman, A., Bonan, G. B., Brovkin, V., Cruz, F., Delire, C., Gayler, V., van den Hurk, B. J. J. M., Lawrence, P. J., van der Molen, M. K., Müller, C., Reick, C. H., Strengers, B. J., and Voldoire, A. (2012). "Determining Robust Impacts of Land-Use-Induced Land Cover Changes on Surface Climate over North America and Eurasia: Results from the First Set of LUCID Experiments." Journal of Climate, 25(9), 3261-3281.

De, U. S., & Rao, G. P. (2004). Urban climate trends—the Indian scenario. Journal of Indian Geophysical Union, 8(3), 199-203.Caramelo, L., & Orgaz, M. (2007). A study of precipitation variability in the Duero Basin (Iberian Peninsula). International journal of climatology, 27(3), 327-339.

Deep, S., and Saklani, A. (2014). "Urban sprawl modeling using cellular automata." The Egyptian Journal of Remote Sensing and Space Science, 17(2), 179-187.

Dettinger, M. D., Cayan, D. R., Meyer, M. K., & Jeton, A. E. (2004). Simulated hydrologic responses to climate variations and change in the Merced, Carson, and American River basins, Sierra Nevada, California, 1900–2099. Climatic Change, 62(1-3), 283-317.

Dewan, A. M., and Yamaguchi, Y. (2009). "Using remote sensing and GIS to detect and monitor land use and land cover change in Dhaka Metropolitan of Bangladesh during 1960-2005." Environmental monitoring and assessment, 150(1), 237-249.

Dibike, Y. B., and Coulibaly, P. (2005). "Hydrologic impact of climate change in the Saguenay watershed: comparison of downscaling methods and hydrologic models." Journal of Hydrology, 307(1-4), 145-163.

Diro, G. T., Grimes, D. I. F., Black, E., O'Neill, A., and Pardo-Iguzquiza, E. (2009). "Evaluation of reanalysis rainfall estimates over Ethiopia." International Journal of Climatology, 29(1), 67-78.

Donigan, A. S., Imhoff, J. C., Bicknell, B. R., and Kittle, J. L. (1984). "Application Guide for Hydrological Simulation Program: FORTRAN(HSPF)." EPA-600/3-84-065 June 1984. Environmental Research Laboratory, Athens, GA. 177 p, 19 fig, 17 tab, 3 app, 20 ref. 68-01-6207.

Duan, Q., Sorooshian, S., and Gupta, V. (1992). "Effective and efficient global optimization for conceptual rainfall?runoff models." Water resources research, 28(4), 1015-1031.

Duhan, D., & Pandey, A. (2015). Statistical downscaling of temperature using three techniques in the Tons River basin in Central India. Theoretical and applied climatology, 121(3-4), 605-622.

Duhan, D., Pandey, A., Gahalaut, K. P. S., and Pandey, R. P. (2013). "Spatial and temporal variability in maximum, minimum and mean air temperatures at Madhya Pradesh in central India." Comptes Rendus Geoscience, 345(1), 3-21.

Ebtehaj, I., Bonakdari, H., Hossein Zaji, A., Hin Joo Bong, C., & Ab Ghani, A. (2016). Design of a new hybrid artificial neural network method based on decision trees for calculating the Froude number in rigid rectangular channels. Journal of Hydrology and Hydromechanics, 64(3), 252-260.

Eldho, T. I., & Kulkarni, A. T. (2014). Watershed Based Integrated Modelling Approach for Hydrologic Simulation Using Numerical Models and Geo Spatial Techniques. Hydrology and Watershed Management: Ecosystem Resilience-Rural and Urban Water Requirements, 1, 3.

Emori, S., and Brown, S. (2005). "Dynamic and thermodynamic changes in mean and extreme precipitation under changed climate." Geophysical Research Letters, 32(17).

Epule, Terence Epule, et al. "Climate change adaptation in the Sahel." Environmental Science & Policy 75 (2017): 121-137.

Errasti, I., Ezcurra, A., Sáenz, J., and Ibarra-Berastegi, G. (2011). "Validation of IPCC AR4 models over the Iberian Peninsula." Theor Appl Climatol, 103(1-2), 61-79.

Evan, K., Subimal, G., and Auroop, R. G. (2012). "Evaluation of global climate models for Indian monsoon climatology." Environmental Research Letters, 7(1), 014012.

Ezber, Y., Lutfi Sen, O., Kindap, T., and Karaca, M. (2007). "Climatic effects of urbanization in Istanbul: a statistical and modeling analysis." International Journal of Climatology, 27(5), 667-679.

Fan, F., Wang, Y., and Wang, Z. (2008). "Temporal and spatial change detecting (1998-2003) and predicting of land use and land cover in Core corridor of Pearl River Delta (China) by using TM and ETM+ images." Environmental Monitoring and Assessment, 137(1), 127-147.

Fedora, M., and Beschta, R. (1989). "Storm runoff simulation using an antecedent precipitation index (API) model." Journal of hydrology, 112(1-2), 121-133.

Feldman, A. D. (1994). "HEC Models for Urban Hydrologic Analysis." Hydrologic Engineering Center DAVIS CA.

Feldman, A. D. (2000). Hydrologic modeling system HEC-HMS: technical reference manual, US Army Corps of Engineers, Hydrologic Engineering Center.

Fennessy, M. J., Kinter, J. L., Kirtman, B., Marx, L., Nigam, S., Schneider, E., Shukla, J., Straus, D., Vernekar, A., Xue, Y., and Zhou, J. (1994). "The Simulated Indian Monsoon: A GCM Sensitivity Study." Journal of Climate, 7(1), 33-43.

Ficklin, D. L., Luo, Y., Luedeling, E., and Zhang, M. (2009). "Climate change sensitivity assessment of a highly agricultural watershed using SWAT." Journal of Hydrology, 374(1), 16-29.

Fischer, G., Tubiello, F. N., van Velthuizen, H., and Wiberg, D. A. (2007). "Climate change impacts on irrigation water requirements: Effects of mitigation, 1990-2080." Technological Forecasting and Social Change, 74(7), 1083-1107.

Flanagan, D. C., Frankenberger, J. R., Cochrane, T. A., Renschler, C. S., & Elliot, W. J. (2013). Geospatial application of the water erosion prediction project (WEPP) model. Transactions of the ASABE, 56(2), 591-601.

Foody, G. M. (2002). "Status of land cover classification accuracy assessment." Remote sensing of environment, 80(1), 185-201.

Franczyk, J., and Chang, H. (2009). "The effects of climate change and urbanization on the runoff of the Rock Creek basin in the Portland metropolitan area, Oregon, USA." Hydrological Processes, 23(6), 805-815.

Frei, C., Christensen, J. H., Déqué, M., Jacob, D., Jones, R. G., and Vidale, P. L. (2003). "Daily precipitation statistics in regional climate models: Evaluation and intercomparison for the European Alps." Journal of Geophysical Research: Atmospheres, 108(D3), 4124.

Fu, G., Liu, Z., Charles, S. P., Xu, Z., and Yao, Z. (2013). "A score-based method for assessing the performance of GCMs: A case study of southeastern Australia." Journal of Geophysical Research: Atmospheres, 118(10), 4154-4167.

Gamon, J. A., Huemmrich, K. F., Stone, R. S., and Tweedie, C. E. (2013). "Spatial and temporal variation in primary productivity (NDVI) of coastal Alaskan tundra: Decreased vegetation growth following earlier snowmelt." Remote Sensing of Environment, 129, 144-153.

Geng, X., Wang, X., Yan, H., Zhang, Q., and Jin, G. (2014). "Land Use/Land Cover Change Induced Impacts on Water Supply Service in the Upper Reach of Heihe River Basin." Sustainability, 7(1), 366-383.

Georgakakos, K. P. (1987). "Real-time flash flood prediction." Journal of Geophysical Research: Atmospheres, 92(D8), 9615-9629.

Georgakakos, K. P., and Foufoula-Georgiou, E. (1991). "Real-time coupling of hydrologic and meteorological models for flood forecasting." Recent advances in the modeling of hydrologic systems, 169-184.

Georgakakos, K. P., Li, S., and Viswesvaran, C. (1988). Integrated Hydrometeorological Forecast System: IHFS, Version 1, a User's Manual, Department of Civil and Environmental Engineering.

Gessesse, B., Bewket, W., and Bräuning, A. (2015). "Model-Based Characterization and Monitoring of Runoff and Soil Erosion in Response to Land Use/land Cover Changes in the Modjo Watershed, Ethiopia." Land Degradation & Development, 26(7), 711-724.

Ghani, A. A., & Azamathulla, H. M. (2014). Development of GEP-based functional relationship for sediment transport in tropical rivers. Neural Computing and Applications, 24(2), 271-276.

Ghosh, S. (2010). SVM-PGSL coupled approach for statistical downscaling to predict rainfall from GCM output. Journal of Geophysical Research: Atmospheres, 115(D22).

Ghosh, S., Roy, M., and Ghosh, A. (2014). "Semi-supervised change detection using modified self-organizing feature map neural network." Applied Soft Computing, 15, 1-20.

Gocic, M., and Trajkovic, S. (2013). "Analysis of changes in meteorological variables using Mann-Kendall and Sen's slope estimator statistical tests in Serbia." Global and Planetary Change, 100, 172-182.

Gong, L., Xu, C.-y., Chen, D., Halldin, S., and Chen, Y. D. (2006). "Sensitivity of the Penman-Monteith reference evapotranspiration to key climatic variables in the Changjiang (Yangtze River) basin." Journal of Hydrology, 329(3), 620-629.

Gosain, A. K., Rao, S., & Basuray, D. (2006). Climate change impact assessment on hydrology of Indian river basins. Current science, 346-353.

Gosain, A., Rao, S., and Arora, A. (2011). "Climate change impact assessment of water resources of India." Current Science, 356-371.

Gowda, K.K., Majuantha, K., Manjunath, B.M., Putty, Y.R., 2008. Study of climate changes at Davangere region by using climatological data. Water Energy Int. 65 (3), 66–77.

Gowda, P. H., Senay, G. B., Colaizzi, P. D., & Howell, T. A. (2008). Simplified surface energy balance (SSEB) approach for estimating actual ET: An evaluation with lysimeter data. In 2008 Providence, Rhode Island, June 29–July 2, 2008 (p. 1). American Society of Agricultural and Biological Engineers.

Graham, D. N., and Butts, M. B. (2005). "Flexible, integrated watershed modelling with MIKE SHE." Watershed models, 849336090, 245-272.

Graham, L. P., Andréasson, J., and Carlsson, B. (2007). "Assessing climate change impacts on hydrology from an ensemble of regional climate models, model scales and linking methods - a case study on the Lule River basin." Climatic Change, 81(1), 293-307.

Graham, L. P., Hagemann, S., Jaun, S., and Beniston, M. (2007). "On interpreting hydrological change from regional climate models." Climatic Change, 81(1), 97-122.

Green, C., and Vangriensven, A. (2008). "Autocalibration in hydrologic modeling: Using SWAT2005 in small-scale watersheds." Environmental Modelling & Software, 23(4), 422-434.

Green, C., Tomer, M., Di Luzio, M., and Arnold, J. (2006). "Hydrologic evaluation of the soil and water assessment tool for a large tile-drained watershed in Iowa." Transactions of the ASABE, 49(2), 413-422.

Groisman, P. Y., Karl, T. R., Easterling, D. R., Knight, R. W., Jamason, P. F., Hennessy, K. J., Suppiah, R., Page, C. M., Wibig, J., and Fortuniak, K. (1999). "Changes in the probability of heavy precipitation: important indicators of climatic change." Climatic Change, 42(1), 243-283.

Guo, H., Hu, Q., and Jiang, T. (2008). "Annual and seasonal streamflow responses to climate and land-cover changes in the Poyang Lake basin, China." Journal of Hydrology, 355(1-4), 106-122.

Haddeland, I., Heinke, J., Biemans, H., Eisner, S., Florke, M., Hanasaki, N., Konzmann, M., Ludwig, F., Masaki, Y., Schewe, J., Stacke, T., Tessler, Z. D., Wada, Y., and Wisser, D. (2014). "Global water resources affected by human interventions and climate change." Proceedings of the National Academy of Sciences of the United States of America, 111(9), 3251-3256.

Halmy, M. W. A., Gessler, P. E., Hicke, J. A., and Salem, B. B. (2015). "Land use/land cover change detection and prediction in the north-western coastal desert of Egypt using Markov-CA." Applied Geography, 63, 101-112.

Han, K.-S., Champeaux, J.-L., and Roujean, J.-L. (2004). "A land cover classification product over France at 1 km resolution using SPOT4/VEGETATION data." Remote Sensing of Environment, 92(1), 52-66.

Hartigan, J. A., and Wong, M. A. (1979). "Algorithm AS 136: A k-means clustering algorithm." Journal of the Royal Statistical Society. Series C (Applied Statistics), 28(1), 100-108.

Hassan, Z., Harun, S., & Malek, M. A. (2012). Application of ANNs Model with the SDSM for the Hydrological Trend Prediction in the Sub-catchment of Kurau River, Malaysia. Journal of Environmental Science and Engineering. B, 1(5B).

Hay, L. E., Clark, M. P., Wilby, R. L., Gutowski Jr, W. J., Leavesley, G. H., Pan, Z., ... & Takle, E. S. (2002). Use of regional climate model output for hydrologic simulations. Journal of Hydrometeorology, 3(5), 571-590.

He, X., Shao, C., and Xiong, Y. (2016). "A non-parametric symbolic approximate representation for long time series." Pattern Analysis and Applications, 19(1), 111-127.

Healy, J. D. (1987). "A note on multivariate CUSUM procedures." Technometrics, 29(4), 409-412.

Heo, J., Yu, J., Giardino, J. R., and Cho, H. (2015). "Impacts of climate and land-cover changes on water resources in a humid subtropical watershed: a case study from East Texas, USA." Water and Environment Journal, 29(1), 51-60.

Hietel, E., Waldhardt, R., and Otte, A. (2004). "Analysing land-cover changes in relation to environmental variables in Hesse, Germany." Landscape ecology, 19(5), 473-489.

Hoekstra, A. Y. (2008). Globalization of water, Wiley Online Library.

Hoekstra, A. Y., and Hung, P. Q. (2002). "Virtual water trade." A quantification of virtual water flows between nations in relation to international crop trade. Value of water research report series, 11, 166.

Holland, G., Done, J., Bruyere, C., Cooper, C. K., & Suzuki, A. (2010, January). Model investigations of the effects of climate variability and change on future Gulf of Mexico tropical cyclone activity. In Offshore Technology Conference. Offshore Technology Conference.

Holman, I. P. (2005). "Climate change impacts on groundwater recharge- uncertainty, shortcomings, and the way forward?" Hydrogeology Journal, 14(5), 637-647.

Houghton, J. T., Ding, Y., Griggs, D. J., Noguer, M., van der Linden, P. J., Dai, X., Maskell, K., and Johnson, C. A. (2001). Climate change 2001: the scientific basis, The Press Syndicate of the University of Cambridge.

Huber, W. C., Dickinson, R. E., Barnwell Jr, T. O., and Branch, A. (1988). "Storm water management model; version 4." Environmental Protection Agency, United States.

Im, S., Kim, H., Kim, C., and Jang, C. (2009). "Assessing the impacts of land use changes on watershed hydrology using MIKE SHE." Environmental geology, 57(1), 231-239.

Iqbal, M. F., and Khan, I. A. (2014). "Spatiotemporal Land Use Land Cover change analysis and erosion risk mapping of Azad Jammu and Kashmir, Pakistan." The Egyptian Journal of Remote Sensing and Space Science, 17(2), 209-229.

Ivanov, P. C., Rosenblum, M. G., Peng, C., Mietus, J., Havlin, S., Stanley, H., and Goldberger, A. L. (1996). "Scaling behaviour of heartbeat intervals obtained by wavelet-based time-series analysis." Nature, 383(6598), 323-327.

Jain, S., Kumar, V., and Saharia, M. (2013). "Analysis of rainfall and temperature trends in northeast India." International Journal of Climatology, 33(4), 968-978.

Jaiswal, R. K., Saxena, R., and Mukherjee, S. (1999). "Application of remote sensing technology for land use/land cover change analysis." Journal of the Indian Society of Remote Sensing, 27(2), 123.

Jat, M. K., Garg, P. K., and Khare, D. (2008). "Modelling of urban growth using spatial analysis techniques: a case study of Ajmer city (India)." International Journal of Remote Sensing, 29(2), 543-567.

Jat, M. K., Garg, P. K., and Khare, D. (2008). "Monitoring and modelling of urban sprawl using remote sensing and GIS techniques." International Journal of Applied Earth Observation and Geoinformation, 10(1), 26-43.

Jat, M. K., Khare, D., Garg, P. K., & Shankar, V. (2009). Remote sensing and GIS-based assessment of urbanisation and degradation of watershed health. Urban Water Journal, 6(3), 251-263.

Jha, M. (2004). "Impacts of climate change on streamflow in the Upper Mississippi River Basin: A regional climate model perspective." Journal of Geophysical Research, 109(D9).

Jhajharia, D., and Singh, V. P. (2011). "Trends in temperature, diurnal temperature range and sunshine duration in Northeast India." International Journal of Climatology, 31(9), 1353-1367.

Jhajharia, D., Yadav, B. K., Maske, S., Chattopadhyay, S., and Kar, A. K. (2012). "Identification of trends in rainfall, rainy days and 24h maximum rainfall over subtropical Assam in Northeast India." Comptes Rendus Geoscience, 344(1), 1-13.

Jiang, F.-Q., ZHU, C., and HU, R.-J. (2002). "Trend Analysis of Precipitation over Northern Xinjiang for the Period 1961-1997 [J]." Scientia Geographica Sinica, 6, 004.

Johari, N. E., Abdul-Talib, S., Wahid, M. A., & Ghani, A. A. (2016). Trend of Total Phosphorus on Total Suspended Solid Reduction in Constructed Wetland Under Tropical Climate. In ISFRAM 2015 (pp. 273-280). Springer Singapore.

Johnson, F., and Sharma, A. (2009). "Measurement of GCM Skill in Predicting Variables Relevant for Hydroclimatological Assessments." Journal of Climate, 22(16), 4373-4382.

Joshi, N., Gupta, D., Suryavanshi, S., Adamowski, J., and Madramootoo, C. A. (2016). "Analysis of trends and dominant periodicities in drought variables in India: A wavelet transform based approach." Atmospheric Research, 182, 200-220.

K. A. Dhore, D. Khare, P. K. Garg, M. K. Jat, 2006, Conceptual Framework of DecisionSupport System for Watershed Management in India, Earth & Life (http://www.geofinds.com), 2006-12- 4, 1(4): 1-17.

Kabba, V. T. S., and Li, J. (2011). "Analysis of land use and land cover changes, and their ecological implications in Wuhan, China." Journal of Geography and Geology, 3(1), 104.

Kahya, E., and Kalayc?, S. (2004). "Trend analysis of streamflow in Turkey." Journal of Hydrology, 289(1-4), 128-144.

Kampata, J. M., Parida, B. P., & Moalafhi, D. B. (2008). Trend analysis of rainfall in the headstreams of the Zambezi River Basin in Zambia. Physics and Chemistry of the Earth, Parts A/B/C, 33(8), 621-625

Kang, I. S., Jin, K., Wang, B., Lau, K. M., Shukla, J., Krishnamurthy, V., Schubert, S., Wailser, D., Stern, W., Kitoh, A., Meehl, G., Kanamitsu, M., Galin, V., Satyan, V., Park, C. K., and Liu, Y. (2002). "Intercomparison of the climatological variations of Asian summer monsoon precipitation simulated by 10 GCMs." Climate Dynamics, 19(5-6), 383-395.

Kawasaki, A., Yamamoto, A., Koudelova, P., Acierto, R., Nemoto, T., Kitsuregawa, M., & Koike, T. (2017). Data Integration and Analysis System (DIAS) Contributing to Climate Change Analysis and Disaster Risk Reduction. Data Science Journal, 16.

Kay, A. L., Davies, H. N., Bell, V. A., & Jones, R. G. (2009). Comparison of uncertainty sources for climate change impacts: flood frequency in England. Climatic Change, 92(1-2), 41-63.

Kenabatho, P. K., Parida, B. P., & Moalafhi, D. B. (2012). The value of large-scale climate variables in climate change assessment: The case of Botswana's rainfall. Physics and Chemistry of the Earth, Parts A/B/C, 50, 64-71.

Keylock, C. J. (2007). "The visualization of turbulence data using a wavelet-based method." Earth Surface Processes and Landforms, 32(4), 637-647.

Khare D., Garg, P.K., Jat M.K and Dhore K. A, 'Selection of Optimum CanalAlignment Using GIS: River Interlinking Perspective", Indian Journal of Power and River Valley Development, Vol. 56 Nos.5 &6, March-April 2007, pp 112-121.

Khare, D., Patra, D., Mondal, A., and Kundu, S. (2015). "Impact of landuse/land cover change on run-off in a catchment of Narmada river in India." Applied Geomatics, 1(7), 23-35.

Khare, D., Patra, D., Mondal, A., and Kundu, S. (2017). "Impact of landuse/land cover change on run-off in the catchment of a hydro power project." Applied Water Science, 7(2), 787-800.

Kisi, O., and Cimen, M. (2012). "Precipitation forecasting by using wavelet-support vector machine conjunction model." Engineering Applications of Artificial Intelligence, 25(4), 783-792.

Knisel, W. G. (1980). "CREAMS: a field scale model for Chemicals, Runoff, and Erosion from Agricultural Management Systems [USA]." United States. Dept. of Agriculture. Conservation research report (USA).

Kokkonen, T. (2003). Rainfall-runoff modelling: comparison of modelling strategies with a focus on ungauged predictions and model integration, Helsinki University of Technology.

Kondratyev, K. Y., & Cracknell, A. P. (1998). Observing global climate change. CRC Press.

Konstantinos, A., & Pijanowski, B. C. (2009). Assessing multiagent parcelization performance in the MABEL simulation model using Monte Carlo replication experiments. Environment and Planning B: Planning and Design, 34(2), 223-244.

Koomen, E., Kuhlman, T., Groen, J., and Bouwman, A. (2005). "Simulating the future of agricultural land use in the Netherlands." Tijdschrift voor economische en sociale geografie, 96(2), 218-224.

Kothawale, D., Munot, A., and Kumar, K. K. (2010). "Surface air temperature variability over India during 1901-2007, and its association with ENSO." Climate Research, 42(2), 89-104.

Kothyari, U., Singh, V., and Aravamuthan, V. (1997). "An investigation of changes in rainfall and temperature regimes of the Ganga Basin in India." Water resources management, 11(1), 17-34.

Kouwen, N., and Mousavi, S. (2002). "WATFLOOD/SPL9 hydrological model and flood forecasting system." Mathematical models of large watershed hydrology, 649-685.

Kralisch, S., Krause, P., and David, O. (2005). "Using the object modeling system for hydrological model development and application." Advances in Geosciences, 4, 75-81.

KS, R., and D, N. K. (2014). "Ranking of global climate models for India using multicriterion analysis." Climate Research, 60(2), 103-117.

Kucukmehmetoglu, M., and Geymen, A. (2006). "The spatial impacts of rapid urbanization on the limited surface water resources in Istanbul."

Kuczera, G., and Parent, E. (1998). "Monte Carlo assessment of parameter uncertainty in conceptual catchment models: the Metropolis algorithm." Journal of Hydrology, 211(1), 69-85.

Kulkarni, A. T., Bodke, S. S., Rao, E. P., & Eldho, T. I. (2014). Hydrologic impact on change in land use/land cover in an urbanizing catchment of Mumbai: a case study. ISH Journal of Hydraulic Engineering, 20(3), 314-323.

Kumar, R., Jat, M. K., & Shankar, V. (2012). Methods to estimate irrigated reference crop evapotranspiration–a review. Water Science and Technology, 66(3), 525-535.

Kundzewicz, Z. W., Mata, L. J., Arnell, N. W., DÖLl, P., Jimenez, B., Miller, K., Oki, T., En, Z., and Shiklomanov, I. (2008). "The implications of projected climate change for freshwater resources and their management." Hydrological Sciences Journal, 53(1), 3-10.

Kunkel, K. E., Andsager, K., and Easterling, D. R. (1999). "Long-term trends in extreme precipitation events over the conterminous United States and Canada." Journal of climate, 12(8), 2515-2527.

Labat, D. (2005). "Recent advances in wavelet analyses: Part 1. A review of concepts." Journal of Hydrology, 314(1-4), 275-288.

Labat, D., Ronchail, J., and Guyot, J. L. (2005). "Recent advances in wavelet analyses: Part 2-Amazon, Parana, Orinoco and Congo discharges time scale variability." Journal of Hydrology, 314(1-4), 289-311.

Lafon, T., Dadson, S., Buys, G., and Prudhomme, C. (2013). "Bias correction of daily precipitation simulated by a regional climate model: a comparison of methods." International Journal of Climatology, 33(6), 1367-1381.

Lal, M., Singh, K., Srinivasan, G., Rathore, L., Naidu, D., and Tripathi, C. (1999). "Growth and yield responses of soybean in Madhya Pradesh, India to climate variability and change." Agricultural and Forest Meteorology, 93(1), 53-70.

Lambin, E. F., Geist, H. J., and Lepers, E. (2003). "Dynamics of land-use and land-cover change in tropical regions." Annual review of environment and resources, 28(1), 205-241.

Lambin, E. F., Turner, B. L., Geist, H. J., Agbola, S. B., Angelsen, A., Bruce, J. W., Coomes, O. T., Dirzo, R., Fischer, G., Folke, C., George, P. S., Homewood, K., Imbernon, J., Leemans, R., Li, X., Moran, E. F., Mortimore, M., Ramakrishnan, P. S., Richards, J. F., Skånes, H., Steffen, W., Stone, G. D., Svedin, U., Veldkamp, T. A., Vogel, C., and Xu, J. (2001). "The causes of land-use and land-cover change: moving beyond the myths." Global Environmental Change, 11(4), 261-269.

Laroche, A.-M., Gallichand, J., Lagacé, R., and Pesant, A. (1996). "Simulating atrazine transport with HSPF in an agricultural watershed." Journal of Environmental Engineering, 122(7), 622-630.

Lee, Y., and Singh, V. (1999). "Tank model using Kalman filter." Journal of hydrologic engineering, 4(4), 344-349.

Lee, Y., and Singh, V. (2005). "Tank model for sediment yield." Water Resources Management, 19(4), 349-362.

Lehner, B., Döll, P., Alcamo, J., Henrichs, T., & Kaspar, F. (2006). Estimating the impact of global change on flood and drought risks in Europe: a continental, integrated analysis. Climatic Change, 75(3), 273-299.

Li, L., Xu, C. Y., Zhang, Z., & Jain, S. K. (2014). Validation of a new meteorological forcing data in analysis of spatial and temporal variability of precipitation in India. Stochastic environmental research and risk assessment, 28(2), 239-252.

Li, W., Zhang, C., Willig, M. R., Dey, D. K., Wang, G., and You, L. (2015). "Bayesian Markov chain random field cosimulation for improving land cover classification accuracy." Mathematical Geosciences, 47(2), 123-148.

Li, X., and Yeh, A. G.-O. (2004). "Analyzing spatial restructuring of land use patterns in a fast growing region using remote sensing and GIS." Landscape and Urban planning, 69(4), 335-354.

Li, Z., Deng, X., Wu, F., and Hasan, S. S. (2015). "Scenario analysis for water resources in response to land use change in the middle and upper reaches of the Heihe River Basin." Sustainability, 7(3), 3086-3108.

Lindström, G., Johansson, B., Persson, M., Gardelin, M., and Bergström, S. (1997). "Development and test of the distributed HBV-96 hydrological model." Journal of hydrology, 201(1-4), 272-288.

Liu, G. H., Luan, Z. Q., Yan, B. X., Guo, Y. D., and Wang, Z. X. (2015). "Response of hydrological processes to land use change and climate variability in the upper Naoli River watershed, northeast China." Water Resour, 42(4), 438-447.

Liu, L., Liu, Z., Ren, X., Fischer, T., and Xu, Y. (2011). "Hydrological impacts of climate change in the Yellow River Basin for the 21st century using hydrological model and statistical downscaling model." Quaternary International, 244(2), 211-220.

Liu, M., and Lu, J. (2015). "Predicting the impact of management practices on river water quality using SWAT in an agricultural watershed." Desalination and Water Treatment, 54(9), 2396-2409.

Loaiciga, H. A., Valdes, J. B., Vogel, R., Garvey, J., & Schwarz, H. (1996). Global warming and the hydrologic cycle. Journal of Hydrology, 174(1-2), 83-127.

López, E., Bocco, G., Mendoza, M., and Duhau, E. (2001). "Predicting land-cover and land-use change in the urban fringe: A case in Morelia city, Mexico." Landscape and Urban Planning, 55(4), 271-285.

Loukas, A., & Quick, M. C. (1996). Spatial and temporal distribution of storm precipitation in southwestern British Columbia. Journal of hydrology, 174(1-2), 37-56.

Lu, M., Renschler, C., & Nearing, M. (2014, May). Climate change and its impact on precipitation, runoff, and erosion in a small semi-arid watershed of the American Southwest. In EGU General Assembly Conference Abstracts (Vol. 16).

Maheswaran, R., and Khosa, R. (2012). "Wavelet-Volterra coupled model for monthly stream flow forecasting." Journal of Hydrology, 450-451, 320-335.

Mala, S., Jat, M. K., & Pradhan, P. (2014). An Approach to analyse Drought occurrences using Geospatial Techniques.

Mall, R. K., Singh, R., Gupta, A., Srinivasan, G., and Rathore, L. S. (2006). "Impact of Climate Change on Indian Agriculture: A Review." Climatic Change, 78(2-4), 445-478.

Mall, R., Gupta, A., Singh, R., Singh, R., and Rathore, L. (2006). "Water resources and climate change: an Indian perspective." Current science, 1610-1626.

Marhaento, H., Booij, M. J., Rientjes, T. H. M., and Hoekstra, A. Y. (2017). "Attribution of changes in the water balance of a tropical catchment to land use change using the SWAT model." Hydrological Processes, 31(11), 2029-2040.

Marshall, E., and Randhir, T. O. (2008). "Spatial modeling of land cover change and watershed response using Markovian cellular automata and simulation." Water Resources Research, 44(4).

Matondo, J. I., & Msibi, K. M. (2001). Estimation of the impact of climate change on hydrology and water resources in Swaziland. Water International, 26(3), 425-434.

Matondo, J. I., Peter, G., and Msibi, K. M. (2004). "Evaluation of the impact of climate change on hydrology and water resources in Swaziland: Part II." Physics and Chemistry of the Earth, Parts A/B/C, 29(15-18), 1193-1202.

Matouq, M. (2008). "Predicting the impact of global warming on the Middle East region: Case Study on Hashemite Kingdom of Jordan using the application of geographical information system." Journal of Applied Sciences, 8(3), 462-470.

McAlpine, C. A., Syktus, J., Deo, R. C., Lawrence, P. J., McGowan, H. A., Watterson, I. G., & Phinn, S. R. (2007). Modeling the impact of historical land cover change on Australia's regional climate. Geophysical Research Letters, 34(22).

McMahon, T. A., Peel, M. C., and Karoly, D. J. (2015). "Assessment of precipitation and temperature data from CMIP3 global climate models for hydrologic simulation." Hydrol. Earth Syst. Sci., 19(1), 361-377.

Meehl, G. A., Stocker, T. F., Collins, W. D., Friedlingstein, P., Gaye, A. T., Gregory, J. M., Kitoh, A., Knutti, R., Murphy, J. M., and Noda, A. (2007). "Global climate projections." Climate change, 283.

Mehrotra, R., Sharma, A., Nagesh Kumar, D., and Reshmidevi, T. V. (2013). "Assessing future rainfall projections using multiple GCMs and a multi-site stochastic downscaling model." Journal of Hydrology, 488, 84-100.

Mendis, W., and Wadigamangawa, A. (1996). "Integration of Remote Sensing and GIS for Land Use/Land Cover Mapping in Nil Wala Basin. GIS Development."

Mersha, A. N., de Fraiture, C., Mehari, A., Masih, I., & Alamirew, T. (2016). Integrated Water Resources Management: contrasting principles, policy, and practice, Awash River Basin, Ethiopia. Water Policy, 18(2), 335-354.

Mersha, A. N., Masih, I., de Fraiture, C., & Alamirew, T. (2017). Evaluating the Impact of Future Scenarios on Water Availability and Demand Based on Stakeholders Prioritized Water Management Options in the Upper Awash Basin, Ethiopia. World Academy of Science, Engineering and Technology, International Journal of Environmental and Ecological Engineering, 4(4).

Meshesha, T. W., Tripathi, S. K., and Khare, D. (2016). "Analyses of land use and land cover change dynamics using GIS and remote sensing during 1984 and 2015 in the Beressa Watershed Northern Central Highland of Ethiopia." Model. Earth Syst. Environ., 2(4), 168.

Meyer, W. B., and BL Turner, I. (1994). Changes in land use and land cover: a global perspective, Cambridge University Press.

Mialhe, F., Gunnell, Y., Ignacio, J. A. F., Delbart, N., Ogania, J. L., and Henry, S. (2015). "Monitoring land-use change by combining participatory land-use maps with standard remote sensing techniques: Showcase from a remote forest catchment on Mindanao, Philippines." International Journal of Applied Earth Observation and Geoinformation, 36, 69-82.

Miao, C., Duan, Q., Sun, Q., Huang, Y., Kong, D., Yang, T., Ye, A., Di, Z., and Gong, W. (2014). "Assessment of CMIP5 climate models and projected temperature changes over Northern Eurasia." Environmental Research Letters, 9(5), 055007.

Michael P. Clementsa, P. H. F., Norman R. Swansonc (2004). "Forecasting economic and financial time-series with non-linear models." International Journal of Forecasting, 20, 169-183.

Mirza, M., Warrick, R., Ericksen, N., and Kenny, G. (1998). "Trends and persistence in precipitation in the Ganges, Brahmaputra and Meghna river basins." Hydrological Sciences Journal, 43(6), 845-858.

Mishra, A. K., Özger, M., and Singh, V. P. (2009). "Trend and persistence of precipitation under climate change scenarios for Kansabati basin, India." Hydrological processes, 23(16), 2345-2357.

Mitsova, D., Shuster, W., and Wang, X. (2011). "A cellular automata model of land cover change to integrate urban growth with open space conservation." Landscape and Urban Planning, 99(2), 141-153.

Mohanty, P. K., Barik, S. K., Kar, P. K., Behera, B., and Mishra, P. (2015). "Impacts of ports on shoreline change along Odisha coast." Procedia Engineering, 116, 647-654.

Mondal, A., and Mujumdar, P. P. (2012). "On the basin-scale detection and attribution of human-induced climate change in monsoon precipitation and streamflow." Water Resources Research, 48(10).

Mondal, A., Khare, D., Kundu, S., Meena, P. K., Mishra, P., and Shukla, R. (2014). "Impact of climate change on future soil erosion in different slope, land use, and soil-type conditions in a part of the Narmada River Basin, India." Journal of Hydrologic Engineering.

Mondal, A., Khare, D., Kundu, S., Mishra, P. K., & Meena, P. K. (2014). Landuse change prediction and its impact on surface run-off using fuzzy c-mean, Markov chain and curve number methods. In Proceedings of the Third International Conference on Soft Computing for Problem Solving (pp. 365-376). Springer, New Delhi.

Moriasi, D. N., Arnold, J. G., Van Liew, M. W., Bingner, R. L., Harmel, R. D., and Veith, T. L. (2007). "Model evaluation guidelines for systematic quantification of accuracy in watershed simulations." Trans. Asabe, 50(3), 885-900.

Moss, R. H., Edmonds, J. A., Hibbard, K. A., Manning, M. R., Rose, S. K., Van Vuuren, D. P., Carter, T. R., Emori, S., Kainuma, M., and Kram, T. (2010). "The next generation of scenarios for climate change research and assessment." Nature, 463(7282), 747-756.

Mubea, K. W., Mundia, C. N., & Kuria, D. N. (2010). The Use of Markov Chain Analysis in Predicting Land Use/Cover Change in Nyeri. Journal of agricultural, science and technology, 12(2), 123-129.

Mukhopadhyay, A., Mondal, A., Mukherjee, S., Khatua, D., Ghosh, S., Mitra, D., and Ghosh, T. (2014). "Forest cover change prediction using hybrid methodology of geoinformatics and Markov chain model: A case study on sub-Himalayan town Gangtok, India." Journal of Earth System Science, 123(6), 1349-1360.

Mundia, C. N., and Aniya, M. (2005). "Analysis of land use/cover changes and urban expansion of Nairobi city using remote sensing and GIS." International Journal of Remote Sensing, 26(13), 2831-2849.

Murphy, A. H. (1988). "Skill Scores Based on the Mean Square Error and Their Relationships to the Correlation Coefficient." Monthly Weather Review, 116(12), 2417-2424.

Murphy, A. H. (1993). "What Is a Good Forecast? An Essay on the Nature of Goodness in Weather Forecasting." Weather and Forecasting, 8(2), 281-293.

Murty, P. S., Pandey, A., and Suryavanshi, S. (2014). "Application of semi-distributed hydrological model for basin level water balance of the Ken basin of Central India." Hydrological Processes, 28(13), 4119-4129.

Muttitanon, W., and Tripathi, N. (2005). "Land use/land cover changes in the coastal zone of Ban Don Bay, Thailand using Landsat 5 TM data." International Journal of Remote Sensing, 26(11), 2311-2323.

Myint, S. W., Gober, P., Brazel, A., Grossman-Clarke, S., and Weng, Q. (2011). "Per-pixel vs. object-based classification of urban land cover extraction using high spatial resolution imagery." Remote sensing of environment, 115(5), 1145-1161.

Nagendra, H., Munroe, D. K., and Southworth, J. (2004). "From pattern to process: landscape fragmentation and the analysis of land use/land cover change." Agriculture, Ecosystems & Environment, 101(2), 111-115.

Nalley, D., Adamowski, J., and Khalil, B. (2012). "Using discrete wavelet transforms to analyze trends in streamflow and precipitation in Quebec and Ontario (1954-2008)." Journal of Hydrology, 475, 204-228.

Nalley, D., Adamowski, J., Khalil, B., and Ozga-Zielinski, B. (2013). "Trend detection in surface air temperature in Ontario and Quebec, Canada during 1967-2006 using the discrete wavelet transform." Atmospheric Research, 132, 375-398.

Nam, W.-H., Hong, E.-M., and Choi, J.-Y. (2015). "Has climate change already affected the spatial distribution and temporal trends of reference evapotranspiration in South Korea?" Agricultural Water Management, 150, 129-138.

Narsimlu, B., Gosain, A. K., & Chahar, B. R. (2013). Assessment of future climate change impacts on water resources of upper sind river basin, India using SWAT model. Water resources management, 27(10), 3647-3662.

Narsimlu, B., Gosain, A. K., and Chahar, B. R. (2013). "Assessment of future climate change impacts on water resources of upper sind river basin, India using SWAT model." Water resources management, 27(10), 3647-3662.

Narsimlu, B., Gosain, A. K., Chahar, B. R., Singh, S. K., & Srivastava, P. K. (2015). SWAT model calibration and uncertainty analysis for streamflow prediction in the Kunwari River Basin, India, using sequential uncertainty fitting. Environmental Processes, 2(1), 79-95.

Neitsch, S. L., Arnold, J. G., Kiniry, J. R., and Williams, J. R. (2011). "Soil and water assessment tool theoretical documentation version 2009." Texas Water Resources Institute.

Neupane, R. P., and Kumar, S. (2015). "Estimating the effects of potential climate and land use changes on hydrologic processes of a large agriculture dominated watershed." Journal of Hydrology, 529, Part 1, 418-429.

Niraula, R., Meixner, T., and Norman, L. M. (2015). "Determining the importance of model calibration for forecasting absolute/relative changes in streamflow from LULC and climate changes." Journal of Hydrology, 522, 439-451.

Nourani, V., Komasi, M., and Mano, A. (2009). "A multivariate ANN-wavelet approach for rainfall-runoff modeling." Water resources management, 23(14), 2877-2894.

Nouri, J., Gharagozlou, A., Arjmandi, R., Faryadi, S., & Adl, M. (2014). Predicting urban land use changes using a CA–Markov model. Arabian Journal for Science and Engineering, 39(7), 5565-5573.

Nyong, A., Adesina, F., & Elasha, B. O. (2007). The value of indigenous knowledge in climate change mitigation and adaptation strategies in the African Sahel. Mitigation and Adaptation strategies for global Change, 12(5), 787-797.

O'Brien, K., Leichenko, R., Kelkar, U., Venema, H., Aandahl, G., Tompkins, H., Javed, A., Bhadwal, S., Barg, S., Nygaard, L., and West, J. (2004). "Mapping vulnerability to multiple stressors: climate change and globalization in India." Global Environmental Change, 14(4), 303-313.

Oetter, D. R., Cohen, W. B., Berterretche, M., Maiersperger, T. K., and Kennedy, R. E. (2001). "Land cover mapping in an agricultural setting using multiseasonal Thematic Mapper data." Remote Sensing of Environment, 76(2), 139-155.

Ojha, C. S. P., Goyal, M. K., & Adeloye, A. J. (2010). Downscaling of precipitation for lake catchment in arid region in India using linear multiple regression and neural networks. Open Hydrology Journal, 4(1), 122-136.

Ojha, R., Kumar, D., Sharma, A., and Mehrotra, R. (2013). "Assessing GCM Convergence for India Using the Variable Convergence Score." Journal of Hydrologic Engineering, 19(6), 1237-1246.

Ojha, R., Nagesh Kumar, D., Sharma, A., and Mehrotra, R. (2012). "Assessing Severe Drought and Wet Events over India in a Future Climate Using a Nested Bias-Correction Approach." Journal of Hydrologic Engineering, 18(7), 760-772.

Oki, T., & Kanae, S. (2006). Global hydrological cycles and world water resources. science, 313(5790), 1068-1072.

Olofsson, P., Foody, G. M., Stehman, S. V., and Woodcock, C. E. (2013). "Making better use of accuracy data in land change studies: Estimating accuracy and area and quantifying uncertainty using stratified estimation." Remote Sensing of Environment, 129, 122-131.

Omer, A., Wang, W., Basheer, A. K., and Yong, B. (2017). "Integrated assessment of the impacts of climate variability and anthropogenic activities on river runoff: a case study in the Hutuo River Basin, China." Hydrology Research, 48(2), 416-430.

Pachauri, R. K., Allen, M. R., Barros, V. R., Broome, J., Cramer, W., Christ, R., Church, J. A., Clarke, L., Dahe, Q., and Dasgupta, P. (2014). Climate change 2014: synthesis report. Contribution of Working Groups I, II and III to the fifth assessment report of the Intergovernmental Panel on Climate Change, IPCC.

Pandey, B. K., Gosain, A., Paul, G., and Khare, D. (2016). "Climate change impact assessment on hydrology of a small watershed using semi-distributed model." Applied Water Science, 1-13.

Parida, B. P., Kgaodi, D., Moalafhi, D. B., & Dube, O. P. (2006). The Effect of Climate Variability and Land Use/Land Cover on the Runoff Characteristic of Limpopo Basin, Botswana. In Proceedings of the IASTED International Conference on Environmentally Sound Technology in Water Resources Management, September (pp. 11-13).

Parida, B.P., (1999). Modelling of Indian Summer Monsoon Rainfall Using a Four-Parameter Kappa Distribution, Intl. Jr. of Climatology, UK , 19, p.1389-1398

Parida, B.P., and Moalafhi, D.B. (2008). Study on the Impact of Climate Variability through a Regional rainfall Frequency Analysis for Botswana using the Radial basis function network and L-moments. Journal of Physics and Chemistry of the Earth. ,Elsevier Pub., 33 (8-13), p.614 - 620

Partal, T., and Kahya, E. (2006). "Trend analysis in Turkish precipitation data." Hydrological processes, 20(9), 2011-2026.

Parth Sarthi, P., Ghosh, S., and Kumar, P. (2015). "Possible future projection of Indian Summer Monsoon Rainfall (ISMR) with the evaluation of model performance in Coupled Model Inter-comparison Project Phase 5 (CMIP5)." Global and Planetary Change, 129(0), 92-106.

Patra, J. P., Mishra, A., Singh, R., and Raghuwanshi, N. (2012). "Detecting rainfall trends in twentieth century (1871-2006) over Orissa State, India." Climatic Change, 111(3-4), 801-817.

Patricola, C. M., & Cook, K. H. (2010). Northern African climate at the end of the twenty-first century: an integrated application of regional and global climate models. Climate Dynamics, 35(1), 193-212.

Perkins, S. E., Pitman, A. J., Holbrook, N. J., and McAneney, J. (2007). "Evaluation of the AR4 Climate Models' Simulated Daily Maximum Temperature, Minimum Temperature, and Precipitation over Australia Using Probability Density Functions." Journal of Climate, 20(17), 4356-4376.

Pervez, M. S., and Henebry, G. M. (2014). "Assessing the impacts of climate and land use and land cover change on the freshwater availability in the Brahmaputra River basin." Journal of Hydrology: Regional Studies.

Petit, C., Scudder, T., and Lambin, E. (2001). "Quantifying processes of land-cover change by remote sensing: Resettlement and rapid land-cover changes in south-eastern Zambia." International Journal of Remote Sensing, 22(17), 3435-3456.

Petit, C., Scudder, T., and Lambin, E. (2001). "Quantifying processes of land-cover change by remote sensing: Resettlement and rapid land-cover changes in south-eastern Zambia." International Journal of Remote Sensing, 22(17), 3435-3456.

Pijanowski, B. C., Brown, D. G., Shellito, B. A., and Manik, G. A. (2002). "Using neural networks and GIS to forecast land use changes: a land transformation model." Computers, environment and urban systems, 26(6), 553-575.

Pingale, S. M., Khare, D., Jat, M. K., and Adamowski, J. (2014). "Spatial and temporal trends of mean and extreme rainfall and temperature for the 33 urban centers of the arid and semi-arid state of Rajasthan, India." Atmospheric Research, 138, 73-90.

Pontius, R. G., Cornell, J. D., and Hall, C. A. (2001). "Modeling the spatial pattern of land-use change with GEOMOD2: application and validation for Costa Rica." Agriculture, Ecosystems & Environment, 85(1), 191-203.

Poulin, A., Brissette, F., Leconte, R., Arsenault, R., & Malo, J. S. (2011). Uncertainty of hydrological modelling in climate change impact studies in a Canadian, snow-dominated river basin. Journal of Hydrology, 409(3-4), 626-636.

Prabhakar, A., and Tiwari, H. (2015). "Land use and land cover effect on groundwater storage." Model. Earth Syst. Environ., 1(4), 1-10.

Prakasam, C. (2010). "Land use and land cover change detection through remote sensing approach: A case study of Kodaikanal taluk, Tamil nadu." International journal of Geomatics and Geosciences, 1(2), 150.

Prudhomme, C., Reynard, N., and Crooks, S. (2002). "Downscaling of global climate models for flood frequency analysis: where are we now?" Hydrological Processes, 16(6), 1137-1150.

Quinn, P., Beven, K., and Lamb, R. (1995). " How to calculate it and how to use it within the topmodel framework." Hydrological processes, 9(2), 161-182.

Radi, V., and Clarke, G. K. C. (2011). "Evaluation of IPCC Models' Performance in Simulating Late-Twentieth-Century Climatologies and Weather Patterns over North America." Journal of Climate, 24(20), 5257-5274.

Ragab, R., and Prudhomme, C. (2002). "Sw-soil and Water: climate change and water resources management in arid and semi-arid regions: prospective and challenges for the 21st century." Biosystems engineering, 81(1), 3-34.

Rahmani, V., Hutchinson, S. L., Harrington Jr, J. A., Hutchinson, J., and Anandhi, A. (2015). "Analysis of temporal and spatial distribution and change?points for annual precipitation in Kansas, USA." International Journal of Climatology, 35(13), 3879-3887.

Rai, P. K., Chahar, B. R., & Dhanya, C. T. (2017). GIS-based SWMM model for simulating the catchment response to flood events. Hydrology Research, 48(2), 384-394.

Raj, K. B. G., and Fleming, K. (2008). "Surface temperature estimation from Landsat ETM data for a part of the Baspa Basin, NW Himalaya, India." Bulletin of Glaciological Research, 25, 19-26.

Raju, K. S., and Kumar, D. N. (2014). "Ranking of global climate models for India using multicriterion analysis." Climate Research, 60(2), 103-117.

Ramankutty, N., and Foley, J. A. (1999). "Estimating historical changes in global land cover: Croplands from 1700 to 1992." Global Biogeochemical Cycles, 13(4), 997-1027.

Randall, D. A., Wood, R. A., Bony, S., Colman, R., Fichefet, T., Fyfe, J., Kattsov, V., Pitman, A., Shukla, J., and Srinivasan, J. (2007). "Climate models and their evaluation." Climate Change 2007: The physical science basis. Contribution of Working Group I to the Fourth Assessment Report of the IPCC (FAR), Cambridge University Press, 589-662.

Ranger, N., Hallegatte, S, Bhattacharya, S., Bachu, M., Priya, S.; Dhore, K., Rafique, F.,Mathur, P, Naville, N., Henriet, F., Herweijer, C., Pohit, S., Corfee-Morlot, J. (2011) "A Preliminary Assessment of the Potential Impact of Climate Change on Flood Risk in Mumbai" Climatic Change, 104, pg. 139-167, DOI 10.1007/s10584-010-9979-2.

Rao, K. S., and Pant, R. (2001). "Land use dynamics and landscape change pattern in a typical micro watershed in the mid elevation zone of central Himalaya, India." Agriculture, Ecosystems & Environment, 86(2), 113-124.

Revadekar, J., Patwardhan, S., and Rupa Kumar, K. (2011). "Characteristic features of precipitation extremes over India in the warming scenarios." Advances in Meteorology, 2011.

Revi, A. (2008). "Climate change risk: an adaptation and mitigation agenda for Indian cities." Environment and Urbanization, 20(1), 207-229.

Ridd, M. K., and Liu, J. (1998). "A comparison of four algorithms for change detection in an urban environment." Remote sensing of environment, 63(2), 95-100.

Rodriguez-Galiano, V. F., Ghimire, B., Rogan, J., Chica-Olmo, M., and Rigol-Sanchez, J. P. (2012). "An assessment of the effectiveness of a random forest classifier for land-cover classification." ISPRS Journal of Photogrammetry and Remote Sensing, 67, 93-104.

Rossman, L. A. (2010). Storm water management model user's manual, version 5.0, National Risk Management Research Laboratory, Office of Research and Development, US Environmental Protection Agency Cincinnati.

Rozenstein, O., and Karnieli, A. (2011). "Comparison of methods for land-use classification incorporating remote sensing and GIS inputs." Applied Geography, 31(2), 533-544.

Saadat, H., Adamowski, J., Bonnell, R., Sharifi, F., Namdar, M., and Ale-Ebrahim, S. (2011). "Land use and land cover classification over a large area in Iran based on single date analysis of satellite imagery." ISPRS Journal of Photogrammetry and Remote Sensing, 66(5), 608-619.

Sahoo, D., and Smith, P. (2009). "Hydroclimatic trend detection in a rapidly urbanizing semi-arid and coastal river basin." Journal of Hydrology, 367(3), 217-227.

Sahoo, G., Ray, C., and De Carlo, E. (2006). "Calibration and validation of a physically distributed hydrological model, MIKE SHE, to predict streamflow at high frequency in a flashy mountainous Hawaii stream." Journal of Hydrology, 327(1), 94-109.

Saleh, A., and Du, B. (2004). "Evaluation of SWAT and HSPF within BASINS program for the upper North Bosque River watershed in central Texas." Transactions of the ASAE, 47(4), 1039.

Salzmann, N., Frei, C., Vidale, P. L., & Hoelzle, M. (2007). The application of Regional Climate Model output for the simulation of high-mountain permafrost scenarios. Global and Planetary Change, 56(1-2), 188-202.

Sang, Y.-F. (2013). "A review on the applications of wavelet transform in hydrology time series analysis." Atmospheric Research, 122, 8-15.

Sang, Y.-F., Singh, V. P., Sun, F., Chen, Y., Liu, Y., and Yang, M. (2016). "Wavelet-based hydrological time series forecasting." Journal of Hydrologic Engineering, 21(5), 06016001.

Saulnier, G.-M., Beven, K., and Obled, C. (1997). "Including spatially variable effective soil depths in TOPMODEL." Journal of hydrology, 202(1), 158-172.

Sayasane, R., Kawasaki, A., Shrestha, S., and Takamatsu, M. (2016). "Assessment of potential impacts of climate and land use changes on stream flow: A case study of the Nam Xong Watershed in Lao PDR." Journal of Water and Climate Change, 7(1), 184-197.

Scharffenberg, W., Fleming, M., and Feldman, A. "The Hydrologic Modeling System (HEC-HMS): Toward a Complete Framework for Hydrologic Engineering." Proc., World Water & Environmental Resources Congress 2003, 1-8.

Schilling, K. E., Jha, M. K., Zhang, Y. K., Gassman, P. W., and Wolter, C. F. (2008). "Impact of land use and land cover change on the water balance of a large agricultural watershed: Historical effects and future directions." Water Resources Research, 44(7).

Seibert, J. (1997). "Estimation of parameter uncertainty in the HBV model." Hydrology Research, 28(4-5), 247-262.

Sen, Z. (2011). "Innovative trend analysis methodology." Journal of Hydrologic Engineering, 17(9), 1042-1046.

Seneviratne, S. I., Nicholls, N., Easterling, D., Goodess, C. M., Kanae, S., Kossin, J., ... & Reichstein, M. (2012). Changes in climate extremes and their impacts on the natural physical environment.

Setegn, S. G., Srinivasan, R., Dargahi, B., and Melesse, A. M. (2009). "Spatial delineation of soil erosion vulnerability in the Lake Tana Basin, Ethiopia." Hydrological Processes, 23(26), 3738-3750.

Sethi, R., Pandey, B. K., Krishan, R., Khare, D., and Nayak, P. C. (2015). "Performance evaluation and hydrological trend detection of a reservoir under climate change condition." Model. Earth Syst. Environ., 1(4), 1-10.

Setiawan, Y., and Yoshino, K. (2012). "Change detection inland-use and land-cover dynamics at a regional scale from modis time-series imagery." ISPRS Annals of the Photogrammetry, Remote Sensing and Spatial Information Sciences, 7.

Shadmani, M., Marofi, S., and Roknian, M. (2012). "Trend analysis in reference evapotranspiration using Mann-Kendall and Spearman's Rho tests in arid regions of Iran." Water resources management, 26(1), 211-224.

Shalaby, A., and Tateishi, R. (2007). "Remote sensing and GIS for mapping and monitoring land cover and land-use changes in the Northwestern coastal zone of Egypt." Applied Geography, 27(1), 28-41.

Shi, P., Qiao, X., Chen, X., Zhou, M., Qu, S., Ma, X., and Zhang, Z. (2014). "Spatial distribution and temporal trends in daily and monthly precipitation concentration indices in the upper reaches of the Huai River, China." Stochastic environmental research and risk assessment, 28(2), 201.

Shifteh Some'e, B., Ezani, A., and Tabari, H. (2012). "Spatiotemporal trends and change point of precipitation in Iran." Atmospheric Research, 113, 1-12.

Singh, P., and Kumar, N. (1997). "Impact assessment of climate change on the hydrological response of a snow and glacier melt runoff dominated Himalayan river." Journal of Hydrology, 193(1), 316-350.

Singh, R., Subramanian, K., and Refsgaard, J. (1999). "Hydrological modelling of a small watershed using MIKE SHE for irrigation planning." Agricultural Water Management, 41(3), 149-166.

Singh, S. K., Mustak, S., Srivastava, P. K., Szabó, S., and Islam, T. (2015). "Predicting spatial and decadal LULC changes through cellular automata Markov chain models using Earth observation datasets and geo-information." Environmental Processes, 2(1), 61-78.

Singh, V., & Bhallamudi, S. M. (1997). Hydrodynamic modeling of basin irrigation. Journal of irrigation and Drainage Engineering, 123(6), 407-414.

Singh, V., Goyal, M. K., and Chu, X. (2015). "Multicriteria evaluation approach for assessing parametric uncertainty during extreme peak and low flow conditions over snow glaciated and inland catchments." Journal of Hydrologic Engineering, 21(1), 04015044.

Sinha, S., Routh, P. S., Anno, P. D., and Castagna, J. P. (2005). "Spectral decomposition of seismic data with continuous-wavelet transform." Geophysics, 70(6), P19-P25.

Sittner, W. T., Schauss, C. E., and Monro, J. C. (1969). "Continuous hydrograph synthesis with an API type hydrologic model." Water Resources Research, 5(5), 1007-1022.

Smith, L. C., Turcotte, D. L., and Isacks, B. L. (1998). "Stream flow characterization and feature detection using a discrete wavelet transform." Hydrological processes, 12(2), 233-249.

Sneyers, R. (1997). "Climate chaotic instability: statistical determination and theoretical background." Environmetrics, 8(5), 517-532.

Solomon, S. (2007). Climate change 2007-the physical science basis: Working group I contribution to the fourth assessment report of the IPCC, Cambridge University Press.

Some'e, B. S., Ezani, A., and Tabari, H. (2012). "Spatiotemporal trends and change point of precipitation in Iran." Atmospheric research, 113, 1-12.

Sonali, P., and Kumar, D. N. (2013). "Review of trend detection methods and their application to detect temperature changes in India." Journal of Hydrology, 476, 212-227.

Sorooshian, S., and Gupta, V. K. (1983). "Automatic calibration of conceptual rainfall?runoff models: The question of parameter observability and uniqueness." Water Resources Research, 19(1), 260-268.

Soulis, E., Snelgrove, K., Kouwen, N., Seglenieks, F., and Verseghy, D. (2000). "Towards closing the vertical water balance in Canadian atmospheric models: coupling of the land surface scheme CLASS with the distributed hydrological model WATFLOOD." Atmosphere-Ocean, 38(1), 251-269.

Srinivas, C., Hariprasad, D., Bhaskar Rao, D., Anjaneyulu, Y., Baskaran, R., and Venkatraman, B. (2013). "Simulation of the Indian summer monsoon regional climate using advanced research WRF model." International Journal of Climatology, 33(5), 1195-1210.

Srivastava, P. K., Han, D., Rico-Ramirez, M. A., Bray, M., and Islam, T. (2012). "Selection of classification techniques for land use/land cover change investigation." Advances in Space Research, 50(9), 1250-1265.

Stathopoulou, M., and Cartalis, C. (2007). "Daytime urban heat islands from Landsat ETM+ and Corine land cover data: An application to major cities in Greece." Solar Energy, 81(3), 358-368.

Steele-Dunne, S., Lynch, P., McGrath, R., Semmler, T., Wang, S., Hanafin, J., & Nolan, P. (2008). The impacts of climate change on hydrology in Ireland. Journal of Hydrology, 356(1-2), 28-45.

Stefanov, W. L., Ramsey, M. S., and Christensen, P. R. (2001). "Monitoring urban land cover change: An expert system approach to land cover classification of semiarid to arid urban centers." Remote sensing of Environment, 77(2), 173-185.

Su, F., Duan, X., Chen, D., Hao, Z., and Cuo, L. (2012). "Evaluation of the Global Climate Models in the CMIP5 over the Tibetan Plateau." Journal of Climate, 26(10), 3187-3208.

Subha Sinha, V Singh and M P Jakhanwal, Rainfall Runoff Modeling Of Punpun River Basin Using ANN –A Case Study. International Journal of Research in Engineering and Social Sciences. 5(5) - 2015,32-49,

Sugawara, M. (1979). "Automatic calibration of the tank model/L'étalonnage automatique d'un modèle à cisterne." Hydrological Sciences Journal, 24(3), 375-388.

Sugawara, M. (1995). "Tank model." Computer models of watershed hydrology.

Tabari, H., and Marofi, S. (2011). "Changes of pan evaporation in the west of Iran." Water Resources Management, 25(1), 97-111.

Tabari, H., and Talaee, P. H. (2011). "Analysis of trends in temperature data in arid and semi-arid regions of Iran." Global and Planetary Change, 79(1), 1-10.

Tabari, H., Somee, B. S., and Zadeh, M. R. (2011). "Testing for long-term trends in climatic variables in Iran." Atmospheric Research, 100(1), 132-140.

Takamatsu, M., Kawasaki, A., Rogers, P. P., & Malakie, J. L. (2014). Development of a land-use forecast tool for future water resources assessment: case study for the Mekong River 3S Sub-basins. Sustainability science, 9(2), 157-172

Tebakari, T., Yoshitani, J., and Suvanpimol, C. (2005). "Time-space trend analysis in pan evaporation over Kingdom of Thailand." Journal of Hydrologic Engineering, 10(3), 205-215.

Teng, J., Chiew, F. H. S., Timbal, B., Wang, Y., Vaze, J., and Wang, B. (2012). "Assessment of an analogue downscaling method for modelling climate change impacts on runoff." Journal of Hydrology, 472-473, 111-125.

Thompson, J., Sørenson, H. R., Gavin, H., and Refsgaard, A. (2004). "Application of the coupled MIKE SHE/MIKE 11 modelling system to a lowland wet grassland in southeast England." Journal of Hydrology, 293(1), 151-179.

Ting, M., and Wang, H. (1997). "Summertime US Precipitation Variability and Its Relation toPacific Sea Surface Temperature." Journal of Climate, 10(8), 1853-1873.

Torrence, C., and Compo, G. P. (1998). "A practical guide to wavelet analysis." Bulletin of the American Meteorological society, 79(1), 61-78.

Trang, N. T. T., Shrestha, S., Shrestha, M., Datta, A., & Kawasaki, A. (2017). Evaluating the impacts of climate and land-use change on the hydrology and nutrient yield in a transboundary river basin: A case study in the 3S River Basin (Sekong, Sesan, and Srepok). Science of The Total Environment, 576, 586-598.

Tripathi, S., Singh, M., and Pandey, A. (2007). "Agroclimatic Variability Analysis of Roorkee, Uttarakhand." Journal of Indian Water Resources Society, 27, 24-30.

Tsihrintzis, V. A., and Hamid, R. (1998). "Runoff quality prediction from small urban catchments using SWMM." Hydrological Processes, 12(2), 311-329.

Uhlenbrook, S., Seibert, J., Leibundgut, C., and Rodhe, A. (1999). "Prediction uncertainty of conceptual rainfall-runoff models caused by problems in identifying model parameters and structure." Hydrological Sciences Journal, 44(5), 779-797.

Ullrich, A., and Volk, M. (2009). "Application of the Soil and Water Assessment Tool (SWAT) to predict the impact of alternative management practices on water quality and quantity." Agricultural Water Management, 96(8), 1207-1217.

Van Griensven, A., Meixner, T., Grunwald, S., Bishop, T., Diluzio, M., and Srinivasan, R. (2006). "A global sensitivity analysis tool for the parameters of multi-variable catchment models." Journal of hydrology, 324(1), 10-23.

Veettil, A. V., and Mishra, A. K. (2016). "Water security assessment using blue and green water footprint concepts." Journal of Hydrology, 542, 589-602.

Verburg, P. H. (2006). "Simulating feedbacks in land use and land cover change models." Landscape Ecology, 21(8), 1171-1183.

Verburg, P. H., de Nijs, T. C. M., Ritsema van Eck, J., Visser, H., and de Jong, K. (2004). "A method to analyse neighbourhood characteristics of land use patterns." Computers, Environment and Urban Systems, 28(6), 667-690.

Verdhen, A., Chahar, B.R., and Sharma, O.P. (2014). “Snowmelt Modelling Approaches in Watershed Models: Computation and Comparison of Efficiencies under Varying Climatic Conditions.” Water Resources Management, DOI:10.1007/s11269-014-0662-7.

Vitousek, P. M. (1994). "Beyond global warming: ecology and global change." Ecology, 75(7), 1861-1876.

Vivekanand Singh, Vijay Kumar and Avinash Agarwal, Reference Evapotranspiration by various methods for Kashmir Valley. Journal of Indian Water Resources Society (IWRS). 26(3-4) - 2006,1-4,

Wang, W., and Ding, J. (2003). "Wavelet network model and its application to the prediction of hydrology." Nature and Science, 1(1), 67-71.

Weng, Q. (2002). "Land use change analysis in the Zhujiang Delta of China using satellite remote sensing, GIS and stochastic modelling." Journal of environmental management, 64(3), 273-284.

Widmann, M., and Schär, C. (1997). "A principal component and long?term trend analysis of daily precipitation in Switzerland." International Journal of Climatology, 17(12), 1333-1356.

Wilby, R. L., & Harris, I. (2006). A framework for assessing uncertainties in climate change impacts: Low-flow scenarios for the River Thames, UK. Water Resources Research, 42(2).

Wilby, R. L., Beven, K. J., & Reynard, N. S. (2008). Climate change and fluvial flood risk in the UK: more of the same. Hydrological processes, 22(14), 2511-2523.

Williams, J., and Nicks, A. "CREAMS hydrology model-Option one." Proc., Applied Modeling Catchment Hydrology. Proc. Int. Symp. Rainfall-Runoff Modeling, 18-21.

Willmott, C. J., Robeson, S. M., and Matsuura, K. (2012). "A refined index of model performance." International Journal of Climatology, 32(13), 2088-2094.

Wolock, D. M., and McCabe, G. J. (1995). "Comparison of single and multiple flow direction algorithms for computing topographic parameters in TOPMODEL." Water Resources Research, 31(5), 1315-1324.

Wu, H., and Qian, H. (2016). "Innovative trend analysis of annual and seasonal rainfall and extreme values in Shaanxi, China, since the 1950s." International Journal of Climatology.

Wu, Q., Li, H.-q., Wang, R.-s., Paulussen, J., He, Y., Wang, M., Wang, B.-h., and Wang, Z. (2006). "Monitoring and predicting land use change in Beijing using remote sensing and GIS." Landscape and urban planning, 78(4), 322-333.

Wu, T. H., Hall, J. A., and Bonta, J. V. (1993). "Evaluation of runoff and erosion models." Journal of irrigation and drainage engineering, 119(2), 364-382.

Wu, W. "Land use and cover change detection and modelling for North Ningxia, China." Proc., Proceedings of Map Asia 2002, GIS Development, Webpage (http://www. gisdevelopment. net/application/environment/overview/envo0008pf. htm).

Wu, W., & Lynch, A. H. (2000). Response of the seasonal carbon cycle in high latitudes to climate anomalies. Journal of Geophysical Research: Atmospheres, 105(D18), 22897-22908.

Wu, Y., and Liu, S. (2012). "Automating calibration, sensitivity and uncertainty analysis of complex models using the R package Flexible Modeling Environment (FME): SWAT as an example." Environmental Modelling & Software, 31, 99-109.

Xiao, J., Shen, Y., Ge, J., Tateishi, R., Tang, C., Liang, Y., and Huang, Z. (2006). "Evaluating urban expansion and land use change in Shijiazhuang, China, by using GIS and remote sensing." Landscape and urban planning, 75(1), 69-80.

Xu, K., Milliman, J. D., and Xu, H. (2010). "Temporal trend of precipitation and runoff in major Chinese Rivers since 1951." Global and Planetary Change, 73(3), 219-232.

Xu, Z., Takeuchi, K., and Ishidaira, H. (2003). "Monotonic trend and step changes in Japanese precipitation." Journal of hydrology, 279(1), 144-150.

Xu, Z.-x., and Zhang, N. (2006). "Long-term trend of precipitation in the Yellow River basin during the past 50 years." Geographical Research, 1, 003.

Yang, J., Yu, K., Gong, Y., and Huang, T. "Linear spatial pyramid matching using sparse coding for image classification." Proc., Computer Vision and Pattern Recognition, 2009. CVPR 2009. IEEE Conference on, IEEE, 1794-1801.

Yang, M., Sang, Y.-F., Liu, C., and Wang, Z. (2016). "Discussion on the Choice of Decomposition Level for Wavelet Based Hydrological Time Series Modeling." Water, 8(5), 197.

Yang, T., Li, H., Wang, W., Xu, C. Y., & Yu, Z. (2012). Statistical downscaling of extreme daily precipitation, evaporation, and temperature and construction of future scenarios. Hydrological Processes, 26(23), 3510-3523.

Yang, X., Zheng, X.-Q., and Chen, R. (2014). "A land use change model: Integrating landscape pattern indexes and Markov-CA." Ecological Modelling, 283, 1-7.

Yuan, F., Sawaya, K. E., Loeffelholz, B. C., and Bauer, M. E. (2005). "Land cover classification and change analysis of the Twin Cities (Minnesota) Metropolitan Area by multitemporal Landsat remote sensing." Remote sensing of Environment, 98(2), 317-328.

Yue, S., Pilon, P., and Cavadias, G. (2002). "Power of the Mann-Kendall and Spearman's rho tests for detecting monotonic trends in hydrological series." Journal of hydrology, 259(1), 254-271.

Zhang, Y., You, Q., Chen, C., and Ge, J. (2016). "Impacts of climate change on streamflows under RCP scenarios: A case study in Xin River Basin, China." Atmospheric Research, 178-179, 521-534.

Zhu, J. (2013). "Impact of Climate Change on Extreme Rainfall across the United States." Journal of Hydrologic Engineering, 18(10), 1301-1309.

Zope, P. E., Eldho, T. I., & Jothiprakash, V. (2017). Hydrological impacts of land use–land cover change and detention basins on urban flood hazard: a case study of Poisar River basin, Mumbai, India. Natural Hazards, 1-17.

ANNEXURE-1 (A)

Ranking (best to poor) of Global Climate Models (GCMs) for Annual Period

Annual Ranking	*North Mountainous India*	*North West India*	*North Central India*	*West Penninsular India*	*East Penninsular India*	*South Penninsular India*	*Northeast India*
1	ukmo_hadcm3	mpi_echam5	ingv_echam4	gfdl_cm2_1	gfdl_cm2_0	bccr_bcm2_0	ingv_echam4
2	gfdl_cm2_0	gfdl_cm2_1	mpi_echam5	mpi_echam5	gfdl_cm2_1	gfdl_cm2_0	csiro_mk3_0
3	mpi_echam5	ingv_echam4	csiro_mk3_0	gfdl_cm2_0	ingv_echam4	cccma_cgcm3_1_t63	cccma_cgcm3_1
4	cccma_cgcm3_1_t63	cccma_cgcm3_1	gfdl_cm2_0	csiro_mk3_0	ncar_pcm1	mpi_echam5	csiro_mk3_5
5	gfdl_cm2_1	cccma_cgcm3_1_t63	miroc3_2_hires	bccr_bcm2_0	giss_aom	cccma_cgcm3_1	gfdl_cm2_1
6	ingv_echam4	ukmo_hadcm3	cccma_cgcm3_1	cccma_cgcm3_1	miroc3_2_hires	ukmo_hadcm3	mpi_echam5
7	miroc3_2_medres	csiro_mk3_0	cccma_cgcm3_1_t63	miroc3_2_medres	bccr_bcm2_0	miroc3_2_medres	ukmo_hadgem1
8	cccma_cgcm3_1	csiro_mk3_5	csiro_mk3_5	miub_echo_g	cccma_cgcm3_1_t63	csiro_mk3_0	ncar_ccsm3_0
9	csiro_mk3_0	gfdl_cm2_0	gfdl_cm2_1	ukmo_hadcm3	iap_fgoals1_0_g	gfdl_cm2_1	gfdl_cm2_0
10	miroc3_2_hires	miroc3_2_hires	ukmo_hadcm3	ukmo_hadgem1	mpi_echam5	giss_aom	miroc3_2_hires
11	ukmo_hadgem1	miroc3_2_medres	ukmo_hadgem1	cccma_cgcm3_t63	ukmo_hadgem1	iap_fgoals1_0_g	ukmo_hadcm3
12	bccr_bcm2_0	ukmo_hadgem1	mri_cgcm2_3_2a	giss_aom	cccma_cgcm3_1	ingv_echam4	cccma_cgcm3_t63
13	csiro_mk3_5	miub_echo_g	inmcm3_0	iap_fgoals1_0_g	csiro_mk3_0	inmcm3_0	miroc3_2_medres
14	ncar_ccsm3_0	bccr_bcm2_0	ipsl_cm4	ingv_echam4	inmcm3_0	miroc3_2_hires	mri_cgcm2_3
15	giss_aom	iap_fgoals1_0_g	miroc3_2_medres	miroc3_2_hires	miroc3_2_medres	cnrm_cm3	giss_aom
16	ipsl_cm4	ncar_ccsm3_0	ncar_ccsm3_0	cnrm_cm3	ukmo_hadcm3	ukmo_hadgem1	miub_echo_g
17	miub_echo_g	giss_aom	ncar_pcm1	csiro_mk3_5	cnrm_cm3	csiro_mk3_5	ncar_pcm1
18	mri_cgcm2_3_2a	inmcm3_0	bccr_bcm2_0	ncar_ccsm3_0	ipsl_cm4	giss_model_e_h	inmcm3_0
19	ncar_pcm1	mri_cgcm2_3_2a	iap_fgoals1_0_g	giss_model_e_h	miub_echo_g	ipsl_cm4	iap_fgoals1_0_g
20	cnrm_cm3	ncar_pcm1	miub_echo_g	ipsl_cm4	csiro_mk3_5	mri_cgcm2_3_2a	bccr_bcm2_0
21	iap_fgoals1_0_g	ipsl_cm4	cnrm_cm3	ncar_pcm1	giss_model_e_h	giss_model_e_r	giss_model_e_h
22	giss_model_e_h	cnrm_cm3	giss_aom	inmcm3_0	mri_cgcm2_3_2a	miub_echo_g	ipsl_cm4
23	inmcm3_0	giss_model_e_h	giss_model_e_h	mri_cgcm2_3_2a	ncar_ccsm3_0	ncar_pcm1	cnrm_cm3
24	giss_model_e_r	giss_model_e_r	giss_model_e_r	giss_model_e_r	giss_model_e_r	ncar_ccsm3_0	giss_model_e_r

ANNEXURE-1 (B)

Ranking (best to poor) of Global Climate Models (GCMs) for Monsoon Period

Monsoon Ranking	*North Mountainous India*	*North West India*	*North Central India*	*West Penninsular India*	*East Penninsular India*	*South Penninsular India*	*Northeast India*
1	mpi_echam5	cccma_cgcm3_1_t63	ingv_echam4	miroc3_2_hires	miroc3_2_hires	bccr_bcm2_0	ingv_echam4
2	cccma_cgcm3_1_t63	ingv_echam4	cccma_cgcm3_1	cccma_cgcm3_1	gfdl_cm2_1	cccma_cgcm3_1_t63	csiro_mk3_0
3	gfdl_cm2_1	mpi_echam5	miroc3_2_hires	miroc3_2_medres	ncar_pcm1	gfdl_cm2_1	csiro_mk3_5
4	ingv_echam4	cccma_cgcm3_1	csiro_mk3_0	csiro_mk3_0	ingv_echam4	miroc3_2_hires	ukmo_hadgem1
5	ukmo_hadcm3	gfdl_cm2_1	gfdl_cm2_0	gfdl_cm2_1	cccma_cgcm3_1_t63	cnrm_cm3	cccma_cgcm3_1
6	ukmo_hadgem1	csiro_mk3_0	mpi_echam5	mpi_echam5	cccma_cgcm3_1	gfdl_cm2_0	gfdl_cm2_1
7	cccma_cgcm3_1	ukmo_hadcm3	ukmo_hadcm3	ncar_pcm1	mpi_echam5	ingv_echam4	mpi_echam5
8	gfdl_cm2_0	csiro_mk3_5	cccma_cgcm3_1_t63	ukmo_hadgem1	miroc3_2_medres	miroc3_2_medres	cccma_cgcm3_1_t3
9	miroc3_2_hires	gfdl_cm2_0	csiro_mk3_5	giss_aom	gfdl_cm2_0	mpi_echam5	ukmo_hadcm3
10	miroc3_2_medres	miroc3_2_medres	gfdl_cm2_1	ingv_echam4	csiro_mk3_5	ncar_ccsm3_0	gfdl_cm2_0
11	csiro_mk3_5	miroc3_2_hires	ukmo_hadgem1	bccr_bcm2_0	csiro_mk3_0	csiro_mk3_0	ncar_pcm1
12	ncar_ccsm3_0	ukmo_hadgem1	ncar_ccsm3_0	cccma_cgcm3_1_t63	bccr_bcm2_0	cccma_cgcm3_1	miroc3_2_hires
13	csiro_mk3_0	bccr_bcm2_0	inmcm3_0	cnrm_cm3	inmcm3_0	ncar_pcm1	miroc3_2_medres
14	giss_aom	iap_fgoals1_0_g	miroc3_2_medres	csiro_mk3_5	cnrm_cm3	ukmo_hadcm3	miub_echo_g
15	bccr_bcm2_0	miub_echo_g	iap_fgoals1_0_g	miub_echo_g	miub_echo_g	ukmo_hadgem1	ncar_ccsm3_0
16	ipsl_cm4	ncar_ccsm3_0	ipsl_cm4	ncar_ccsm3_0	giss_aom	giss_aom	cnrm_cm3
17	ncar_pcm1	ncar_pcm1	mri_cgcm2_3_2a	gfdl_cm2_0	ukmo_hadgem1	giss_model_e_r	giss_aom
18	cnrm_cm3	cnrm_cm3	ncar_pcm1	giss_model_e_h	ukmo_hadcm3	iap_fgoals1_0_g	ipsl_cm4
19	iap_fgoals1_0_g	giss_aom	miub_echo_g	iap_fgoals1_0_g	ncar_ccsm3_0	inmcm3_0	mri_cgcm2_3_2a
20	miub_echo_g	inmcm3_0	bccr_bcm2_0	ipsl_cm4	iap_fgoals1_0_g	mri_cgcm2_3_2a	giss_model_e_h
21	giss_model_e_h	mri_cgcm2_3_2a	giss_aom	mri_cgcm2_3_2a	mri_cgcm2_3_2a	csiro_mk3_5	iap_fgoals1_0_g
22	giss_model_e_r	giss_model_e_h	cnrm_cm3	ukmo_hadcm3	ipsl_cm4	giss_model_e_h	inmcm3_0
23	inmcm3_0	ipsl_cm4	giss_model_e_h	inmcm3_0	giss_model_e_r	miub_echo_g	bccr_bcm2_0
24	mri_cgcm2_3_2a	giss_model_e_r	giss_model_e_r	giss_model_e_r	giss_model_e_h	ipsl_cm4	giss_model_e_r

ANNEXURE-1 (C)

Ranking (best to poor) of Global Climate Models (GCMs) for Non-monsoon Period

Non-monsoon Ranking	*North Mountainous India*	*North West India*	*North Central India*	*West Penninsular India*	*East Penninsular India*	*South Penninsular India*	*Northeast India*
1	ukmo_hadcm3	miroc3_2_medres	mpi_echam5	gfdl_cm2_1	ipsl_cm4	cccma_cgcm3_1	mpi_echam5
2	cccma_cgcm3_1_t63	gfdl_cm2_1	ipsl_cm4	mpi_echam5	gfdl_cm2_0	gfdl_cm2_0	ncar_ccsm3_0
3	mpi_echam5	mpi_echam5	miroc3_2_medres	ipsl_cm4	giss_aom	ipsl_cm4	csiro_mk3_0
4	gfdl_cm2_0	ukmo_hadgem1	cccma_cgcm3_1	giss_aom	iap_fgoals1_0_g	bccr_bcm2_0	cccma_cgcm3_1_t63
5	ingv_echam4	inmcm3_0	cccma_cgcm3_1_t63	iap_fgoals1_0_g	ukmo_hadgem1	gfdl_cm2_1	csiro_mk3_5
6	csiro_mk3_5	ipsl_cm4	csiro_mk3_0	miub_echo_g	bccr_bcm2_0	giss_aom	gfdl_cm2_1
7	gfdl_cm2_1	miroc3_2_hires	gfdl_cm2_1	bccr_bcm2_0	csiro_mk3_0	iap_fgoals1_0_g	ingv_echam4
8	ipsl_cm4	ncar_ccsm3_0	ingv_echam4	cccma_cgcm3_1	gfdl_cm2_1	mpi_echam5	miroc3_2_hires
9	miroc3_2_hires	ukmo_hadcm3	mri_cgcm2_3_2a	gfdl_cm2_0	ingv_echam4	ukmo_hadcm3	miroc3_2_medres
10	miroc3_2_medres	cccma_cgcm3_1_t63	ncar_ccsm3_0	inmcm3_0	ukmo_hadcm3	cccma_cgcm3_1_t63	cccma_cgcm3_1
11	mri_cgcm2_3_2a	csiro_mk3_0	ncar_pcm1	csiro_mk3_0	cccma_cgcm3_1_t63	miroc3_2_medres	gfdl_cm2_0
12	ncar_ccsm3_0	giss_aom	miroc3_2_hires	miroc3_2_medres	cnrm_cm3	ukmo_hadgem1	ukmo_hadgem1
13	bccr_bcm2_0	iap_fgoals1_0_g	ukmo_hadcm3	mri_cgcm2_3_2a	inmcm3_0	giss_model_e_h	ipsl_cm4
14	csiro_mk3_0	miub_echo_g	gfdl_cm2_0	ncar_ccsm3_0	miub_echo_g	inmcm3_0	miub_echo_g
15	miub_echo_g	mri_cgcm2_3_2a	miub_echo_g	ukmo_hadgem1	mpi_echam5	csiro_mk3_0	mri_cgcm2_3_2a
16	giss_aom	csiro_mk3_5	ukmo_hadgem1	cccma_cgcm3_1_t63	ncar_pcm1	miroc3_2_hires	ncar_pcm1
17	iap_fgoals1_0_g	gfdl_cm2_0	csiro_mk3_5	cnrm_cm3	cccma_cgcm3_1	miub_echo_g	ukmo_hadcm3
18	inmcm3_0	ingv_echam4	giss_aom	ukmo_hadcm3	miroc3_2_hires	mri_cgcm2_3_2a	giss_aom
19	ukmo_hadgem1	cccma_cgcm3_1	iap_fgoals1_0_g	csiro_mk3_5	ncar_ccsm3_0	csiro_mk3_5	inmcm3_0
20	cnrm_cm3	bccr_bcm2_0	inmcm3_0	giss_model_e_h	miroc3_2_medres	giss_model_e_r	cnrm_cm3
21	cccma_cgcm3_1	ncar_pcm1	bccr_bcm2_0	ingv_echam4	csiro_mk3_5	ingv_echam4	iap_fgoals1_0_g
22	giss_model_e_h	cnrm_cm3	cnrm_cm3	miroc3_2_hires	giss_model_e_h	ncar_pcm1	bccr_bcm2_0
23	ncar_pcm1	giss_model_e_h	giss_model_e_h	giss_model_e_r	giss_model_e_r	cnrm_cm3	giss_model_e_h
24	giss_model_e_r	giss_model_e_r	giss_model_e_r	ncar_pcm1	mri_cgcm2_3_2a	ncar_ccsm3_0	giss_model_e_r

ANNEXURE-2

Detailed Land Use, Soil and Slope distribution for SWAT Model

Detailed LAND USE distribution for SWAT model		Area [ha]	% Area
Basin		**3274522**	
Number of Sub-basins: 54			
Number of HRUs: 856			
LAND USE			
1.	RESIDENTIAL-MEDIUM DENSITY --> URMD	18473	0.57
2.	DRYLAND CROPLAND AND PASTURE --> CRDY	41	0.00
3.	CROPLAND/GRASSLAND MOSAIC --> CRGR	701857	21.77
4.	SHRUBLAND --> SHRB	208266	6.46
5.	MIXED GRASSLAND/SHRUBLAND --> MIGS	33548	1.04
6.	SAVANNA --> SAVA	273962	8.50
7.	DECIDUOUS BROADLEAF FOREST --> FODB	2920	0.09
8.	DECIDUOUS NEEDLELEAF FOREST --> FODN	189717	5.88
9.	EVERGREEN BROADLEAF FOREST --> FOEB	293563	9.10
10.	MIXED FOREST --> FOMI	92033	2.85
11.	WATER BODIES --> WATB	384112	11.91
12.	WOODED WETLAND --> WEWO	1026028	31.82

Detailed SOIL/SLOPE distribution for SWAT Model		Area [ha]	% .Area
SOILS			
1.	Bv12-3b-3696	20574	0.64
2.	I-bc-3735	549384	17.04
3.	I-Bc-Lc-3714	31303	0.97
4.	Lc75-1b-3780	57812	1.79
5.	Vc21-3a-3859	15778	0.49
6.	Vc43-3ab-3861	1853718	57.49
7.	Vp20-3a-3866	695952	21.58
SLOPE			
1.	0-0.75	285712	8.86
2.	0.75-2	790104	24.50
3.	02-04	756871	23.47
4.	04-06	392022	12.16
5.	06--99	999813	31.01

ANNEXURE-3

Distribution of Sub-basins area in the basin

(Location of Sub-basins given in Figure 7.3)

Sub-basin	Area (ha)	% Area	Sub-basin	Area (ha)	% Area	Sub-basin	Area (ha)	% Area
1	56761.72	1.76	19	98028.65	3.04	37	200466	6.22
2	17597.98	0.55	20	138025.2	4.28	38	51912.01	1.61
3	116738.5	3.62	21	75200.28	2.33	39	34631.83	1.07
4	20291.98	0.63	22	241753.6	7.5	40	28836.46	0.89
5	51572.67	1.6	23	19863.93	0.62	41	55532.71	1.72
6	83735.29	2.6	24	39866.53	1.24	42	82094.61	2.55
7	49776.96	1.54	25	65836.74	2.04	43	24421.68	0.76
8	58712.46	1.82	26	3730.09	0.12	44	74863.53	2.32
9	29982.79	0.93	27	9643.45	0.3	45	56229.47	1.74
10	28513.49	0.88	28	65792.82	2.04	46	52352.97	1.62
11	25410.4	0.79	29	33029.9	1.02	47	110502.2	3.43
12	54687.82	1.7	30	28932.06	0.9	48	57618.67	1.79
13	90565.03	2.81	31	90972.4	2.82	49	79727.02	2.47
14	35080.55	1.09	32	56561.91	1.75	50	32726.74	1.01
15	5061.58	0.16	33	45978.84	1.43	51	27244.01	0.84
16	46095.97	1.43	34	52222.06	1.62	52	57520.48	1.78
17	71482.25	2.22	35	26103.71	0.81	53	33338.23	1.03
18	24774.8	0.77	36	67292.26	2.09	54	138827.1	4.31

LIST OF PUBLICATIONS

Peer reviewed Journals/ Conferences / Book Chapter

- **Brij K Pandey**, Deepak Khare (2018) "Identification of Trend over Narmada River Basin (India) of long term Precipitation and Reference Evapotranspiration series "*Global and Planetary Change, Elsevier*. DOI: 10.1016/j.gloplacha.2017, Volume 161, Pages 172-182.

- **Brij K Pandey**, H. Tiwari, D. Khare (2017) "Trend analysis using discrete wavelet transforms (DWT) for long term precipitation (1851-2006) over India" *Hydrological Science Journal, Taylor & Francis .DOI:10.1080/02626667.2017. 1371849. Issue 13, Volume 23, 2017. Pages: 2187-2208.*

- **Brij K Pandey**, Deepak Khare (2017) "Analyzing and modelling of a large river basin dynamics applying Integrated Cellular Automata and Markov Model" *Environment Earth Science, Springer. DOI: 10.1007/s12665-017-7133-4.*

- **Brij K Pandey**, Deepak Khare, A. Kawasaki, P.K. Mishra (2018) "Climate Change Impact assessment on Blue and Green Water by Coupling of Representative CMIP5 Climate Models with physical based Hydrological Model" *Water Resources Management, Springer.* ***(Accepted)***

- **Brij K Pandey**, Deepak Khare (2017) "Assessment of Reference Evapotranspiration in the context of climate change for Central India (Madhya Pradesh)" *DOI: 10.1007/978-3-319-55125-8-21.(Book : Development of Water Resources in India; Publisher: Water Science and Technology Library, Springer; Edition: Vol. 84,)* ***(Book Chapter)***

- **Brij K Pandey**, A. K. Gosain, G. Paul, D. Khare (2017) "Climate change impact assessment on hydrology of small watershed using semi- distributed model" *Applied Water Science, Springer. DOI:10.1007/s13201-016-0383-6.*

- **Brij K Pandey**, D. Khare (2017) "Hydrological Response Simulation for River Basin under Climate Change Scenario " for *International Conference 'Asia Oceania Geoscience Society-2017'* at Singapore from 06-11 August 2017. **(Poster Presentation)**

- **Brij K Pandey**, A K Gosain, G. Paul, D. Khare "Hydrological Modeling of Watershed: Impact and Coping strategies towards Climate Change*"* of *International conference on Modeling Tools for Sustainable Water Resources Management (MTSWRM)* at IIT Hyderabad 28-29 December 2014. **(Paper Presentation).**

- **Brij K Pandey**, Deepak Khare, H. Tiwari "Analyzing and visualization of annual extremes meteorological parameters employing Innovative Trend Analysis and Discrete Wavelet Transform", *Journal of Hydrology*. (Under Review)

- **Brij K Pandey**, Deepak Khare, Patricia Sanchez "Evaluation of AR4 Climate Models for India using Multi-Criteria Analysis and Akaike Information Criteria" *Theoretical and Applied Climatology*. (Under Review)